6-14-2021 10:00 AM

Characterization and modulatory influence of pyruvate kinase muscle isoforms 1 and 2 within the murine pluripotent continuum

Joshua G. Dierolf, *The University of Western Ontario*

Supervisor: Betts, Dean H., *The University of Western Ontario*

A thesis submitted in partial fulfillment of the requirements for the Doctor of Philosophy degree in Physiology and Pharmacology

Abstract

Mouse embryonic stem cells (mESCs) and mouse epiblast stem cells (mEpiSCs) represent opposite ends of a pluripotency continuum, respectively referred to as naïve and primed pluripotent states. A third, recently discovered intermediate state has been described as the 'formative state'. Metabolism has been traditionally regarded as a by-product of cell fate; however, recent evidence now supports metabolism as promoting stem cell fate. Pyruvate kinase muscle isoforms 1 and 2 (PKM1 and PKM2) catalyze the final, rate limiting step of glycolysis generating adenosine triphosphate (ATP) and pyruvate; however, the precise role(s) of these isozymes in naïve, formative, and primed pluripotency is unclear. Steric-blocking morpholino oligonucleotides were employed to modulate the levels of PKM1/2; this thesis characterized the cellular expression, localization patterns, and contributions of PKM1 and PKM2 in mESCs, chemically transitioned mouse epiblast-like cells (mEpiLCs) representing formative pluripotency, and mEpiSCs using immunoblotting, flow cytometry, and confocal microscopy. My results indicate that PKM1 and PKM2 are not only localized to the cytoplasm, but also accumulate in distinct subnuclear regions of mESCs, mEpiLCs, and mEpiSCs as determined by a comprehensive and quantitative, confocal microscopy colocalization methodology.

In Chapters 2 and 3, I employed orthogonal projections, and airyscan processing to investigate the localization patterns of PKM1/2. I determined that the subnuclear localization of PKM1/2 shifts during the pluripotent development across mESCs, mEpiLCs, and mEpiSCs. The appropriateness and power of the Pearson's Correlation Coefficient and Manders' Overlap Coefficient for assessing nuclear and cytoplasmic

protein colocalization in pluripotent stem cells (PSCs) by immunofluorescence confocal microscopy was validated and expanded upon. In Chapter 4, I describe a key research tool of this thesis using flow cytometry, this improved technique allows for the identification of formative pluripotency cells from naïve and primed populations using the cell surface markers SSEA1 and CD24. Additionally, I utilized this advanced methodology in Chapter 5 to assess the influence of PKM1/2 modulation on pluripotency state. Altering PKM1/2 levels affected the ability of naïve state cells to transition to the formative state, it also influenced the transition of formative cells to a primed-like state. In conclusion, the results suggest that nuclear PKM1/2 assists with distinct pluripotency state maintenance and lineage priming by non-canonical mechanisms. These results advance our understanding of the overall mechanisms controlling naïve, formative, and primed pluripotency.

Lay Summary

Prior to implantation, an embryo is referred to as a blastocyst. The blastocyst contains a small pocket of cells called the inner cell mass. These cells can become all cell types of an individual, a characteristic coined ‘pluripotency’. Isolated inner cell mass cells can be grown in the lab to study how the embryo develops and how pluripotent stem cells function. Stem cells require sources of energy to maintain themselves and growth with the process of metabolism. Pluripotent stem cells progressively specialize over the timeline of the pluripotent continuum. The first stage of the continuum is called the naïve state, where a cell is pluripotent, but is not fully ready to turn into a new cell. First, a naïve cell must develop into a formative state cell, this state is an intermediate point needed to gain the ability to turn into any cell of the fetus, and the only state that a cell can turn into a germ cell. Before making the decision to leave pluripotency, the cell enters the final stage, the primed state, where it is ‘primed’ for cell lineage choices. This thesis examined two main proteins that are known to aid in cellular digestion of the building blocks needed to grow and generate energy, pyruvate kinase muscle isoforms 1 and 2 (PKM1/2). PKM1/2 affect the ability of pluripotent stem cells to stay as naïve cells or develop into becoming formative, or primed stem cells. This thesis utilized several improved methods to examine the effects of altering the levels and localization of PKM1/2 on pluripotent and metabolic state of the naïve, formative, and primed stages. This knowledge helps us to understand how embryonic stem cells stay pluripotent and specialize into other types of cells.

Keywords:

Aerobic glycolysis; Differentiation; Embryonic stem cells; Formative pluripotency; Glycolysis; Metabolism; Murine development; Naïve pluripotency; Oxidative phosphorylation; Pluripotent continuum; Primed pluripotency; Pyruvate kinase muscle isoforms 1 and 2.

Co-Authorship Statement

Chapter two is adapted from a submitted manuscript: **3D immunofluorescent image colocalization quantification in mouse epiblast stem cells**. Dierolf, J.G., Watson, A.J., Betts, D.H. (2021). Chapter two has been submitted to *Methods in Molecular Biology*. This methodology was conceived to improve upon existing strategies by Dierolf, J.D.

Chapter three is adapted from a submitted manuscript: **Differential localization patterns of pyruvate kinase isoforms in murine naïve, formative, and primed pluripotent states**. Dierolf, J.G., Watson, A.J., Betts, D.H. (2021). Submitted to *Experimental Cell Research*. J.G. Dierolf designed all experiments with the assistance of Drs. A.J. Watson and D.H. Betts. All data was generated by J.G. Dierolf in the laboratories of AJ Watson, and D.H. Betts. All figures were prepared by J.G. Dierolf. The manuscript was written by J.G. Dierolf with the assistance of A.J. Watson and D.H. Betts.

Chapter four is adapted from a submitted manuscript: **Flow cytometric characterization of pluripotent cell protein markers in naïve, formative, and primed pluripotent stem cells**. Dierolf, J.G., Brooks, C., Chadwick, K., Watson, A.J., Betts, D.H. (2021). Chapter four has been submitted to *Methods in Molecular Biology*. Chapter four is presented as work completed with the help of the stem cell technician C. Brooks and the flow cytometry facility manager Dr. K. Chadwick. C. Brooks helped to grow cells and stain treatments for the flow cytometric analysis. Experimental design was completed by J.G. Dierolf with the assistance of C. Brooks and Dr. D.H. Betts. Flow cytometry was completed by J.G. Dierolf under the advisement of Dr. K. Chadwick of the London Regional Flow Cytometry Facility of Robarts at Western University.

Chapter five is adapted from a submitted manuscript: **Modulation of PKM1/2 levels alters the metabolic and pluripotent state of murine pluripotent stem cells**. Dierolf, J.G., Hunter, H., Watson, A.J., Betts, D.H. (2021). Submitted to *Scientific Reports*. J.G. Dierolf designed all experiments with the assistance of Drs. A.J. Watson and D.H. Betts. All data was generated by J.G. Dierolf in the laboratories of AJ Watson and D.H. Betts. H. Hunter retested and generated additional transcript abundance raw data following cDNA synthesis and prior experiments completed by J.G. Dierolf. All figures were prepared by J.G. Dierolf. The manuscript was written by J.G. Dierolf with the assistance of A.J. Watson, H. Hunter, and D.H. Betts. Cell maintenance, morpholino transfection, flow cytometry analysis, and writing were completed by J.G. Dierolf.

Epigraph

> "We can judge our progress by the courage of our questions and the depth of our answers, our willingness to embrace what is true rather than what feels good."
>
> Dr. Carl Sagan

Since starting this project in 2015, I have struggled with the concept of progression and finding contentment with the answers I was generating. Failure was a big part of the first 3 years of my PhD, few experiments worked, even fewer produced results worthy of further investigation. During my first year in the lab, I witnessed PKM1 appearing to reside in the nucleus of my stem cells under a basic fluorescent microscope, something that had never been reported in any cell type at the time. Naturally, I doubted this initial finding, but I thought it was interesting enough to present to my lab resulting in discussion. This small qualitative finding was the seed to give me the courage to not only investigate whether it was in fact in the nucleus, but also create my own, more comprehensive, and improved methodology for nuclear cytoplasmic colocalization. I embraced my ideas and forged a path to success. By finding courage in my questions and working to improve the field, I was able to begin answering my query. Showing nuclear PKM1 felt like real progress, but it required asking deeper questions and answering those question in new and better ways. Science is not static; science is highly dynamic and craves both improvement and change; this project resulted in enhancements to current methodologies that will benefit projects well outside of the scope of my study. Overall, this project required a willingness to embrace the scientific method, and despite setbacks and troubleshooting, I was able to turn kernels of proof into more substantial evidence of something novel.

Dedication

This thesis is dedicated to those who encouraged my research interests and fostered my curiosity the most, my grandparents Manfred and Joan Dierolf.

Acknowledgements

This thesis would not have been possible without my outstanding lab mates, family, friends, and mentors. Thank you to all my lab mates, especially Courtney Brooks for teaching me tips, tricks, and best practises in growing pluripotent stem cells. Thank you to my ever-supportive wife Micky Agrawal for standing by me through successes and failures; for getting me back on my feet and sharing in my excitement in the pursuit of excellence. This project would not have been possible without a certain special presence in my life, I felt a great deal of comfort during the hardest of times from my loyal dog Milly, thank you sweet girl. My parents, Jennifer and George Dierolf provided me with love and lodging throughout this difficult and formative process, you helped shape me into who I am today and for that I am eternally grateful.

Two core technical concepts that I worked to improve in the field are colocalization by confocal microscopy and methodology in distinguishing between pluripotent states by flow cytometry, these concepts were largely introduced to me by Drs. Julia Abitbol and Kristin Chadwick respectively. Without your instruction and our dialogue into the equipment, protocols, and scope of the technology, my research dreams would not have reached fruition. I am exceedingly grateful for your interest in my project, thank you both so much.

My supervisor, Dr. Dean Betts and the principal investigators of our research wing, Drs. Timothy Regnault, Daniel Hardy, and Andrew Watson supported me through their provision of research materials, space, and advice. Thank you for your interest in my research and giving me the opportunity to share my opinions and ideas. I really

appreciated the opportunity to pioneer a project of my own under the supervisor of Dr. Betts, and watch it develop from initial findings into peer reviewed publications. The members of our lab, including the research associates, lab technicians, post-docs, graduate students, fourth year thesis students, and volunteers have largely become my extended family. Thank you for being with me during this process as we grew together. Without the bonds we formed, this experience would not have been nearly as successful or enjoyable. Finally, my lab mates Alex Kozlov and Hailey Hunter were the biggest supporters of my research and gave me the emotional support needed to succeed.

I so am grateful for our amazing department of Physiology and Pharmacology for their amazing administrative staff and researchers. Our department is truly second to none at Western and I have never felt more supported during my over a decade experience at Western as I have during my PhD studies. There were several brilliant opportunities including: the student council, working on subcommittees within the department, and having the option to be a teaching assistant, that helped to shape the researcher and teacher I have developed into. Thank you to Drs. Dean Betts and Andrew Watson for creating a positive working space and encouraging me to excel and grow as a scientist. Additionally, thank you to Drs. Anita Woods, Cheryle Séguin, and David Hess for the incredible teaching experience in our second and fourth-year courses, I learned so much about how to share my love of science and stem cell biology with others. The opportunities to be involved were fantastic; I am so glad to give back to our stem cell community.

My research at Western University was greatly benefited by the extracurricular development provided by the Ontario Institute of Regenerative Medicine (OIRM) and the Stem Cell Network (SCN) of Canada. Thanks to these two outstanding organizations, I was able to learn critical skills needed in my studies. Both organizations gave me many reasons to stay in science and continue my dreams of researching stem cells for future regenerative medical innovations. Thank you to all members of the OIRM and SCN for your tireless efforts to promote Canadian science and trainee development. Being the chair of the SCN Trainee Communications Committee has been an incredible honor and further helped me to develop as a confident stem cell scientist.

Finally, this project would not have been possible without my three sensational mentors, Drs. Cheryle Séguin, Andrew Watson, and John Di Guglielmo. I can't begin to express my appreciation for your investment in my success and development, thank you. I found my niche thanks to you three.

Table of Contents

List of Abbreviations

2i	small molecule inhibitor cocktail; MEK/GSK
Acetyl-CoA	Acetyl coenzyme A
ADP	Adenosine diphosphate
Aldoa	Aldolase A
ANOVA	Analysis of variance
APC	Allophycocyanin
ATP	Adenosine triphosphate
BMP	Bone morphogenic protein
cDNA	Copy deoxyribonucleic acid
Cer1	Cerberus 1
cESC	Canine embryonic stem cells
CRISPR	Clustered regularly interspaced short palindromic repeats
DNA	Deoxyribonucleic acid
Dnmt3	DNA methyltransferase 3
Dppa3	Developmental pluripotency associated 3
E	Embryonic day
Eno1	Enolase 1
Eras	Embryonic stem cell expressed ras
Erk	Extracellular regulated kinases
ESC	Embryonic stem cell
Esrrb	Estrogen related receptor beta

FA	FGF-2/ACTIVIN A media
FACS	Fluorescently activated cell sorting
FBP	Fructose 1-6, bisphosphate
FBS	Fetal bovine serum
FCSB	Flow cytometry staining buffer
FGF-2	Fibroblast growth factor-2
Fh1	Fumarate hydratase 1
g	Gravity
Gapdh	Glyceraldehyde 3-phosphate dehydrogenase
GCDB	Gentle cell dissociation buffer
Gpi	Glucose-6-phosphate isomerase
GSK3β	Glycogen synthase kinase 3 beta
hESC	Human embryonic stem cells
Hif-1α	Hypoxia inducible factor 1-alpha
Hk2	Hexokinase 2
Hnf-4α	Hepatocyte nuclear factor 4 alpha
hnRNPI/hnRNP1/hnRNP2	Heterogenous nuclear ribonucleoproteins
HRP	Horseradish peroxidase
ICM	Inner cell mass
Idh2	Isocitrate dehydrogenase
iPSC	Induced pluripotent stem cell
Jmjd	Jumonji C domain-containing protein
Klf2	Krüppel-like Factor 2

Klf4	Krüppel-like Factor 4
Klf5	Krüppel-like Factor 5
Lef1	Lymphoid enhancer binding factor 1
LIF	Leukemia inhibitory factor
Mdh2	Malate dehydrogenase 2
MEFs	Mouse embryonic fibroblasts
Mek	Mitogen-activated protein kinase kinase
MEM	Minimum essential media
mEpiLCs	Mouse epiblast-like cells
mEpiSCs	Mouse epiblast stem cells
mESCs	Mouse embryonic stem cells
MO	Morpholino
MOC	Manders' overlap coefficient
mPSC	Mouse pluripotent stem cells
mRNA	Messenger ribonucleic acid
NAD	Nicotinamide adenine dinucleotide
NNEA	Non-essential amino acids
Nfκb	Nuclear factor kappa B
Nr0b1	Nuclear Receptor Subfamily 0 Group B Member 1
OA	Oroxylin A
Oct4/6	Octamer-binding transcription factor 4/6
OXPHOS	Oxidative phosphorylation
PBS	Phosphate-buffered saline

PCC	Pearson correlation coefficient
Pdk/Pdhk	Pyruvate dehydrogenase kinase
PE	Phycoerythrin
Pecam	Platelet endothelial cell adhesion molecule
Pfk1	Phosphofructokinase 1
PGCLC	Primordial germ cell-like cell
Pgam1	Phosphoglycerate mutase 1
Pgm	Phosphoglucomutase-1
Pklr	Pyruvate kinase - liver and red blood cells
Pkm1	Pyruvate kinase muscle isoform 1
Pkm2	Pyruvate kinase muscle isoform 2
Pml	Promyelocytic leukemia protein
pPkm2	Phosphorylated pyruvate kinase muscle isoform 2
PSC	Pluripotent stem cell
PVDF	Polyvinylidene difluoride
QCA	Quantitative colocalization analysis
qPCR	Quantitative polymerase chain reaction
qRT-PCR	Quantitative Real time polymerase chain reaction
rcf	Relative centrifugal force
REAP	Rapid, Efficient and Practical fractionation method
Rex1 (Zfp42)	Zinc finger protein 42
RIPA	Radioimmunoprecipitation assay buffer
RNA	Ribonucleic acid

RT-PCR	Real time polymerase chain reaction
	Reverse transcription polymerase chain reaction
Sall2	Spalt-like gene 2
SCLC	Small cell lung cancer
SD	Standard deviation
SEM	Standard error of means
shRNA	Small hairpin ribonucleic acid
siRNA	Small interference ribonucleic acid
Sox2	Sex determining region Y box transcription factor 2
SSEA1	Stage specific embryonic antigen 1
Stat3	Signal transducer and activator of transcription
Suclg1	Succinate-CoA ligase GDP/ADP-forming subunit alpha
T(Bra)	Brachyury
TALEN	Transcription activator-like effector nucleases
Tbp	TATA-binding protein
TBS	Tris-buffered saline
Tcfcp2l1	Transcription factor CP2-like protein 1
TE	Trophectoderm
Zic2	Zinc finger of the cerebellum 2

Lists of Figures

List of Tables

Chapter 1

1.0.0. Preface.

1.0.1. Mammalian blastocyst inner cell mass development.

Following fertilization by the union of a sperm and egg, the first mammalian cell differentiation event yields two distinct cell lineages, the trophectoderm (TE) and the inner cell mass (ICM) (Marikawa and Alarcón 2009). The TE and ICM are cellular precursors of the placenta and embryonic germ cell layers respectively. The eutherian placenta provides a necessary means for maternal nourishment of the developing embryo and this unique feature is conserved in the eutherian evolution of the TE. The cells of the ICM will go onto specialize into the cells of the adult organism, including the germ cells. These ICM cells are classified as pluripotent, they have the capability to self-renew indefinitely or specialize into any cell derivative of the three germ cell layers.

1.0.2. The first cell lineage determination.

Approximately 16-20 hours post-fertilization, the first cleavage of the zygote occurs resulting in the formation of two blastomeres. The subsequent cleavage events that follow, occur in 12- to 24-hour intervals. Between the third and fourth cleavage events, individual blastomeres undergo a morphogenetic change called ‘compaction’, resulting in a dramatic increase in cell-to-cell contact. This is fueled by the formation and action of E-Cadherin (Cadhern1; Cdh1) mediated adherens junction formation that transitions the eight-cell stage preimplantation embryo from a grape-like cluster into a fully mulberry-like compacted cell mass called the morula. Aside from providing cell-to-cell adhesion,

E-Cadherin also plays a critical and indirect role in generating the contractile forces needed for tissue compaction by removing acto-myosin from ectopic cell-to-cell surfaces (Stephenson, Yamanaka, and Rossant 2010; Klompstra et al. 2015; S. Yamada and Nelson 2007). This allows acto-myosin to accumulate and form a shell-like surface around the embryo, and generates the contraction necessary for compaction to occur (Maître et al. 2015). The formation of the ICM begins following the fifth cleavage event, where secreted vacuoles from outer TE blastomeres begin to form, grow, and combine within the embryo to form the fluid-filled blastocyst cavity (Aziz and Alexandre 1991). It is here that the TE and ICM combine to make up what is now referred to as the 'blastocyst'. The TE epithelializes from the outer blastomeres with the ICM forming on the basal surface from aggregated cells on the opposite side of the blastocyst cavity, this orientation is referred to as the 'embryonic and abembryonic poles' respectively and forms the embryonic-abembryonic axis.

1.1.0. The pluripotent continuum.

Within the developing murine embryo, naïve embryonic stem cells (mESCs) are derived from the inner cell mass (ICM) of an embryo at the pre-implantation blastocyst-stage, whereas primed epiblast stem cells (mEpiSCs) are more developmentally differentiated and can be derived from the late post-implantation epiblast (Nichols and Smith 2009). These two pluripotent states exist as the beginning and end of the pluripotent continuum. Both states have several distinguishing features aside from their developmental timeline. Morphologically, naïve cells are domed with a glistening appearance in culture, and their colonies are tolerant to single cell dissociation, whereas primed cells are characteristically flattened and respond poorly to enzymatic passaging (Tesar et al. 2007). In females, naïve

cells contain two activated X chromosomes, the paternally inherited X chromosome is inactivated in extraembryonic lineages following cleavage and is correspondingly inactivated in primed cells (Heard 2004). In terms of signalling, mESCs maintain the ability to indefinitely self-renew through activation of the transcription factor 'signal transducer and activator of transcription 3' (*Stat3*) by leukemia inhibitory factor (LIF) supplementation (Williams et al. 1988; A. G. Smith et al. 1988; H Niwa et al. 1998). When cultured with serum and LIF, mESCs can be maintained *in vitro*, however, they exist in a heterogenous composition that includes both naïve and cells exiting naïve state. In contrast, homogenous mESC cell culture is maintained through LIF supplementation with a small molecule blockage strategy referred to as 2i, a small molecular cocktail containing inhibitors of mitogen-activated protein kinase and glycogen synthase kinase 3 (Wray et al. 2011; Burdon et al. 1999). The combination of LIF/2i supplementation in the absence of sera promotes naïve cell homogeneity by suppressing differentiation without hindering cell division, the resulting state is referred to as the 'ground-state'. Alternatively, mEpiSCs do not require LIF or 2i, instead they require activin and fibroblast growth factor (FGF, together FA supplemented media) addition to their medium to achieve a stable, proliferative primed state (Brons et al. 2007; Tesar et al. 2007). Either end of the pluripotent continuum is hallmarked with unique metabolic preferences, with naïve cells are metabolically bivalent, utilizing both glycolytic and oxidative phosphorylation (OXPHOS), whereas primed cells are preferentially glycolytic even in oxygen rich environments (Figure 1.1.) (Zhou et al. 2012).

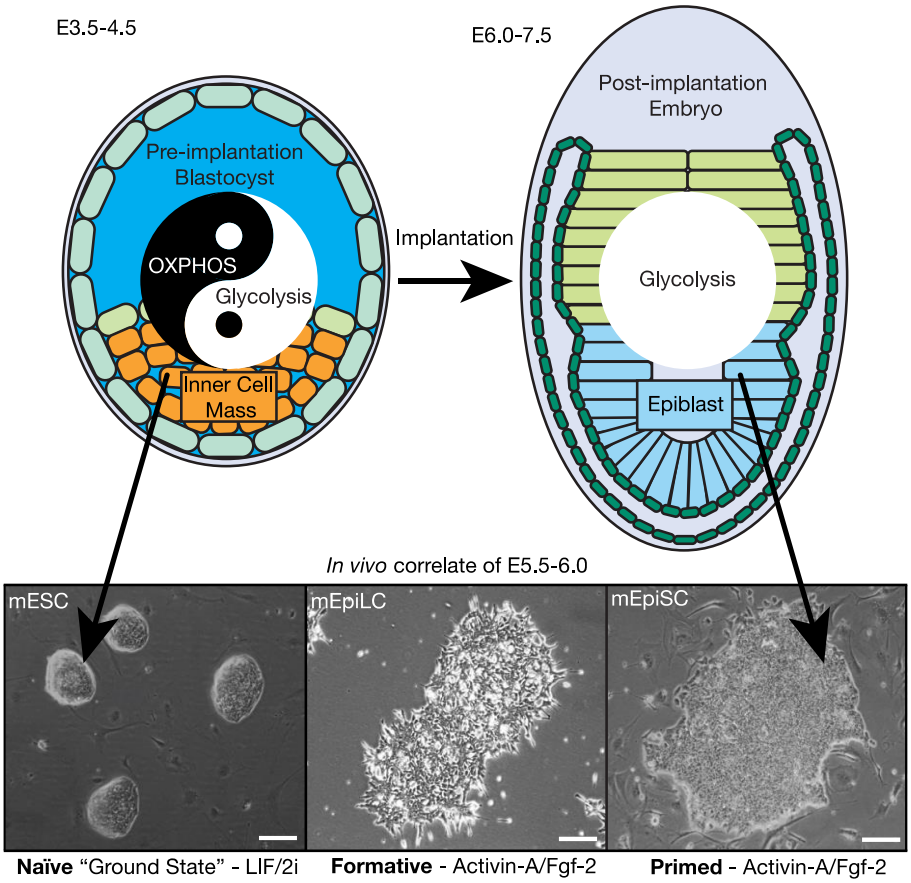

Figure 1.1. Pluripotent stem cells of the pre- and post- implantation murine blastocyst and corresponding metabolic preferences.

Phase contrast microscopy imaging of mESCs, mEpiLCs and mEpiSCs. Explanting cells of the inner cell mass of between Embryonic day (E) 3.5 and E4.5, supplemented with LIF and 2i media promotes domed colonies of cells with glistening borders representing the naïve pluripotent state. The formative state can be modelled by exchanging LIF/2i supplementation with FA media over 48 hours, these mEpiLCs are like the cells of the E5.5 to E6.0 post-implantation epiblast. Explanting cells of the post-implantation epiblast between E6.0 and E7.5 cultured in FA results in flattened colonies of cells representing the primed pluripotent state. The naïve and primed pluripotent states differ in metabolic preferences as naïve cells are bivalent utilizing glycolysis and OXPHOS and primed cells preferentially utilizing aerobic glycolysis. Scale bars represent 200 μm.

Between either end of the pluripotent continuum exists an interval of pluripotency hallmarked by the primordial germ cell and lineage differentiation competency. This executive, intermediate phase is referred to as formative pluripotency, and corresponds with E5.5-6.0 in the mouse embryo (A. Smith 2017). While naïve and primed pluripotent states are well characterized, the intermediate formative state and how stem cells exit pluripotency during differentiation is an area with much to still understand. One area that has been particularly neglected is an investigation of formative state's metabolic preferences. In this thesis, mESCs were exposed to FA for 48, 72, and 96 hours to produce and model the formative state and exit of the naïve and formative states towards a primed-like state. After 48 hours of FA treatment, mEpiLCs become reminiscent of E5.75 mouse ICM cells (Hayashi et al. 2011). At 72 hours following FA media supplementation, mEpiLCs exhibit a apoptosis event, cementing them towards a primed-like pluripotent fate path (Hayashi et al. 2011). Through additional passages and continued FA media treatment, primed-like pluripotent state cells are achieved. These conditions and timelines were employed to simulate a primed-like pluripotent state by exposing mESCs to FA over 96 hours with a single passage at 48 hours (Morgani, Nichols, and Hadjantonakis 2017).

Recently, stable formative pluripotent lines have been derived from humans and mice (Kinoshita et al. 2020). Stable formative lines can be generated though the addition of traditional FA media and supplementation of a tankyrase inhibitor, which works to inhibit Wnt/β-Catenin signalling (Menon et al. 2019). This is a ground-breaking finding as the formative pluripotent state works to promotes the phased progression model of

pluripotent development, which dictates that during development and achievement of competency for cell lineage specification, cells of the naïve pluripotent state will progress through formative into the primed pluripotent state before differentiating into a somatic cell (A. Smith 2017). Additionally, formative state cells are the only stem cell capable of efficient differentiation into primordial germ-like cells (PGCLCs). This demonstrates a competency for germ cell generation that is not inherent to naïve pluripotency (Hayashi et al. 2011). If correct, the phased progression model of pluripotent development would benefit from an effective method in studying phased progression transitioning efficiency. The cell surface markers Stage specific embryonic antigen 1 (SSEA1) and CD24 have been used to distinguish between the naïve and primed pluripotent states *via* flow cytometry (Shakiba et al. 2015). SSEA1 has elevated expression in naïve cells, whereas CD24 is elevated in primed pluripotency (Shakiba et al. 2015). For these reasons I was inspired to pursue the investigation of cell surface marker expression in transitioning formative state pluripotency cells, relative to both naïve and primed state cells. Currently, there are few effective methods for discriminating the formative state from naïve or primed pluripotency, and with the advent of a stable formative cell line (Kinoshita et al. 2020), the study of exiting the naïve state and traversing through the phased progression model of cell specification is better enabled. Delineation of naïve, formative, and primed states is important to the field of pluripotency as recent advances allow researchers to stably culture formative stem cells for the study of specification and development. Until recently, primed pluripotency was the only stable culture of human PSCs, as the naïve state is a transient stage outside of mouse and rat models (Ying and Smith 2017).

1.1.1. Non-canonical roles of metabolism.

Increasing evidence promotes metabolism as having a critical role in the establishment, maintenance, and differentiation of pluripotent stem cells. Elevated reactive oxygen species (ROS) associated with OXPHOS has been implicated not only with apoptosis, but also in cell differentiation acting as second messengers and influencing the epigenetic landscape (Sarsour et al. 2009; Maryanovich and Gross 2013). When there is a demand for cells to proliferate, the proliferative state has a metabolic precursor response, whereby pyruvate shunting to the mitochondria is decreased. In addition, there is an elevated glycolytic response resulting in an upregulation of anabolic gene expression and biosynthetic pathways. This trend is profiled by a simultaneous increase in aerobic glycolysis, and decrease in OXPHOS; such phenotype is evident in both tumor and embryonic development (Vander Heiden, Cantley, and Thompson 2009). When reprogramming from the primed-to-naïve pluripotent state through overactivation of LIF, the reverse metabolic shift is witnessed, a transition from aerobic glycolysis to increased OXPHOS and metabolic bivalency (Carbognin et al. 2016). As OXPHOS is dependent on mitochondrial respiration, this shift also demonstrates mitochondrial reprogramming. Overactivation of LIF promotes the gene *Stat3*, which is critical in self-renewal, can bind to the mitochondrial genome and promotes the naïve phenotype and reversion of primed pluripotency (Carbognin et al. 2016). Elevated Stat3 also promotes naïve associated genes, increases stem cell proliferation, and both OXPHOS and mitochondrial gene transcription (Carbognin et al. 2016). My investigation sheds light on the role of metabolism and pyruvate shuttling during early development and enhances knowledge of

cell conversion, this may advance the ability to effectively model disease, and eventually apply cell replacement therapies through enhanced cell differentiation.

Traditionally, human induced pluripotent stem cells (hiPSCs) reflect metabolic trends of primed PSCs, exhibiting increased glycolytic flux and decreased OXPHOS. Relative to their somatic cell origins, iPSCs are proliferative, requiring a greater amount of energy, yet have a substantial decrease in OXPHOS activity. Indeed, hiPSCs exhibit aerobic glycolytic metabolism like primed cells, showing distinct similarities to cancer cell metabolism and structural differences within the mitochondria (Jasanoff 1992; Ishida et al. 2020). Epigenetic changes are partially responsible for these metabolic trends. One alternate route for this glycolytic flux is contribution towards the pentose phosphate pathway (PPP), which is implicated in having an a key role in energy flux in iPSCs (Prigione et al. 2015). HIF-1α and HIF-2β are required during the initial stages of reprogramming and counter intuitively, HIF-2β, if stabilized, can hinder reprogramming efficiency. During early reprogramming of iPSCs from somatic cells, there is a sudden and unexpected burst of OXPHOS, this event is referred to as OXPHOS burst. This sudden burst is required for reprogramming, despite the end iPSC metabolic fate being preferentially glycolytic. Induction of the OXPHOS burst event upregulates estrogen-related nuclear receptors and PGC-1α/β (co-factors). Recent evidence suggests that the OXPHOS burst is necessary to cause HIF-1α activation by increasing the activity of NRF2 promoting a switch in metabolism from being OXPHOS to glycolytic (Hawkins et al. 2016).

1.1.2. Pyruvate kinase muscle isoforms.

Mammals express four tissue specific pyruvate kinase (PK) isozymes: M1, M2, L, and R, each with unique properties and tissue expression to meet specific metabolic demands (K. Yamada and Noguchi 1999). PK-Liver and Red Blood (LR) gene expresses L and R in a tissue-promotor specific manner. L is present in the kidneys and liver tissue, whereas R in red blood cells (W. Yang and Lu 2015). PKM1/2 is the enzyme responsible for catalyzing the final and rate limiting step of glycolysis, the enzyme plays a role in directing the fate of pyruvate towards lactate or acetyl CoA for glycolysis and OXPHOS (W. Yang and Lu 2015). This step involves the catalysis of phosphate from phosphoenolpyruvate (PEP) to ADP producing the second ATP of glycolysis and pyruvate.

PKM1/2 are alternatively spliced isoforms from the PKM gene (Figure 1.2) (Wong, De Melo, and Tang 2013). Heterogeneous nuclear ribonucleoproteins A1/A2 and polypyrimidine-tract binding protein work to splice PKM1 through the exclusion of exon 9 and inclusion of exon 10, whereas PKM2 is spliced to include exon 10 and exclude exon 9 (K. Yamada and Noguchi 1999). PKM1 is expressed in most somatic tissues that have a high energy requirement. The overexpression or replacement of PKM2 in place of PKM1 restricts tumorigenesis and cancer progression (Anastasiou et al. 2012; Chaneton and Gottlieb 2012). However, PKM2 is the predominant pyruvate kinase isoform in cancer cells, but is also expressed in most somatic cells apart from liver, brain, and paradoxically muscle in adult tissues (W. Yang and Lu 2015; Christofk et al. 2008). PKM1/2 activity is regulated based on expression level, and both homotropic and

heterotropic allosteric interactions with fructose 1,6-bisphosphate (FBP) and PEP respectively, allosteric interactions are not evident with M1 isozyme, which maintains an active homotetrameric conformation (Boles et al. 1997; Imamura and Tanaka 1982). When FBP levels decrease, PKM2 homotetramers dissociate into homodimers, these conformations are interconvertible (Wong, De Melo, and Tang 2013). The PKM2 dimer is associated with aerobic glycolysis and anabolism, this isoform is also formed in the presence of Tyr phosphorylated peptides regardless of FBP levels. In turn, this causes phosphorylation on Y105 which prevents FBP binding, a key trait of Warburg metabolism (the Warburg Effect), where even in the presence of oxygen, cells are preferentially glycolytic (Gupta and Bamezai 2010). The Warburg Effect is the metabolic preference for glycolysis, and it is typical of most cancers (O. Warburg. 1924). Despite appearing to be a poor method of generating maximal ATP levels, most cancer cells do not reply on mitochondrial respiration, but rather employ aerobic glycolysis, despite apparent oxygen availability. This metabolic preference was first characterized in 1924, yet we are only now starting to understand the mechanisms and rationale behind this counterintuitive process. Mouse and human primed pluripotent cells are similar to specific cancer cells regarding their metabolic preferences as both are preferentially glycolytic despite oxygen being available (Zhou et al. 2012). Given this similarity, the results of this thesis document PKM2 residing within the nucleus of these highly proliferative stem cells, this is a key trait of the Warburg Effect. PKM2 is a target for many cancer treatments, and the results of my study demonstrate that PKM1 and PKM2 isoforms have novel expression patterns between pluripotent states. As human ESCs (hESCs) and most cancer cell lines exhibit the Warburg Effect, studying the unknown

mechanisms of PKM2 interactions within PSCs is a critical area of focus (X. Liu et al. 2019; Shyh-Chang, Daley, and Cantley 2013).

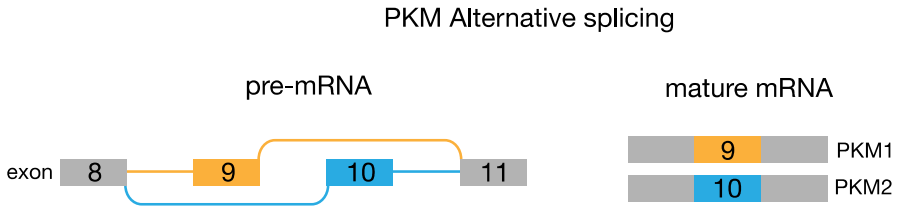

Figure 1.2. Alternative splicing schematic of pyruvate kinase muscle isoforms 1/2.

Pyruvate kinase muscle isoforms 1 and 2 (PKM1/2) is alternatively spliced from the PKM gene. Mature PKM1 mRNA excludes exon 10, and conversely, mature PKM2 mRNA excludes exon 9. Image was created by Joshua Dierolf and Martin Krzywinski.

PKM2 interacts with: OCT4, a marker of pluripotency in ESCs, HIF-1α master regulator of metabolism, STAT3, and β-CATENIN (W. Yang and Lu 2015). Interestingly, the interaction of OCT4 increases during a transition from the dimeric and phosphorylated conformation associated with the Warburg Effect (Morfouace et al. 2014). It is currently assumed that the interaction of PKM2 and OCT4 has a role in mitosis and tumor nourishment, however, this mechanism has yet to be delineated (Hitoshi Niwa, Miyazaki, and Smith 2000). Dimeric PKM2 also associates with HIF-1α, this interaction promotes transcriptional coactivation of HIF-1α through positive feedback regulation, additionally, this promotes the Warburg Effect in at least two ways. Firstly, when PKM2 is hydroxylated by and bound to prolyl hydroxylase 3, there is an interaction with HIF-1 α that results in transactivation of the glycolytic enzymes lactate dehydrogenase A (LDHA) and pyruvate dehydrogenase kinase 1 (PDK1), transactivation of vascular endothelial growth factor can also occur. PKM2 also transactivates HIF1α target genes such as GLUT1, LDHA and PDK1 (which inhibits OXPHOS via pyruvate shunting) by altering interactions at hypoxia response elements (HRE), and these alterations include improved recruitment of p300 and enhanced binding of HIF-1α (Luo et al. 2011). HIF-1 works to regulate PKM expression for both isozymes (M1/M2), with only dimeric PKM2 interacting directly with HIF-1α by enhancing HIF1α binding and enlisting p300 at HREs, this in turn transactivates key glycolytic enzymes required for the Warburg Effect. Additionally, HIF-1α transcriptionally regulates OCT4, further implicating PKM2 as an important gene in proliferation and aerobic glycolysis (Prigione et al. 2015). Within the nucleus, dimeric PKM2 can operate as a protein kinase through phosphorylation of STAT3 (Tyr705), thus enhancing the transcriptional activity of STAT3, and subsequently

activating MEK5 and histone H3 (Thr11) (Gao et al. 2012). PKM2 can translocate to the nucleus through epidermal growth factor induction by transactivation of β-CATENIN through the phosphorylation of tyrosine Y333 (Figure 1.3). This interaction contributes to c-MYC and cyclin D transcription. However, an interaction with Wnt and PKM2 is not evident (Weiwei Yang et al. 2011). Interactions with c-MYC require more research, but interestingly a depletion of c-MYC in naïve cells will force mESC into a 'diapause' like state of quiescence (Scognamiglio et al. 2016). PKM2 can also be methylated, for example, methylation by coactivator-associated arginine methyltransferase 1 (CARM1). Protein-protein interaction of PKM2 and CARM1 along with methylation of PKM2's C-domain also promotes the Warburg effect and activates a transition from oxidative phosphorylation to aerobic glycolysis (F. Liu et al. 2017). Downregulating intragenic DNA methylation can influence pre-splicing of alternative splice events for PKM1/2. Importantly, CARM1 does not methylate PKM1, however, CARM1 and PKM1 proteins do interact, and CARM1 primarily methylates dimeric PKM2 over the tetrameric conformation. Currently, epigenetic regulation of PKM2 in PSCs has not been thoroughly investigated (Singh et al. 2017). Pyruvate destined for an OXPHOS is irreversibly decarboxylated into acetyl CoA within the mitochondria by pyruvate dehydrogenase complex (PDC) for processing within the tricarboxylic acid cycle. PKM2, PDC-(E2 subunit), and histone acetyltransferase p300 form a complex with the CYP1A1 enhancer of arylhydrocarbon receptor. Through this complexing, nuclear PKM2 promotes cell proliferation through enhanced detoxification of detrimental endogenous metabolites and aids in acetyl CoA production (Matsuda et al. 2016). The mechanism of how transcriptional activation fully regulates these enzymes, and their function is still largely unknown. Relative to PKM2, the alternative isozyme PKM1 has been vastly

understudied, however, recent publications have determined PKM1 is involved in chemoresistance, and may have additional non-canonical roles (Fushida et al. 2018; Wei et al. 2017). Indeed, PKM1 has been recently documented binding with Hepatocyte Nuclear Factor 4∝ (HNF4∝), before translocating to the nucleus of hepatoma cells(Wei et al. 2017). This may suggest a potential non-canonical role for the traditional cytoplasmic metabolic enzyme. PKM1 has been found present in chemo-resistant cancerous cells and following knockdown increased cellular chemotherapy sensitivity (Taniguchi et al. 2016). There is a clinical need to study PKM1/2 modulation in metabolically active cells as PKM1/2 are heavily implicated in the transition of healthy cells to utilizing Warburg Effect over OXPHOS. As such PKM2, and now PKM1 is the target of several cancer related approaches (Wei et al. 2017; W. Yang and Lu 2015). As this transition is similar to the bivalent-to-glycolytic switch from naïve to primed pluripotency, there is a developmental importance in studying the influence of PKM1/2 modulation. Current strategies have included knocking in alleles of PKM1/2 (Konno, Ishii, et al. 2015), using siRNA (Goldberg and Sharp 2012) and shRNA (Qin et al. 2017) strategies, lentiviral overexpression (Qin et al. 2017), pharmacological approaches (Giannoni et al. 2015; Hasenoehrl et al. 2017; Wei et al. 2017) and miRNAs (Konno, Koseki, et al. 2015; Taniguchi et al. 2015).

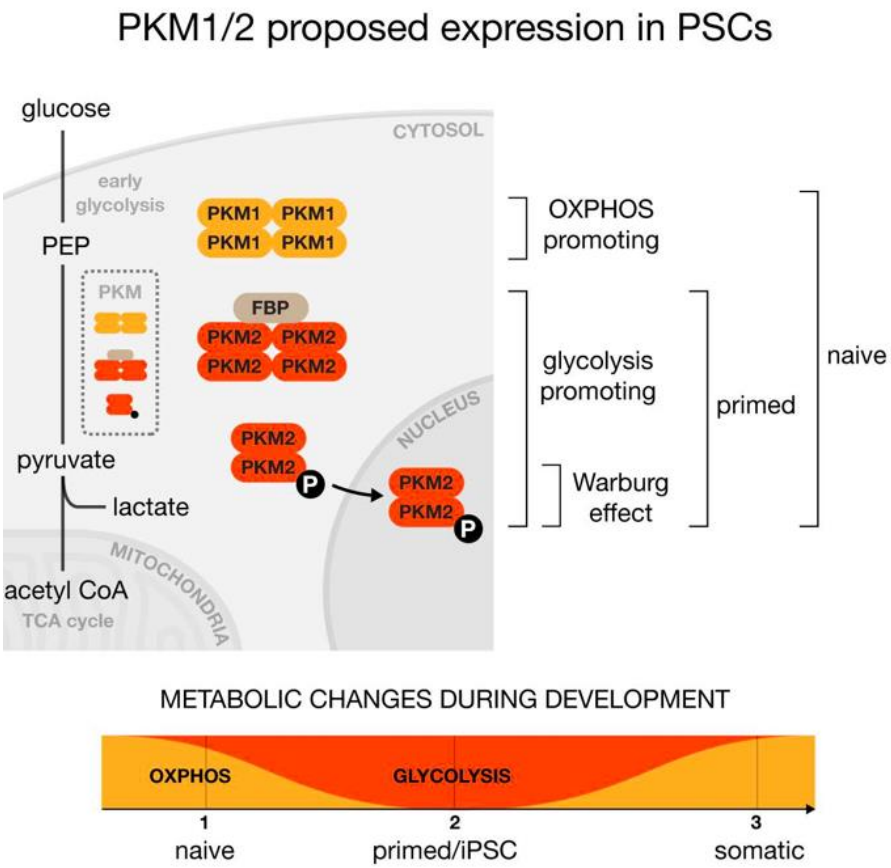

Figure 1.3. A proposed model of PKM1/2 isoforms in naïve and primed pluripotent stem cells.

Intracellular PKM1/2 exist as active tetramers, the PKM2 tetrameric conformation is destabilized following phosphorylation promoting a dimeric conformation. Dimeric PKM2 is translocated to nuclei and promotes the Warburg Effect. As primed cells have been described as preferentially aerobic glycolytic in metabolic preference, nuclear PKM2 by dimeric PKM2 translocation is proposed. As naïve cells are metabolically bivalent, a mix of OXPHOS and glycolytic promoting conformations is presumed. Image created by Joshua Dierolf and Martin Krzywinski in Illustrator.

My thesis is focused on providing an increased understanding of the mechanisms controlling early cell differentiation and enhanced cell reprogramming through modulation of metabolic processes. This is an area of interest in stem cell biology as other groups have successfully and are continually attempting to achieve increased reprogramming efficiencies in iPSCs by promoting the characterized iPSC metabolism of elevated glycolysis and decreased OXPHOS. A well-established example is the upregulation of HIF activity to promote glycolysis, which interestingly also increases PKM2 activity. Likewise, pyruvate dehydrogenase kinase (PDHK) activity inhibits pyruvate dehydrogenase (PDH), stunting for OXPHOS to occur and even the addition of FBP treatment promotes a metabolic switch to glycolysis and increased reprogramming efficiency (Folmes et al. 2011; Zhu et al. 2010). By promoting OXPHOS instead, cellular reprogramming efficiency of somatic cells can alternatively be decreased. While cancer cells and primed pluripotent stem cells share a preference for aerobic glycolysis, there is still an apparent role for OXPHOS in PSCs, this is an area in need of greater research and PKM1/2 may have a vital role in this capacity. Recent studies have no longer alluded to metabolism as influencing pluripotency, but have claimed that metabolism actively promotes pluripotency (Ryall et al. 2015). When considering the metabolic preferences of naïve and primed pluripotent states, and the switch from aerobic to anaerobic metabolism, it is important to consider their *in vivo* counterparts, the cells of the pre- and post- implantation embryo. These metabolic preferences are thought to be intrinsically programmed into these states due to the limited oxygen availability of their *in vivo* origins within the reproductive tract (Carbognin et al. 2016). Further study into the metabolic preferences of the formative state, and the formative interval of embryo development is needed. If the phased progression model of pluripotent development is correct, and the

notion of intrinsic programming based on *in vivo* origins holds true, then it would be expected that the shift towards aerobic glycolysis is established during the formative interval and in the formative state.

1.2.0. Rationale.

PKM1/2 have been independently implicated in naïve and primed cells, yet their role in the developmental transition between pluripotent states has yet to be fully elucidated (Konno, Ishii, et al. 2015; Qin et al. 2017). Knocking in an allele of either the *Pkm1* or *Pkm2* gene indicates that Pkm2, but not Pkm1 has a role in maintaining the naïve state following a differentiation stimuli as determined by a transcriptional assay in mESCs (Konno, Ishii, et al. 2015). Overexpression of either PKM1 or PKM2 increases pluripotent transcript abundance in naïve mESCs. Additionally, it has been demonstrated that PKM2 can translocate to the nuclei of primed hESCs, when silenced, cells do not exhibit altered glucose metabolism suggesting a non-canonical role for PKM2 (Christensen, Calder, and Houghton 2015). PKM2, and recently PKM1 have been implicated to have other potential non-canonical roles, outside of metabolic enzymatic activities, such as promoting aerobic glycolytic activity and proliferation typical of cancerous cells (Hamabe et al. 2014; Wei et al. 2018; Palsson-McDermott et al. 2015; Stone et al. 2018; Weiwei Yang and Lu 2013; Growth 2018; Wei et al. 2017; Fushida et al. 2018). With the advent of new flow cytometric approaches and improved characterization of the formative state, this thesis seeks to delineate expression, localization, and influence of PKM1/2 on the naïve, formative, and primed pluripotent states of murine embryonic stem cells.

1.3.0. Governing Hypothesis.

Pyruvate kinase muscle isoform 1 and 2 expression are differentially expressed in naïve, formative, and primed pluripotent states; and enhance the progression of pluripotent state development in murine embryonic stem cells.

1.4.0. Thesis Objectives.

This research investigates the role of PKM1/2 in the maintenance and differentiation of naïve, formative, primed-like, and primed pluripotent states through the following objectives:

1. Optimize quantitative confocal colocalization of fluorescently tagged antisera against PKM1 and PKM2 to subcellular regions of naïve, formative, and primed mESCs
2. Characterize protein and transcript abundance along with subcellular localization of PKM1/2 isoforms in naïve, formative, and primed mPSCs.
3. Optimise the application of flow cytometry using SSEA and CD24 cell surface markers to delineate naïve, formative and primed pluripotent states.
4. Determine the influence of modulating PKM1/2 in naïve mESCs and primed mEpiSCs and transitioning towards formative mEpiLCs and primed-like mEpiLCs.

1.5.0. References:

Anastasiou, Dimitrios, Yimin Yu, William J. Israelsen, Jian Kang Jiang, Matthew B. Boxer, Bum Soo Hong, Wolfram Tempel, et al. 2012. "Pyruvate Kinase M2 Activators Promote Tetramer Formation and Suppress Tumorigenesis." *Nature Chemical Biology* 8 (10): 839–47. https://doi.org/10.1038/nchembio.1060.

Aziz, M, and H Alexandre. 1991. "The Origin of the Nascent Blastocoele in Preimplantation Mouse Embryos Ultrastructural Cytochemistry and Effect of Chloroquine." *Roux's Archives of Developmental Biology* 200 (2): 77–85. https://doi.org/10.1007/BF00637187.

Boles, Eckhard, Frank Schulte, Thomas Miosga, Kerstin Freidel, Elke Schlüter, Friedrich K. Zimmermann, Cornelis P. Hollenberg, and Jürgen J. Heinisch. 1997. "Characterization of a Glucose-Repressed Pyruvate Kinase (Pyk2p) in Saccharomyces Cerevisiae That Is Catalytically Insensitive to Fructose-1,6-Bisphosphate." *Journal of Bacteriology* 179 (9): 2987–93. https://doi.org/10.1128/jb.179.9.2987-2993.1997.

Brons, I Gabrielle M, Lucy E Smithers, Matthew W B Trotter, Peter Rugg-Gunn, Bowen Sun, Susana M Chuva de Sousa Lopes, Sarah K Howlett, et al. 2007. "Derivation of Pluripotent Epiblast Stem Cells from Mammalian Embryos." *Nature* 448 (June): 191. https://doi.org/10.1038/nature05950.

Burdon, T, C Stracey, I Chambers, J Nichols, and A Smith. 1999. "Suppression of SHP-2 and ERK Signalling Promotes Self-Renewal of Mouse Embryonic Stem Cells." *Developmental Biology* 210 (1): 30–43. https://doi.org/10.1006/dbio.1999.9265.

Carbognin, Elena, Riccardo M Betto, Maria E Soriano, Austin G Smith, and Graziano Martello. 2016. "Stat3 Promotes Mitochondrial Transcription and Oxidative Respiration during Maintenance and Induction of Naive Pluripotency." *The EMBO Journal* 35 (6): 618–34. https://doi.org/https://doi.org/10.15252/embj.201592629.

Chaneton, Barbara, and Eyal Gottlieb. 2012. "Rocking Cell Metabolism: Revised Functions of the Key Glycolytic Regulator PKM2 in Cancer." *Trends in Biochemical Sciences* 37 (8): 309–16. https://doi.org/10.1016/j.tibs.2012.04.003.

Christensen, David R, Philip C Calder, and Franchesca D Houghton. 2015. "GLUT3 and PKM2 Regulate OCT4 Expression and Support the Hypoxic Culture of Human Embryonic Stem Cells." *Scientific Reports* 5 (December): 17500. https://doi.org/10.1038/srep17500.

Christofk, Heather R., Matthew G. Vander Heiden, Marian H. Harris, Arvind Ramanathan, Robert E. Gerszten, Ru Wei, Mark D. Fleming, Stuart L. Schreiber, and Lewis C. Cantley. 2008. "The M2 Splice Isoform of Pyruvate Kinase Is Important for Cancer Metabolism and Tumour Growth." *Nature* 452 (7184): 230–33. https://doi.org/10.1038/nature06734.

Folmes, Clifford D L, Timothy J. Nelson, Almudena Martinez-Fernandez, D. Kent Arrell, Jelena Zlatkovic Lindor, Petras P. Dzeja, Yasuhiro Ikeda, Carmen Perez-Terzic, and Andre Terzic. 2011. "Somatic Oxidative Bioenergetics Transitions into Pluripotency-Dependent Glycolysis to Facilitate Nuclear Reprogramming." *Cell Metabolism* 14 (2): 264–71. https://doi.org/10.1016/j.cmet.2011.06.011.

Fushida, Sachio, Katsunobu Oyama, Tetsuo Ohta, Itasu Ninomiya, Shinichi Harada, Jun Kinoshita, Tomoya Tsukada, Tomoharu Miyashita, and Mitsuyoshi Okazaki. 2018. "The Effect of HIF-1α and PKM1 Expression on Acquisition of Chemoresistance."

Cancer Management and Research Volume 10: 1865–74. https://doi.org/10.2147/cmar.s166136.

Gao, Xueliang, Haizhen Wang, Jenny J. Yang, Xiaowei Liu, and Zhi Ren Liu. 2012. "Pyruvate Kinase M2 Regulates Gene Transcription by Acting as a Protein Kinase." *Molecular Cell* 45 (5): 598–609. https://doi.org/10.1016/j.molcel.2012.01.001.

Giannoni, Elisa, Maria Letizia Taddei, Andrea Morandi, Giuseppina Comito, Maura Calvani, Francesca Bianchini, Barbara Richichi, et al. 2015. "Targeting Stromal-Induced Pyruvate Kinase M2 Nuclear Translocation Impairs Oxphos and Prostate Cancer Metastatic Spread." *Oncotarget* 6 (27): 24061–74. https://doi.org/10.18632/oncotarget.4448.

Goldberg, Michael S., and Phillip A. Sharp. 2012. "Pyruvate Kinase M2-Specific SiRNA Induces Apoptosis and Tumor Regression." *The Journal of Experimental Medicine* 209 (2): 217–24. https://doi.org/10.1084/jem.20111487.

Growth, Cell-autonomous Tumor Cell. 2018. "PKM1 Confers Metabolic Advantages and Promotes Article PKM1 Confers Metabolic Advantages and Promotes Cell-Autonomous." *Cancer Cell* 33 (3): 355-367.e7. https://doi.org/10.1016/j.ccell.2018.02.004.

Gupta, Vibhor, and Rameshwar N K Bamezai. 2010. "Human Pyruvate Kinase M2: A Multifunctional Protein." *Protein Science* 19 (11): 2031–44. https://doi.org/10.1002/pro.505.

Hamabe, Atsushi, Masamitsu Konno, Nobuhiro Tanuma, Hiroshi Shima, Kenta Tsunekuni, Koichi Kawamoto, Naohiro Nishida, et al. 2014. "Role of Pyruvate Kinase M2 in Transcriptional Regulation Leading to Epithelial–Mesenchymal Transition." *Proceedings of the National Academy of Sciences* 111 (43): 15526 LP – 15531. https://doi.org/10.1073/pnas.1407717111.

Hasenoehrl, Carina, Gert Schwach, Nassim Ghaffari-Tabrizi-Wizsy, Robert Fuchs, Nadine Kretschmer, Rudolf Bauer, and Roswitha Pfragner. 2017. "Anti-Tumor Effects of Shikonin Derivatives on Human Medullary Thyroid Carcinoma Cells." *Endocrine Connections* 6 (2): 53–62. https://doi.org/10.1530/EC-16-0105.

Hawkins, Kate E., Shona Joy, Juliette M.K.M. Delhove, Vassilios N. Kotiadis, Emilio Fernandez, Lorna M. Fitzpatrick, James R. Whiteford, et al. 2016. "NRF2 Orchestrates the Metabolic Shift during Induced Pluripotent Stem Cell Reprogramming." *Cell Reports* 14 (8): 1883–91. https://doi.org/10.1016/j.celrep.2016.02.003.

Hayashi, Katsuhiko, Hiroshi Ohta, Kazuki Kurimoto, Shinya Aramaki, and Mitinori Saitou. 2011. "Reconstitution of the Mouse Germ Cell Specification Pathway in Culture by Pluripotent Stem Cells." *Cell* 146 (4): 519–32. https://doi.org/10.1016/j.cell.2011.06.052.

Heard, Edith. 2004. "Recent Advances in X-Chromosome Inactivation." *Current Opinion in Cell Biology* 16 (3): 247–55. https://doi.org/10.1016/j.ceb.2004.03.005.

Heiden, Matthew Vander, Lewis Cantley, and Craig Thompson. 2009. "Understanding the Warburg Effect: The Metabolic Requiremetns of Cell Proliferation." *Science* 324 (5930): 1029–33. https://doi.org/10.1126/science.1160809.Understanding.

Imamura, Kuchi, and Takehiko Tanaka. 1982. "Pyruvate Kinase Isozymes from Rat." *Methods in Enzymology* 90 (C): 150–65. https://doi.org/10.1016/S0076-6879(82)90121-5.

Ishida, Tomoaki, Shu Nakao, Tomoe Ueyama, Yukihiro Harada, and Teruhisa

Kawamura. 2020. “Metabolic Remodeling during Somatic Cell Reprogramming to Induced Pluripotent Stem Cells: Involvement of Hypoxia-Inducible Factor 1.” *Inflammation and Regeneration* 40 (1): 8. https://doi.org/10.1186/s41232-020-00117-8.

Jasanoff, Sheila. 1992. “Science, Politics, and the Renegotiation of Expertise at EPA.” *Osiris* 740 (3): 194–217. https://doi.org/10.1086/677353.Stem.

Kinoshita, Masaki, Michael Barber, William Mansfield, Yingzhi Cui, Daniel Spindlow, Giuliano Giuseppe Stirparo, Sabine Dietmann, Jennifer Nichols, and Austin Smith. 2020. “Capture of Mouse and Human Stem Cells with Features of Formative Pluripotency.” *Cell Stem Cell*. https://doi.org/https://doi.org/10.1016/j.stem.2020.11.005.

Klompstra, Diana, Dorian C Anderson, Justin Y Yeh, Yuliya Zilberman, and Jeremy Nance. 2015. “An Instructive Role for C. Elegans E-Cadherin in Translating Cell Contact Cues into Cortical Polarity.” *Nature Cell Biology* 17 (6): 726–35. https://doi.org/10.1038/ncb3168.

Konno, Masamitsu, Hideshi Ishii, Jun Koseki, Nobuhiro Tanuma, Naohiro Nishida, Koichi Kawamoto, Tatsunori Nishimura, et al. 2015. “Pyruvate Kinase M2, but Not M1, Allele Maintains Immature Metabolic States of Murine Embryonic Stem Cells.” *Regenerative Therapy* 1: 63–71. https://doi.org/10.1016/j.reth.2015.01.001.

Konno, Masamitsu, Jun Koseki, Koichi Kawamoto, Naohiro Nishida, Hidetoshi Matsui, Dyah Laksmi Dewi, Miyuki Ozaki, et al. 2015. “Embryonic MicroRNA-369 Controls Metabolic Splicing Factors and Urges Cellular Reprograming.” *PLoS ONE* 10 (7): e0132789. https://doi.org/10.1371/journal.pone.0132789.

Liu, Fabao, Fengfei Ma, Yuyuan Wang, Ling Hao, Hao Zeng, Chenxi Jia, Yidan Wang, et al. 2017. “PKM2 Methylation by CARM1 Activates Aerobic Glycolysis to Promote Tumorigenesis.” *Nature Cell Biology* 19 (11): 1358–70. https://doi.org/10.1038/ncb3630.

Liu, Xin, Meiyan Wang, Tao Jiang, Jingjin He, Xuemei Fu, and Yang Xu. 2019. “IDO1 Maintains Pluripotency of Primed Human Embryonic Stem Cells by Promoting Glycolysis.” *Stem Cells (Dayton, Ohio)* 37 (9): 1158–65. https://doi.org/10.1002/stem.3044.

Luo, Weibo, Hongxia Hu, Ryan Chang, Jun Zhong, Matthew Knabel, Robert O’Meally, Robert N. Cole, Akhilesh Pandey, and Gregg L. Semenza. 2011. “Pyruvate Kinase M2 Is a PHD3-Stimulated Coactivator for Hypoxia-Inducible Factor 1.” *Cell* 145 (5): 732–44. https://doi.org/10.1016/j.cell.2011.03.054.

Maître, Jean-Léon, Ritsuya Niwayama, Hervé Turlier, François Nédélec, and Takashi Hiiragi. 2015. “Pulsatile Cell-Autonomous Contractility Drives Compaction in the Mouse Embryo.” *Nature Cell Biology* 17 (7): 849–55. https://doi.org/10.1038/ncb3185.

Marikawa, Yusuke, and Vernadeth B Alarcón. 2009. “Establishment of Trophectoderm and Inner Cell Mass Lineages in the Mouse Embryo.” *Molecular Reproduction and Development* 76 (11): 1019–32. https://doi.org/10.1002/mrd.21057.

Maryanovich, Maria, and Atan Gross. 2013. “A ROS Rheostat for Cell Fate Regulation.” *Trends in Cell Biology* 23 (3): 129–34. https://doi.org/10.1016/j.tcb.2012.09.007.

Matsuda, Shun, Jun Adachi, Masaru Ihara, Nobuhiro Tanuma, Hiroshi Shima, Akira Kakizuka, Masae Ikura, Tsuyoshi Ikura, and Tomonari Matsuda. 2016. “Nuclear Pyruvate Kinase M2 Complex Serves as a Transcriptional Coactivator of

Arylhydrocarbon Receptor." *Nucleic Acids Research* 44 (2): 636–47. https://doi.org/10.1093/nar/gkv967.

Menon, Malini, Richard Elliott, Leandra Bowers, Nicolae Balan, Rumana Rafiq, Sara Costa-Cabral, Felix Munkonge, et al. 2019. "A Novel Tankyrase Inhibitor, MSC2504877, Enhances the Effects of Clinical CDK4/6 Inhibitors." *Scientific Reports* 9 (1): 201. https://doi.org/10.1038/s41598-018-36447-4.

Morfouace, M., L. Lalier, L. Oliver, M. Cheray, C. Pecqueur, P. F. Cartron, and F. M. Vallette. 2014. "Control of Glioma Cell Death and Differentiation by PKM2-Oct4 Interaction." *Cell Death and Disease* 5 (1): e1036-8. https://doi.org/10.1038/cddis.2013.561.

Morgani, Sophie, Jennifer Nichols, and Anna-Katerina Hadjantonakis. 2017. "The Many Faces of Pluripotency: In Vitro Adaptations of a Continuum of in Vivo States." *BMC Developmental Biology* 17 (1): 7. https://doi.org/10.1186/s12861-017-0150-4.

Nichols, Jennifer, and Austin Smith. 2009. "Naive and Primed Pluripotent States." *Cell Stem Cell* 4 (6): 487–92. https://doi.org/10.1016/j.stem.2009.05.015.

Niwa, H, T Burdon, I Chambers, and A Smith. 1998. "Self-Renewal of Pluripotent Embryonic Stem Cells Is Mediated via Activation of STAT3." *Genes & Development* 12 (13): 2048–60. https://doi.org/10.1101/gad.12.13.2048.

Niwa, Hitoshi, Jun Ichi Miyazaki, and Austin G. Smith. 2000. "Quantitative Expression of Oct-3/4 Defines Differentiation, Dedifferentiation or Self-Renewal of ES Cells." *Nature Genetics* 24 (4): 372–76. https://doi.org/10.1038/74199.

O. Warburg., K. Posener. 1924. "Negelein: Ueber Den Stoffwechsel Der Tumoren." *Biochemische Zeitschrift* Vol. 152 (1): 319–44.

Palsson-McDermott, Eva M, Anne M Curtis, Gautam Goel, Mario A R Lauterbach, Frederick J Sheedy, Laura E Gleeson, Mirjam W M van den Bosch, et al. 2015. "Pyruvate Kinase M2 Regulates Hif-1α Activity and IL-1β Induction and Is a Critical Determinant of the Warburg Effect in LPS-Activated Macrophages." *Cell Metabolism* 21 (1): 65–80. https://doi.org/10.1016/j.cmet.2014.12.005.

Prigione, Alessandro, María Victoria Ruiz-Pérez, Raul Bukowiecki, and James Adjaye. 2015. "Metabolic Restructuring and Cell Fate Conversion." *Cellular and Molecular Life Sciences* 72 (9): 1759–77. https://doi.org/10.1007/s00018-015-1834-1.

Qin, Shengtang, Danli Yang, Kang Chen, Haolan Li, Liqiang Zhang, Yuan Li, Rongrong Le, Xiaojie Li, Shaorong Gao, and Lan Kang. 2017. "Pkm2 Can Enhance Pluripotency in ESCs and Promote Somatic Cell Reprogramming to IPSCs." *Oncotarget* 8 (48): 84276. https://doi.org/10.18632/ONCOTARGET.20685.

Ryall, James G., Tim Cliff, Stephen Dalton, and Vittorio Sartorelli. 2015. "Metabolic Reprogramming of Stem Cell Epigenetics." *Cell Stem Cell* 17 (6): 651–62. https://doi.org/10.1016/j.stem.2015.11.012.

Sarsour, Ehab H., Maneesh G. Kumar, Leena Chaudhuri, Amanda L. Kalen, and Prabhat C. Goswami. 2009. "Redox Control of the Cell Cycle in Health and Disease." *Antioxidants & Redox Signaling* 11 (12): 2985–3011. https://doi.org/10.1089/ars.2009.2513.

Scognamiglio, Roberta, Nina Cabezas-Wallscheid, Marc Christian Thier, Sandro Altamura, Alejandro Reyes, Áine M. Prendergast, Daniel Baumgärtner, et al. 2016. "Myc Depletion Induces a Pluripotent Dormant State Mimicking Diapause." *Cell* 164 (4): 668–80. https://doi.org/10.1016/j.cell.2015.12.033.

Shakiba, Nika, Carl A. White, Yonatan Y. Lipsitz, Ayako Yachie-Kinoshita, Peter D.

Tonge, Samer M.I. Hussein, Mira C. Puri, et al. 2015. “CD24 Tracks Divergent Pluripotent States in Mouse and Human Cells.” *Nature Communications* 6: 7329. https://doi.org/10.1038/ncomms8329.

Shyh-Chang, N., G. Q. Daley, and L. C. Cantley. 2013. “Stem Cell Metabolism in Tissue Development and Aging.” *Development* 140 (12): 2535–47. https://doi.org/10.1242/dev.091777.

Singh, Smriti, Sathiya Pandi Narayanan, Kajal Biswas, Amit Gupta, Neha Ahuja, Sandhya Yadav, Rajendra Kumar Panday, Atul Samaiya, Shyam K. Sharan, and Sanjeev Shukla. 2017. “Intragenic DNA Methylation and BORIS-Mediated Cancer-Specific Splicing Contribute to the Warburg Effect.” *Proceedings of the National Academy of Sciences*, 201708447. https://doi.org/10.1073/pnas.1708447114.

Smith, A G, J K Heath, D D Donaldson, G G Wong, J Moreau, M Stahl, and D Rogers. 1988. “Inhibition of Pluripotential Embryonic Stem Cell Differentiation by Purified Polypeptides.” *Nature* 336 (6200): 688–90. https://doi.org/10.1038/336688a0.

Smith, Austin. 2017. “Formative Pluripotency: The Executive Phase in a Developmental Continuum.” *Development* 144 (3): 365–73. https://doi.org/10.1242/dev.142679.

Stephenson, Robert Odell, Yojiro Yamanaka, and Janet Rossant. 2010. “Disorganized Epithelial Polarity and Excess Trophectoderm Cell Fate in Preimplantation Embryos Lacking E-Cadherin.” *Development* 137 (20): 3383 LP – 3391. https://doi.org/10.1242/dev.050195.

Stone, Oliver A, Mohamed El-Brolosy, Kerstin Wilhelm, Xiaojing Liu, Ana M Romão, Elisabetta Grillo, Jason K H Lai, et al. 2018. “Loss of Pyruvate Kinase M2 Limits Growth and Triggers Innate Immune Signaling in Endothelial Cells.” *Nature Communications* 9 (1): 4077. https://doi.org/10.1038/s41467-018-06406-8.

Taniguchi, Kohei, Miku Sakai, Nobuhiko Sugito, Yuki Kuranaga, Minami Kumazaki, Haruka Shinohara, Hiroshi Ueda, et al. 2016. “PKM1 Is Involved in Resistance to Anti-Cancer Drugs.” *Biochemical and Biophysical Research Communications* 473 (1): 174–80. https://doi.org/https://doi.org/10.1016/j.bbrc.2016.03.074.

Taniguchi, Kohei, Nobuhiko Sugito, Minami Kumazaki, Haruka Shinohara, Nami Yamada, Yoshihito Nakagawa, Yuko Ito, et al. 2015. “MicroRNA-124 Inhibits Cancer Cell Growth through PTB1/PKM1/PKM2 Feedback Cascade in Colorectal Cancer.” *Cancer Letters* 363 (1): 17–27. https://doi.org/10.1016/J.CANLET.2015.03.026.

Tesar, Paul J., Josh G. Chenoweth, Frances A. Brook, Timothy J. Davies, Edward P. Evans, David L. Mack, Richard L. Gardner, and Ronald D.G. McKay. 2007. “New Cell Lines from Mouse Epiblast Share Defining Features with Human Embryonic Stem Cells.” *Nature* 448 (7150): 196–99. https://doi.org/10.1038/nature05972.

Wei, Libin, Yuanyuan Dai, Yuxin Zhou, Zihao He, Jingyue Yao, Li Zhao, Qinglong Qiqiang Guo, et al. 2018. “Pyruvate Kinase M2 Is a PHD3-Stimulated Coactivator for Hypoxia-Inducible Factor 1.” *Development* 8 (1): 1–16. https://doi.org/10.1016/j.cell.2011.03.054.

Wei, Libin, Yuanyuan Dai, Yuxin Zhou, Zihao He, Jingyue Yao, Li Zhao, Qinglong Guo, and Lin Yang. 2017. “Oroxylin A Activates PKM1/HNF4 Alpha to Induce Hepatoma Differentiation and Block Cancer Progression.” *Cell Death & Disease* 8 (7): e2944. https://doi.org/10.1038/cddis.2017.335.

Williams, R Lindsay, Douglas J Hilton, Shirley Pease, Tracy A Willson, Colin L Stewart, David P Gearing, Erwin F Wagner, Donald Metcalf, Nicos A Nicola, and Nicholas

M Gough. 1988. “Myeloid Leukaemia Inhibitory Factor Maintains the Developmental Potential of Embryonic Stem Cells.” *Nature* 336 (6200): 684–87. https://doi.org/10.1038/336684a0.

Wong, Nicholas, Jason De Melo, and Damu Tang. 2013. “PKM2, a Central Point of Regulation in Cancer Metabolism.” *International Journal of Cell Biology* 2013 (Figure 1). https://doi.org/10.1155/2013/242513.

Wray, Jason, Tüzer Kalkan, Sandra Gomez-Lopez, Dominik Eckardt, Andrew Cook, Rolf Kemler, and Austin Smith. 2011. “Inhibition of Glycogen Synthase Kinase-3 Alleviates Tcf3 Repression of the Pluripotency Network and Increases Embryonic Stem Cell Resistance to Differentiation.” *Nature Cell Biology* 13 (7): 838–45. https://doi.org/10.1038/ncb2267.

Yamada, K, and T Noguchi. 1999. “Regulation of Pyruvate Kinase Gene Expression.” *Biochem. J* 337: 1–11. https://doi.org/PMC1219928.

Yamada, Soichiro, and W James Nelson. 2007. “Localized Zones of Rho and Rac Activities Drive Initiation and Expansion of Epithelial Cell–Cell Adhesion .” *Journal of Cell Biology* 178 (3): 517–27. https://doi.org/10.1083/jcb.200701058.

Yang, W., and Z. Lu. 2015. “Pyruvate Kinase M2 at a Glance.” *Journal of Cell Science* 128 (9): 1655–60. https://doi.org/10.1242/jcs.166629.

Yang, Weiwei, and Zhimin Lu. 2013. “Nuclear PKM2 Regulates the Warburg Effect.” *Cell Cycle* 12 (19): 3154–58. https://doi.org/10.4161/cc.26182.

Yang, Weiwei, Yan Xia, Haitao Ji, Yanhua Zheng, Ji Liang, Wenhua Huang, Xiang Gao, Kenneth Aldape, and Zhimin Lu. 2011. “Nuclear PKM2 Regulates β-Catenin Transactivation upon EGFR Activation.” *Nature* 480 (7375): 118–22. https://doi.org/10.1038/nature10598.

Ying, Qi-Long, and Austin Smith. 2017. “The Art of Capturing Pluripotency: Creating the Right Culture.” *Stem Cell Reports* 8 (6): 1457–64. https://doi.org/https://doi.org/10.1016/j.stemcr.2017.05.020.

Zhou, Wenyu, Michael Choi, Daciana Margineantu, Lilyana Margaretha, Jennifer Hesson, Christopher Cavanaugh, C. Anthony Blau, et al. 2012. “HIF1α Induced Switch from Bivalent to Exclusively Glycolytic Metabolism during ESC-to-EpiSC/HESC Transition.” *EMBO Journal* 31 (9): 2103–16. https://doi.org/10.1038/emboj.2012.71.

Zhu, Saiyong, Wenlin Li, Hongyan Zhou, Wanguo Wei, Rajesh Ambasudhan, Tongxiang Lin, Janghwan Kim, Kang Zhang, and Sheng Ding. 2010. “Reprogramming of Human Primary Somatic Cells by OCT4 and Chemical Compounds.” *Cell Stem Cell* 7 (6): 651–55. https://doi.org/10.1016/j.stem.2010.11.015.

Chapter 2

2.0.0. Chapter Title: 3D immunofluorescence image colocalization quantification in embryonic mouse pluripotent stem cells

A version of this Chapter has been accepted for publication in *Methods in Molecular Biology.*

2.0.1. CRediT Author Statement:

Joshua Dierolf: Conceptualization, Methodology, Validation, Formal Analysis, Investigation, Writing – Original Draft, Writing – Review & Editing, Visualization

Dean Betts: Resources, Writing – Review & Editing, Funding Acquisition, Supervision

Andrew Watson: Writing – Review & Editing, Funding Acquisition, Supervision

2.0.2. Summary:

This chapter details 3D morphological topography of mouse pluripotent stem cell colony architecture optimization and nuclear protein localization by co-immunofluorescence confocal microscopy analysis. Colocalization assessment of nuclear and cytoplasmic cell regions is detailed to demonstrate nuclear localization in mouse epiblast stem cells (mEpiSCs) by confocal microscopy and orthogonal colocalization assessment. Protein colocalization within mouse embryonic stem cells (mESCs), mouse epiblast-like cells (mEpiLCs), and mEpiSCs, or any pluripotent stem cell with a high nuclear-to-cytoplasmic ratio, can be efficiently completed using these optimized protocols.

2.1.0. Introduction:

Immunofluorescence microscopy allows for the visualization of fluorescence light energy emitted from a fluorophore representing the cellular localization of a specific protein of interest. Activation of a fluorophore can be direct or indirect, depending on whether it is conjugated to a primary or secondary antibody respectively (Joshi and Yu 2017). Observable differences in immunofluorescence localization is readily distinguished within a cell using this technique, however, quantification of target protein levels is challenging. Colocalization is an effective quantitative method of comparison between two images within a specific region of interest (ROI), and their level of correlated spatial overlap in pixels used to determine quantity (Adler and Parmryd 2012). The following methods have been developed to quantitatively compare the levels of nuclear and cytoplasmic colocalization for a gene of interest within a specific ROI using immunofluorescence imaging by confocal microscopy.

Pluripotency markers such as octamer-binding transcription factor 4 (OCT4), sex determining region Y – box 2 (SOX2), and NANOG are nuclear localized transcription factors that are expressed within pluripotent stem cells (PSCs). They represent ideal candidate nuclear markers that can be contrasted with overall nuclear DNA staining using Hoechst DNA or an equivalent binding dye as a nuclear reference. Since PSCs, such as mouse epiblast stem cells (mEpiSCs), are typically grown on a feeder cell layer of mouse embryonic fibroblasts (MEFs) for support, OCT4, SOX2, and NANOG become useful stem cell colocalization proteins, as they are not expressed in the MEFs. Choosing the optimal control protein is key, as PSCs have high nuclear to cytoplasmic size ratios, increasing the difficulty in distinguishing between nuclear and cytoplasmic protein localizations (Oh et al. 2005; Pagliara et al. 2014).

The protein of interest in this protocol is pyruvate kinase muscle isoform 2 (PKM2), a metabolic protein that can translocate from the cytoplasm to the nucleus in cancer cells (Yang and Lu 2013). The metrics described compare spatial overlap and correlation between two fluorescent channels include the algorithms for calculating Manders's Overlap Coefficient (MOC) and Pearson Correlation Coefficient (PCC), these metrics are published for induced PSCs and neuronal differentiation (Seibler et al. 2011). The MOC is a measure of the spatial overlap of pixels between two images within a ROI (Manders, Verbeek, and Aten 1993). However, the MOC is quite sensitive to photobleaching, therefore ensuring proper confocal imaging with appropriate laser intensities is paramount (Dunn, Kamocka, and McDonald 2011)(Zinchuk, Zinchuk, and Okada 2007). By applying the removal of non-relevant pixels, non-oversaturated images can eliminate

problems associated with the signal-to-noise sensitivity affected by photobleaching. Therefore, the MOC is a valuable tool in determining if the pixels associated with the two validated proteins exist in the same spatially-relevant ROI (Aaron, Taylor, and Chew 2019). Conversely, the PCC is a measure of covariance between pixels. It is more accommodating in terms of what images can be compared, and represents the other main measurable parameter of colocalization, correlation of pixel distribution between images (Dunn, Kamocka, and McDonald 2011). The PCC of pluripotent stem cell colonies may be decreased compared to individual cells as the PCC measures pixel correlation, therefore, examining the subcellular structures of individual cells will be emphasized more than areas representing extra, non-relevant pixels found in generalized regions of cell colonies (Dunn, Kamocka, and McDonald 2011). Due to the large nuclear-cytoplasmic size ratio of pluripotent stem cells, this limitation of PCC, should not be an issue, and in my experience, there is little to no change between individual cells and total colony PCC or MOC. Proper optimization and consistency in cell fixation and processing is critical for consistency and successful colocalization in all studies of this type. It is essential that all samples, specimens, treatments, and replicates are consistently exposed to well thought out, empirically determined protocols that are consistently applied throughout the entire process and across all experimental replicates. Additionally, the following protocol is also effective for quantifying protein colocalization within naïve mouse embryonic stem cells (mESCs) and formative mouse epiblast-like cells (mEpiLCs), but should work well for any colocalization study, especially for pluripotent stem cells or cell with a high nuclear-to-cytoplasmic ratio.

The mechanisms controlling PKM1 and PKM2 nuclear translocation are largely unknown, however, PKM1 may complex with hepatocyte nuclear factor 4∝ (HNF4∝), and this can be enhanced with the addition of the drug Oroxylin A (OA) and the oncogene JMJD5 is implicated in the nuclear translocation of PKM2 (Wei et al. 2017; Wang et al. 2014). Nuclear translocation of PKM2 as a characteristic of the Warburg effect is well supported by fluorescent imaging and nuclear-to-cytoplasmic fractionation (Yang et al. 2011, 2012; Yang and Lu 2013; Prakasam et al. 2017; Giannoni et al. 2015). Typical confocal image analysis employing visual interpretation of overlaid fluorescent images is a purely qualitative means of spatial localization, however, accurate quantitative measurement of spatial localization can effectively occur within the context of a well-controlled comparison of two fluorophores to determine the degree of colocalization (Wu et al. 2012). Quantitative colocalization analysis (QCA) is most commonly divided into two metrics representing the relationship between two fluorophores, these measures are the degree of, i) overlap and ii) correlation (Dunn, Kamocka, and McDonald 2011). The degree of spatial location by overlapping images was first quantified by Otsu in 1979, where pixels of two images were overlapped after applying a threshold (Otsu 1979). Manders's Overlap Coefficient (MOC) better distinguishes pixels ignored from the threshold from higher intensity pixels but at the cost of being influenced by autofluorescence and an insensitively to differences between the signal-to-noise ratios of the two fluorophores (Manders, Verbeek, and Aten 1993; Aaron, Taylor, and Chew 2019). While the MOC is a measure of co-occurrence of two fluorophores, within the spatially shared regions of a cell, two markers may interact or share a similar trend in intensity localization and may be functionally related or interact. Thus, the colocalization metric of correlation can indicate that two fluorophores share an associative relationship

(Aaron, Taylor, and Chew 2019). The Pearson Correlation Coefficient (PCC) compares the variation of signal intensity between the intersection of two images, taking into account the total population of pixels (Aaron, Taylor, and Chew 2019). As such, this calculation can determine the direction of linear association between the fluorophores (Aaron, Taylor, and Chew 2019; Pearson and Henrici 1896). The MOC and the PCC are commonly used calculations to quantify fluorescent protein spatial overlap and correlation (Adler and Parmryd 2012). Despite the accuracy and power of QCA, this technique has been not been utilized to its full extent, especially so, in its application to measuring protein colocalization in pluripotent stem cells (Dunn, Kamocka, and McDonald 2011). This may be due to an on-going debate within the field of QCA over the correct use and interpretation of overlap and correlation metrics (Adler and Parmryd 2010; Aaron, Taylor, and Chew 2019). Thus, a second primary objective of my study was to contrast both PCC versus MOC in the analysis of PKM1/2 colocalization with nuclear and cytoplasmic protein markers during naïve, formative, and primed pluripotency cell cultures (Zinchuk, Wu, and Grossenbacher-Zinchuk 2013).

The measurement of colocalization is a complicated and hotly debated area of biology (Adler and Parmryd 2010; Aaron, Taylor, and Chew 2019). The term colocalization is largely used to measure two main components with different applications, namely correlation or co-occurrence of two fluorophores to each other based on pixel distribution (Aaron, Taylor, and Chew 2019). Co-occurrence in immunofluorescence is the presentation of fluorescent pixels existing in the same spatial distribution, it is an indicator of overlap between markers, whereas correlation is a measurement of the relationship between the pixel intensities and may indicate a biochemical interaction

(Manders, Verbeek, and Aten 1993). There are several coefficients used to quantify colocalization such as M1, M2, k1, k2 (Manders's coefficients), MOC, PCC, Spearman's rank correlation, and the intensity correlation quotient (Manders, Verbeek, and Aten 1993; Agnati et al. 2005; Adler and Parmryd 2012). The controversy lies specifically in the usefulness and relevance of the MOC, and the alleged superiority of the PCC. In 2010, Alder and Parmryd first published work that diminished the usefulness of MOC in colocalization studies, outlining the metric as a hybrid measurement of correlations and co-occurrences, and arguing that the MOC was not a suitable metric for either colocalization by correlation or co-occurrence (Adler and Parmryd 2010). This was determined by an additive offset of pixels which did not affect the PCC but increased the MOC to a higher level of co-occurrence. As such, the MOC has been criticized as not being the best metric of co-occurrence due to the influence of correlation (Adler and Parmryd 2010). However, this view has since been contested using biological samples demonstrating that both the MOC and PCC are valid measures of colocalization that add different qualities to determining interactions between two fluorochromes and their target proteins (Aaron, Taylor, and Chew 2019). Immunofluorescence is commonly considered as primarily a qualitative technique and the literature into colocalization often uses generalized descriptors, such as 'moderate' or 'strong' association within PCC ranges. To bring greater consistency to the field, and offer greater validity to the quantitative nature of colocalization, a method of colocalization range descriptors has been developed by Zinchuk *et al.* (Zinchuk, Wu, and Grossenbacher-Zinchuk 2013), and it is this approach that was implemented in this thesis to assign a quantitative designate to the colocalization of PKM1 and PKM2 within mESCs. Zinchuk *et al.* labelled PCC values within set ranges to a classification, that included: Correlation: very weak: -1 – -0.27,

weak: -0.26 - 0.09, moderate: 0.1 – 0.48, strong: 0.49 – 0.84, and very strong: 0.85 – 1.0 (Zinchuk, Wu, and Grossenbacher-Zinchuk 2013). MOC values fall into set ranges of: Overlap: very weak: 0 – 0.49, weak: 0.50 – 0.70, moderate: 0.71 – 0.88, strong: 0.89 – 0.97, and very strong: 0.98 – 1.0 (Zinchuk, Wu, and Grossenbacher-Zinchuk 2013). My results support claims that the MOC is a valuable metric of colocalization. By comparing MOC and PCC values relative to a positive and negative biological reference, a stronger baseline set than that produced by using only the improved descriptors. Nuclear (OCT4) and cytoplasmic (GAPDH) proteins were uniquely employed as control markers to correlate their nuclear localization with a well characterized DNA intercalating nuclear stain- Hoechst, which established a robust positive and negative reference to nuclear colocalization, allowing for the direct comparison of MOC and PCC values to one another. Comparing these well-defined positive references to the qualifying range standards set by Zinchuk *et al*. has produced data that supports comparing colocalization by correlation as being superior to spatial overlap in my system (Zinchuk, Wu, and Grossenbacher-Zinchuk 2013). However, there is still valuable knowledge to gain from the MOC, but the PCC data shows a greater distinction between internal reference controls.

2.2.0. Materials:

1. Washing Solution: Dulbecco's Phosphate Buffered Saline (no magnesium, no calcium) (DPBS(-/-))(Gibco^{TM} 14190144).
2. Permeabilization solution: 0.1 % Triton X-100 (Sigma-Aldrich TX1568-1) diluted in DPBS(-/-).

3. Sterilizing Ethanol: 70 % lab-grade ethanol diluted in MilliQ water.
4. Antibody Dilution Solution: 10 % serum from host-species of secondary antibody diluted in DPBS(-/-)-T (0.1 % Tween-20).

Primary Antibodies:

- OCT4: Oct-3/4 Antibody (C-10) (Santa Cruz sc-5279) – 1:50 dilution.
- GAPDH: GAPDH (6C5) (Santa Cruz sc-32233) – 1:50 dilution.
- PKM2: PKM2-specific Polyclonal antibody (ProteinTech 15822-1-AP) – 1:50 dilution.

Secondary Antibodies:

- Goat anti-Rabbit IgG (H+L) Highly Cross-Adsorbed Secondary Antibody, Alexa Fluor Plus 555 (Invitrogen A32732) – 10 μg/mL dilution.
- Goat anti-Mouse IgG (H+L) Cross-Adsorbed Secondary Antibody, Alexa Fluor 488 (Invitrogen A11001) – 1 μg/mL dilution.

5. mESC and mEpiLC substratum: 0.1 % porcine gelatin (Sigma-Aldrich G2500) in MilliQ water and autoclave sterilized.
6. mEpiSC substratum: 10 μg/mL/cm^2 sterile fibronectin (Roche 11051407001) MilliQ water.
7. 1.25mm glass coverslips.
8. Kimberly-Clark Professional™ Kimtech Science™ Kimwipes™ Delicate Task Wipers, 1-Ply (Kimberly-Clark Professional™ 34155).
9. Parafilm™ M Wrapping Film (Fisher Scientific S37441).
10. Humidified container (i.e., Pyrex dish filled with a small amount of water and covered in plastic wrap).

11. Light-tight box.
12. 6-Well cell culture plates (Thermo Scientific Nunc™ Cell-Culture treated Multidishes 140675).
13. Tweezers (the finer tipped, the better).
14. Nuclear stain such as NucBlue™ Live Ready Probes™ Reagent (Invitrogen R37605).
15. Mounting medium such as ProLong™ Gold Antifade Mountant (ThermoFisher Scientific P10144).

2.3.0. Methods:

The quantification of immunofluorescence colocalization protocol requires detailed planning of the experimental design prior to starting. The theory behind the set-up of this methodology is similar to a multi-stain flow cytometry experiment, where controls of each cell type including unstained, single florescent stains, and multi-fluorescent stains (including both antibody stains and live/dead viability stains) are required in biological triplicate. To complete an accurate colocalization experiment or perform an optimal immunofluorescence study, it is advised that an antibody titration (concentration dilution series) be completed for each new cell type or antiserum used. A control sample of each cell type with a single Hoechst stain or another DNA binding equivalent should be included. If an isotype control for each marker is not available, minimally include a secondary only control. A dual fluorescent stain of Hoechst to the nuclear or pluripotency marker of choice will provide a valuable nuclear reference as well. It is recommended that each biological replicate be run in technical triplicate to ensure that

colonies within each passage and imaging set are representative of the true post-imaging calculations. All biological replications within a statistical set should be run within a single sitting of an experimental run by confocal microscopy, including the identical laser settings and general threshold parameters. Deviating from these will result in inconsistent measures. A benefit to completing this modality that cannot be accomplished with flow cytometry is that you can revisit the imaging process of coverslips at any point in time using confocal microscopy if controls are re-analyzed and new thresholds are set.

2.3.1. Coverslip Preparation.

Wash 1.25 mm thick coverslips with 70 % ethanol diluted in MilliQ water. Dry the coverslip with a Kimwipe and UV within a covered 6-well culture dish in a biosafety cabinet for 1 hour to sterilize and dry (*see* **Note 1**). Coat coverslips with 200 μL of sterile 0.1 % gelatin or substratum of choice. Incubate overnight in an incubator (37 °C at 5 % CO_2). Alternatively, for mEpiSCs weaned off MEFs, coat coverslips with 200 μL of 10 μg/mL/cm^2 fibronectin for 45 minutes at room temperature (*see* **Note 2**). Aspirate residual substratum. Plate cells on the outline of the substratum. Eject cell suspension in place of the substratum (*see* **Note 2**). Allow for cells to attach for 1 hour before gently filling the well with the corresponding cell media for overnight incubation (*see* **Note 3**).

2.3.2. Staining Preparation.

Wash cells once with Dulbecco's Phosphate-Buffered Saline without calcium/magnesium (DPBS(-/-)) (*see* **Note 4**). Incubate coverslips in chilled 4 % paraformaldehyde (Sigma - Aldrich) diluted in DPBS(-/-) for 10 minutes. Wash once with chilled DPBS(-/-) for 10 minutes (*see* **Note 5**). Permeabilize adhered cells with 0.1% TritonX-100 for 10 minutes

(*see* **Note 6**). Wash once for 10 minutes with chilled DPBS(-/-). Block the samples by incubating the colony adhered coverslips in 10 % serum (from host-species of secondary antibody) diluted in chilled DPBS(-/-)-T (0.1 % Tween-20) for 30 minutes. No additional washing step is required.

2.3.3. Simultaneous Primary Antibody Staining.

Dilute primary antibodies in 10 % serum (from host-species of secondary antibody) diluted in chilled DPBS(-/-)-T. On a piece of parafilm, pipette 100 μL per coverslip spaced out 5 cm apart (*see* **Note 7**). Using a pair of sterile tweezers, lift each coverslip from the corner and gently dry the coverslip by touching the edge of the glass with a folded Kimwipe (*see* **Note 8**). Once dry, place the coverslip cell-side-down on the diluted antibody. The solution should fully cover the surface of the glass in contact with the parafilm if done correctly. Incubate coverslips with primary antibodies in blocking serum overnight at 4℃. To avoid dehydration of the coverslip, allow the incubation to take place in a humidified container. All samples should incubate for the same length of time to be comparable by colocalization. Remove the coverslip from the humified container by lifting the upside-down coverslip from the parafilm slowly. Place the coverslip in a 6-well plate cell side-up submerged in chilled DPBS(-/-). Wash coverslip(s) once for 10 minutes each in chilled DPBS(-/-). Dilute secondary antibodies in 10% serum (from host-species of secondary antibody) diluted in chilled DPBS(-/-)-T. On a piece of parafilm, pipette 100 μL per coverslip spaced out 5 cm apart. The surface tension will hold the diluted antibody in place. Incubate coverslips with secondary antibodies in blocking serum for 1 hour at room temperature. Humidified incubation is not necessary for this duration of time. All samples incubating with a secondary antibody are now light

sensitive, it is recommended that handling and future steps are completed under dim-lighting. Wash coverslip(s) with chilled DPBS(-/-), add 4 drops/mL of NucBlue™ Live Ready Probes™ Reagent (Hoechst 33342) for 5 minutes. Not all samples will get a Hoechst staining step, always pay attention to your experimental design. Wash once with chilled DPBS(-/-) for 10 minutes.

2.3.4. Mounting and Slide Preparation.

Mount onto 70 % ethanol cleaned, dry, and labelled microscope slides using a commercially available mounting media such as ProLong™ Gold Antifade Mountant. Place the coverslip cell side-down on an edge held up by the cover using tweezers and gently drop the lifted edge over the mounting media to avoid bubbles. Seal with nail polish unless using an adhesive resin-based mounting media (*see* **Note 9**). Store in a light-tight box until you are ready to image on a fluorescent microscope.

2.3.5. Immunofluorescence Colocalization Optimization and Analysis.

To accurately image, quantify, and compare mESCs, mEpiLCs and mEpiSCs, one must establish and apply a single, consistent set of laser parameters for each marker. My analysis was completed on a ZEISS LSM800 confocal microscope with an Airyscan detector and ZEISS Zen system imaging software. Zen Lite, while a free option, does not have the ability to do colocalization analysis in suite. The basic steps of this protocol should be effective for all confocal immunofluorescence microscopic systems, however, if ZEISS Zen system software is unavailable, ImageJ/FIJI are free softwares that offer similar colocalization capabilities and other valuable plugins such as particle analysis and noise reduction that will work with the described protocol.

a)

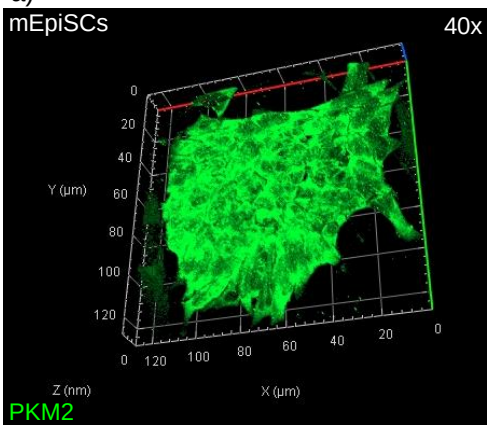
mEpiSCs
40x
Y (µm)
Z (nm)
X (µm)
PKM2

b)

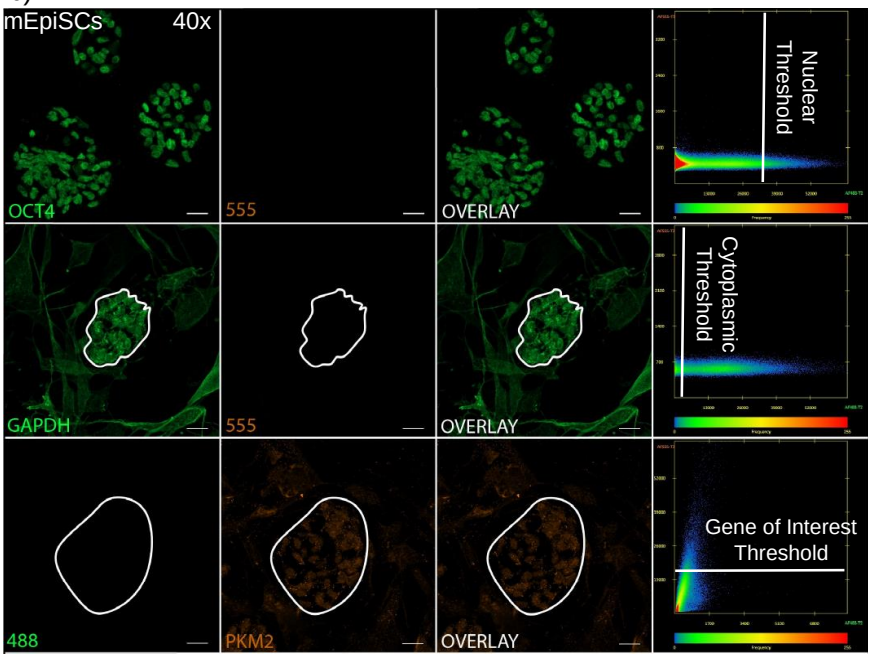
mEpiSCs
40x
OCT4
555
OVERLAY
Nuclear Threshold
GAPDH
555
OVERLAY
Cytoplasmic Threshold
488
PKM2
OVERLAY
Gene of Interest Threshold

c)

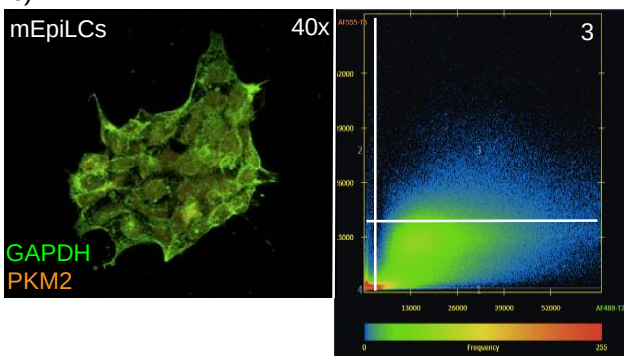
mEpiLCs
40x
GAPDH
PKM2
3
Frequency

Figure 2.1. Nuclear and cytoplasmic colocalization optimization of mEpiSCs.

a) 3D representation of a mEpiSC colony generated from a Z-stack before being processed into an orthogonal projection. X, Y and Z dimensions can be measured, as mEpiSC colonies have a flattened morphology, this approach is useful when comparing the morphologically domed/glistening, naïve mESCs. b) Nuclear, cytoplasmic and protein of interest thresholds of the markers OCT4, GAPDH, and PKM2 respectively in mEpiSCs. Channel thresholds are set to just above the solid green phase of the scatterplots in single stained controls with both lasers running at their optimized intensities. c) Dual stained mEpiLC for GAPDH (green) and PKM2 (orange). Scatterplot of the dual stained specimens detailing nuclear to protein of interest areas of colocalization. Pixel correlation and overlap are measured above the thresholds. Scale bars represent 20 μm.

Identify the appropriate stage settings and focus onto colonies at 40x and 63x objectives using a Hoechst or equivalent single stained samples (*see* **Notes 10 and 11**). Optimize the corresponding laser to each protein marker of interest to the brightest specimen. All the select laser parameters should not result in autofluorescence of any cell type in that laser configuration. If your microscope does not contain a Z-stack module (*see* **Note 12)**. Complete a Z-stack series at 40x magnification set to just beyond the top and bottom of a centered colony. For mESCs, mEpiSCs and mEpiSC, 40x should allow for an entire medium size colony to be in view. These images can be used to examine and visually compare the 3D topography of each pluripotent state colony (Figure 2.1.a) (*see* **Note 13**). Process z-stacks into orthogonal projections (*see* **Note 14**). Select the brightest samples of each single stained marker to set the base threshold. Select the colocalization or scatterplot option, in Zeiss software this is a tab labelled 'Colocalization'. This should appear as a quadrant with a crosshair containing two, adjustable thresholds (Figure 2.1.b). Set the x-axes to one of the channels examined and the y-axes to the other channel. Threshold should be adjusted to keep the signal below the solid green fluorescence (Figure 2.1.b) (*see* **Note 15**). Once the threshold is set, use these settings on each of the dual stained images (Figure 2.1.c), the quadrant labelled '3' represents pixels beyond both control thresholds. A corresponding table with completed calculations is available on the Zeiss Zen system under the table option. Depending on your software, you may need to calculate the MOC and PCC.

Use the following formulae and compare biological replicates as mean ±SEM (Dunn, Kamocka, and McDonald 2011):

$$MOC = \frac{\sum_i (R_i \times G_i)}{\sqrt{\sum_i R_i^2 \times \sum_i G_i^2}} \qquad PCC = \frac{\sum_i (R_i - \bar{R}) \times (G_i - \bar{G})}{\sqrt{\sum_i (R_i - \bar{R})^2 \times \sum_i (G_i - \bar{G})^2}}$$

Where 'R' and 'G' represent the fluorophore intensities of the first and second laser channels respectively. As a check compare Hoechst-stained controls (nuclear reference) to nuclear protein markers such as OCT4, SOX2, or NANOG to verify the accuracy of overlap and correlation to nuclear staining.

2.3.5. Qualifying Descriptors:

PCC and MOC ranges can be qualified into useful and publishable descriptors (Zinchuk, Wu, and Grossenbacher-Zinchuk 2013).

PCC: [very weak: -1 – -0.27], [weak: -0.26 - 0.09], [moderate: 0.1 – 0.48], [strong: 0.49 – 0.84], [very strong: 0.85 – 1.0]

MOC: [very weak: 0 – 0.49], [weak: 0.50 – 0.70], [moderate: 0.71 – 0.88], [strong: 0.89 – 0.97], [very strong: 0.98 – 1.0]

2.4.0. Notes:

Note 1: *To avoid coverslips from sticking to the dish, prop coverslips onto a wall of the dish.*

Note 2*: Allow for surface tension to hold the selected substratum in place on the coverslip.*

Note 3. *If seeding MEFs prior to mEpiSCs, repeat this step 24-hours post-MEF seeding with mEpiSCs.*

Note 4. *Typical protocols state to wash cells up to 3 times, however, mEpiSCs do not stick to their substratum very well, especially when coated onto feeders. The generation of mEpiLCs results in a mass-apoptosis event 48 hours into generation, it is highly recommended that they be treated with the utmost care during washing steps. All washing steps need to be completed gently and all liquid ejection needs to be directed off the adhered cells. Avoid agitation of the plate during washing steps to improve adherence.*

Note 5. *Take care that the DPBS(-/-) is in liquid form without slush that may increase mechanical stress upon ejection.*

Note 6. *This concentration and duration allow for small, medium, and large colonies maintaining either the domed or flattened morphologies of mESCs or mEpiSCs to be permeabilization throughout the structure and underlying MEF layer. Exceeding this concentration or duration will lead to decreased adherence and morphological integrity leading to poor 3D topographical imaging.*

Note 7. *The surface tension will hold the diluted antibody in place.*

Note 8. *Residual liquid will be pulled off of the coverslip without physically contacting the adhered cells or subjecting them to unnecessary aspiration. Lifting the coverslips is performed easier in liquid, reducing the surface tension effect of the glass on the plate.*

Note 9. *Clear, viscous nail polish works best if no resin-based mounting media is available.*

Note 10. *If your microscope has the option to save stage settings, save this parameter for each cell type examined for future reference.*

Note 11. *If you are unsure of which protein marker will fluoresce, the brightest out of the cell types or treatments you are examining, briefly image each and select the brightest and least bright of each protein marker.*

Note 12. *If your microscope does not contain a Z-stack module. Single slice images can still be compared using this protocol, proceed to Step.6. Individual cells can be outlined in both modes, this is especially important for examining only mEpiSCs if grown on feeders (Figure 2.1. B)) or if comparing individual cells to the total colony.*

Note 13. *If time and memory space is not an issue, use the smallest slice size possible at the greatest resolution for optimal imaging.*

Note 14. *These images retain data from the individual slices and are easier to compute for post-image analysis.*

Note 15. *Some microscopes have a Costes algorithm included, if this option is opted for, double check that the crosshair is accurately placed.*

2.5.0. Discussion:

Traditionally, colocalization is employed to investigate close interaction between two proteins of interest through fluorescent imaging. However, this view is myopic and understates the power that a well-controlled and optimized colocalization study can demonstrate. Colocalization is not simply a method to propose interaction, but rather a form of quantitative analysis that demonstrates correlation between proteins indicative of biomolecular interaction and localization overlap within a defined cellular region. Colocalization is actually a physics-based approach to determining trends in pixel orientation between two sets of data (Comeau, Costantino, and Wiseman 2006). From

this approach, when a greater quantity pixel of one set of data occupies the same space, they will overlap to a higher degree than another set that is offset. Additionally, when compared based on a scatterplot of pixel orientation, trends in pixel distribution can determine if there is a correlation to their placement (Dunn, Kamocka, and McDonald 2011). Taken together, two fluorophores that occupy the same cellular space can be measured in terms of overlap and two fluorophores that show similar pixel distribution may also correlate in pixel intensity. These two metrics can be measured by the Manders's overlap coefficient (MOC) and Pearson's correlation coefficient (PCC) respectively and represent the two components of colocalization (Dunn, Kamocka, and McDonald 2011).

These methods will accurately and comprehensively determine differences in nuclear and cytoplasmic expression and changes by fluorescence imaging. Due to the high nuclear-to-cytoplasmic size ratio, traditional methods of nuclear translocation validation, such as nuclear extraction and subsequent immunoblotting, present a challenge in separating the cytoplasmic and nuclear fractions within stem cells (Oh et al. 2005). Nuclear-to-cytoplasmic ratios are valuable for validating pluripotency state, due to the defined nuclear localization of OCT4, SOX2, and NANOG, imaging studies are of particular relevance to establishing mPSC pluripotency (Perestrelo et al. 2017).

The accuracy of this methodology relies on the addition of the nuclear reference, namely Hoechst relative to OCT4. Comparing two nuclear references ensures that the localization differences between the proteins of interest (in example; PKM2) and the nuclear comparison marker (OCT4) are valid. Other studies using colocalization have not

utilized this methodology however my unpublished works show that this is an invaluable tool of validation (Dierolf, Watson, and Betts 2020). Additionally, I apply an entire additional dimension relative to a typical colocalization by analysing orthogonal projections of three-dimensional stacks of colonies as opposed to a two-dimensional comparison, this is beneficial as cells are not 2-dimensional and their expressed proteins do not simply conform to a single layer of expression and localization (Dunn, Kamocka, and McDonald 2011). The main challenge of applying this methodology is the difficulty associated with transitioning and plating pluripotent states. When transitioning from naïve-to-primed-like states your samples will also shift from expressing E- to N-cadherins and undergo a period of mass apoptosis 48 hours into transitioning (Theunissen et al. 2016; Hayashi et al. 2011). Taken together, cell adhesion and viability are extraordinarily difficult to optimize and control for during this pivotal stage of the protocol (Hayashi et al. 2011). This is one of the few, if not only colocalization methods designed specifically for cells grown in colonies and with cells having high nuclear-to-cytoplasmic size ratios, as such, other colocalization methodologies likely will not provide for accurate colocalization of proteins in these cell types. Additionally, I further improved this methodology by implementing qualified descriptor sets for MOC and PCC ranges to serve as accurate descriptors and metrics of spatial overlap and correlation (Zinchuk, Wu, and Grossenbacher-Zinchuk 2013).

The field of colocalization microscopy is mired in controversy, and perhaps rightly so, as the variety and reproducibility of techniques leaves much to be desired and the lack of proper guidelines is evident (Adler and Parmryd 2010; Aaron, Taylor, and Chew 2019; Wu et al. 2012). Currently, several groups are contemplating the validity of the MOC as

a way to measure spatial overlap or as a metric of colocalization at all (Aaron, Taylor, and Chew 2019; Adler and Parmryd 2010). These varying points of view stem from differences in opinion on biologic relevance and physics-based approaches on validation (Adler and Parmryd 2010, 2012; Zinchuk, Zinchuk, and Okada 2007). This doubt in the MOC is valid in a poorly optimized study as the MOC is sensitive to the intensity of undesired signals of interest due to high saturation or poor imaging techniques (Aaron, Taylor, and Chew 2019). When poorly imaged or oversaturated MOC is elevated, however, I circumvent such an artefact in three ways; 1) by setting a threshold on a titrated sample in the cell type of the highest expression for each parameter, 2) by outlining areas/regions of interest to avoid any potential non-specific binding sites, and finally 3) using a the nuclear reference to the nuclear comparison marker allows for any potential elevated MOC value to be precisely localized. In a poorly executed study, an elevated MOC would show little difference between controls and the additional nuclear reference. These results promote the MOC is a valuable metric of spatial overlap for stem cell related colocalization studies. In the context of the traditional misconception of colocalization, the MOC is will not demonstrate any level of molecular interaction between two proteins of interest.

The ways in which the degree of interaction between two or more molecules is determined by the metric of correlation or the degree of colocalization. With regards to correlation, the algorithm recommended in this study and that which is used in most publications is PCC. PCC is not as controversial as MOC, however, it can be improved upon by calculating the Spearman coefficient, a metric of correlation that identifies non-linear relationships between pixel distribution that are otherwise masked by the PCC

which is only sensitive to direct, linear relationships (Aaron, Taylor, and Chew 2019). The Spearman coefficient measures intensity in ranks instead of raw intensity like the PCC, allowing for an averaging of intensities that will reveal correlated, non-linear relationships to be portrayed and analyzed as linear scatterplots. Unlike the MOC, the PCC is sensitive to a high signal to noise ratio, similar to the recommendations for a quality MOC measurement, a well-controlled and calibrated study needs to take place for an accurate PCC value, otherwise, increases the signal-to-noise ratio will decrease any measured correlation (Dunn, Kamocka, and McDonald 2011). To accurately compare PCC values amongst groups it is important that colony size and cell culture parameters are as similar as possible to allow for the highest signal-to-noise ratio possible. Together the metrics of MOC and PCC are the basic, core components of colocalization and work together to inform the relationship of two fluorophores co-occurrence and correlation with each other. This metholodology comprehensively assesses all these parameters and has applied both PCC and MOC to functions to measure differences accurately and precisely in nuclear and cytoplasmic protein localization patterns in pluripotent stem cells.

2.6.0. Acknowledgements:

mESC and mEpiSC pluripotent stem cell lines were graciously gifted from Dr. Janet Rossant. This research was funded by a Canadian Institutes of Health Research operating grant to A.J.W. and D.H.B. and Natural Sciences and Engineering Research Council of Canada grant to D.H.B. The funding sources played no role in design, data collection, analysis, decision to publish, or preparation of this study and manuscript.

2.7.0. References:

Aaron, Jesse S, Aaron B Taylor, and Teng-Leong Chew. 2019. "The Pearson's Correlation Coefficient Is Not a Universally Superior Colocalization Metric. Response to 'Quantifying Colocalization: The MOC Is a Hybrid Coefficient – an Uninformative Mix of Co-Occurrence and Correlation.'" *Journal of Cell Science* 132 (1): jcs227074. https://doi.org/10.1242/jcs.227074.

Adler, Jeremy, and Ingela Parmryd. 2010. "Quantifying Colocalization by Correlation: The Pearson Correlation Coefficient Is Superior to the Mander's Overlap Coefficient." *Cytometry Part A* 77A (8): 733–42. https://doi.org/10.1002/cyto.a.20896.

———. 2012. "Colocalization Analysis in Fluorescence Microscopy." *Methods in Molecular Biology* 931: 97–109. https://doi.org/10.1007/978-1-62703-56-4_5.

Agnati, Luigi F, Kjell Fuxe, Maria Torvinen, Susanna Genedani, Rafael Franco, Stan Watson, Gastone G Nussdorfer, Giuseppina Leo, and Diego Guidolin. 2005. "New Methods to Evaluate Colocalization of Fluorophores in Immunocytochemical Preparations as Exemplified by a Study on A2A and D2 Receptors in Chinese Hamster Ovary Cells." *Journal of Histochemistry & Cytochemistry* 53 (8): 941–53. https://doi.org/10.1369/jhc.4A6355.2005.

Comeau, Jonathan W D, Santiago Costantino, and Paul W Wiseman. 2006. "A Guide to Accurate Fluorescence Microscopy Colocalization Measurements." *Biophysical Journal* 91 (12): 4611–22. https://doi.org/10.1529/biophysj.106.089441.

Dierolf, Joshua G, Andrew J Watson, and Dean H Betts. 2020. "Differential Localization Patterns of Pyruvate Kinase Isoforms in Murine Naïve, Formative and Primed Pluripotent States." *BioRxiv*, January, 2020.04.12.036251. https://doi.org/10.1101/2020.04.12.036251.

Dunn, Kenneth W., Malgorzata M. Kamocka, and John H. McDonald. 2011. "A Practical Guide to Evaluating Colocalization in Biological Microscopy." *American Journal of Physiology-Cell Physiology* 300 (4): C723–42. https://doi.org/10.1152/ajpcell.00462.2010.

Giannoni, Elisa, Maria Letizia Taddei, Andrea Morandi, Giuseppina Comito, Maura Calvani, Francesca Bianchini, Barbara Richichi, et al. 2015. "Targeting Stromal-Induced Pyruvate Kinase M2 Nuclear Translocation Impairs Oxphos and Prostate Cancer Metastatic Spread." *Oncotarget* 6 (27): 24061–74. https://doi.org/10.18632/oncotarget.4448.

Hayashi, Katsuhiko, Hiroshi Ohta, Kazuki Kurimoto, Shinya Aramaki, and Mitinori Saitou. 2011. "Reconstitution of the Mouse Germ Cell Specification Pathway in Culture by Pluripotent Stem Cells." *Cell* 146 (4): 519–32. https://doi.org/10.1016/j.cell.2011.06.052.

Joshi, Sonali, and Dihua Yu. 2017. "Chapter 8 - Immunofluorescence." In , edited by Morteza Jalali, Francesca Y L Saldanha, and Mehdi B T - Basic Science Methods for Clinical Researchers Jalali, 135–50. Boston: Academic Press. https://doi.org/https://doi.org/10.1016/B978-0-12-803077-6.00008-4.

Manders, EMM, FJ Verbeek, and JA Aten. 1993. "Measurement of Co-Localization of Objects in Dual-Colour Confocal Images." *Journal of Microscopy* 169 (3): 375–82. https://doi.org/10.1111/j.1365-2818.1993.tb03313.x.

Oh, Sun Kyung, Hee Sun Kim, Hee Jin Ahn, Hye Won Seol, Yoon Young Kim, Yong

Bin Park, Chul Jong Yoon, Dong-Wook Kim, Seok Hyun Kim, and Shin Yong Moon. 2005. “Derivation and Characterization of New Human Embryonic Stem Cell Lines: SNUhES1, SNUhES2, and SNUhES3.” *STEM CELLS* 23 (2): 211–19. https://doi.org/https://doi.org/10.1634/stemcells.2004-0122.

Otsu, Nobuyuki. 1979. “A Threshold Selection Method from Gray-Level Histograms.” *IEEE Transactions on Systems, Man and Cybernetics* 20 (1): 62–66. https://doi.org/0018-9472/79/0100-0062$00.75.

Pagliara, Stefano, Kristian Franze, Crystal R McClain, George W Wylde, Cynthia L Fisher, Robin J M Franklin, Alexandre J Kabla, Ulrich F Keyser, and Kevin J Chalut. 2014. “Auxetic Nuclei in Embryonic Stem Cells Exiting Pluripotency.” *Nature Materials* 13 (6): 638–44. https://doi.org/10.1038/nmat3943.

Pearson, Karl, and Olaus Magnus Friedrich Erdmann Henrici. 1896. “VII. Mathematical Contributions to the Theory of Evolution.—III. Regression, Heredity, and Panmixia.” *Philosophical Transactions of the Royal Society of London. Series A, Containing Papers of a Mathematical or Physical Character* 187 (January): 253–318. https://doi.org/10.1098/rsta.1896.0007.

Perestrelo, Tânia, Weitong Chen, Marcelo Correia, Christopher Le, Sandro Pereira, Ana S Rodrigues, Maria I Sousa, João Ramalho-Santos, and Denis Wirtz. 2017. “Pluri-IQ: Quantification of Embryonic Stem Cell Pluripotency through An Image-Based Analysis Software.” *Stem Cell Reports* 9 (2): 697–709. https://doi.org/10.1016/j.stemcr.2017.06.006.

Prakasam, Gopinath, Rajnish Kumar Singh, Mohammad Askandar Iqbal, Sunil Kumar Saini, Ashu Bhan Tiku, and Rameshwar N K Bamezai. 2017. “Pyruvate Kinase M Knockdown–Induced Signaling via AMP-Activated Protein Kinase Promotes Mitochondrial Biogenesis, Autophagy, and Cancer Cell Survival.” *Journal of Biological Chemistry* 292 (37): 15561–76. https://doi.org/10.1074/jbc.M117.791343.

Seibler, Philip, John Graziotto, Hyun Jeong, Filip Simunovic, Christine Klein, and Dimitri Krainc. 2011. “Mitochondrial Parkin Recruitment Is Impaired in Neurons Derived from Mutant PINK1 Induced Pluripotent Stem Cells.” *The Journal of Neuroscience* 31 (16): 5970 LP – 5976. https://doi.org/10.1523/JNEUROSCI.4441-10.2011.

Theunissen, Thorold W, Marc Friedli, Yupeng He, Evarist Planet, Ryan C O’Neil, Styliani Markoulaki, Julien Pontis, et al. 2016. “Molecular Criteria for Defining the Naive Human Pluripotent State.” *Cell Stem Cell* 19 (4): 502–15. https://doi.org/10.1016/j.stem.2016.06.011.

Wang, H.-J., Y.-J. Hsieh, W.-C. Cheng, C.-P. Lin, Y.-S. Lin, S.-F. Yang, C.-C. Chen, et al. 2014. “JMJD5 Regulates PKM2 Nuclear Translocation and Reprograms HIF-1 -Mediated Glucose Metabolism.” *Proceedings of the National Academy of Sciences* 111 (1): 279–84. https://doi.org/10.1073/pnas.1311249111.

Wei, Libin, Yuanyuan Dai, Yuxin Zhou, Zihao He, Jingyue Yao, Li Zhao, Qinglong Guo, and Lin Yang. 2017. “Oroxylin A Activates PKM1/HNF4 Alpha to Induce Hepatoma Differentiation and Block Cancer Progression.” *Cell Death & Disease* 8 (7): e2944. https://doi.org/10.1038/cddis.2017.335.

Wu, Yong, Vadim Zinchuk, Olga Grossenbacher-Zinchuk, and Enrico Stefani. 2012. “Critical Evaluation of Quantitative Colocalization Analysis in Confocal Fluorescence Microscopy.” *Interdisciplinary Sciences: Computational Life Sciences*

4 (1): 27–37. https://doi.org/10.1007/s12539-012-0117-x.
Yang, Weiwei, and Zhimin Lu. 2013. “Nuclear PKM2 Regulates the Warburg Effect.” *Cell Cycle* 12 (19): 3154–58. https://doi.org/10.4161/cc.26182.
Yang, Weiwei, Yan Xia, Haitao Ji, Yanhua Zheng, Ji Liang, Wenhua Huang, Xiang Gao, Kenneth Aldape, and Zhimin Lu. 2011. “Nuclear PKM2 Regulates β-Catenin Transactivation upon EGFR Activation.” *Nature* 480 (7375): 118–22. https://doi.org/10.1038/nature10598.
Yang, Weiwei, Yanhua Zheng, Yan Xia, Haitao Ji, Xiaomin Chen, Fang Guo, Costas A. Lyssiotis, Kenneth Aldape, Lewis C. Cantley, and Zhimin Lu. 2012. “ERK1/2-Dependent Phosphorylation and Nuclear Translocation of PKM2 Promotes the Warburg Effect.” *Nature Cell Biology* 14 (12): 1295–1304. https://doi.org/10.1038/ncb2629.
Zinchuk, Vadim, Yong Wu, and Olga Grossenbacher-Zinchuk. 2013. “Bridging the Gap between Qualitative and Quantitative Colocalization Results in Fluorescence Microscopy Studies.” *Scientific Reports* 3 (1): 1365. https://doi.org/10.1038/srep01365.
Zinchuk, Vadim, Olga Zinchuk, and Teruhiko Okada. 2007. “Quantitative Colocalization Analysis of Multicolor Confocal Immunofluorescence Microscopy Images: Pushing Pixels to Explore Biological Phenomena.” *ACTA HISTOCHEMICA ET CYTOCHEMICA* 40 (4): 101–11. https://doi.org/10.1267/ahc.07002.

Chapter 3

A version of this Chapter has been accepted for publication in *Experimental Cell Research.*

3.0.0. Chapter Title: Differential localization patterns of pyruvate kinase isoforms in murine naïve, formative, and primed pluripotent states

3.0.1. CRediT Author Statement:

Joshua Dierolf: Conceptualization, Methodology, Validation, Formal Analysis, Investigation, Writing – Original Draft, Writing – Review & Editing, Visualization
Dean Betts: Resources, Writing – Review & Editing, Funding Acquisition, Supervision
Andrew Watson: Resources, Writing – Review & Editing, Funding Acquisition, Supervision

3.1.0. Abstract:

Mouse embryonic stem cells (mESCs) and mouse epiblast stem cells (mEpiSCs) represent opposite ends of a pluripotency continuum, referred to as naïve and primed pluripotent states, respectively. These divergent pluripotent states differ in several ways including growth factor requirements, transcription factor expression, DNA methylation patterns, and metabolic profiles. Naïve cells employ both glycolysis and oxidative phosphorylation (OXPHOS), whereas primed cells preferentially utilize aerobic glycolysis, a trait shared with cancer cells referred to as the 'Warburg Effect'. Until recently, metabolism has been regarded as a by-product of cell fate, however, evidence now supports metabolism as being a promoter of stem cell state and fate decisions. Pyruvate kinase muscle isoforms (PKM1 and PKM2) are important for generating and maintaining pluripotent stem cells (PSCs) and mediating the Warburg Effect. Both isoforms catalyze the last step of glycolysis generating adenosine triphosphate and pyruvate, however, the precise role(s) of PKM1/2 in naïve and primed pluripotency is not well understood. The primary objective of this study was to characterize the cellular expression and localization patterns of PKM1 and PKM2 in mESCs, chemically transitioned epiblast-like cells (mEpiLCs) representing formative pluripotency, and mEpiSCs using immunoblotting and confocal microscopy. The results indicate that PKM1 and PKM2 are not only localized to the cytoplasm, but also accumulate in differential subnuclear regions of mESC, mEpiLCs, and mEpiSCs as determined by a quantitative, confocal microscopy colocalization employing orthogonal projections, and airyscan processing. Importantly, the results demonstrate subnuclear localization of PKM1/2 shifts during the transition from mESCs, mEpiLCs, and mEpiSCs. Finally, the methodology used comprehensively validates the appropriateness and power of the

Pearson's correlation coefficient and Manders's overlap coefficient for assessing nuclear and cytoplasmic protein colocalization in PSCs by immunofluorescence confocal microscopy. I propose that nuclear PKM1/2 may assist with distinct pluripotency state maintenance and lineage priming by non-canonical mechanisms. These results advance the understanding of the overall mechanisms controlling naïve, formative, and primed pluripotency.

3.2.0. Introduction:

Pluripotent stem cells (PSCs) have the capacity for indefinite self-renewal and the potential to differentiate into the cell types of all three germ layers including the germ line (Nichols and Smith 2009). The potency of PSCs, such as embryonic stem cells (ESCs), exists within a continuum with opposite ends described as naïve and primed states (Nichols and Smith 2009). In mice, naïve mESCs are derived from the inner cell mass (ICM) of an early, embryonic day (E)3.5 to E4.5, blastocyst-stage embryo, whereas primed mouse epiblast stem cells (mEpiSCs) are derived later from the epiblast of E5.0-8.0 post-implantation embryos (Morgani, Nichols, and Hadjantonakis 2017; Evans and Kaufman 1981; Brons et al. 2007; Tesar et al. 2007; Martin 1981). However, when cultured *in vitro,* mEpiSCs more closely resemble the epiblast of E7.25-E8.0 embryos (Joo et al. 2014; Tesar et al. 2007; Morgani, Nichols, and Hadjantonakis 2017; Kojima et al. 2014). Human ESCs (hESCs) have traditionally been stabilized at the primed pluripotent state, however, a naïve hESC line has been recently derived (Ge Guo et al. 2016). Between both ends of the pluripotent continuum exists a recently described intermediate state called the 'formative pluripotent state' (Kalkan and Smith 2014; Smith

2017). Formative pluripotency is an executive phase and may represent the gene expression patterns and attributes of mouse epiblast cells within E5.5-6.25 embryo (Morgani, Nichols, and Hadjantonakis 2017). Like naïve and primed PSCs, formative PSCs also express NANOG, OCT4, and SOX2 (Chambers et al. 2003; Kalkan and Smith 2014; Hayashi et al. 2011). However, unlike naïve and primed PSCs, the formative mouse epiblast-like cells (mEpiLCs) can efficiently differentiate into primordial germ cell-like cells when presented with the appropriate growth factors such as bone morphogenic protein 4 (Morgani, Nichols, and Hadjantonakis 2017; Ohinata et al. 2009). Each pluripotent state has several distinguishing features such as unique morphology, growth factor dependencies, gene expression profiles, epigenetic status, and metabolic preferences (Morgani, Nichols, and Hadjantonakis 2017; Nichols and Smith 2009). Morphologically, naïve PSCs are more rounded in appearance and grow as colonies with glistening edges compared to flattened primed PSC colonies (Nichols and Smith 2009). This hemispherical morphology of naïve cells is largely due to greater Cdh1 expression, which can be replicated in mEpiSCs following overexpression of Cdh1 (Ohtsuka, Nishikawa-Torikai, and Niwa 2012). Culture of mESCs requires leukemia inhibitor factor (LIF) which promotes 'ground state' naïve pluripotency and resists differentiation through activation of the transcription factor STAT3 (Ohtsuka, Nakai-Futatsugi, and Niwa 2015). Stabilizing naïve pluripotency requires LIF and the addition of two small molecule inhibitors (LIF/2i) of MEK1/2 (PD00032) and glycogen synthase kinase-3 (CHIR99021) (Ying et al. 2008; Silva and Smith 2008). Formative cells can be chemically transitioned from mESCs-to-mouse epiblast-like cells (mEpiLCs) over 48 hours as a transient and heterogenous population (Kinoshita and Smith 2018; Hayashi et al. 2011). To maintain primed pluripotency and exit the naïve state, mEpiSCs and

chemically transitioned mEpiLCs are cultured with ACTIVIN-A and FGF-2. While naïve and primed cells express the core pluripotency associated genes Oct4, Sox2, Nanog, both states differ in transcriptional programs with Rex1, Esrrb, Dppa3, Klf2/4/5, Tcfcp2l1, and Pecam delineating the naïve state, and Zic2, T (Brachyury), and Cer1, to list a few, distinguishing the primed pluripotent state (Morgani, Nichols, and Hadjantonakis 2017). The formative pluripotent state is reported to highly express Lef1, Pou1fc, and Dnmt3 (Kalkan et al. 2019). Naïve and primed pluripotent states also differ in terms of their epigenetic landscape, including X-activation and chromatin methylation status (Takahashi, Kobayashi, and Hiratani 2018). Female primed PSCs display random X chromosome inactivation, whereas naïve PSCs display activation of both X chromosomes (Heard 2004). Relative to primed cells, naïve PSCs contain larger regions of active chromatin as indicated by higher levels of H2k4me3 and histone acetylation (G. Guo et al. 2009; Gafni et al. 2013). Importantly, naïve and primed PSCs also differ in terms of their metabolic preferences (W. Zhou et al. 2012). Naïve cells are characterised as being metabolically bivalent, utilizing both glycolytic and oxidative phosphorylation (OXPHOS) processes, whereas primed cells are preferentially glycolytic (W. Zhou et al. 2012). Even when cultured in oxygen rich conditions, primed PSCs utilize aerobic glycolysis and display low OXPHOS gene expression, which, is characteristic of the Warburg Effect that is active in many cancer cells (Prigione et al. 2010).

Despite the original observations of Dr. Otto Warburg that cells exhibiting the Warburg Effect consume elevated glucose and direct increased levels of pyruvate towards lactate formation, most cancers do not gain ATP by glycolysis primarily (Weinhouse et al. 1956). In actuality, glycolysis in the majority of cancer cells is not increased to generate

ATP, but rather increase precursors necessary for enhancing anabolic processes (DeBerardinis and Chandel 2016). Indeed, glucose oxidation by OXPHOS still produces the bulk of ATP in most cancer cells with anaplerotic flux of metabolic intermediates produced by glutaminolysis and lactic acid fermentation into the TCA cycle including α-ketoglutarate and even lactate respectively (Feron 2009). The sourcing of metabolites for ATP production appears to be dependent on the surrounding microenvironments and cancer subtype (Hensley et al. 2016). For example, non-small cell lung cancer (NSCLC) cells illustrate metabolic heterogeneity and preferential aerobic and non-aerobic metabolism processes (Hensley et al. 2016). Within cells exhibiting the Warburg Effect, an increase in lactate production would be expected within NSCLC cells, elevated lactate is used a carbon source in the TCA cycle and other increased expression of pyruvate carboxylase promote higher levels of anaplerotic processes feeding into the TCA cycle compared to normal lung tissue (Hensley et al. 2016). Misconceptions in distinguishing the concepts of anabolic processes for cellular proliferation and energy generation relating to the Warburg Effect need to be tackled not only in cancer research, but also in stem cell research going forward (DeBerardinis and Chandel 2016).

The Warburg Effect is orchestrated by an upregulation of key transcription factors including: Oct4, c-Myc, Hif-1∝, and Nfκb along with the glycolytic genes: Hk2, Pgm, Pdk, and pyruvate kinase muscle isoform 2 (Pkm2) (Levine and Puzio-Kuter 2010). When upregulated, these aerobic glycolytic associated genes promote anabolism and ATP generation to boost glycolytic flux (Feron 2009; Guppy, Greiner, and Brand 1993). It is hypothesized that the high glycolytic flux of mESC maintains their high proliferative capacity and as such, cellular metabolic state should be considered as a mediator of

pluripotency and as a regulator of gene expression controlling cell proliferation and differentiation (Kondoh et al. 2007; Zhang et al. 2018). While metabolism has traditionally been viewed as a by-product of cell fate decisions, the manipulation of metabolic genes and their products in stem cells can promote or resist cellular differentiation and reprogramming (Hawkins et al. 2016; Rodrigues et al. 2015; W. Zhou et al. 2012). Thus, the developmental progression of naïve-to-primed transitioning occurs in synchrony with metabolic programming to influence cell fate and pluripotent state as both a driver and a passenger (Dahan et al. 2019).

Recently, pyruvate kinase muscle isoforms 1 and 2 (PKM1/2) have been implicated in regulating pluripotency, proliferation, and in the generation of pluripotent stem cells during reprogramming (Qin et al. 2017). PKM1 and PKM2 are the metabolic enzymes responsible for catalyzing the final, rate limiting step of glycolysis by directing pyruvate towards either a lactate or acetyl-CoA fate (Noguchi et al. 1987; Christofk et al. 2008). Mammals express four tissue specific pyruvate kinase isozymes; M1, M2, L, and R, each with unique properties and tissue expression patterns to meet specific metabolic demands (Yamada and Noguchi 1999). PKM1/2 are alternatively spliced isoforms from the PKM gene and both PKL and PKR are encoded by the PKLR gene (Noguchi et al. 1987). The M1 and M2 isoforms are spliced by three different heterogenous nuclear ribonucleoproteins; hnRNPI/hnRNP1/hnRNP2 that involve the inclusion of exon 9 or 10, respectively (David et al. 2010). PKM1/2 activity is regulated by homotropic and heterotropic allosteric interactions with fructose 1,6-bisphosphate (FBP) and phosphoenolpyruvate respectively (Boles et al. 1997; Imamura and Tanaka 1982). PKM1 is expressed primarily in somatic cells, whereas fetal tissues along with essentially all

cancer cell types exhibit elevated PKM2 with certain types of tumours such as glioblastomas displaying a complete isoform switch from PKM1 to PKM2 (Desai et al. 2013). The elevated PKM2 found in cancer cells is predominantly the inactive PKM2 homodimer form, which is due to pulsatile phosphofructokinase (Shi, You, and Luo 2019). The active homotetramer is typically bound to its cofactor FBP, however, when the PKM2 homodimer is phosphorylated (Y105) by the oncogenic linked fibroblast growth factor receptor type 1, the homotetrameric configuration is disrupted (Hitosugi et al. 2009; Christofk, H. R., Vander Heiden, M. G., Wu, N., Asara, J. M. & Cantley 2008). This interrupts glucose oxidation and increases glycolysis and lactate production in aerobic glycolytic preferential cancer cells, even in the presence of abundant oxygen levels. In contrast, PKM1 operates as a constitutively active homotetramer without a described allosteric binding site (Jurica et al. 1998).

PKM2 has additional non-canonical roles including its function as a protein kinase, cytosolic receptor, transcriptional co-activator, and is also implicated in cytokinesis and chromosome segregation (W. Yang and Lu 2015; Jiang, Wang, et al. 2014; Jiang, Li, et al. 2014). PKM2 can form a complex with OCT4 resulting in decreased OCT4 transcriptional activity and stemness with increased apoptosis and differentiation (Lee et al. 2008; Morfouace et al. 2014). Studies also indicate that the interaction of PKM2 and OCT4 affects mitosis and tumor energy production (Niwa, Miyazaki, and Smith 2000). PKM2 is implicated in pluripotency through its interaction and transcriptional regulation of OCT4 in hESCs (Christensen, Calder, and Houghton 2015). Knockdown of PKM2 in hESCs exhibited no change in lactate production or glucose uptake, however, OCT4 expression decreased substantially (Christensen, Calder, and Houghton 2015). PKM2 is

observed in the nuclei of the hESCs cultured under both normoxic (20%), and hypoxic (5%) oxygen conditions, but a significant reduction in PKM2 expression was observed under normoxia (Christensen, Calder, and Houghton 2015). Overexpression of either PKM1 or PKM2 results in increased transcript abundance of the pluripotency associated genes; Eras, Rex1, and Nanog in mESCs (Qin et al. 2017). Upon knockdown of total PKM, pluripotency associated gene transcript abundance also decreases, but self-renewal and morphology appear unperturbed (Qin et al. 2017). During reprogramming of somatic cells into iPSCs, both PKM1 and PKM2 are upregulated within the first 8 days (Qin et al. 2017). Additionally, the knockdown of total PKM during this period hinders reprogramming and overexpression of PKM2 significantly increases the generation of iPSC colonies (Qin et al. 2017). PKM1 was originally thought to only be expressed in the cells of non-proliferative tumors, however, PKM1 has recently been localized in the nuclei of hepatoma (HepG2 and SMMC-7721 cell lines) cells following Oroxylin A (OA) treatment and this localization was concluded to promote cellular differentiation to hepatocytes-like cells (Wei et al. 2017; Israelsen et al. 2013).

Quantitative colocalization analysis (QCA) is most commonly divided into two metrics, these measures are the degree of overlap and correlation (Dunn, Kamocka, and McDonald 2011). Both MOC and the PCC are commonly used to quantify fluorescent protein spatial overlap and correlation (Adler and Parmryd 2012). Despite the accuracy and power of QCA, this technique has been not been utilized to its full extent, especially so, in its application to measuring protein colocalization in pluripotent stem cells (Dunn, Kamocka, and McDonald 2011). This study contrasted both PCC versus MOC in our

analysis of PKM1/2 colocalization with nuclear and cytoplasmic protein markers during naïve, formative, and primed pluripotency within mouse ES cell cultures

This study, for the first time, comprehensively characterized the subcellular localization and expression patterns of PKM1 and PKM2 isoforms during transition from naïve, through the formative and onto the primed murine embryonic pluripotent states. I accomplished this by optimizing a confocal microscopy colocalization approach comparing correlation and co-occurrence of PKM1 and PKM2 localization to nuclear localized OCT4 and cytoplasmic localized GAPDH. Degrees of colocalization were then applied to our measured values of overlap and correlation using qualified ranges indicating a spectrum of 'very weak' to 'very strong' variables of colocalization (Zinchuk, Wu, and Grossenbacher-Zinchuk 2013). Using these approaches, the data suggests an elevated nuclear presence of PKM1 and PKM2 in naïve mESCs, formative state mEpiLCs and primed mEpiSCs as assessed by spatial overlap of PKM1 and PKM2 localization to OCT4 localization. The results also demonstrate a moderate association of PKM1 and PKM2 to OCT4 localization in naïve mESCs and a strong association between PKM1 and OCT4 in formative mEpiLCs. Together, the findings suggest a novel, non-canonical role for PKM1 in pluripotent stem cells.

3.3.0. Materials and methods:

3.3.1. Antibody specificity:

Rabbit polyclonal antibodies specific for PKM1 and PKM2 (Proteintech 15821-1-AP, 15822-1-AP) were used to distinguish between PKM1 and PKM2 protein localization and

abundance in this study. These PKM1 and PKM2 antibodies recognize the corresponding immunogens of LVRASSHSTDLMEAMAMGSV and LRRLAPITSDPTEATAVGAV, respectively, and have been knockdown-verified confirming their isoform specificity (Nakatsu et al. 2015; Horiuchi et al. 2017; Christofk et al. 2008; Ma et al. 2019; Jianan Chen et al. 2018).

3.3.2. Feeder cell derivation and culture conditions:

Mouse embryonic fibroblasts (MEFs) (CF1 cell line, ThermoFisher) derived from E12.5 mouse embryos were plated and expanded on 0.1% porcine gelatin (Sigma G2500) coated dishes and irradiated (8000 rads). Irradiated MEFs were cultured in media containing the following: DMEM (ThermoFisher11960044), 8.9% Qualified FBS (ThermoFisher 12483020, lot# 1936657), 1.1% MEM NEAA (100x) (ThermoFisher 11140050), 1.1% GlutaMAX (ThermoFisher 35050061). Irradiated MEFs were plated on 0.1% gelatin dishes and cultured for a minimum of 1 hour prior to mEpiSC plating for immunofluorescence and 24 hours for all other molecular analyses.

3.3.3. Stem cell culture conditions:

Feeder-free, naïve, mouse embryonic stem cells (mESCs, R1 strain – 129X1 x 129S1; provided courtesy of Dr. Janet Rossant, Hospital for Sick Children, Toronto, Canada), feeder-free, primed-like mouse epiblast-like cells (mEpiLCs, chemically converted R1 mESCs) and primed mouse epiblast stem cells (mEpiSCs, strain – 129S2; also provided by Dr. Janet Rossant) were cultured in the following base media; a 1:1 mixture of KnockOut DMEM/F12 (ThermoFisher 12660012) and Neurobasal Media (ThermoFisher 21103049) with 0.1% 2-Mercaptoethanol (Gibco 21985-029), 0.25% GlutaMAX

(ThermoFisher 35050061), 1.0% N2 Supplement (100x) (ThermoFisher 17502048), 2.0% B27 Supplement (50x) (ThermoFisher 17504044). Base media for the culture of mESCs were supplemented with 1000 units/mL ESGRO Recombinant mouse LIF protein (EMD Millipore ESG1107), and 2i small molecule inhibitors: 1 µM PD0325901 (Reagents Direct 39-C68) and 3 µM CHIR99021 (Reagents Direct 27-H76). Base media for the culture of mEpiLCs and mEpiSCs were supplemented with 20ng/mL Activin A from mouse (Sigma-Aldrich SRP6057) and 12ng/mL Fgf-2 from mouse (Sigma-Aldrich SRP3038). mESCs were passaged using Accutase (STEMCELL Technologies 07920) and centrifuged at 244 x g for 5 minutes. Primed mouse epiblast stem cells were cultured in the base medium and supplements as mEpiLCs were along with a substratum of irradiated mouse embryonic fibroblasts (MEFs). One hour prior to passaging, growth medium was replaced. Passaging was completed using Gentle Cell Dissociation Buffer (Gibco 13151-014) for 5 minutes at room temperature. Lifted cells were then centrifuged at 244 x g for 3 minutes and plated at a density of 1:12 onto fibronectin coated dishes with MEFs. RNA and protein abundance studies were completed by excluding MEFS for feeder-free conditions and passaging mEpiSCs with StemPro™ Accutase™ (Thermo Fisher A1110501) to ensure only MEF free lysates were used. Additionally, during the preliminary work for this study it was clear that the MEF feeder cells supporting the mEpiSCs, express the PKM isoforms in abundance. mEpiSCs were weaned off irradiated MEFs by gentle enzymatic passaging onto fibronectin over two passages, this resulted in a clean and healthy population of feeder-free mEpiSCs ready for protein abundance studies.

3.3.4. Real-Time Quantitative qRT-PCR:

RNA isolation was completed using a RNeasy RNA isolation kit (Qiagen 74104) and Trizol (Ambion 15596018) hybrid protocol followed by DNAse treatment (Invitrogen AM1906). cDNA synthesis was completed in accordance with iScript (BioRad 170-8891) protocols. Total RNA was extracted from adherent cells using TRIzol Reagent (Invitrogen) and a RNeasy mini kit (Qiagen). DNAses were then removed using DNAse Free Kit (AM1906). cDNA synthesis using iScript. Primers were tested in temperature gradients before cDNA dilution series to determine primer efficiencies. Relative transcript abundance was compared using mean±SEM with a two-way ANOVA with Tukey's multiple comparison test with three biological replicates. Relative transcript abundance was calculated using the Pfaffl method of quantification, normalized to mESCs and relative to TATA-binding protein (Tbp) transcript abundance. Forward and reverse primer designs and annealing temperatures are available in Table 3.1.

Table 3.1 PCR Primers:

Gene Name	**Potency/ Role**	**Efficiency (%)**	**Annealing Temperature (℃)**	**Sequence (F = Forward, R = Reverse; 5' – 3')**
Tbp	Reference gene	99.42434	57.0 - 63.0	F- TACTGAAGAAAGGGAGAATCATGG R- GAGACTGTTGGTGTTCTGAATAGG
Pecam	Naïve	89.999919	63.0	F- CAAGGCCAAACAGAAACCCG R- GCCTTCCGTTCTCTTGGTGA
Dppa3	Naïve	90.327424	63.0	F- AAAGTCGACCCAATGAAGGA R- CGGGGTTTAGGGTTAGCTTT
Rex1	Naïve	96.622863	63.0	F- AGAAGAAAGCAGGATCGCCT R- TATGACTCACTTCCAGGGGG
Esrrb	Naïve	103.71074	63.0	F- CAGGCAAGGATGACAGACG R- GAGACAGCACGAAGGACTGC

Klf2	Naïve	106.23229	63.0	F- TCGAGGCTAGATGCCTTGTGA R- AAACGAAGCAGGCGGCAGA
Klf4	Naïve	102.51493	63.0	F- TGGTGCTTGGTGAGTTGTGG R- GCTCCCCCGTTTGGTACCTT
Klf5	Naïve	102.58943	63.0	F- TACGGGCGAGAAGCCCTACA R- GGCACACCATGCACTGGAAC
Tcfcp2l1	Naïve	99.564838	60.0	F- CCGCCCCTACAGTATGTGTT R- AGTCCCCTAGCTTCCGATTC
Lef1	Formative	108.05468	57.0	F- AGAAGAAGAAGAGGAAGAGAGAGAAGC R- AGATGTAGGCAGCTGTCATTCTGG
Dnmt3	Formative	99.041999	63.0	F- GGCAAGGACGACGTTTTGTG R- GTTGGACACGTCCGTGTAGTGAG
Pou1fc	Formative	98.95197	59.4	F- TTTCTCAAGTGTCCCAAGCC R- ACCACCTCCTTCTCCAGTTG
Zic2	Primed	89.96254	63.0	F- GGTGACCCACGTCTCTGTG R- CGGATGTGGTTGACCAGTTT
Cer1	Primed	99.767999	60.0	F- ACCTATGTGTGGATGGCTGC R- AGATCCGGCTTGTCTTCTGC
T(Bra)	Primed	104.08831	60.0	F- CGGTGGCGAGAGAAGTGAAG R- CTTCCCTGCGCTCTCTGTG

3.3.5. Western blotting:

Mouse ESCs and mEpiLCs were washed with cold DPBS (calcium chloride/magnesium chloride/) (PBS(+/+)) (Gibco 14040-133) and all cell types were lysed with Pierce™ RIPA Buffer (ThermoScientific 89900) supplemented with 1X Phosphatase Inhibitor Cocktail Set 2 (Calbiochem 5246251) and 1X Protease Inhibitor Cocktail Set 1 (Calbiochem 539131). mEpiSCs passaged off MEF-coated plates onto fibronectin (Roche 11051407001) coated plates for a single passage using StemPro™ Accutase™ to avoid MEF contamination. mEpiSCs were centrifuged at 244 x g and lysed. Lysates were sonicated for five, 30 joule pulses over 30 seconds and were rotated at 4 °C for 30 minutes followed by centrifugation of 12000 rcf at 4 °C for 20 minutes with the

supernatant removed into a fresh, chilled tube. Protein quantification was completed using a Pierce™ BCA Protein Assay kit (Thermo Fisher Scientific 23225). Protein loading mixes were prepared at 10-25 µg samples in MilliQ H_2O, LDS, and Reducing Agent at 70°C for 10 minutes. Loading mixes were loaded in NuPAGE™ 4-12% Bis-Tris Gels (Invitrogen NuPAGE NP0336), the electroporation solution consisting of 1x MOPS (BOLT Invitrogen B000102) and 500 µL of sample reducing agent containing dithiothreitol (Thermofisher NP0009) added. Electrophoresis was completed at 200 V for 50 minutes. Proteins were transferred to a PVDF membrane at 100V for 2 hours in ice-cold conditions. The protein transferred PVDF membrane (EMD Immobilon IPVH00010) was blocked in 5% bovine serum albumin (BSA) (ALB001) for phosphorylated antibodies or 5% skimmed milk (Carnation) in 1x TBST for 1 hour at room temperature with end-to-end agitation. Primary antibodies were introduced to the membrane overnight at 4 °C with rotation. Membranes were washed 3 times for 10 minutes in TBST and HRP conjugated secondary antibodies were introduced for 1 hour at room temperature with rotation. Membranes were then washed three times for 10 minutes each and imaged with Luminata Classico Western HRP Substrate (EMD WBLUC0500) or Immobilon Forte Western HRP Substrate (EMD WBLUF0500) on a ChemiDoc. Membranes were stripped using antibody stripping buffer (FroggaBio ST010) until previous antibody binding was no longer evident. Bands of interest were compared to β-ACTIN and/or Ponceaus S for total lane protein densitometry. Western blotting densitometry results were compared using mean $\pm$ SEM, One-way ANOVA, Tukey's multiple comparison test with three biological replicates. Primary and secondary antibodies and their concentrations are listed in Table 3.2.

Table 3.2 Western blot antibody/marker list:

Primary Antibody/Marker	**Concentration**	**Secondary Antibody**	**Concentration**
β-ACTIN A3854	1:50000	N/A: HRP-linked	N/A: HRP-linked
PKM1 15821-1-AP	1:5000, 5% TBST	Anti-rabbit IgG, HRP-linked Antibody #7074 Cell Signaling Technology	1:2000-10,000, 5% Milk in TBST
pPKM2 (Tyr105) 3827S	1:5000, 5% BSA in TBST	Anti-rabbit IgG, HRP-linked Antibody #7074 Cell Signaling Technology	1:2000-10,000, 5% BSA in TBST
PKM2 15822-1-AP	1:5000, 5% Skim milk in TBST	Anti-rabbit IgG, HRP-linked Antibody #7074 Cell Signaling Technology	1:2000 5%Milk in TBST
OCT4 sc-5279	1:5000 5% Skim milk in TBST	Donkey anti-mouse IgG-HRP sc-2314 Santa Cruz	1:10,000, 5% Skim milk in TBST

GAPDH sc-32233	1:10000 5% Skim milk in TBST	Donkey anti- mouse IgG- HRP sc-2314 Santa Cruz	1:10,000, 5% Skim milk in TBST
LAMIN A Ab26300	1:10000 5% Skim milk in TBST	Anti-rabbit IgG, HRP-linked Antibody #7074 Cell Signaling Technology	1:2000 5% Skim milk in TBST
∝-TUBULIN	1ug/mL 5% Skim milk in TBST	Anti-rabbit IgG, HRP-linked Antibody #7074 Cell Signaling Technology	1:2000 5% Skim milk in TBST
Ponceau Stain	0.1% (w/v), 5% acetic acid	N/A	N/A

3.3.6. Immunofluorescence and confocal microscopy:

Cells were plated onto 1.25mm thick coverslips coated with gelatin. When ready, cells were fixed with 2% paraformaldehyde (PFA) (EMS 15714) in PBS(+/+) for 10 minutes and washed for 5 minutes with chilled PBS(+/+). Following fixation, cells were permeabilized with 0.1% Triton X-100 (TX1568-1) in PBS(+/+) for 10 minutes and washed for 5 minutes with room temperature PBS(+/+). Cells were then blocked in 10% animal serum of the host-species of the secondary antibody, diluted in 0.1% PBS(+/+)-Tween 20 (PBST) for 30 minutes. Primary antibody was diluted in 10% animal serum of

the host-species of secondary antibody, diluted with 0.1% PBST overnight. Following primary incubation, cells were washed once for 5 minutes in PSB(+/+) before incubation in secondary antibody, diluted in 10% animal serum of the host-species of secondary antibody in 0.1% PBST for 1 hour. See supplementary Table 3.3. for primary and secondary antibody dilutions. Hoechst staining was completed where necessary (secondary only controls in the case of colocalization) for 5 minutes in PBS(+/+) followed two washes in PBS(+/+) for 5 minutes per wash. Cells were then mounted onto coverslips with Prolong Gold (P36934). Each experiment and their individual cell types included a secondary only control that was analysed with the same laser intensities as the treatment samples. Individual treatments were completed in three biological replicates. Primary and secondary antibodies and their concentrations are listed in Table 3.3.

Table 3.3 Immunofluorescence antibody and stain list:

Primary Antibody	**Concentration**	**Secondary Antibody**	**Concentration**
PKM1 15821-1-AP	1:50	555-G∝R A32732	10ug/mL
PKM2 15822-1-AP	1:50	555-G∝R A32732	10ug/ml
OCT4 sc-5279	1:50	488-G∝M A11001	1ug/ml
GAPDH sc-32233	1:50	488-G∝M A11001	1ug/ml
mNANOG AF2729	10ug/ml	488-D∝ G A11055	10ug/ml

SOX2 sc-365823	1:50	488-G∝M A11001	1ug/ml
HNF-4α K9218	1:500	488-G∝M A11001	1ug/ml
Phalloidin (647) A22287	4ug/mL	N/A	N/A
Hoechst (NucBlue)	3 drops/mL	N/A	N/A

3.3.7. Colocalization: co-occurrence and correlation by immunofluorescence:

Orthogonal projections of colony optimal slice generated image stacks were taken at 40x and 63x immersed in oil by a Zeiss LSM800 confocal microscope. Thresholds were set by optimized single stain samples (channel 488 - OCT4, GAPDH and channel 555 - PKM1, PKM2) exposed to all tested lasers and exposures. These exposures and laser intensities were tested against secondary antibody only controls. Double stains (PKM1/OCT4, PKM1/GAPDH, PKM2/OCT4 and PKM2/GAPDH) were taken in stacks containing full colonies and processed into orthogonal projections. The projections were then set to the predetermined co-localization thresholds (Costes thresholds were set when applicable) as set from the single stain controls. Each treatment was analysed in at least biological triplicate and each biological replicate was examined for several technical replicates of different colonies within their respective samples. Double stained treatments were compared for co-occurrence and correlation using Manders's Overlap Coefficient (MOC) and Pearson's Correlation Coefficient (PCC) respectively. MOC and PCC represent areas of spatial overlap and correlation between two controlled fluorophores

within regions of interest respectively. Areas of interest and negation of background information was completed using the outline tool to circle colonies and cells of interest while removing staining on MEFs and potential sources of non-specific binding. Additionally, individual cells were compared to whole colonies using airyscan processing under 63x magnification by confocal microscopy. This process increased the signal-to-noise ratio thus increasing signal resolution. Due to the intensity of light during an airyscan process, photobleaching prevented stacks of colonies at 63x when examining the individual cells. PCC values were categorised within set ranges to a classification, that included: correlation: very weak: -1 – -0.27, weak: -0.26 - 0.09, moderate: 0.1 – 0.48, strong: 0.49 – 0.84, and very strong: 0.85 – 1.0 (Zinchuk, Wu, and Grossenbacher-Zinchuk 2013). MOC values fall into set ranges of: overlap: very weak: 0 – 0.49, weak: 0.50 – 0.70, moderate: 0.71 – 0.88, strong: 0.89 – 0.97, very strong: 0.98 – 1.0 (Zinchuk, Wu, and Grossenbacher-Zinchuk 2013). Statistical analysis included application of a two tailed Mann-Whitney test of mean $\pm$SEM MOC and PCC scores run in at least three biological and technical replicates. All tested samples were stained and treated in the same manner and processed in the same session. Between microscopy sessions, single stain laser thresholds were retaken to account for any potential photobleaching. Statistics of PCC and MOC treatments relative to the positive reference represent a two-way ANOVA with Sidak's multiple comparisons test of mean$\pm$SEM PCC and MOC scores where $\propto$=0.05, n=3 biological replicates.

3.3.8. Nuclear and cytoplasmic fractionation.

Rapid isolation of nuclei from cells was completed using the REAP protocol (Nabbi and Riabowol 2015). mESCs were grown to 90% confluency on 10 cm dishes. Prior to collection, culture medium was aspirated, and the cells were washed with ice-cold PBS(-/-) with 1X Protease Inhibitor Cocktail Set 1 (Calbiochem 539131). The PBS was aspirated, and the dish was placed on ice where 1 mL of PBS was added, and the cells were scraped and centrifuged for 10 seconds at 10,000 rpm. The supernatant was aspirated and resuspended in 900 µL of ice-cold 0.1% Tergitol-NP-40 (Sigma NP-40S) in PBS(-/-) before being triturated 5 times. At this point a 300 µL total lysate sample was removed and stabilized in Laemmli buffer and vortexed. This sample was sonicated at 20 kHz for 2 pulses each 8 seconds long and the sample was then boiled for 1 minute and frozen prior to western blotting. The remaining NP-40 suspended sample was then centrifuged at 10,000 rpm for 10 seconds and 300 µL was removed as the cytoplasmic fraction. This fraction was stabilized in Laemmli buffer, vortexed and boiled for 1 minute before being frozen prior to western blotting. The remaining NP-40 suspended sample was aspirated and resuspended in 1 mL 0.1% NP-40 in PBS(-/-) with 1X Protease Inhibitor Cocktail Set 1 before centrifuged at 10,000 rpm. The supernatant was discarded, and the pellet resuspended in water and Laemmli buffer before sonication at 20 kHz for 2 pulses at 8 seconds per pulse. This nuclear fraction was boiled for 1 minute and frozen for future western blotting as described above. Antibody staining for control markers LAMIN A and ∝-TUBULIN and the markers of interest PKM1, pPKM2, and PKM2 were compared relative to total lane protein content by Ponceau staining (0.1% Ponceau, 5% acetic acid). Each cell type's mean densitometry ± SEM was analyzed by

applying a one-way ANOVA with Tukey's multiple comparison test or unpaired, two tailed t-test respectively with 3 biological replicates.

3.4.0. Results:

3.4.1. Characterization of naïve mESCs transitioning towards a primed pluripotent state.

By 72 hours following the removal of mouse LIF and 2i supplementation with the addition of Fgf-2/Activin A (FA media), mESCs approximating a primed-like pluripotent state underwent an apoptotic event with the resulting colonies transitioning to a flattened morphology (Supplementary Figure 3.01.). The mESCs by 72 hours had transitioned to mEpiLCs (primed-like state) and the mESCs, mEpiLCs, and mEpiSCs showed homogenous colony expression of the pluripotency associated genes NANOG, OCT4, and SOX2 (Figure 3.01.A). Secondary antibody only controls confirmed the specificity of the immunofluorescence staining (Supplementary Figure 3.02.).

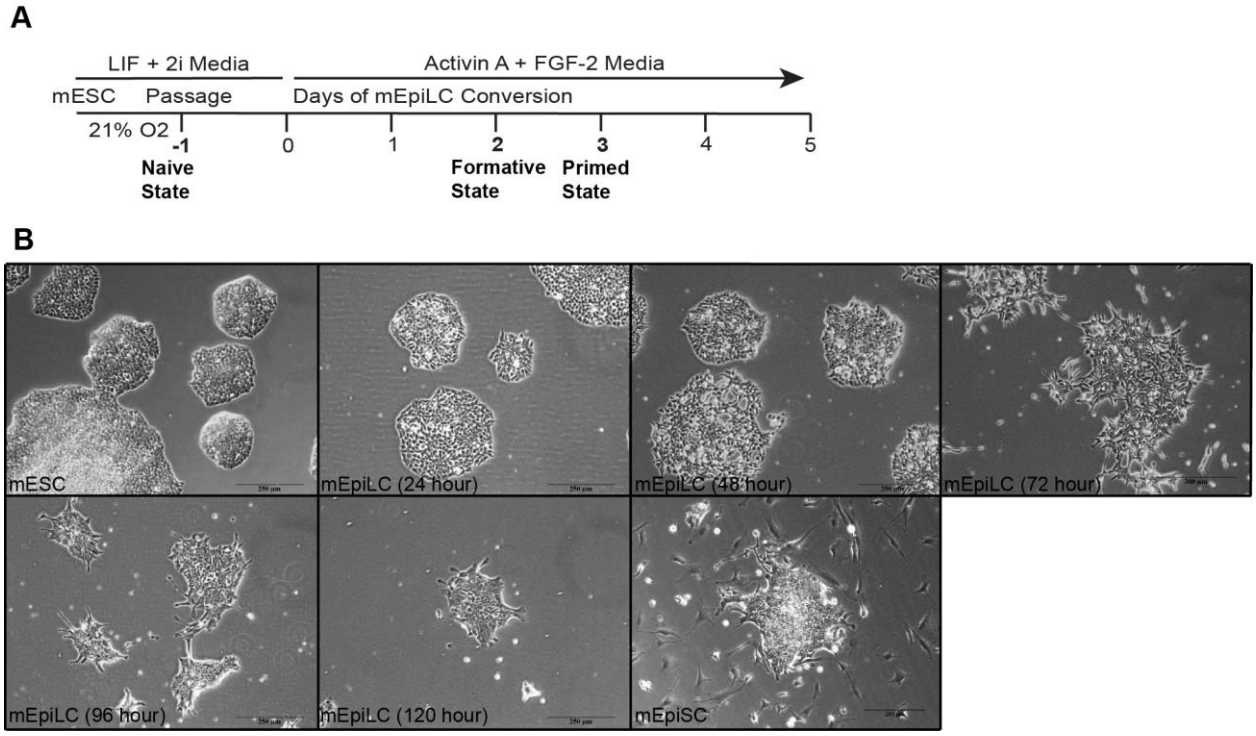

Supplementary Figure 3.01. mEpiLC generation and mPSC cell morphology.

(A) Schematic depicting the generation of mEpiLCs from mESCs and the associated pluripotent states. (B) Phase contrast microscopy of mESCs, mEpiLCs (24, 48, 72, 96, and 120 hours) and mEpiSCs grown on MEFs. Images take using 10x Magnification and scale bars represent 250 and 300 μm (as indicated)**.**

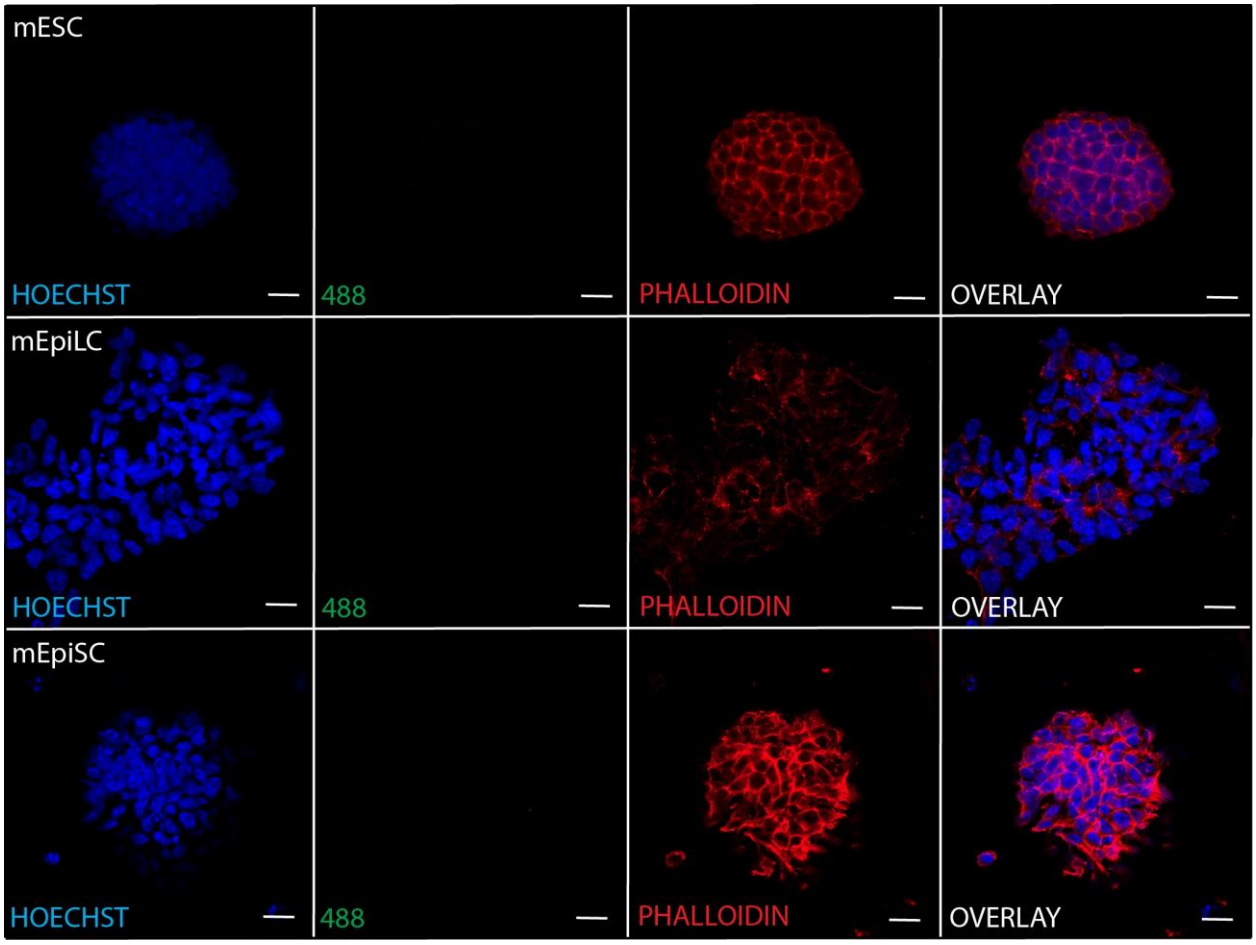

Supplementary Figure 3.02. Secondary antibody only immunofluorescence controls for pluripotency markers.

Immunofluorescence of mESC, mEpiLC, and mEpiSC stained for Hoechst, phalloidin and the secondary antibodies (Table 3.3.) used throughout this study, assessed by confocal microscopy. Images taken using 40x magnification and scale bars represent 20 μm.

Assessment of stage specific transcript abundance of naïve, formative, and primed markers verified the pluripotent state of mESCs, mEpiLCs, and mEpiSCs, respectively (Figure 3.01.). The naïve pluripotent associated genes: Rex1, Esrrb, Pecam, Tcfcp2l1, Klf2, Klf4, Dppa3, and Klf5 all underwent a significant ($p<0.05$) reduction in transcript abundance in mEpiLCs and mEpiSCs relative to mESCs (Figure 3.01.B). The transcript abundance of formative pluripotent associated genes; Lef1, Dnmt3, and Pou1fc were significantly ($p<0.05$) increased in mEpiLCs compared to mESCs with Dnmt3 and Pou1fc mRNAs also significantly ($p<0.05$) elevated in mEpiLCs over that observed in mEpiSCs (Figure 3.01.B). The transcript abundance of primed pluripotent state associated markers Zic2, T(Brachyury), and Cer1 were significantly ($p<0.05$) increased in the mEpiSCs relative to the mESCs (Figure 3.01.B).

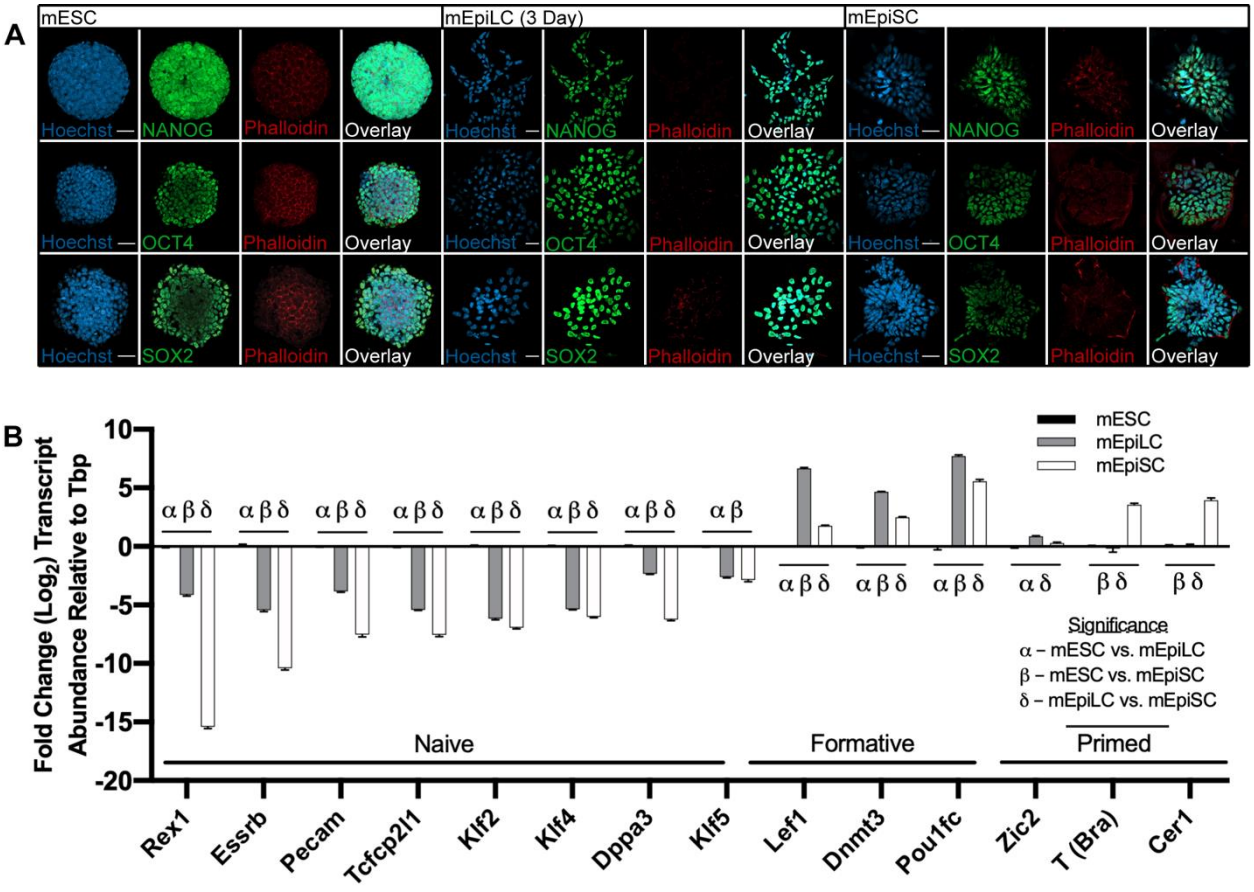

Figure 3.01. mESC, mEpiLC, and mEpiSC populations transcript abundance for pluripotency genes.

(A) Immunofluorescence of mESC, mEpiLC, and mEpiSC stained with Hoechst (blue), phalloidin (red) and the core pluripotency associated markers (green): NANOG, OCT4, SOX2 assessed by confocal microscopy. Images taken using 40x magnification and scale bars represent 20 μm. (B) Histogram of transcript abundance of naïve, formative, and primed pluripotent associated genes relative to Tbp and normalized to mESCs. Error bars represent standard error of the mean (SEM), n=3, *p<0.05. Statistics for the transcript abundance study represent a two-way ANOVA with Tukey's multiple comparisons of mean$\pm$SEM where $\propto$=0.05, n=3 biological replicates run in technical triplicate.

3.4.2. PKM1/2 protein abundance and localization fluctuate in naïve mESCs, primed-like mEpiLCs, and primed mEpiSCs.

There was a significant ($p<0.05$) increase in PKM1 and PKM2 protein abundance relative to β-ACTIN in formative primed-like mEpiLCs cultured in Fgf-2/Activin A (FA medium) compared to naïve mESCs or primed mEpiSCs (Figure 3.02.A). The ratio of phosphorylated (Tyr105), homodimeric conformation of PKM2 to total PKM2 protein abundance relative to β-ACTIN significantly ($p<0.05$) decreased when naïve mESCs were transitioned to formative, primed-like mEpiLCs. However, no significant ($p>0.05$) difference in the ratio of PKM1 to PKM2 protein abundance relative to β-ACTIN was observed in any pluripotency cell state cultures investigated. PKM1 and PKM2 protein fluorescence were detected in the cytoplasm and nuclei of mESCs, mEpiLCs, and mEpiSCs as demonstrated by morphological comparison with Hoechst and rhodamine phalloidin stains representing nuclear and cytoskeletal compartments respectively (Figure 3.02.B). Secondary antibody only controls confirmed the specificity of the PKM1/2 immunofluorescence staining (Supplementary Figure 3.04.).

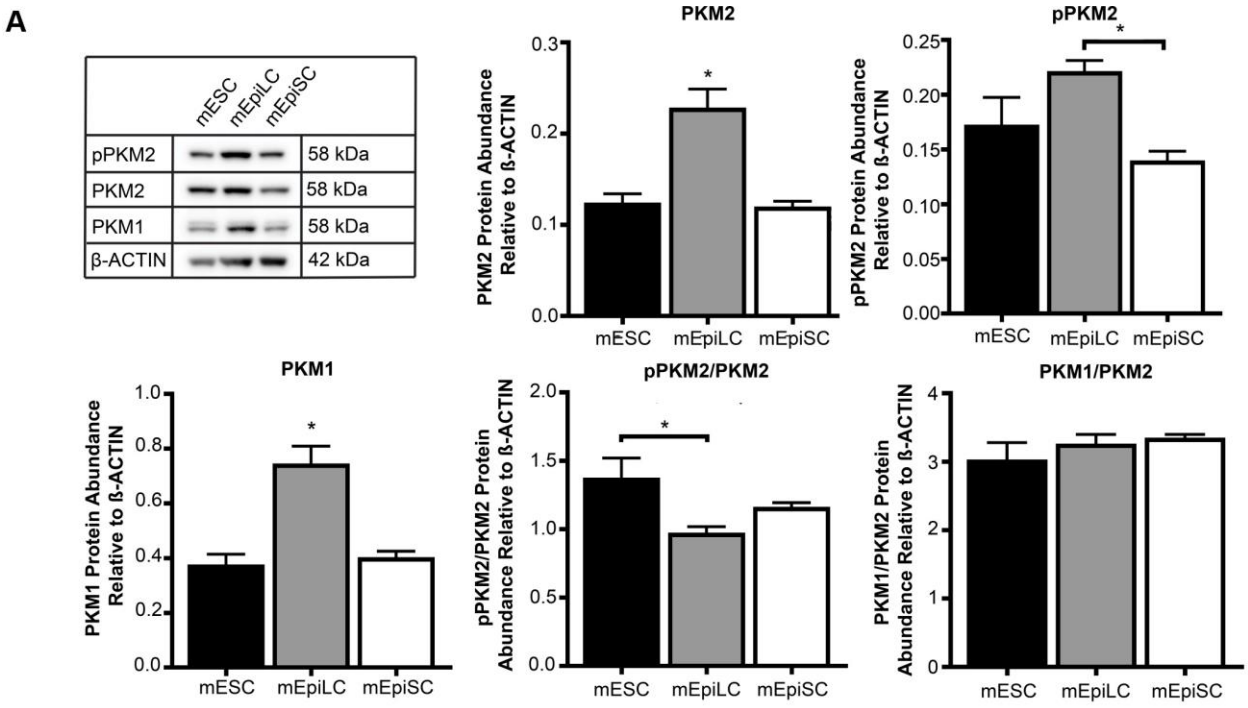
A
mESC
mEpiLC
mEpiSC
pPKM2
PKM2
PKM1
β-ACTIN
58 kDa
58 kDa
58 kDa
42 kDa
PKM2
PKM2 Protein Abundance Relative to ß-ACTIN
pPKM2
pPKM2 Protein Abundance Relative to ß-ACTIN
PKM1
PKM1 Protein Abundance Relative to ß-ACTIN
pPKM2/PKM2
pPKM2/PKM2 Protein Abundance Relative to ß-ACTIN
PKM1/PKM2
PKM1/PKM2 Protein Abundance Relative to ß-ACTIN
mESC
mEpiLC
mEpiSC

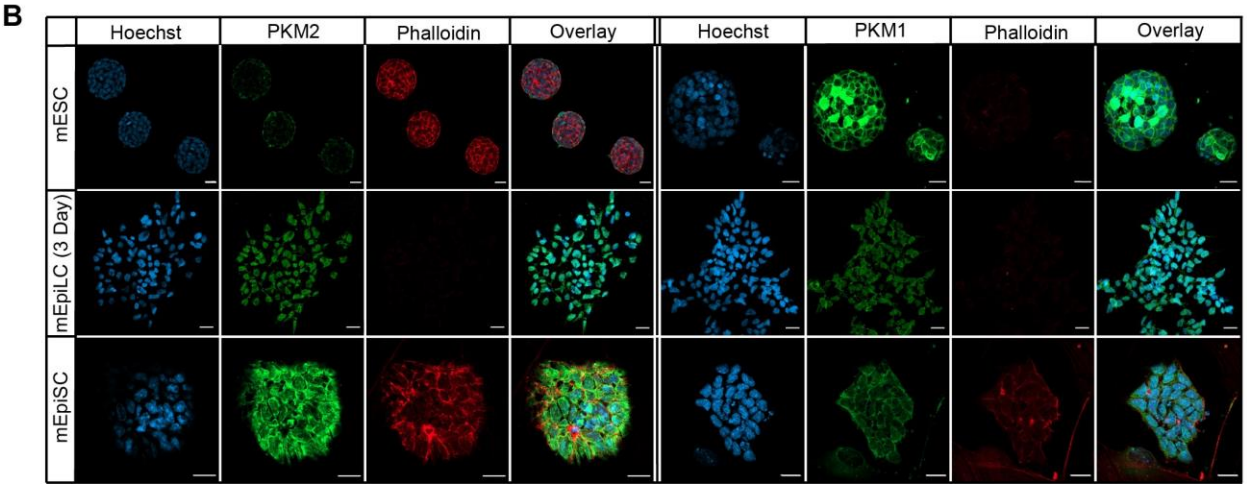
B
Hoechst
PKM2
Phalloidin
Overlay
Hoechst
PKM1
Phalloidin
Overlay
mESC
mEpiLC (3 Day)
mEpiSC

Figure 3.02. Distinct PKM1 and PKM2 protein profiles in mESCs, mEpiLCs, and mEpiSCs.

A) Histogram comparing protein abundance of PKM1, PKM2, and pPKM2 relative to β-ACTIN in mESCs, mEpiLCs, and mEpiSCs in total protein lysates. Error bars represent SEM, n=3, *p<0.05. B) Immunofluorescence of mESC, mEpiLC, and mEpiSC stained for Hoechst (blue), phalloidin (red) and the metabolic markers: PKM1 and PKM2 (green) assessed by confocal microscopy. Images taken using 40x magnification and scale bars represent 20 μm. Error bars represent SEM, n=3, *p<0.05. Statistics represent a one-way ANOVA with Tukey's multiple comparisons of mean$\pm$SEM MOC and PCC scores run in n=3 biological replicates.

3.4.3. Qualitative PKM1/2 nuclear translocation in naïve mESCs, formative mEpiLCs, and primed mEpiSCs

Following the first indication of nuclear PKM1/2 in naïve mESCs, a series of pre-colocalization imaging studies were completed as a precursor for Chapters 2 and 3. Nuclear PKM1/2 was not always clearly visible in colonies or individual cells, this led us to taking a 3-dimension (3D) approach to imaging. Using a confocal microscope, individual slices of fluorescent images were stacked to generate a 3D structure of entire colonies of mESCs and mEpiSCs for PKM1 and PKM2 (Figure 3.03.). Visually examining the 3D architecture of mESCs stained for PKM1 provide our first truly promising evidence of nuclear PKM1 translocation as cells closer to the upper layers of the colony exhibit clear nuclear localization.

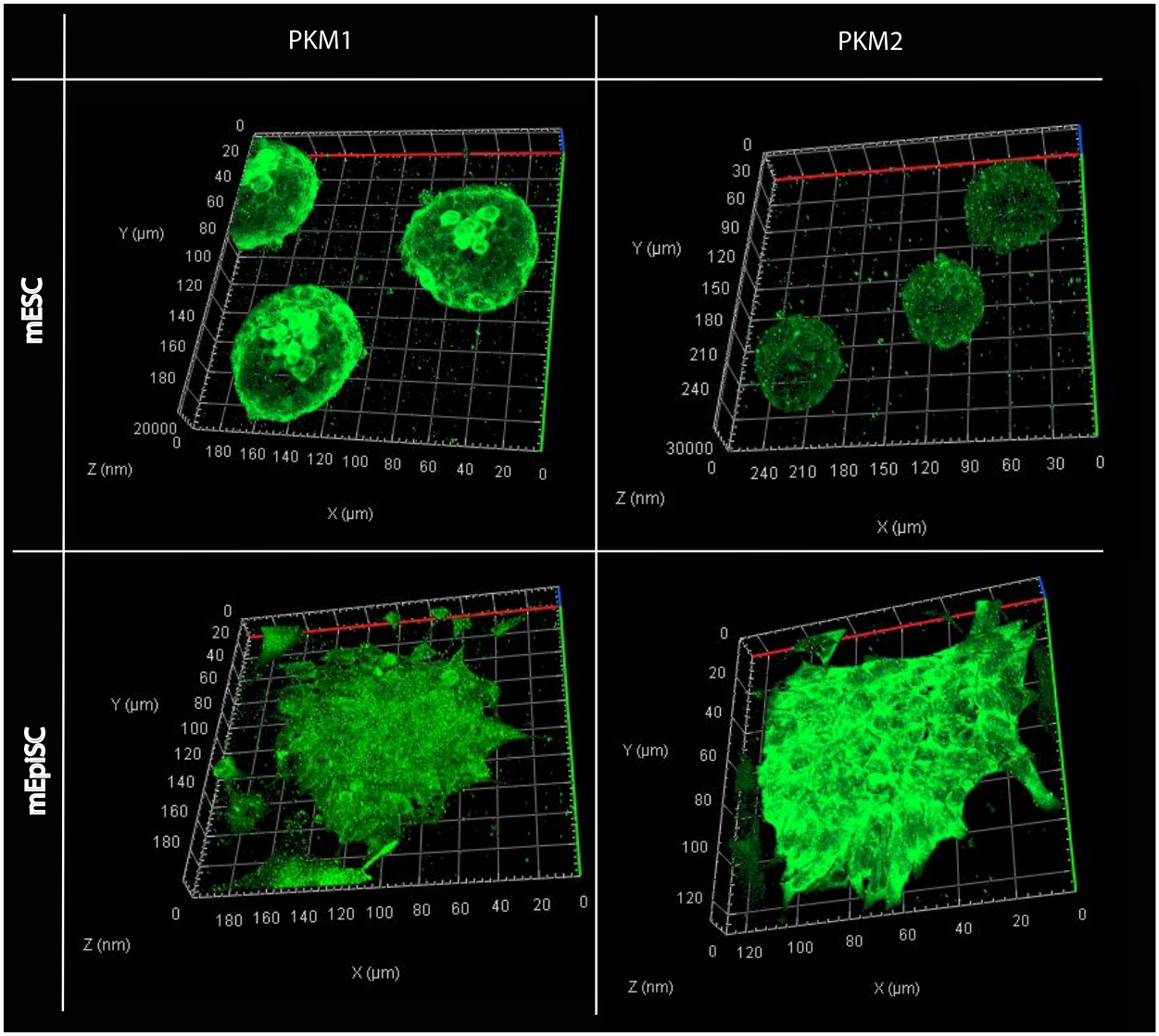

Figure 3.03. 3D rendered immunofluorescence imaging of mESC and mEpiSC PKM1 and PKM2 indicate potential nuclear localization patterns.

Colonies of mESCs and mEpiSCs stained for PKM1 and PKM2 demonstrate a 3D rendering of localization patterns within cells. Nuclear localization of PKM1 in mESCs is visually demonstrated in cells of the upper layers of the colony. Scale bars are depicted on all 3 axes and imaging was completed at 40x objective; scale bars depict measurements in µm.

To further promote the notion of nuclear translocation of PKM1/2 in mESCs and mEpiSCs, I utilized the pharmacological agent Leptomycin B. Leptomycin B is an antibiotic and the first agent found that works to block nuclear export in cells (Wolff, Sanglier, and Wang 1997). As Leptomycin B doesn't impede nuclear import, it served as a useful tool in the study of nuclear PKM1/2 translocation. Leptomycin was first assessed in a time course (Supplementary Figure 3.03, Figures 3.04., and 3.05.). As small colonies visually appeared to show the most consistent nuclear PKM1, I examined the influence of adding the nuclear export blocking agent Leptomycin B in mESCs over 3, 6, 9, and 12 hours comparing no Leptomycin to 2 ng/mL treatments by fluorescence imaging. Based on these images, there is a qualitative increase in nuclear PKM2 at 12 hours (Figure 3.04.) and PKM1 throughout the series (Figure 3.05.).

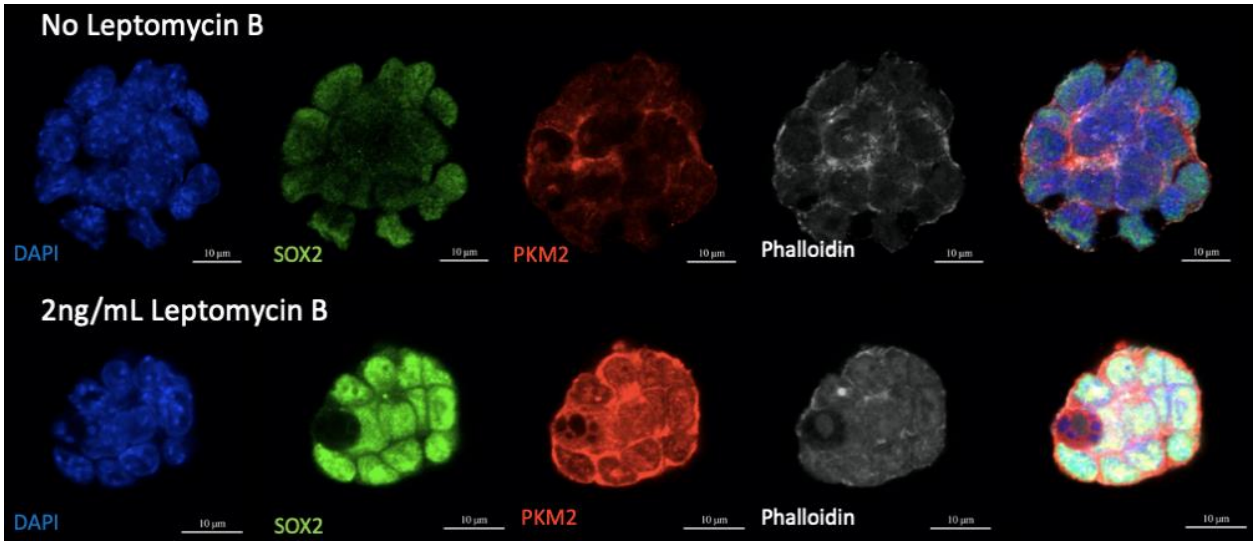

Figure 3.04. Nuclear translocation of PKM2 following Leptomycin B treatment.

Elevated PKM2 nuclear translocation in naïve mESCs were treated with Leptomycin B to block nuclear export over 12 hours. Cells were stained for the nuclear localized pluripotency marker SOX2, DAPI, PKM2, and Phalloidin. Scale bars represent 10 μm. Imaging was completed at 63x objective.

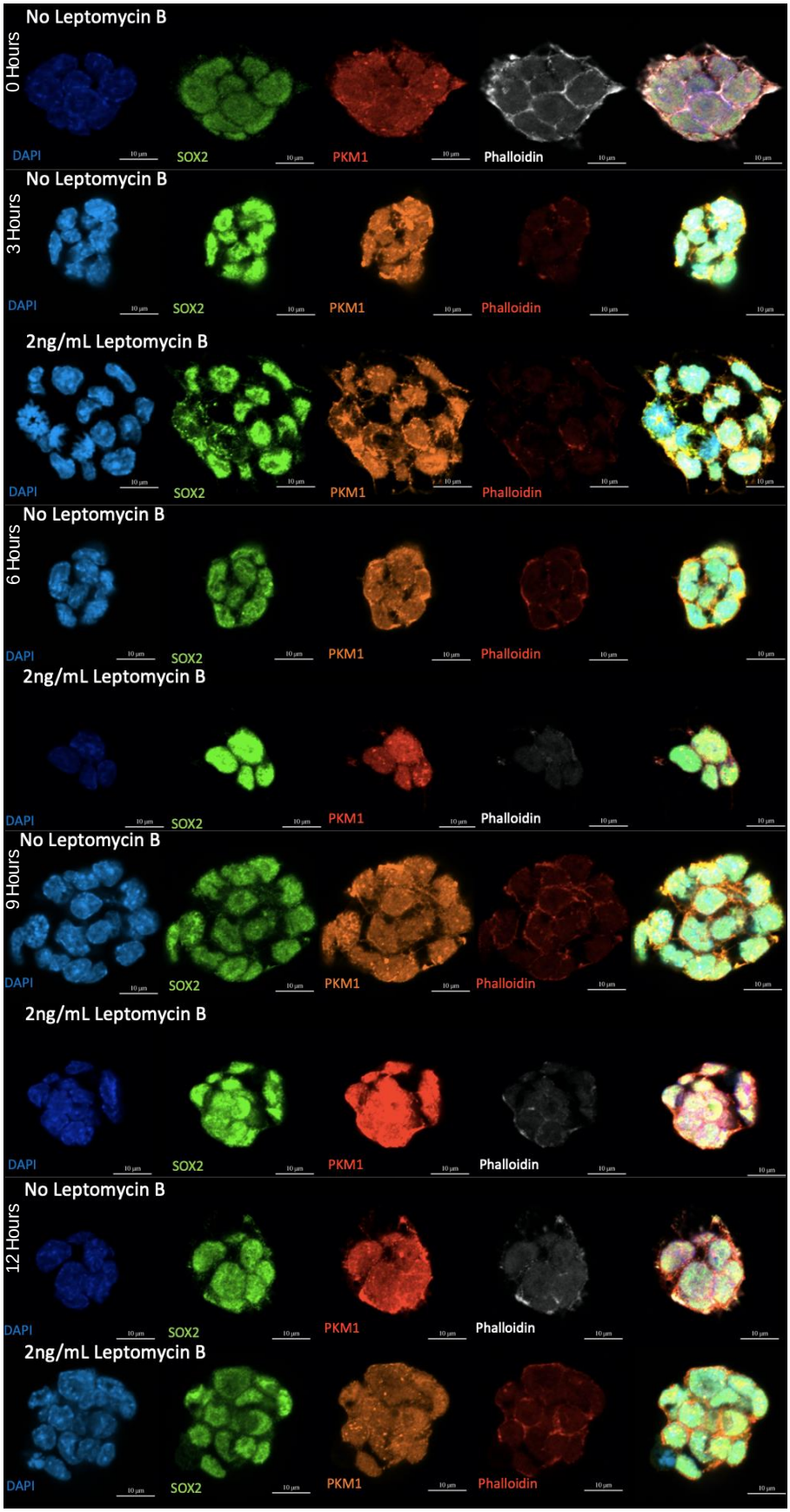
No Leptomycin B
0 Hours
DAPI
SOX2
PKM1
Phalloidin
No Leptomycin B
3 Hours
DAPI
SOX2
PKM1
Phalloidin
2ng/mL Leptomycin B
DAPI
SOX2
PKM1
Phalloidin
No Leptomycin B
6 Hours
DAPI
SOX2
PKM1
Phalloidin
2ng/mL Leptomycin B
DAPI
SOX2
PKM1
Phalloidin
No Leptomycin B
9 Hours
DAPI
SOX2
PKM1
Phalloidin
2ng/mL Leptomycin B
DAPI
SOX2
PKM1
Phalloidin
No Leptomycin B
12 Hours
DAPI
SOX2
PKM1
Phalloidin
2ng/mL Leptomycin B
DAPI
SOX2
PKM1
Phalloidin

Figure 3.05. Nuclear translocation of PKM1 following Leptomycin B treatment time course.

Progression of nuclear translocation of PKM1 in mESCs with the addition of Leptomycin B to hinder nuclear export over 12 hours. Cells were stained for the nuclear localized pluripotency marker SOX2, DAPI, PKM1, and Phalloidin. Scale bars represent 10 μm. Imaging was completed at 63x objective.

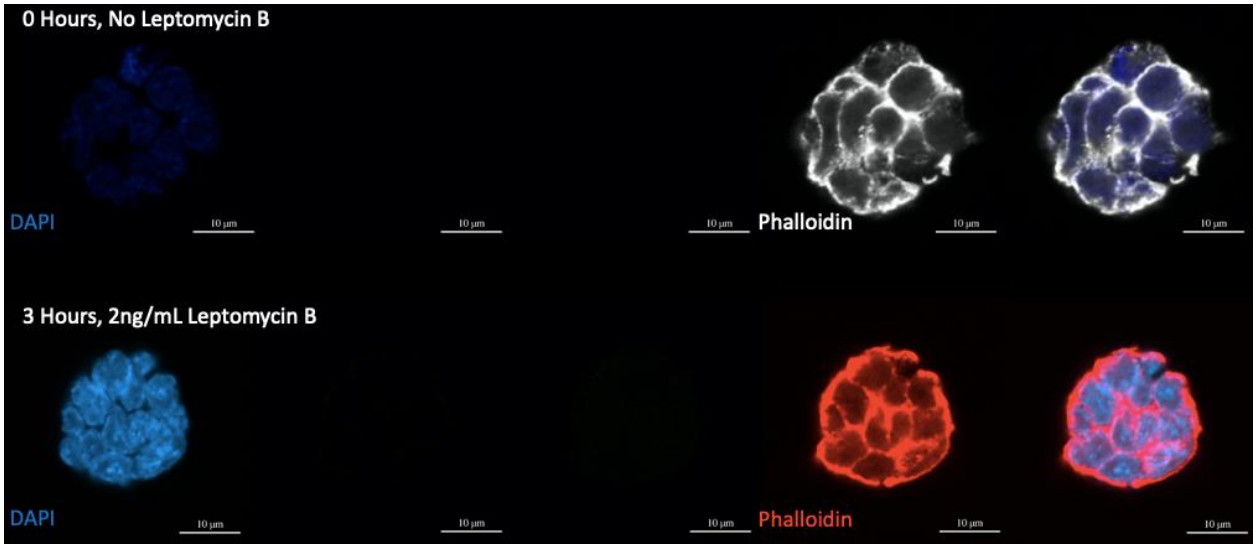

Supplementary Figure 3.03. No Primary controls for small colony nuclear localization imaging.

No primary controls of mESCs grown in small colonies stained with DAPI and Phalloidin. Scale bars represent 10 μm. Imaging was completed at 63x objectives.

The concentration of Leptomycin B was then increased to better demonstrate nuclear localization in larger colonies. Examining mESCs at 5 and 10 hours following the addition of 20 µg/mL of Leptomycin B showed clearer nuclear translocation of PKM1 at 10 hours relative to no leptomycin B treatment (Figure 3.06.). The addition of nuclear and cytoplasmic markers further allowed for a comparison of nuclear translocation. SOX2, Hoechst, and Phalloidin made comparing nuclear PKM1 substantially more evident and further promoted the idea of adding nuclear references to (see Chapter 2 colocalization methodology). It was clear that blocking nuclear export in these cells was detrimental to their viability and not a long-term solution.

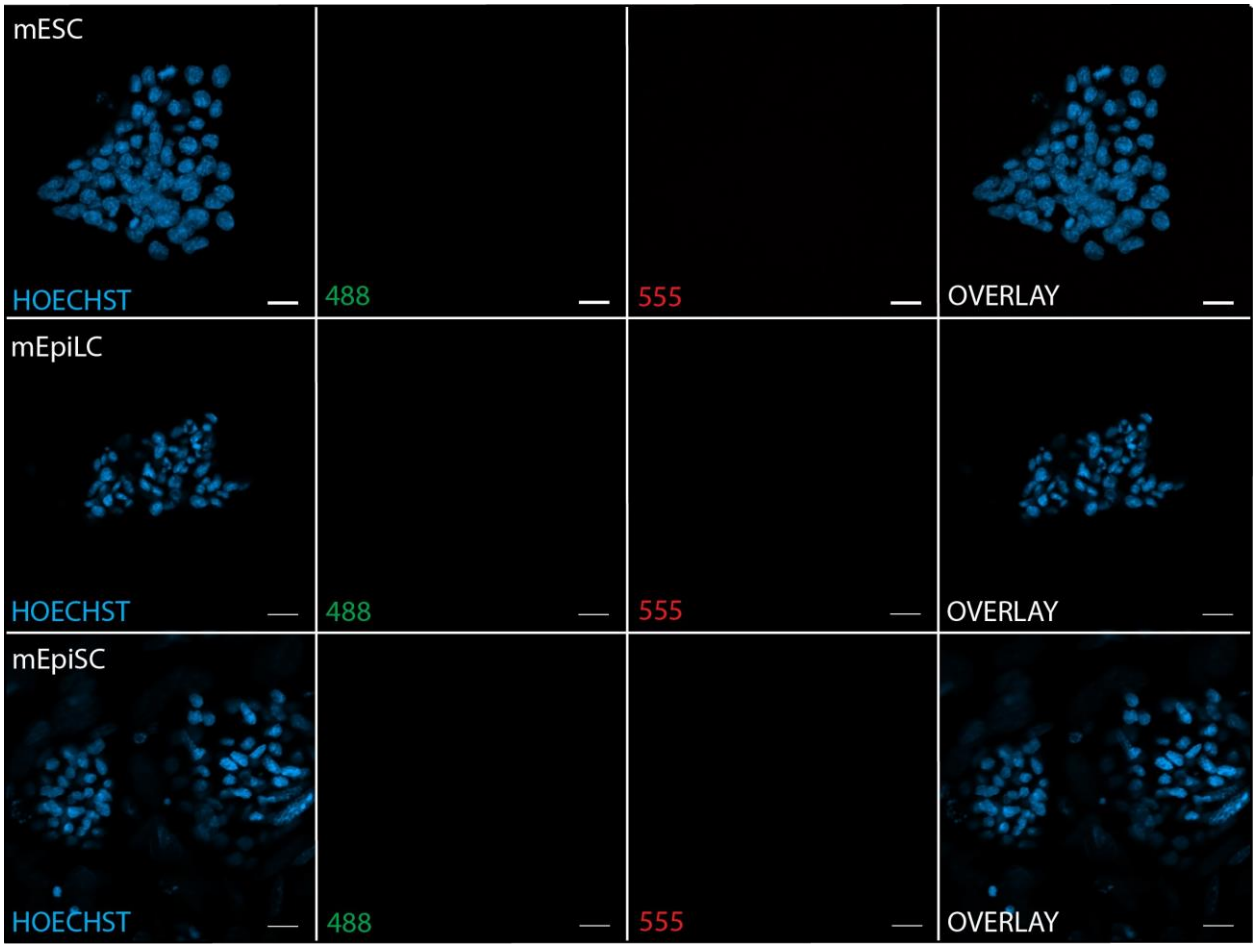

Supplementary Figure 3.04. Secondary antibody only immunofluorescence controls for PKM1 and PKM2 and colocalization study.

Immunofluorescence microscopy of mESC, mEpiLC and mEpiSC stained for Hoechst, phalloidin and the secondary antibodies (Table 3.3.) used throughout this study, assessed by confocal microscopy. Images taken using 40x magnification and scale bars represent 20 μm.

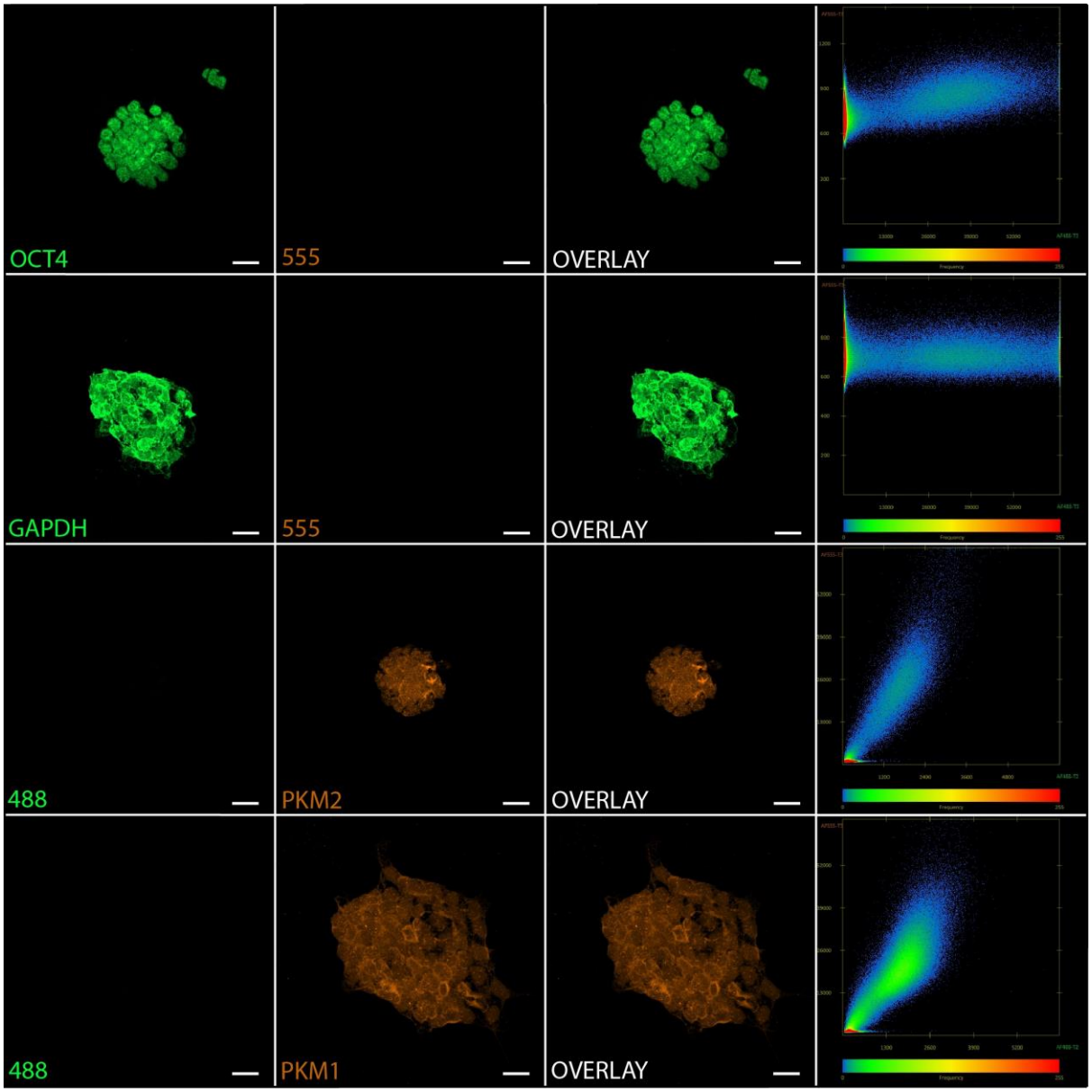

Supplementary Figure 3.05. mESC PKM1, PKM2, OCT4, and GAPDH colocalization settings.

Immunofluorescence microscopy of mESCs demonstrating single fluorescence images for PKM1, PKM2, OCT4, and GAPDH along with their respective thresholds. Images taken using 40x magnification and scale bars represent 20 μm. Confocal laser channels labelled as 488 and 555 corresponding to treatments incubated with OCT4/GAPDH and PKM1/PKM2 respectively.

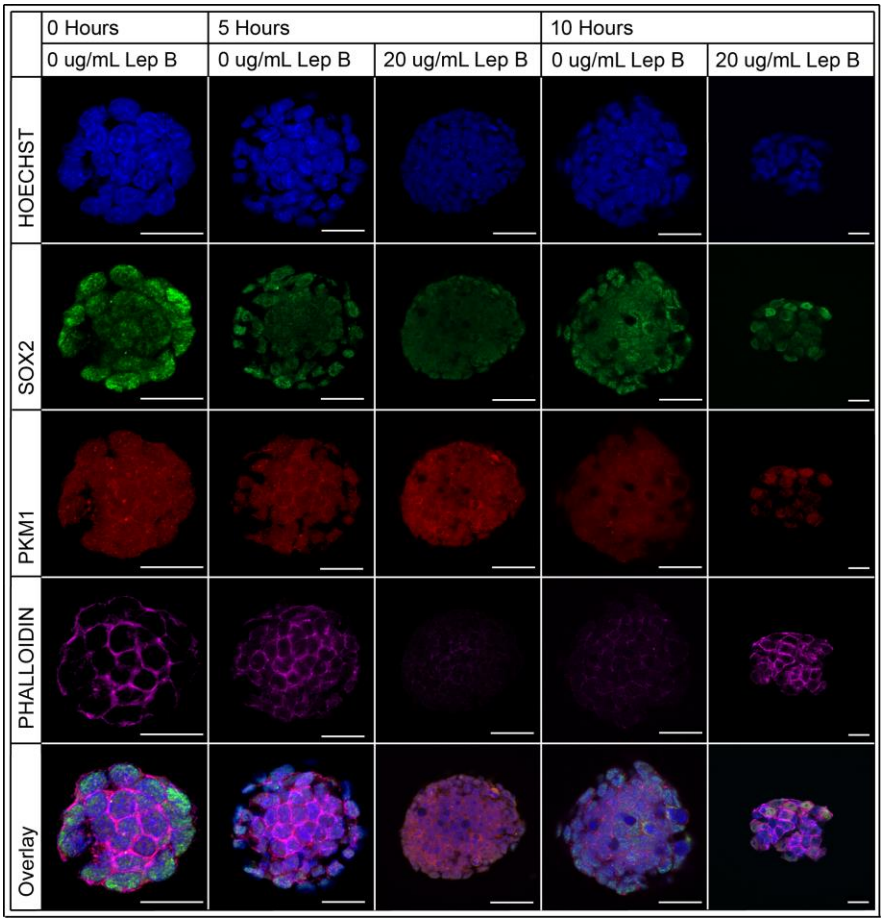

Figure 3.06. Time course fluorescence imaging of mESCs treated with Leptomycin B prevent nuclear export of PKM1.

The addition of the nuclear export blocking agent Leptomycin B to mESCs at 20 µg/mL over 5 and 10 hours demonstrates that PKM1 translocated to the nuclei. Scale bars represent 20 µm and microscopic imaging was completed using a 63x objective.

Finally, I examined both naïve mESCs and primed mEpiSCs for PKM1 and PKM2 protein localization by fluorescence imaging with the addition of 20 μg/ml Leptomycin B (Figure 3.07.). This imaging provided evidence that not only naïve mESCs experience nuclear translocation, but primed mEpiSCs, exhibiting the aerobic glycolytic metabolic preference also have a degree of nuclear PKM1 and PKM2 nuclear translocation. I originally hypothesized that primed mEpiSCs would have nuclear PKM2 as this localization pattern is indicative of dimeric pPKM2 and the Warburg Effect (Weiwei Yang et al. 2012; W. Zhou et al. 2012). Nuclear translocation of PKM1 and PKM2 in either end of the pluripotent continuum naturally led us to investigate what happens in between the naïve and primed states, and ultimately devise a better system of colocalization methodology.

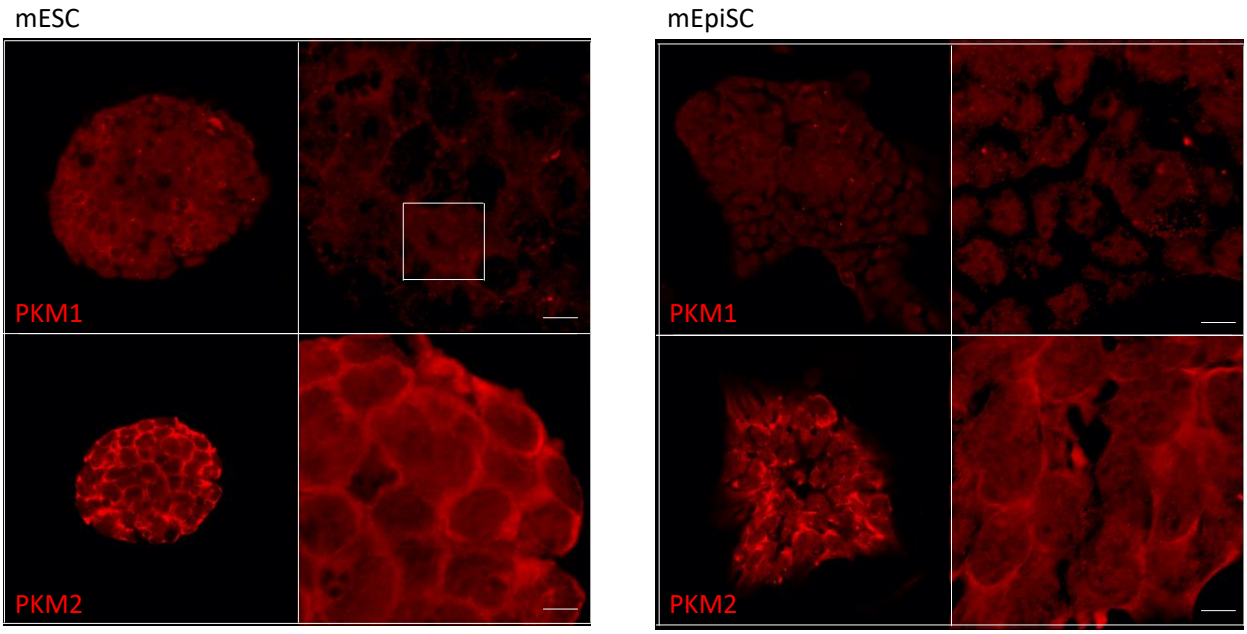

Figure 3.07. Initial results indicating potential nuclear localization of PKM1 in mESCs.

Naïve and primed mPSCs appear to show nuclear localization of the metabolic proteins PKM1 and PKM2. This was an early finding following the addition of Leptomycin B for a nuclear export blockade to demonstrate nuclear translocation of PKM1. Cultured mESCs and mEpiSCs treated with 20 μg/mL of Leptomycin B for 5 hours, stained for PKM1 and PKM2. Scale bars represent 5 μm and imaged at 40x and 63x objectives.

3.4.4. Subnuclear localization of PKM1 and PKM2 with OCT4 within naïve mESCs.

To authenticate the subcellular immunofluorescence results (Figure 3.02.B), a colocalization study investigating spatial co-occurrence or overlap and correlation of PKM1 and PKM2 with the nuclear localized marker OCT4 and the cytoplasmic localized marker GAPDH using confocal microscopy was conducted. Colocalization of immunofluorescent spatial overlap and correlation was compared using Manders's overlap coefficient (MOC) and Pearson's correlation coefficient (PCC), respectively on orthogonal projections with background pixels removed from quantification (Dunn, Kamocka, and McDonald 2011). Using these methods, total mESC colony colocalization of PKM1 and PKM2 with OCT4 and GAPDH showed a high instance of spatial overlap to both marker proteins with a significantly ($p<0.05$) greater overlap to nuclear OCT4 (Figure 3.08.A, B). However, PKM1 displayed significantly ($p<0.05$) higher correlation to OCT4 localization compared to GAPDH (Figure. 3.08. B). Using the standards set by Zinchuk *et al.,* PKM1 and PKM2 exhibited a 'moderate' correlation and a 'strong' overlap to both OCT4 and GAPDH localization (PCC range: moderate = 0.1-0.48, MOC range: strong = 0.89-0.97) (Zinchuk, Wu, and Grossenbacher-Zinchuk 2013). By increasing the signal-to-noise ratio through airyscan processing, the colocalization resolution was improved and the analysis was applied to individual mESCs. Individual cell analysis aligned closely with the colony analysis by indicating a strong correlation for spatial co-occurrence for PKM1 and PKM2 in mESCs (Supplementary Figure 3.06.A, B). Immunofluorescence controls and colocalization thresholds are shown in Supplementary Figure 3.05.

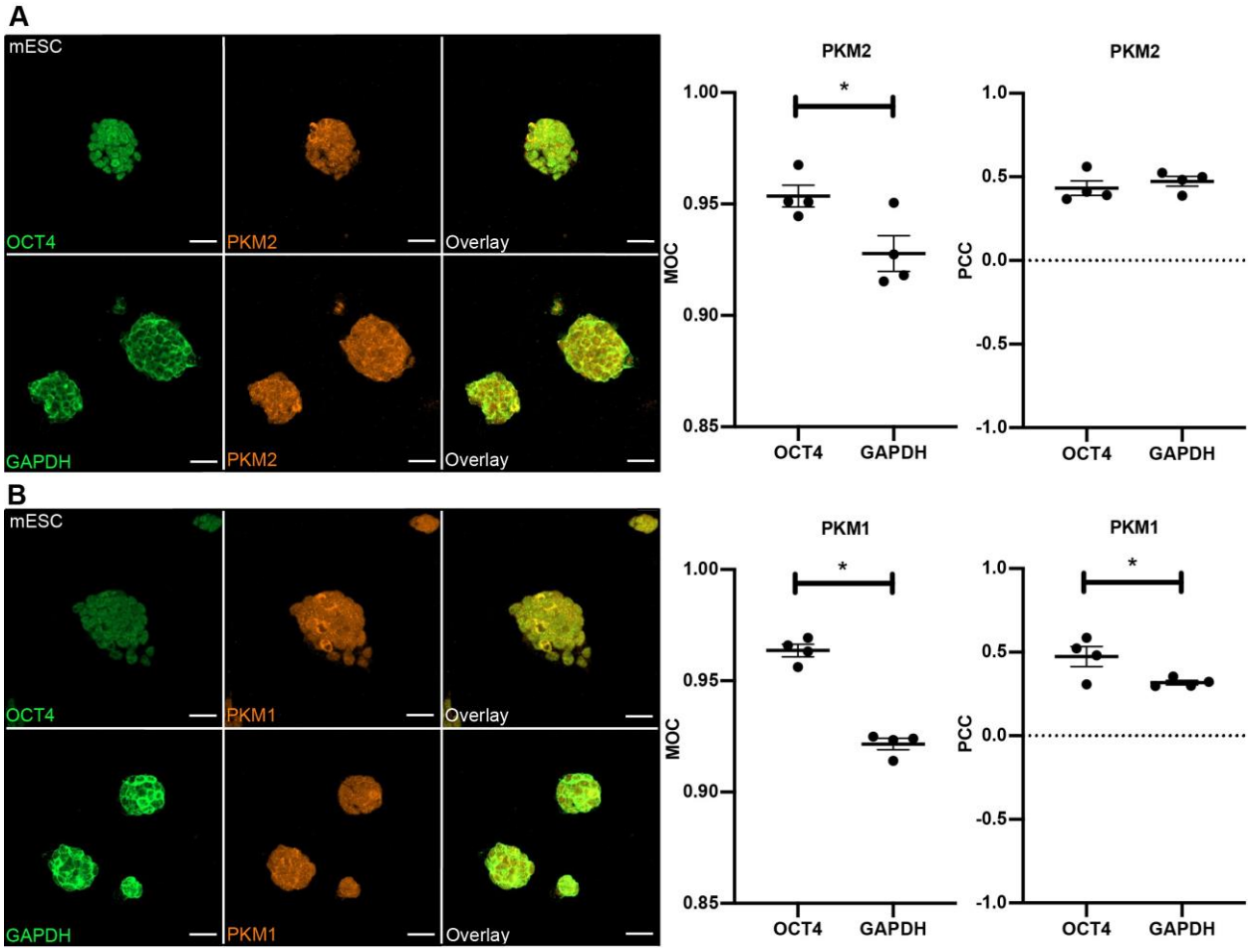

Figure 3.08. PKM1 and PKM2 are translocated to the nuclei of mESCs and both PKM1 and PKM2 are associated with OCT4 and GAPDH localization.

(A) Immunofluorescence of mESCs stained for OCT4 (green), GAPDH (green), and PKM2 (orange) for a confocal, colocalization analysis. Images taken using 40x magnification and scale bars represent 20 μm. Histogram comparing PKM2 to OCT4 and GAPDH spatial localization by Manders's Overlap Coefficient (MOC) and Pearson's Correlation Coefficient (PCC). Error bars represent SEM, n=3, *p<0.05. (B) Immunofluorescence of mESCs stained for OCT4 (green), GAPDH (green), and PKM1 (orange) for a confocal, colocalization analysis. Images taken using 40x magnification and scale bars represent 20 μm. Histogram comparing PKM1 to OCT4 and GAPDH spatial localization by Manders's Overlap Coefficient (MOC) and Pearson's Correlation Coefficient (PCC). Error bars represent SEM, n=3, *p<0.05. Statistics represent a two tailed Mann-Whitney test of mean$\pm$SEM MOC and PCC scores run in n=4 biological replicates and at least a technical triplicate.

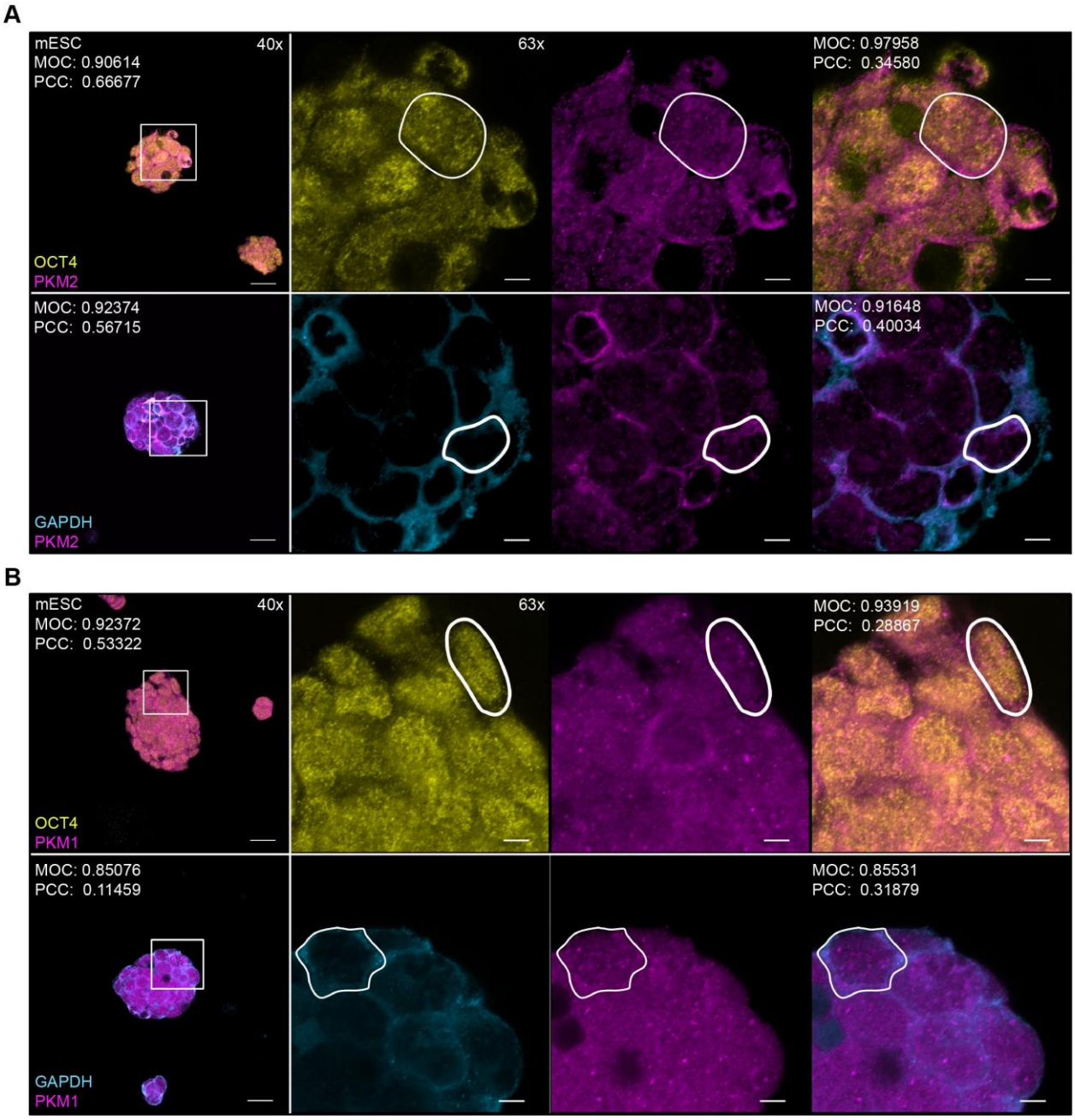
A
mESC
MOC: 0.90614
PCC: 0.66677
40x
63x
MOC: 0.97958
PCC: 0.34580
OCT4
PKM2
MOC: 0.92374
PCC: 0.56715
MOC: 0.91648
PCC: 0.40034
GAPDH
PKM2
B
mESC
MOC: 0.92372
PCC: 0.53322
40x
63x
MOC: 0.93919
PCC: 0.28867
OCT4
PKM1
MOC: 0.85076
PCC: 0.11459
MOC: 0.85531
PCC: 0.31879
GAPDH
PKM1

Supplementary Figure 3.06. PKM1/2 colocalization within individual cells of mESC colonies.

Immunofluorescence microscopy of mESC colonies, colocalization analysis compared MOC and PCC of the total colony to that of a single cell. (A) PKM2 staining versus OCT4 and GAPDH in mESCs comparing orthogonal projections of whole colonies to individual cells by airyscan processing. (B) PKM1 staining versus OCT4 and GAPDH in mESCs comparing orthogonal projections of whole colonies to individual cells by airyscan processing. Images taken using 40x magnification with scale bars represent 20 μm and 63x magnification with scale bars representing 5 μm. Square boxes indicate areas of interest from the 40x for 63x magnification. White outlines around cells represents the area of analysis of the airyscanned images.

3.4.5. Subnuclear localization of PKM1 and PKM2 with Oct4 in mEpiLCs.

Immunofluorescence colocalization was quantified in mEpiLCs cultured in transitioning FA medium at 48 hours via confocal microscopy of orthogonal projections and airyscan processing. These cells represent the formative pluripotent state. I applied total colony and single cell colocalization analysis as described above, and observed co-occurrence of PKM1 and PKM2 compared to OCT4 and GAPDH with a significantly ($p<0.05$) greater PKM1 spatial co-occurrence to OCT4 (Figure 3.09.A, B). Only PKM1 localization was correlated with both OCT4 and GAPDH localization in these cultures (Figure 3.09.B). PKM1 exhibited a 'strong' correlation and a 'strong' overlap with OCT4 localization, a 'moderate' correlation and a 'strong' overlap to GAPDH localization (PCC range: strong = 0.49-0.84, MOC range: strong = 0.89-0.97) (Zinchuk, Wu, and Grossenbacher-Zinchuk 2013). PKM2 displayed a 'weak' correlation to both OCT4 and GAPDH with a 'strong' overlap to OCT4 and a 'moderate' overlap to GAPDH (PCC range: weak = -0.26-0.09, MOC range: moderate = 0.71-0.88, strong = 0.89-0.97). Using airyscan processing, individual cells of mEpiLC colonies displayed consistent correlation and spatial overlap compared to the colony (Supplementary Figure 3.08. A, B). Immunofluorescence controls and colocalization thresholds are shown in Supplementary Figure 3.07.

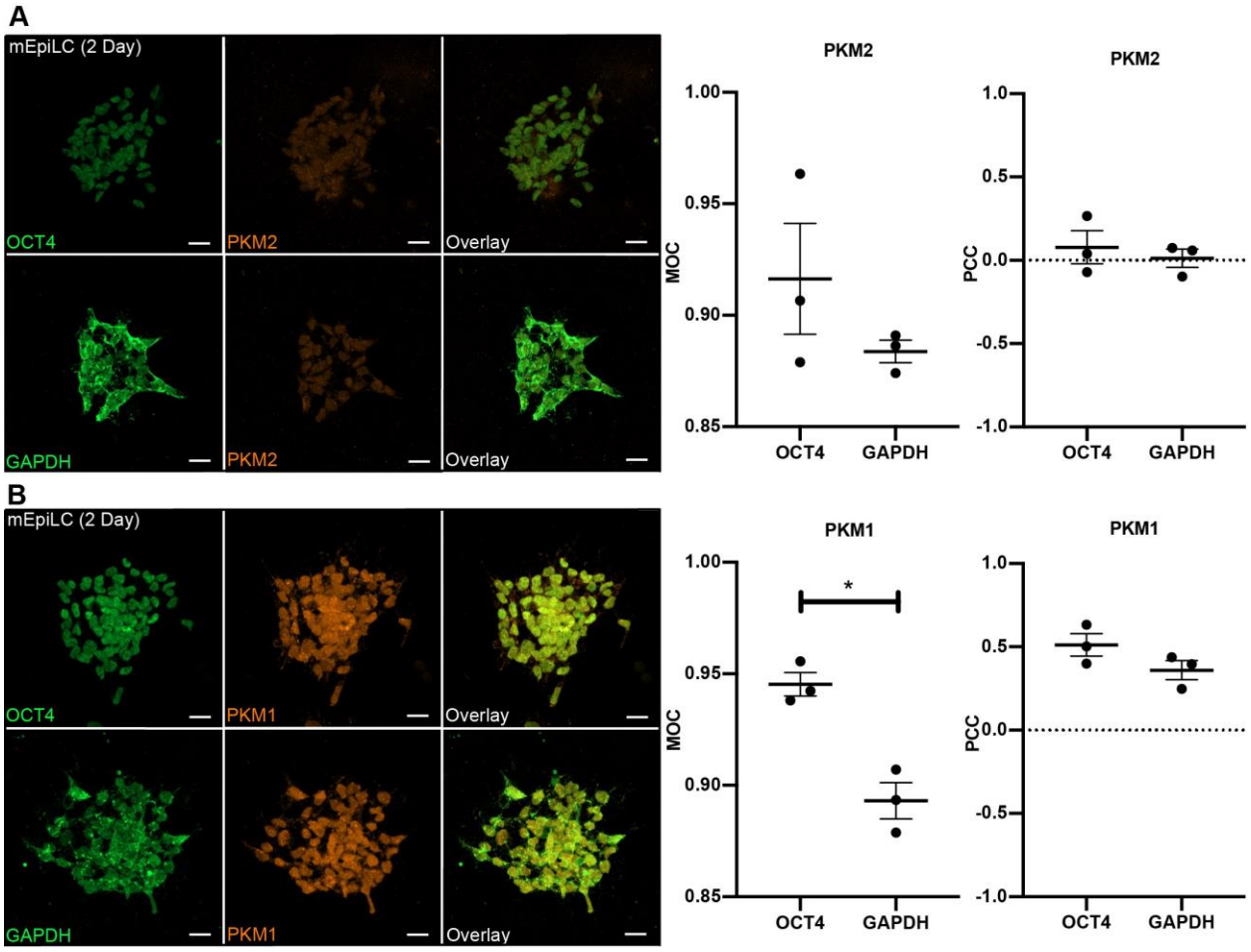

Figure 3.09. PKM1 and PKM2 are translocated to the nuclei of mEpiLCs and PKM1 is associated with OCT4 and GAPDH localization.

A) Immunofluorescence of mEpiLCs stained for OCT4 (green), GAPDH (green), and PKM2 (orange) for a confocal, colocalization analysis. Images taken using 40x magnification and scale bars represent 20 μm. Histogram comparing PKM2 to OCT4 and GAPDH spatial localization by Manders's Overlap Coefficient (MOC) and Pearson's Correlation Coefficient (PCC). Error bars represent SEM, n=3. (B) Immunofluorescence of mEpiLCs stained for OCT4 (green), GAPDH (green) and PKM1 (orange) for a confocal, colocalization analysis. Images taken using 40x magnification and scale bars represent 20 μm. Histogram comparing PKM1 to OCT4 and GAPDH spatial localization by Manders's Overlap Coefficient (MOC) and Pearson's Correlation Coefficient (PCC). Error bars represent SEM, n=3, *p<0.05. Statistics represent a two tailed Mann-Whitney test of mean$\pm$SEM MOC and PCC scores run in at least n=3 biological replicates and at least technical triplicate.

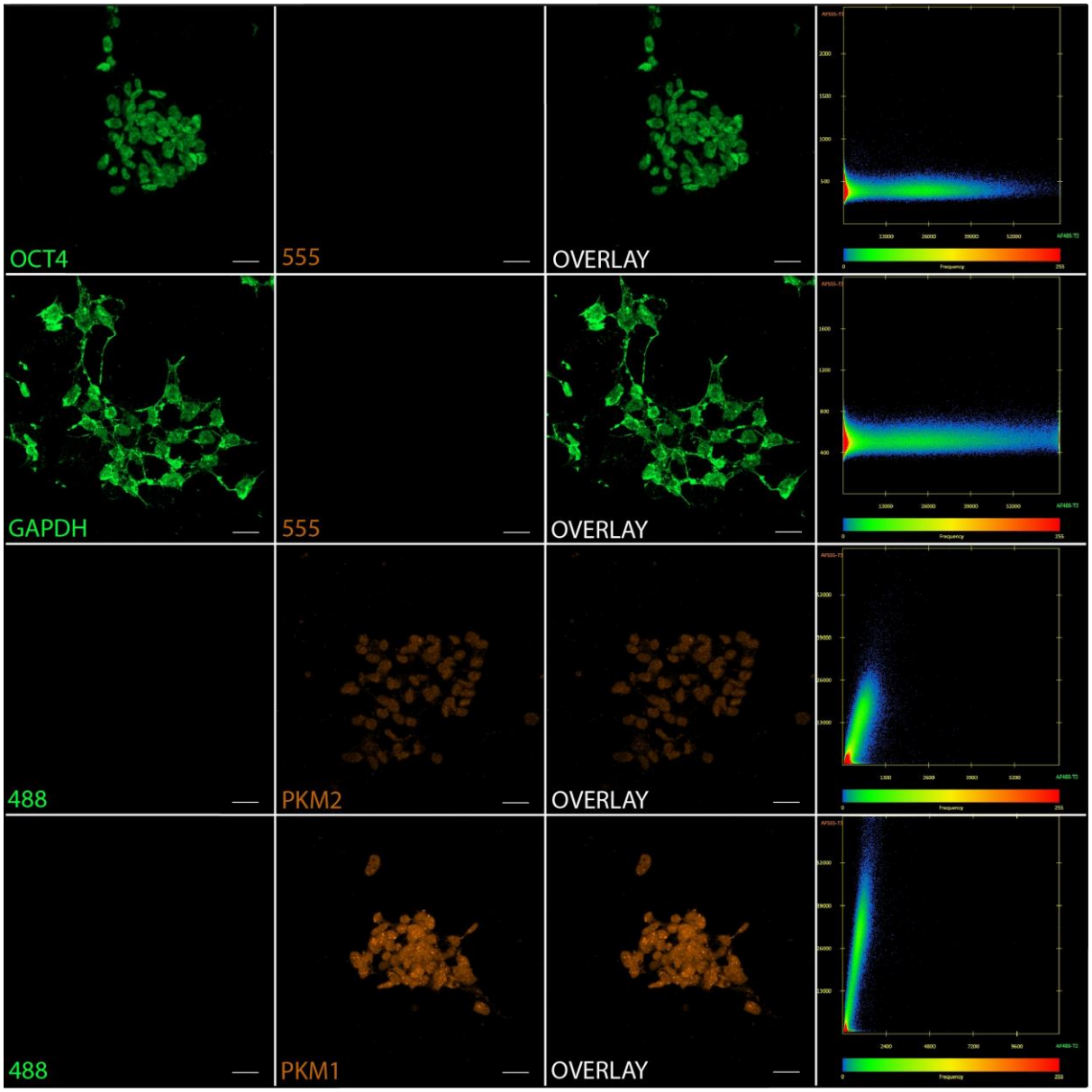

Supplementary Figure 3.07. mEpiLC PKM1, PKM2, OCT4 and GAPDH colocalization settings.

Immunofluorescence microscopy of mEpiLCs demonstrating single fluorescence images for PKM1, PKM2, OCT4, and GAPDH along with their respective thresholds. Images taken using 40x magnification and scale bars represent 20 μm. Confocal laser channels labelled as 488 and 555 corresponding to treatments incubated with OCT4/GAPDH and PKM1/PKM2 respectively.

A

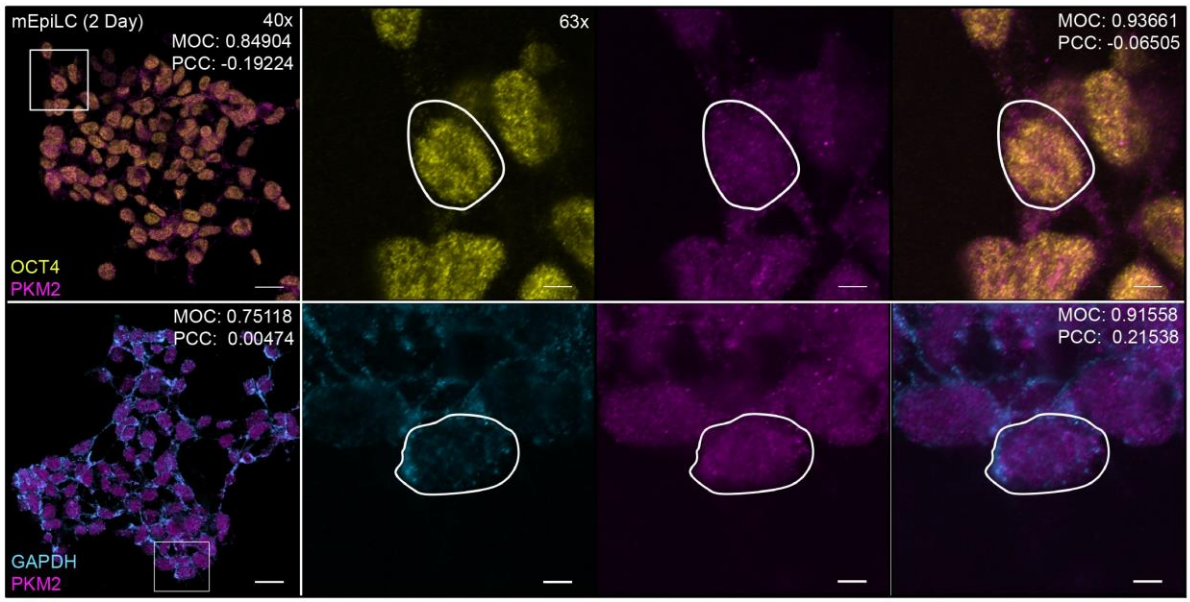
mEpiLC (2 Day)
40x
MOC: 0.84904
PCC: -0.19224
OCT4
PKM2
63x
MOC: 0.93661
PCC: -0.06505
MOC: 0.75118
PCC: 0.00474
GAPDH
PKM2
MOC: 0.91558
PCC: 0.21538

B

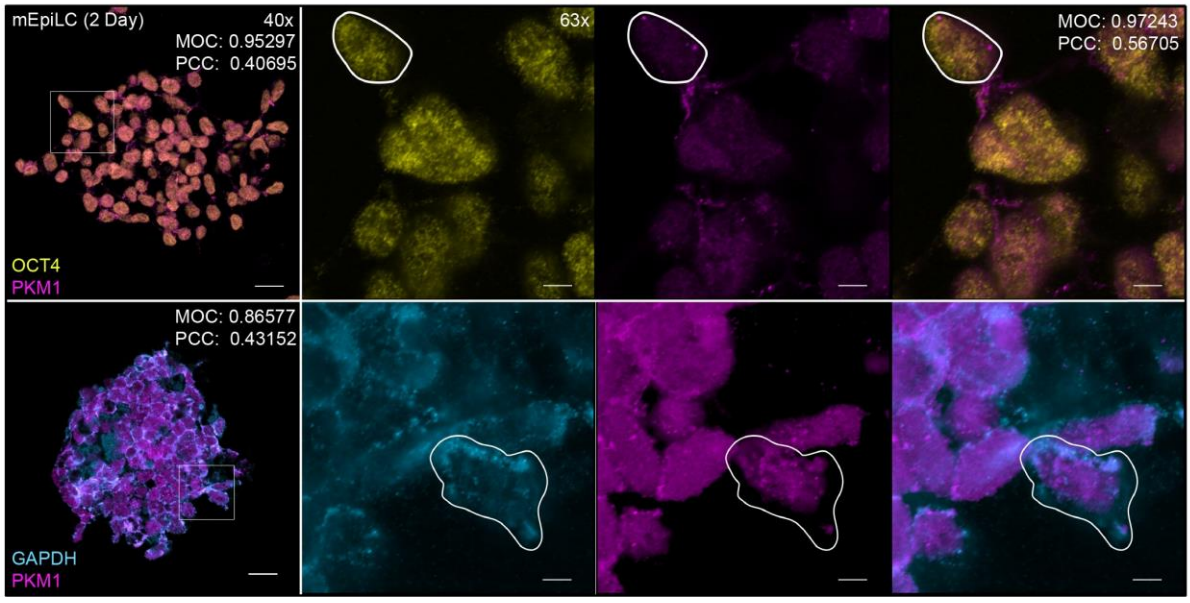
mEpiLC (2 Day)
40x
MOC: 0.95297
PCC: 0.40695
OCT4
PKM1
63x
MOC: 0.97243
PCC: 0.56705
MOC: 0.86577
PCC: 0.43152
GAPDH
PKM1

Supplementary Figure 3.08. PKM1/2 colocalization within individual cells of mEpiLC colonies.

Immunofluorescence microscopy of mEpiLC colonies, colocalization analysis compared MOC and PCC of the total colony to that of a single cell. (A) PKM2 staining versus OCT4 and GAPDH in mEpiLCs comparing orthogonal projections of whole colonies to individual cells by airyscan processing. (B) PKM1 staining versus OCT4 and GAPDH in mEpiLCs comparing orthogonal projections of whole colonies to individual cells by airyscan processing. Images taken using 40x magnification with scale bars represent 20 μm and 63x magnification with scale bars representing 5 μm. Square boxes indicate areas of interest from the 40x for 63x magnification. White outlines around cells represents the area of analysis of the airyscanned images.

3.4.6. Subnuclear Localization of PKM1 and PKM2 with Oct4 in mEpiSCs.

As observed for the naïve mESCs and the formative mEpiLCs, a high degree of PKM1 and PKM2 spatial overlap to both OCT4 and GAPDH in mEpiSCs was observed (Figure 3.10.A, B). However, unlike the mESCs and mEpiLCs, there were only low levels representing no meaningful correlation of PKM1 or PKM2 with OCT4 or GAPDH in these cultures (Figure 3.10.A, B). PKM1 and PKM2 immunofluorescence each showed a 'strong' overlap to both OCT4 and GAPDH immunolocalizations (MOC range: 0.89-0.97) (Zinchuk, Wu, and Grossenbacher-Zinchuk 2013). PKM1 and PKM2 displayed a 'weak' correlation to OCT4 and a 'moderate' correlation to GAPDH (PCC range: weak = -0.26-0.09, moderate = 0.1-.48). Using airyscan processing, individual cells of mEpiLC colonies displayed consistent correlation and spatial overlap compared to the colony (Supplementary Figure 3.10.A, B). Immunofluorescence controls and colocalization thresholds are shown in Supplementary Figure 3.09.

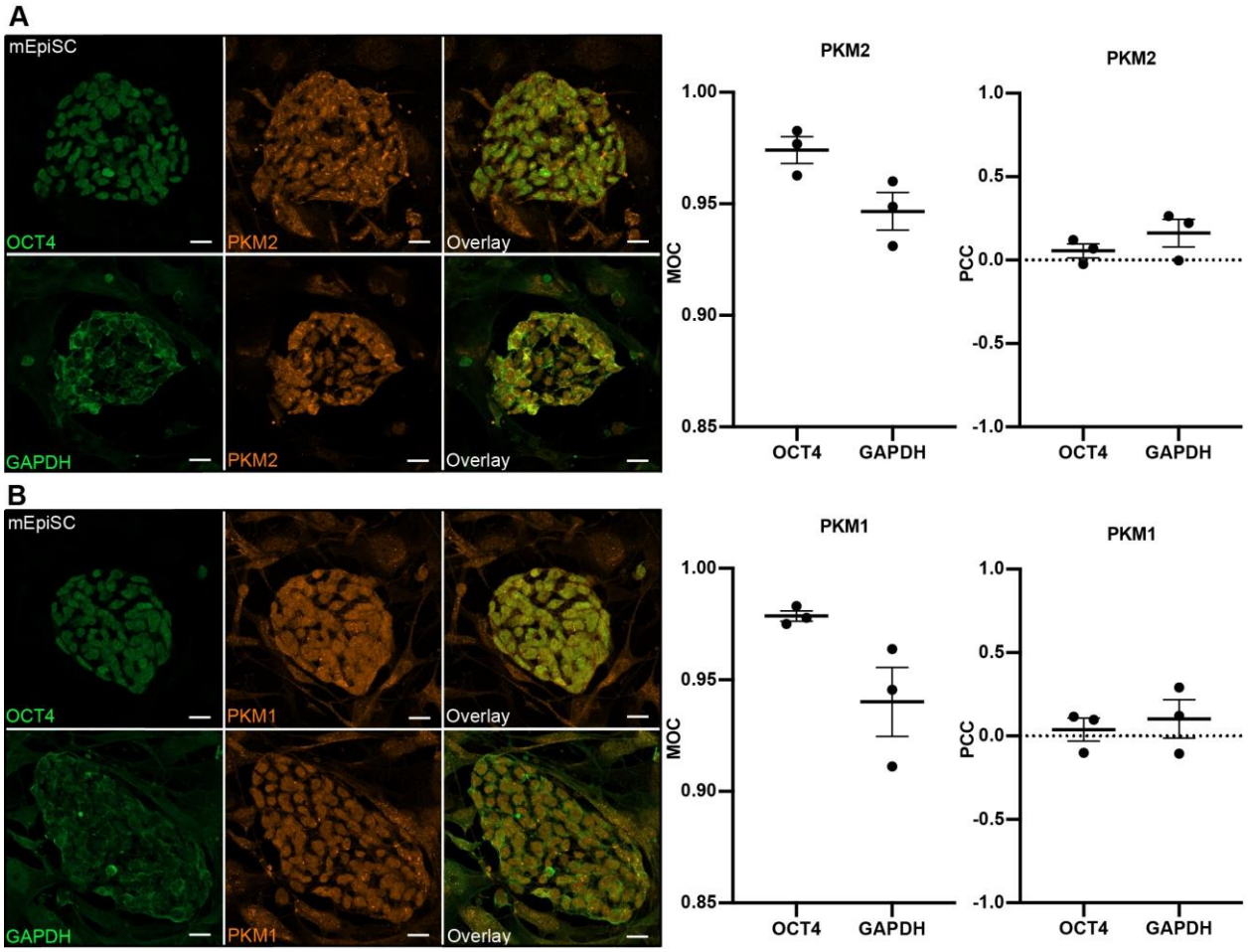

Figure 3.10. PKM1 and PKM2 are translocated to the nuclei of mEpiSCs and neither isoform is associated with OCT4 or GAPDH localization.

(A) Immunofluorescence of mEpiSCs stained for OCT4 (green), GAPDH (green), and PKM2 (orange) for a confocal, colocalization analysis. Images taken using 40x magnification and scale bars represent 20 μm. Histogram comparing PKM2 to OCT4 and GAPDH spatial localization by Manders's Overlap Coefficient (MOC) and Pearson's Correlation Coefficient (PCC). Error bars represent SEM, n=3. (B) Immunofluorescence of mEpiSCs stained for OCT4 (green), GAPDH (green) and PKM1 (orange) for a confocal, colocalization analysis. Images taken using 40x magnification and scale bars represent 20 μm. Histogram comparing PKM1 to OCT4 and GAPDH spatial localization by Manders's Overlap Coefficient (MOC) and Pearson's Correlation Coefficient (PCC). Error bars represent SEM, n=3. Statistics represent a two tailed Mann-Whitney test of mean$\pm$SEM MOC and PCC scores run in at least n=3 biological replicates and at least technical triplicate.

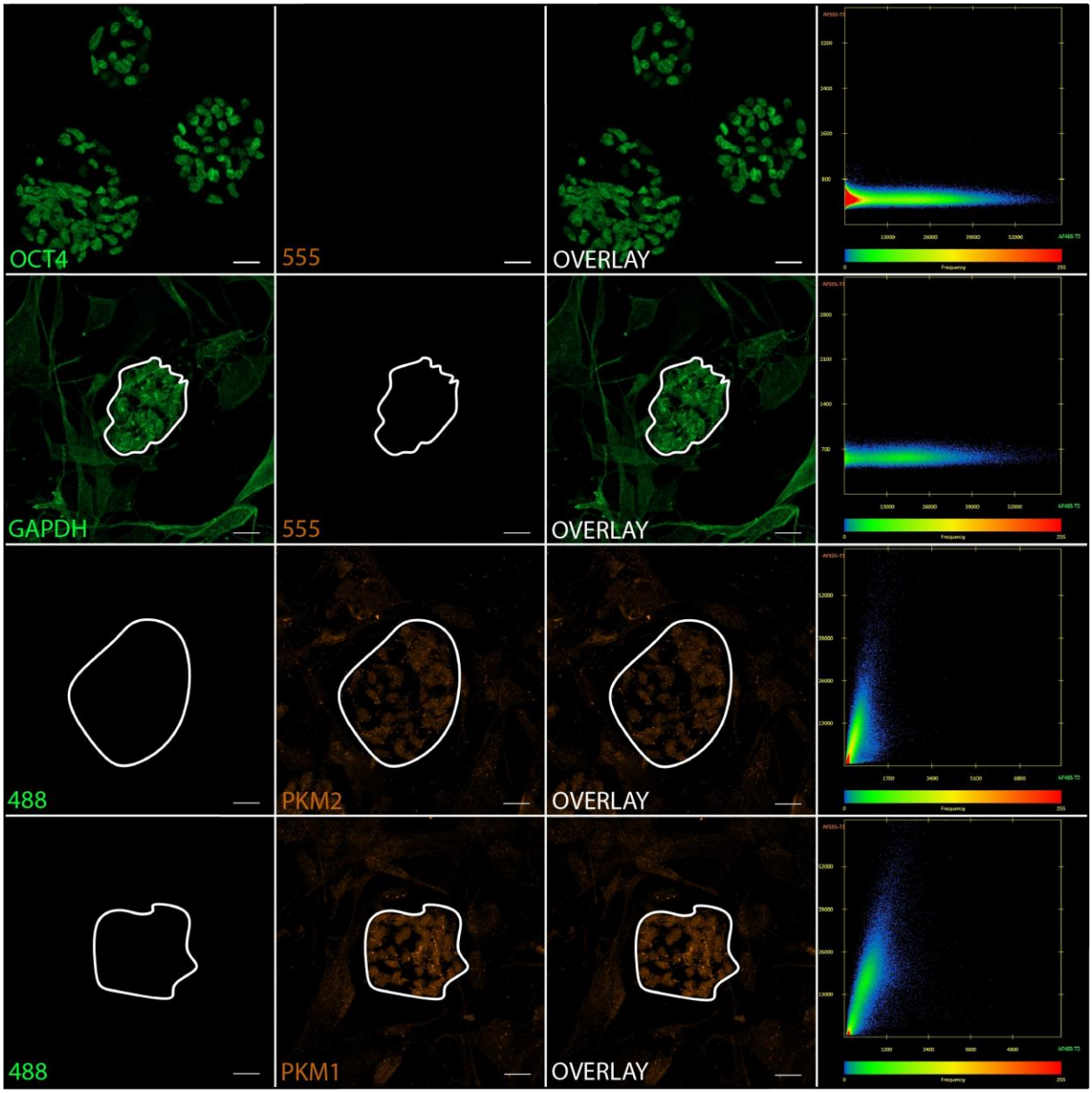

Supplementary Figure 3.09. mEpiSC PKM1, PKM2, OCT4, and GAPDH colocalization settings.

Immunofluorescence microscopy of mEpiSCs demonstrating single fluorescence images for PKM1, PKM2, OCT4, and GAPDH along with their respective thresholds. Images taken using 40x magnification and scale bars represent 20 μm. White outlines represent area of analysis to exclude areas of MEF staining. Confocal laser channels labelled as 488 and 555 corresponding to treatments incubated with OCT4/GAPDH and PKM1/PKM2 respectively.

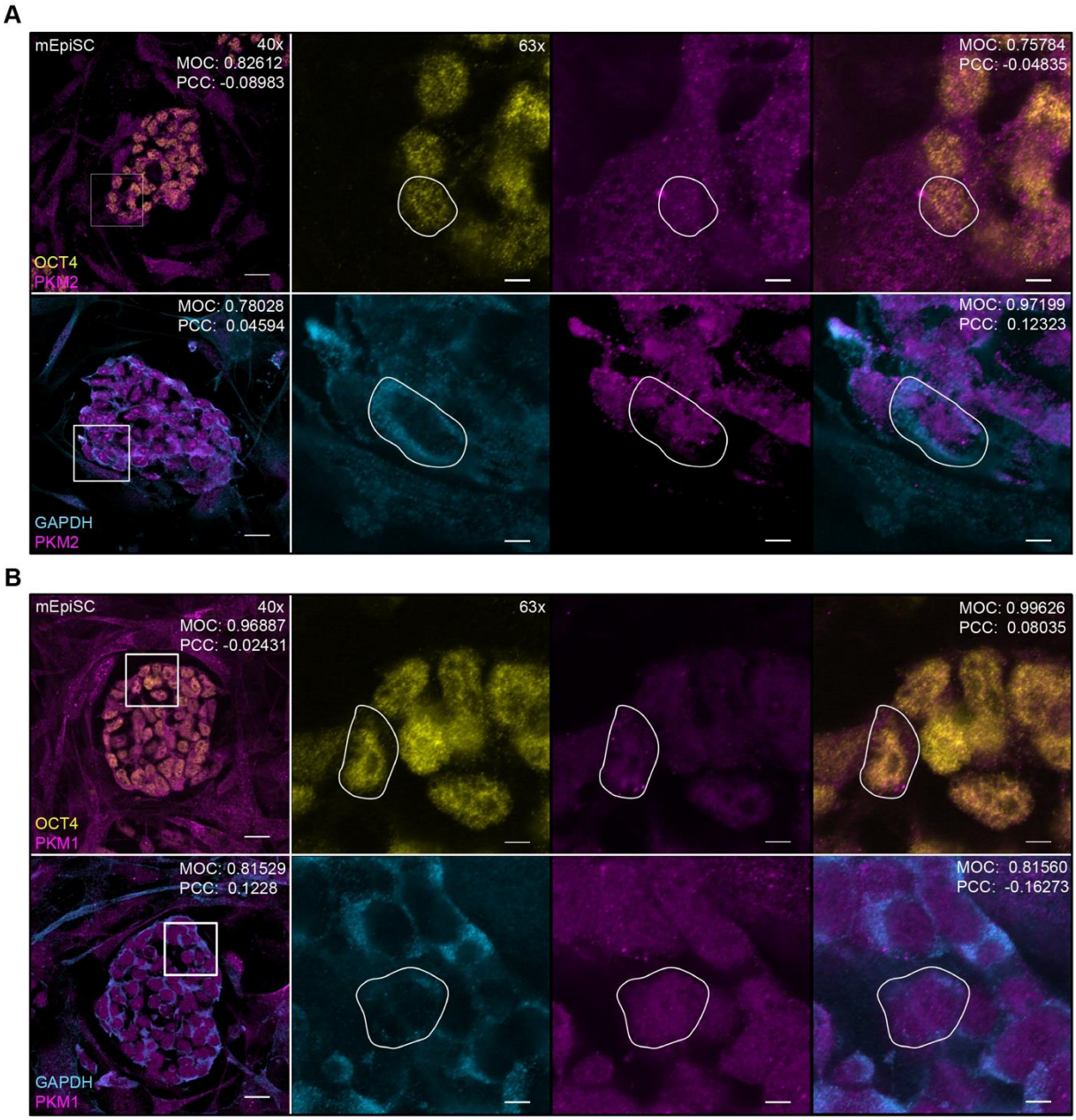
A
mEpiSC
40x
MOC: 0.82612
PCC: -0.08983
63x
MOC: 0.75784
PCC: -0.04835
OCT4
PKM2
MOC: 0.78028
PCC: 0.04594
MOC: 0.97199
PCC: 0.12323
GAPDH
PKM2
B
mEpiSC
40x
MOC: 0.96887
PCC: -0.02431
63x
MOC: 0.99626
PCC: 0.08035
OCT4
PKM1
MOC: 0.81529
PCC: 0.1228
MOC: 0.81560
PCC: -0.16273
GAPDH
PKM1

Supplementary Figure 3.10. PKM1/2 colocalization within individual cells of mEpiSC colonies.

Immunofluorescence microscopy of mEpiSC colonies, colocalization analysis compared MOC and PCC of the total colony to that of a single cell. (A) PKM2 staining versus OCT4 and GAPDH in mEpiSCs comparing orthogonal projections of whole colonies to individual cells by airyscan processing. (B) PKM1 staining versus OCT4 and GAPDH in mEpiSCs comparing orthogonal projections of whole colonies to individual cells by airyscan processing. Images taken using 40x magnification with scale bars represent 20 μm and 63x magnification with scale bars representing 5 μm. Square boxes indicate areas of interest from the 40x for 63x magnification. White outlines around cells represents the area of analysis of the airyscanned images.

3.4.7. PKM1 and PKM2 are differentially localized to OCT4 and GAPDH between naïve, formative, and primed pluripotent states.

To obtain a deeper understanding of the cellular co-occurrence of nuclear PKM1 and PKM2 during the transition from mESCs, mEpiLCs, and mEpiSCs cultures, I contrasted the outcomes between overall co-occurrence (MOC) with Hoechst and OCT4 (positive reference) and Hoechst and GAPDH (negative reference). Relative to the positive reference, there was no significant ($p>0.05$) changes to MOC of PKM1 or PKM2 localization to OCT4 localization in mESCs, mEpiLCs, or mEpiSCs, indicating that PKM1 and PKM2 do indeed occupy nuclear associated regions in these pluripotent cells (Figure 3.12.B). Relative to the positive reference, there was a no significant ($p>0.5$) changes to the MOC of PKM1 or PKM2 localization to GAPDH localization in mESCs and mEpiSCs, indicating that PKM1 and PKM2 do indeed occupy cytoplasmic regions in these cells as well (Figure 3.12.B). However, relative to the positive reference, there was a significant ($p<0.05$) decrease in MOC of PKM1 and PKM2 localization to GAPDH localization in the mEpiLCs, indicating a decreased cytoplasmic presence in these cells (Figure 3.12.B).

To further interrogate the subnuclear association of nuclear PKM1 and PKM2 during transitioning mESCs, mEpiLCs, and mEpiSCs cultures, I compared the outcomes between overall correlation (PCC) with Hoechst and OCT4 (positive reference) and Hoechst and GAPDH (negative reference). Each mPSC state examined showed differential PKM1/2 subnuclear expression correlation to OCT4 and GAPDH compared to the positive reference. Relative to the positive reference indicating nuclear OCT4 association, there was no significant ($p>0.05$) difference in PCC of PKM1 or PKM2

localization to OCT4 or GAPDH in mESCs (Figure. 3.11.B). In contrast, mEpiLCs and mEpiSC displayed significantly ($p<0.05$) less PCC of PKM2 localization to OCT4 relative to the positive reference, however, these values did not reach a meaningful linear correlation level (Figure 3.11.B). Relative to the positive reference indicating nuclear association, there was no significant ($p>0.05$) PCC difference in PKM1 and a significant ($p<0.05$) decrease in correlation of PKM2 localization to OCT4 and GAPDH localization relative to the positive reference in mEpiLCs, suggesting nuclear association of PKM1 and reduced nuclear association of PKM2 with OCT4 (Figure 3.11.B). Relative to the positive reference indicating nuclear association, there was a significant ($p<0.05$) decrease in PCC of PKM1 and PKM2 localization to OCT4 and GAPDH localization relative to the positive reference in mEpiSCs (Figure 3.11.B). However, in the case of mEpiLCs and mEpiSCs, values with PCC = 0 reflect no meaningful linear correlation and a meaningful association of PKM1 or PKM2 localization to these fluorophores of interest cannot be conclusively inferred.

Using the standard ranges set by Zinchuk *et. al.* to describe these values with qualifying terms, there is an observed 'strong correlation' and 'strong overlap' in the Hoechst/OCT4 positive reference (PCC = 0.49 ± 0.06, MOC = 0.95 ± 0.00) and a 'very weak correlation' and 'strong overlap' in the GAPDH/Hoechst negative reference (PCC = -0.07 ± 0.08, MOC =0.89 ± 0.01) (Figure 3.11.A) (Zinchuk, Wu, and Grossenbacher-Zinchuk 2013). These standards promote the superiority of the PCC over the MOC, however, there was a significant difference between the positive and negative references and our sample data indicating a valuable role for the MOC comparison as well.

In summary, PKM1 and PKM2 occupy the same spatial localization as OCT4 nuclear regions and differentially correlate to subnuclear localizations relative to OCT4 and GAPDH localization in mESCs, mEpiLCs, and mEpiSCs. I demonstrate that both the PCC and MOC metrics are valuable in comparison to known positive nuclear references, in this case Hoechst staining. Reference stains and colocalization thresholds are available in Supplementary Figure 3.11.

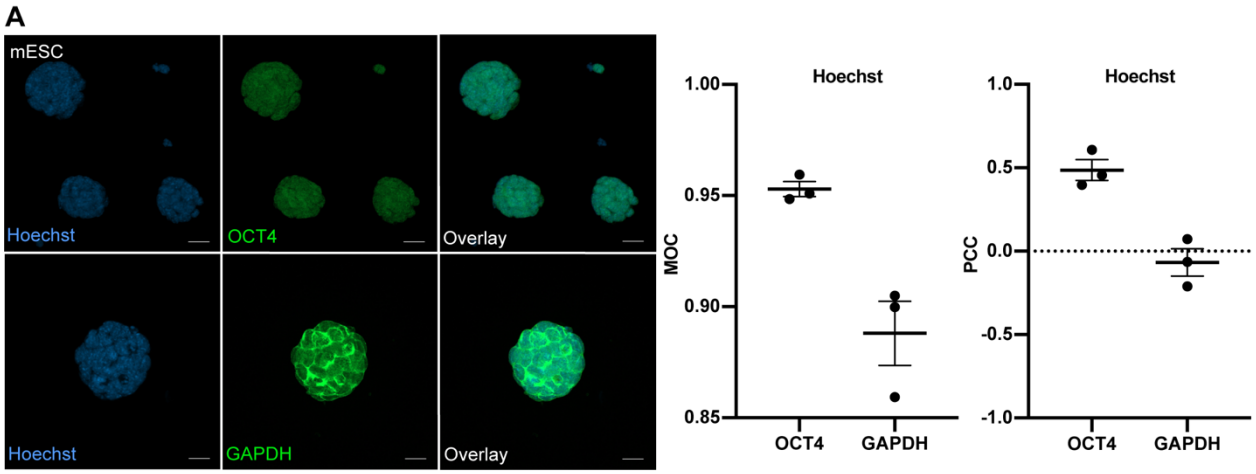
A
mESC
Hoechst
OCT4
Overlay
Hoechst
GAPDH
Overlay
Hoechst
MOC
1.00
0.95
0.90
0.85
OCT4
GAPDH
Hoechst
PCC
1.0
0.5
0.0
-0.5
-1.0
OCT4
GAPDH

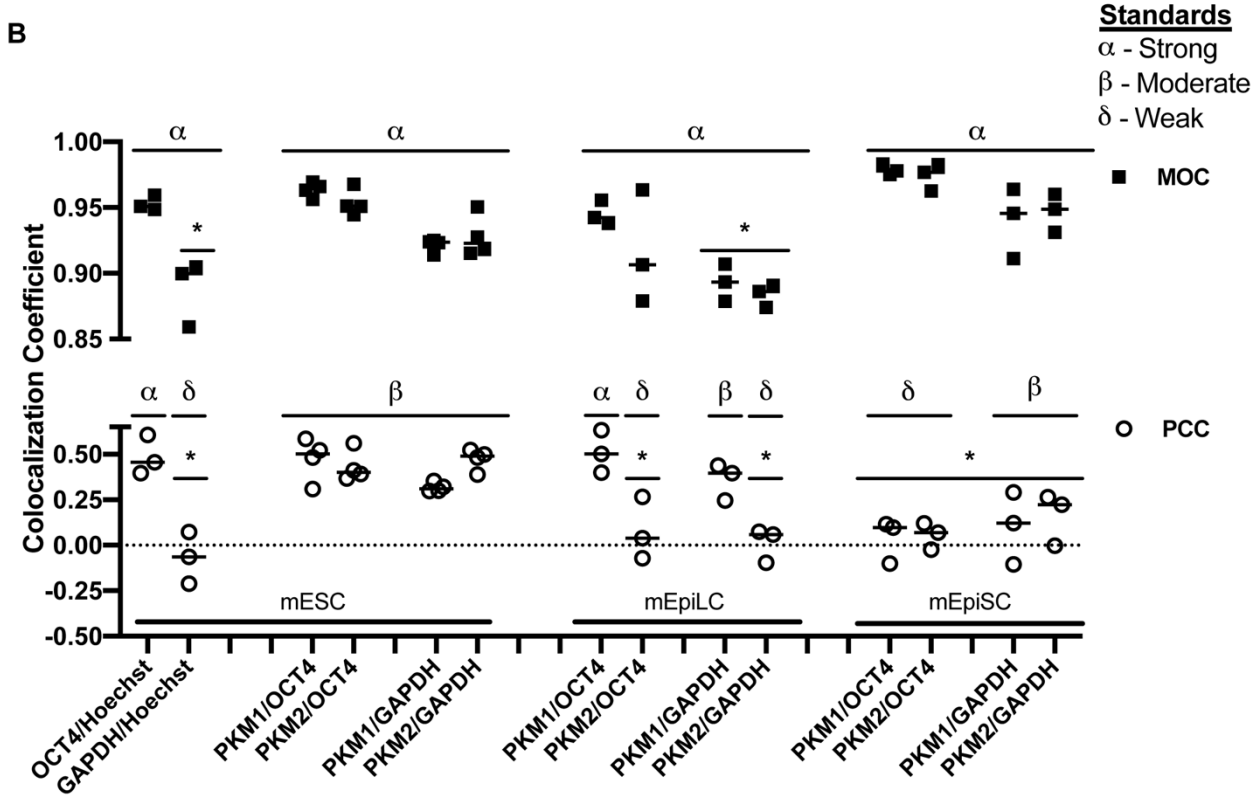
B
Standards
α - Strong
β - Moderate
δ - Weak
MOC
PCC
Colocalization Coefficient
1.00
0.95
0.90
0.85
0.50
0.25
0.00
-0.25
-0.50
mESC
mEpiLC
mEpiSC
OCT4/Hoechst
GAPDH/Hoechst
PKM1/OCT4
PKM2/OCT4
PKM1/GAPDH
PKM2/GAPDH

Figure 3.11. PKM1/2 are moderately associated with OCT4 localization in mESC, PKM1 is strongly associated with OCT4 localization in mEpiLCs, and PKM1/2 overlap in nuclear regions of mESCs, mEpiLCs, and mEpiSCs.

(A) Immunofluorescence of mESCs immuno-stained for OCT4 (green), GAPDH (green), and Hoechst (blue) for a confocal, colocalization analysis. Images taken using 40x magnification and scale bars represent 20 μm. Histogram comparing Hoechst to OCT4 and GAPDH spatial localization by Manders's Overlap Coefficient (MOC) and Pearson's Correlation Coefficient (PCC). Error bars represent SEM, n=3. (B) Total results of colocalization study comparing positive and negative references to mESCs, mEpiLCs, and mEpiSC MOC and PCC values. Standard range qualifiers set by Zinchuk *et al*. (2013) compare overlap and correlation differences. Error bars represent SEM, n=3. Statistics of PCC and MOC treatments relative to the positive reference represent a two-way ANOVA with Sidak's multiple comparisons test of mean$\pm$SEM PCC and MOC scores where $\propto$=0.05, n=3 biological replicates.

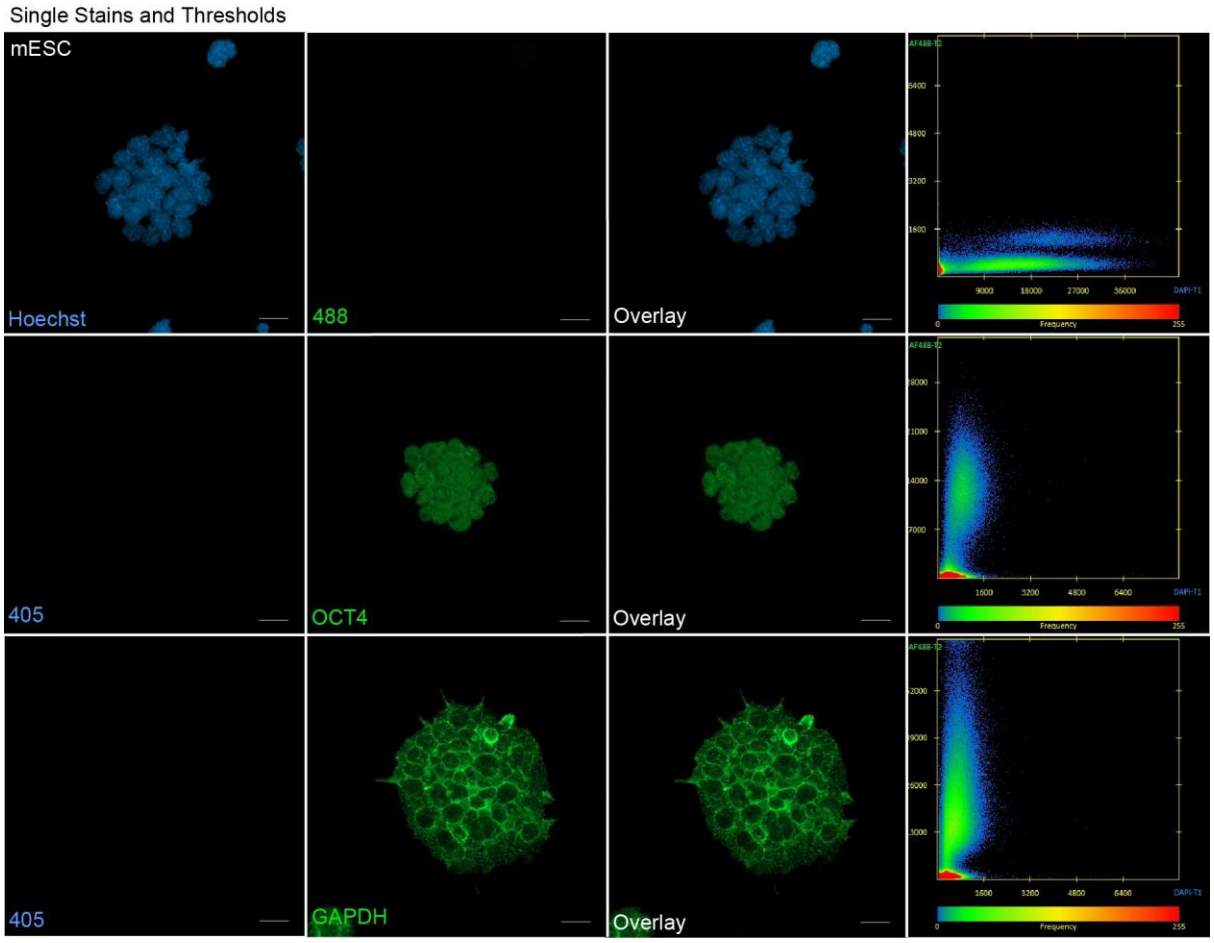

Supplementary Figure 3.11. mESC positive and negative colocalization controls. Immunofluorescence microscopy of mESCs demonstrating single and double stains for Hoechst, OCT4 and GAPDH along with their respective thresholds. Images taken using 40x magnification and scale bars represent 20 μm. Confocal laser channels labelled as 405 nm and 488 nm corresponding to treatments incubated with Hoechst and OCT4/GAPDH respectively.

Nuclear localization of PKM1 and PKM2 in naïve mESCs by cell fractionation

To validate the results of the orthogonal projection immunofluorescence analysis, a nuclear and cytoplasmic fractionation of naïve mESCs using the REAP protocol was conducted (Nabbi and Riabowol 2015). Naïve mESCs were selected as they were the only mPSC that exhibited both a nuclear co-occurrence and correlation of PKM1 and PKM2 with OCT4 immunofluorescence from our colocalization study. The REAP protocol was validated by comparing the nuclear and cytoplasmic fractions with the nuclear marker LAMIN A and the cytoplasmic marker ∝-TUBULIN. A significant ($p<0.05$) increase in ∝-TUBULIN in the cytoplasmic fraction compared to the nuclear fraction validating successful fractionation was observed (Supplementary Figure 3.12. A, B, C). The results effectively demonstrated the nuclear localization of PKM1 from naïve mESC protein lysates (Supplementary Figure 3.12. C). This was evident as the ratio of nuclear-to-cytoplasmic fraction PKM1 trended towards elevated levels of nuclear PKM1 in the mESC, however, this did not reach statistical significance (Supplementary Figure 3.12. C).

A

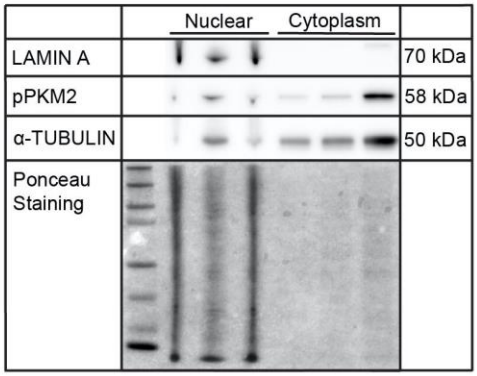
Nuclear
Cytoplasm
LAMIN A
pPKM2
α-TUBULIN
Ponceau Staining
70 kDa
58 kDa
50 kDa

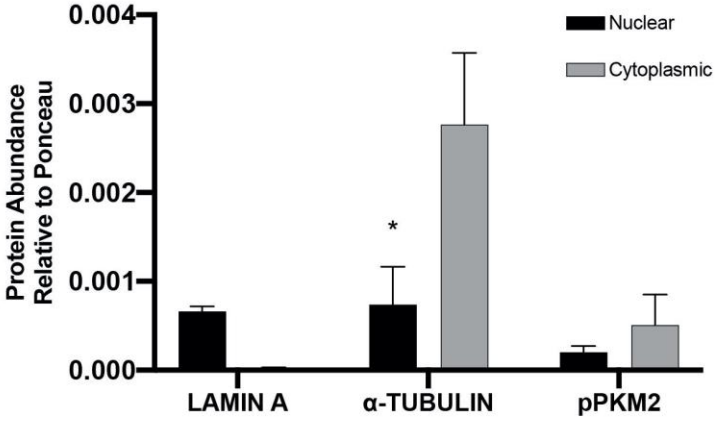
Protein Abundance Relative to Ponceau
0.004
0.003
0.002
0.001
0.000
Nuclear
Cytoplasmic
*
LAMIN A
α-TUBULIN
pPKM2

B

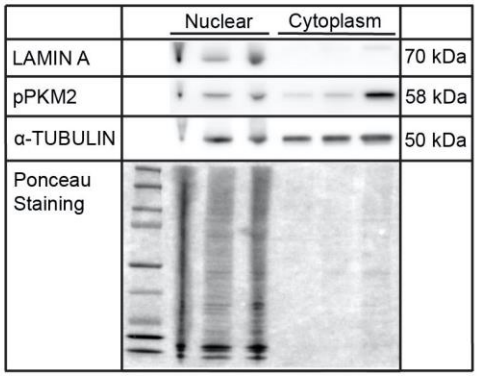
Nuclear
Cytoplasm
LAMIN A
pPKM2
α-TUBULIN
Ponceau Staining
70 kDa
58 kDa
50 kDa

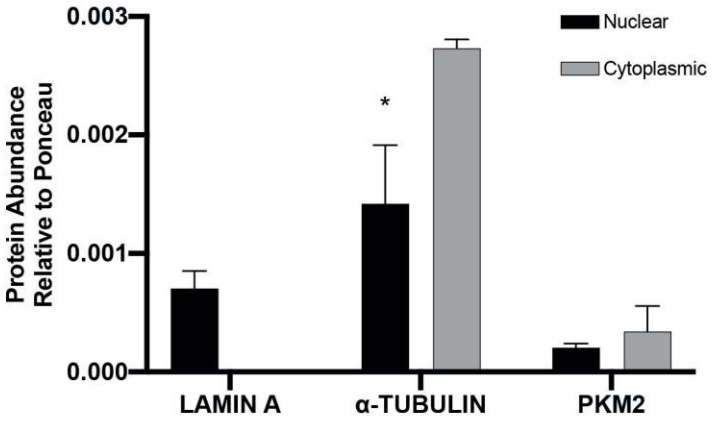
Protein Abundance Relative to Ponceau
0.003
0.002
0.001
0.000
Nuclear
Cytoplasmic
*
LAMIN A
α-TUBULIN
PKM2

C

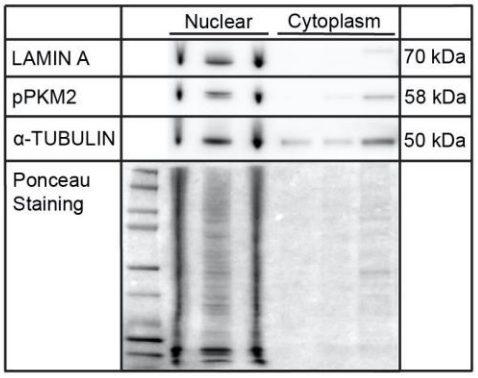
Nuclear
Cytoplasm
LAMIN A
pPKM2
α-TUBULIN
Ponceau Staining
70 kDa
58 kDa
50 kDa

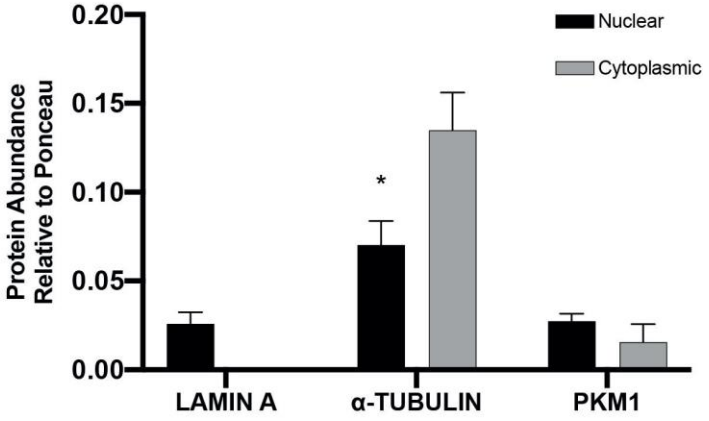
Protein Abundance Relative to Ponceau
0.20
0.15
0.10
0.05
0.00
Nuclear
Cytoplasmic
*
LAMIN A
α-TUBULIN
PKM1

Supplementary Figure 3.12. PKM1 is translocated to the nuclei of mESCs.
(A) Histogram comparing protein abundance of nuclear and cytoplasmic fractioned lysates of pPKM2, ∝-TUBULIN, and LAMIN A relative to total protein Ponceau staining in mESCs. Error bars represent SEM, n=3, *p<0.05. (B) Histogram comparing protein abundance of nuclear and cytoplasmic fractioned lysates of PKM2, ∝-TUBULIN, and LAMIN A relative to total protein Ponceau staining in mESCs. Error bars represent SEM, n=3, *p<0.05. (C) Histogram comparing protein abundance of nuclear and cytoplasmic fractioned lysates of PKM1, ∝-TUBULIN, and LAMIN A relative to total protein Ponceau staining in mESCs. Error bars represent SEM, n=3, *p<0.05.

3.5.0. Discussion:

Despite traditionally being considered a passive trait of cell-fate determination, mounting evidence now supports metabolism as having a direct role in self-renewal, cell fate and differentiation (Dahan et al. 2019). Our study investigated differences in pyruvate kinase muscle isoforms 1 and 2 (PKM1/2) in naïve, formative, and primed pluripotent stem cells and found differential expression and nuclear localization of these metabolic isoforms during pluripotent state transitioning. Densitometry of total protein lysates indicated that over the course of pluripotent progression there is an increase protein abundance of PKM1, PKM2, and phosphorylated PKM2 in the formative state. Despite this increase in protein abundance, the ratio of PKM1 to PKM2, a common ratio used to examine aerobic glycolytic preferential cancer cells, was not different between each pluripotent state, indicating that a stable PKM1/2 ratio is likely required for maintaining pluripotency, which one differentiation occurs is not observed (Qin et al. 2017). There was an observed nuclear immunofluorescence for both PKM1/2 isoforms in naïve mouse embryonic stem cells (mESCs), formative mouse epiblast-like stem cells (mEpiLCs), and primed mouse epiblast stem cells (mEpiSCs). To verify this observation, I conducted an improved confocal colocalization approach to compare differences in nuclear and cytoplasmic localization by contrasting orthogonal projections with well-established reference markers. Using this technique, I determined that in each pluripotent state, PKM1 and PKM2 both reside in nuclear regions and that PKM1 and PKM2 are moderately associated with OCT4 localization patterns in mESCs. PKM1 is strongly associated with OCT4 localization patterns in mEpiLCs and both isoforms have a weak association to OCT4 immunolocalization in mEpiSCs showing a progressive decline in association to the pluripotency gene OCT4 during mouse ES cell pluripotency transitioning.

The measurement of colocalization is a complicated and hotly debated area of biology (Adler and Parmryd 2010; Aaron, Taylor, and Chew 2019). The term colocalization is largely used to measure two main components with different applications, namely correlation or co-occurrence of two fluorophores to each other based on pixel distribution (Aaron, Taylor, and Chew 2018). Co-occurrence in immunofluorescence is the presentation of fluorescent pixels existing in the same spatial distribution, and it is an indicator of overlap between markers (Manders, Verbeek, and Aten 1993). Correlation is a measurement of the relationship between the pixel intensities and may indicate a biochemical interaction (Manders, Verbeek, and Aten 1993). Both the Manders's overlap coefficient (MOC) and Pearson's correlation coefficient (PCC) are valid measures of colocalization, but they inform different biological questions (Aaron, Taylor, and Chew 2019). Immunofluorescence microscopy is commonly thought of as a qualitative technique and the literature into colocalization often uses descriptors such as moderate or strong association within PCC ranges. Zinchuk *et al.* (Zinchuk, Wu, and Grossenbacher-Zinchuk 2013) developed a method of colocalization range descriptors to bring greater consistency to the field and offer more validity to the quantitative nature of colocalization. I implemented a quantitative designate to the colocalization of PKM1 and PKM2 within the mPSCs of this study. This study supports claims that the MOC is a valuable metric of colocalization. By comparing MOC and PCC values to a positive and negative biological reference, I demonstrate that this methodology sets a stronger baseline than using only improved descriptors. OCT4 and GAPDH were used as nuclear and cytoplasmic reference proteins control markers to compare to another known nuclear stain, Hoechst, which set a positive and negative reference to nuclear colocalization that

allowed us to directly compare MOC and PCC values to. Comparing known positive and negative references to the qualifying range standards set by Zinchuk *et al*. this studies data supports comparing colocalization by correlation being superior to spatial overlap (Zinchuk, Wu, and Grossenbacher-Zinchuk 2013). However, while MOC still provided valuable knowledge, the PCC data showed an improved distinction between internal reference controls. These findings demonstrate that it is critical to run positive and negative references relative to dual fluorophore colocalization and that in the case of mouse embryonic stem cells, the spatial overlap data may not be sufficient to reach quality colocalization assessment compared to correlation data when considering the qualifying standards set by Zinchuk *et al*. I observed that the MOC metric in mPSCs did not delineate nuclear and cytoplasmic distinctions by colocalization and that the PCC metric was a highly effective and viable tool for such distinction and analysis. To increase the power of our colocalization study, a simple analysis single images was not employed, instead, I investigated orthogonal projections of stacks examining the data of individual slices to characterize the localization patterns of a true three-dimensional structure. I also accounted for the inherent flaws of the MOC calculation by examining only the individual colonies and individual cells in the orthogonal and airyscanned images respectively to prevent autofluorescence or background pixel offset to influence the algorithm.

Naïve mESCs, in the metabolically bivalent state, proved to be a unique and attractive cell type for colocalization analysis. By examining the correlation of PKM1 and PKM2 immunolocalizations to OCT4 and GAPDH immunolocalizations, not only was an assessment of PKM isoforms occupying similar spaces completed, but the trends in

subnuclear pixel intensity were related was as well. Additonally, both isoforms occupy the same spatial regions in comparison to the controls, and both PKM1 and PKM2 were clearly associated with the localization patterns of both OCT4 and GAPDH. Together, these results promote the concept that PKM1 and PKM2 both translocate to the nuclei of mESCs. A recent study using mass spectroscopy of human lung carcinoma cells determined that PKM1 and PKM2 interact with each other (Prakasam et al. 2017) suggesting a possible PKM1/2 interaction in the nuclei of mouse ESCs. Supporting this claim, I completed a REAP fractionation for nuclear and cytoplasmic protein abundance in mESCs and demonstrate the presence of both PKM1 and PKM2 in nuclear fractions (Nabbi and Riabowol 2015). This methodology was able to cleanly discriminate cytoplasmic fractions from nuclear proteins as controlled by LAMIN A, however, nuclear fractions were not fully separated from cytoplasmic proteins, likely due to the high ratio of nuclear-to-cytoplasm in PSCs.

In the initial PKM protein abundance characterization of total cell lysate, I found that there was an increase of PKM1 and PKM2 levels in mEpiLCs. Despite this increase in protein abundance, the ratio of PKM1 to PKM2 protein abundance did not change between any of the pluripotent cell types examined. As PKM2 switches to increased PKM1 expression during differentiation and development, with the reverse occurring during tumor formation, the role of the PKM1 to PKM2 ratio has become a focus of interest (Morita et al. 2018). It may be more pertinent to examine the nuclear-to-cytoplasmic ratio of PKM1/2 including the dimer to tetramer conformations of PKM2 in various pluripotent states. Surprisingly, the formative state mEpiLCs had significantly decreased in PKM1 and PKM2 colocalization spatial overlap to GAPDH compared with

the positive reference. This demonstrates very low amounts of either isoform occupying the traditional cytoplasmic region occupied by GAPDH for both isoforms. When examining mEpiLCs for correlation of PKM1 and PKM2 colocalization to OCT4 and GAPDH, I determined that PKM1 was associated with both OCT4 and GAPDH compared to the controls. Coupling this finding with the results of the colocalization overlap findings, the formative state mEpiLCs were unique in primarily localizing PKM1 in the nucleus, suggesting that PKM1 may be key in the transition of bivalent metabolism to preferential aerobic glycolysis. Previous studies have shown that the transcription factor promyelocytic leukemia protein (PML), a known PKM2 mediator that maintains the homotetrameric conformation and suppresses the Warburg Effect, interacts with OCT4 and NANOG and is necessary for maintaining naïve pluripotency (Hadjimichael et al. 2017; Jiancong Liang et al. 2008; Shimada, Shinagawa, and Ishii 2008). Knocking down or deleting PML resulted in flat, slower growing mESC colonies with reduced OCT4, SOX2, cMYC and NR0B1 and diminished naïve-associated BMP, LIF/STAT3 and PI3K signaling whereas Activin A and FGF signalling increased (Hadjimichael et al. 2017). Overexpression of PML resists mESC transitioning towards primed pluripotency and is required for efficient iPSC generation (Hadjimichael et al. 2017). Future studies should examine the influence of PML in the generation of formative state mEpiLCs. As mEpiLCs are the only cells currently described that can efficiently give rise to primordial germ-like cells, PML and PKM1/2 may be important targets for controlling cell fate to efficiently produce mEpiLCs (Hayashi et al. 2011).

I determined that of all the mPSCs studied, the primed mEpiSCs had the greatest spatial overlap as assessed by Manders's overlap coefficient (MOC) of PKM1 and PKM2

colocalization to OCT4 and GAPDH yet significantly lower PKM1 and PKM2 correlation (PCC) to OCT4 and GAPDH. This was unexpected as other aerobic glycolytic cells, such as, glioma stem cells display an interaction between PKM2 and OCT4 (Morfouace et al. 2014). The reduced association as assessed by the Pearson correlation coefficient (PCC) of PKM2 and OCT4 may reflect differential chromatin targets in the primed pluripotent state and may be associated with lineage priming and reduced differentiation potential (Morfouace et al. 2014). Interestingly, there is also a decrease in PKM1 correlation to OCT4 as assessed by PCC, but only in the primed mEpiSCs. Using the refined colocalization analysis, I demonstrated that PKM1 and PKM2 co-occur (MOC) in the nuclei of mPSCs across the pluripotent continuum and that PKM1 and PKM2 are differentially correlated (PCC) with OCT4 and GAPDH in each examined pluripotent state. This data suggests that ChIP-sequencing of PKM1 and PKM2 targets should be examined in mPSC varieties encompassing the pluripotent continuum. Further, the correlation of PKM2 colocalization to OCT4 decreases from naïvety through the formative state and into primed pluripotency. As such, I conclude that nuclear PKM1 and PKM2 are implicated as contributors to the maintenance and progression of embryonic stem cell pluripotency.

Recent literature has reported instances of nuclear and mitochondrial translocation of PKM2 (Qi et al. 2019; Ji Liang et al. 2017). The nuclear translocation of PKM2 is implicated in the regulation of the master glycolysis regulator HIF-1α (Wang et al. 2014). Jumonji C Domain-containing dioxygenase 5 (JMJD5)-PKM2 interaction hinders PKM2 tetramer formation, blocks pyruvate kinase activity and promotes translocation of PKM2

into the nucleus to regulate HIF-1α-mediated gene transcription (Wang et al. 2014). JMJD5 regulates the cell cycle and maintains pluripotency in human embryonic stem cells (Zhu, Hu, and Baker 2014), however, its role in the nuclear translocation of PKM2 and regulating metabolism in pluripotent stem cells has not been explored. Overexpression of PKM2 maintains the undifferentiated state by fine tuning redox control in naïve mESCs grown as embryoid bodies (Konno et al. 2015). Future studies treating naïve stem cells with pharmacological agents such as shikonin or DASA-58, which promote the tetrameric conformation of PKM2, may resist formative state transitioning by maintaining the naïve state (J. Chen et al. 2011; Giannoni et al. 2015). Adjusting PKM2 levels has been completed in mESCs and a complete knockout should be feasible as PKM2-null mice are viable though they experience some metabolic distress and have a reliance on PKM1 (Jacks et al. 2016). However, these mice show induction of late onset formation of spontaneous hepatocellular carcinomas (Jacks et al. 2016). PKM2 is certainly a potential target for cancer treatments and likely a key player in cellular reprogramming and differentiation (Jacks et al. 2016; Qin et al. 2017). Despite several non-canonical roles being characterized, it is likely that other roles exist and have yet to be discovered (Weiwei Yang et al. 2011).

While PKM2 has been extensively studied in cancers and stem cells (Morita et al. 2018; Jacks et al. 2016; Konno et al. 2015; Wei et al. 2018; C. C. L. Wong et al. 2014; Taniguchi et al. 2015; N. Wong, De Melo, and Tang 2013), the PKM1 isoform has not been investigated to the same extent. There is a growing body of evidence to suggest that PKM1 may play an important role in early differentiation and within specific cancer

subtypes. Until recently, PKM1 was thought to be only expressed with spatial heterogeneity in non-proliferative cells of tumors, however, recent publications have found this is not always the case (Israelsen et al. 2013; Morita et al. 2018). PKM1 is essential for the proliferation and tumor-promoting capabilities of small cell lung cancer (SCLCs) and other net endocrine tumors (Morita et al. 2018). Oxygen consumption in PKM1 overexpressed cancer cells does not change although there are more mitochondria with a greater rate of mitochondria dysfunction, while there are more reactive oxygen species generated in the PKM2 overexpressed cells compared to the PKM1 overexpressed cells (Morita et al. 2018). These characteristics of PKM1 overexpressed cells are accompanied with increased autophagic flux and increased tumor growth with increased autophagy and mitophagy (Morita et al. 2018). PKM1 could play a non-canonical role in promoting autophagic and mitophagic roles during pluripotent stem cell state transitioning. When either PKM1 or PKM2 was overexpressed in mESCs, it was found that the pluripotency markers Nanog, Eras, and Rex1 were upregulated and an embryoid body formation assay showed that overexpression did not influence differentiation (W. Zhou et al. 2012). Taken together, these results indicate that PKM1 contributes to proliferation, stemness, and pluripotency. Based on this investigation's protein abundance analysis, PKM2 or both isoforms may promote the generation of mEpiLCs and the formative pluripotent state (Qin et al. 2017). The results suggest that preserving an equal ratio of PKM1 to PKM2 may be necessary to maintain mouse pluripotency. Such a trend is not found following lineage specialization into various somatic cells (Qin et al. 2017). I also report a unique localization of PKM1 that suggests a novel, non-canonical role just as nuclear, dimeric pPKM2 has been implicated in several non-metabolic roles associated with stemness and cell growth (W. Yang and Lu 2015).

Recently, the role of PKM1 in highly proliferative cells has been highlighted (Morita et al. 2018). These results along with our current data questions PKM2's role as the traditional prototypic isozyme of development as it is now clear that PKM1 is expressed and likely has non-canonical roles (Morita et al. 2018). Nuclear PKM1 has recently been reported in other highly proliferative cell types such as human liver cancer cells (HepG2 and SMMC-7721) (Wei et al. 2017). Following treatment with drug Oroxylin A (OA), an O-methylated flavonoid derived from the Oroxylum indicum tree, PKM1 is translocated to the nucleus with hepatocyte nuclear factor 4 α (HNF4α), and increases the PKM1 to PKM2 ratio resulting in hepatoma differentiation (Wei et al. 2017). PKM1 overexpressed in embryoid bodies generated from mESCs resulted in increased endoderm transcript abundance of FOXA2, AFP, and HINF1B, implicating PKM1 in endoderm differentiation (Konno et al. 2015). Given the colocalization findings, nuclear localization of PKM1 is certainly implicated in formative state generation, and the addition of a drug such as OA may modulate the occurrence of this transient pluripotent state.

To fully validate to the colocalization study, I examined nuclear and cytoplasmic fractionation protein abundance in the mESCs. Due to the inherent difficulty of nuclear and cytoplasmic extraction and the exceptionally high nuclear-to-cytoplasmic ratio of mESCs, the most successful method of extraction was the REAP (Rapid, Efficient and Practical) method of extraction (Y. Zhou et al. 2016; Nabbi and Riabowol 2015). While nuclear extraction of PSCs is generally considered a challenging technique, clean extractions have been published (Bechard and Dalton 2009). Using this technique, protein densitometry demonstrates PKM1 and PKM2 do have increased nuclear lysate protein abundance. The most important finding of this study was that PKM1 is enriched

in the nuclear fraction compared to the cytoplasmic fraction of mESCs, further supporting that PKM1 is being translocated to the nuclei of naïve mESCs.

In summary, the data supports differential nuclear and subnuclear localization of both PKM1 and PKM2 in mouse pluripotent stem cells and suggest a novel regulatory role for nuclear PKM1. These results establish differential nuclear, subnuclear, and cytoplasmic association of PKM1 and PKM2 in mESC cells as they transition from naïve pluripotency, through formative state (primed-like mEpiLCs) towards primed mEpiSCs (Figure 3.12.). Protein colocalization studies applied to PSCs should give greater weight to their correlation data and not their spatial overlap findings especially if the standards set by Zinchuk *et al.* are implemented (Zinchuk, Wu, and Grossenbacher-Zinchuk 2013). The presence of nuclear PKM1/2 and the dynamic redistribution of PKM1 and PKM2 during pluripotency continuum suggests potential non-canonical roles for both isoforms in maintaining and directing varying pluripotent states.

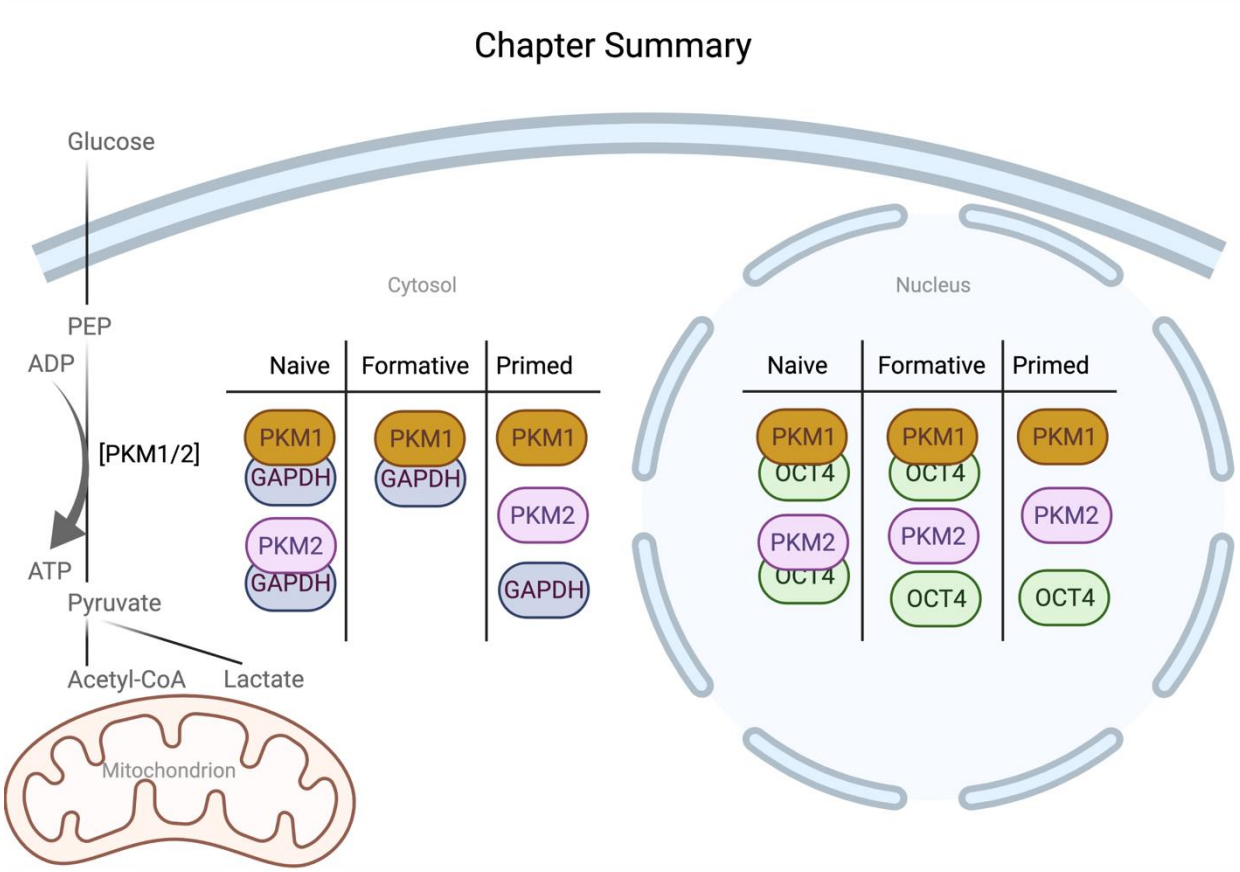

Figure 3.12. PKM1/2 are differentially localized to subcellular regions with potential interaction with OCT4 and GAPDH in naïve, formative, and primed mouse embryonic stem cells.

Pyruvate kinase muscle isoforms are localized to nuclear regions in mESCs, mEpiLCs, and mEpiSCs. There is indication of potential biomolecular interaction of PKM with OCT4 or GAPDH denoted by circled proteins overlapping in the schematic. As mESCs become more developmentally lineage primed for differentiation (mEpiSCs), the correlation of PKM1/2 with OCT4 and GAPDH decreases. This could mean decreased potential for biomolecular interaction of the isoforms with OCT4 and a potential rearrangement of subcellular localization patterns in the cytosol such as mitochondrial colocalization as demonstrated in previous studies (Ji Liang et al. 2017). This illustration was completed using BioRender.

3.6.0. Acknowledgments:

Technical expertise and advisement from Courtney Brooks and Drs. Lin Zhao, Christie Vanderboor, Nicole Edwards, Ian Tobias, Jodi Garner, Amy Wong, and Cheryle Séguin aided to the progress of this work. Confocal and colocalization tips were graciously shared by Dr. Julia Abitbol. Pluripotent cell lines were gifted from Dr. Janet Rossant. This research was funded by a Canadian Institutes of Health Research operating grant to A.J.W. and D.H.B. and Natural Sciences and Engineering Research Council of Canada grant to D.H.B. The funders had no role in study design, data collection and analysis, decision to publish, or preparation of the manuscript.

3.7.0. References:

Aaron, Jesse S, Aaron B Taylor, and Teng-Leong Chew. 2018. “Image Co-Localization – Co-Occurrence versus Correlation.” *Journal of Cell Science* 131 (3): jcs211847. https://doi.org/10.1242/jcs.211847.

———. 2019. “The Pearson’s Correlation Coefficient Is Not a Universally Superior Colocalization Metric. Response to ‘Quantifying Colocalization: The MOC Is a Hybrid Coefficient – an Uninformative Mix of Co-Occurrence and Correlation.’” *Journal of Cell Science* 132 (1): jcs227074. https://doi.org/10.1242/jcs.227074.

Adler, Jeremy, and Ingela Parmryd. 2010. “Quantifying Colocalization by Correlation: The Pearson Correlation Coefficient Is Superior to the Mander’s Overlap Coefficient.” *Cytometry Part A* 77A (8): 733–42. https://doi.org/10.1002/cyto.a.20896.

———. 2012. “Colocalization Analysis in Fluorescence Microscopy.” *Methods in Molecular Biology* 931: 97–109. https://doi.org/10.1007/978-1-62703-56-4_5.

Bechard, Matthew, and Stephen Dalton. 2009. “Subcellular Localization of Glycogen Synthase Kinase 3β Controls Embryonic Stem Cell Self-Renewal.” *Molecular and Cellular Biology* 29 (8): 2092 LP – 2104. https://doi.org/10.1128/MCB.01405-08.

Boles, Eckhard, Frank Schulte, Thomas Miosga, Kerstin Freidel, Elke Schlüter, Friedrich K. Zimmermann, Cornelis P. Hollenberg, and Jürgen J. Heinisch. 1997. “Characterization of a Glucose-Repressed Pyruvate Kinase (Pyk2p) in Saccharomyces Cerevisiae That Is Catalytically Insensitive to Fructose-1,6-Bisphosphate.” *Journal of Bacteriology* 179 (9): 2987–93. https://doi.org/10.1128/jb.179.9.2987-2993.1997.

Brons, I Gabrielle M, Lucy E Smithers, Matthew W B Trotter, Peter Rugg-Gunn, Bowen Sun, Susana M Chuva de Sousa Lopes, Sarah K Howlett, et al. 2007. “Derivation of Pluripotent Epiblast Stem Cells from Mammalian Embryos.” *Nature* 448 (June): 191. https://doi.org/10.1038/nature05950.

Chambers, Ian, Douglas Colby, Morag Robertson, Jennifer Nichols, Sonia Lee, Susan Tweedie, and Austin Smith. 2003. “Functional Expression Cloning of Nanog, a Pluripotency Sustaining Factor in Embryonic Stem Cells.” *Cell* 113 (5): 643–55. https://doi.org/10.1016/S0092-8674(03)00392-1.

Chen, J., J. Xie, Z. Jiang, B. Wang, Y. Wang, and X. Hu. 2011. “Shikonin and Its Analogs Inhibit Cancer Cell Glycolysis by Targeting Tumor Pyruvate Kinase-M2.” *Oncogene* 30 (42): 4297–4306. https://doi.org/10.1038/onc.2011.137.

Chen, Jianan, Yan Yu, Xiaolong Chen, Yuting He, Qiuyue Hu, Hongqiang Li, Qicai Han, et al. 2018. “MiR-139-5p Is Associated with Poor Prognosis and Regulates Glycolysis by Repressing PKM2 in Gallbladder Carcinoma.” *Cell Proliferation* 51 (6): e12510. https://doi.org/10.1111/cpr.12510.

Christensen, David R, Philip C Calder, and Franchesca D Houghton. 2015. “GLUT3 and PKM2 Regulate OCT4 Expression and Support the Hypoxic Culture of Human Embryonic Stem Cells.” *Scientific Reports* 5 (December): 17500. https://doi.org/10.1038/srep17500.

Christofk, H. R., Vander Heiden, M. G., Wu, N., Asara, J. M. & Cantley, L. C. 2008. “Pyruvate Kinase M2 Is a Phosphotyrosine Binding Protein.” *Nature* 452 (March): 181–89. https://doi.org/10.1038/nature06667.

Christofk, Heather R., Matthew G. Vander Heiden, Marian H. Harris, Arvind

Ramanathan, Robert E. Gerszten, Ru Wei, Mark D. Fleming, Stuart L. Schreiber, and Lewis C. Cantley. 2008. "The M2 Splice Isoform of Pyruvate Kinase Is Important for Cancer Metabolism and Tumour Growth." *Nature* 452 (7184): 230–33. https://doi.org/10.1038/nature06734.

Dahan, Perrine, Vivian Lu, Robert M T Nguyen, Stephanie A L Kennedy, and Michael A Teitell. 2019. "Metabolism in Pluripotency: Both Driver and Passenger?" *The Journal of Biological Chemistry* 294 (14): 5420–29. https://doi.org/10.1074/jbc.TM117.000832.

David, Charles J, Mo Chen, Marcela Assanah, Peter Canoll, and James L Manley. 2010. "HnRNP Proteins Controlled by C-Myc Deregulate Pyruvate Kinase MRNA Splicing in Cancer." *Nature* 463 (7279): 364–68. https://doi.org/10.1038/nature08697.

DeBerardinis, Ralph J, and Navdeep S Chandel. 2016. "Fundamentals of Cancer Metabolism." *Science Advances* 2 (5): e1600200. https://doi.org/10.1126/sciadv.1600200.

Desai, Shruti, Minming Ding, Bin Wang, Zhimin Lu, Qi Zhao, Kenna Shaw, W K Alfred Yung, John N Weinstein, Ming Tan, and Jun Yao. 2013. "Tissue-Specific Isoform Switch and DNA Hypomethylation of the Pyruvate Kinase PKM Gene in Human Cancers." *Oncotarget* 5 (18): 1–9. https://doi.org/10.18632/oncotarget.1159.

Dunn, Kenneth W, Malgorzata M Kamocka, and John H McDonald. 2011. "A Practical Guide to Evaluating Colocalization in Biological Microscopy." *American Journal of Physiology-Cell Physiology* 300 (4): C723–42. https://doi.org/10.1152/ajpcell.00462.2010.

Evans, M. J., and M. H. Kaufman. 1981. "Establishment in Culture of Pluripotential Cells from Mouse Embryos." *Nature*. https://doi.org/10.1038/292154a0.

Feron, Olivier. 2009. "Pyruvate into Lactate and Back: From the Warburg Effect to Symbiotic Energy Fuel Exchange in Cancer Cells." *Radiotherapy and Oncology* 92 (3): 329–33. https://doi.org/10.1016/j.radonc.2009.06.025.

Gafni, Ohad, Leehee Weinberger, Abed Alfatah Mansour, Yair S. Manor, Elad Chomsky, Dalit Ben-Yosef, Yael Kalma, et al. 2013. "Derivation of Novel Human Ground State Naive Pluripotent Stem Cells." *Nature* 504 (7479): 282–86. https://doi.org/10.1038/nature12745.

Giannoni, Elisa, Maria Letizia Taddei, Andrea Morandi, Giuseppina Comito, Maura Calvani, Francesca Bianchini, Barbara Richichi, et al. 2015. "Targeting Stromal-Induced Pyruvate Kinase M2 Nuclear Translocation Impairs Oxphos and Prostate Cancer Metastatic Spread." *Oncotarget* 6 (27): 24061–74. https://doi.org/10.18632/oncotarget.4448.

Guo, G., J. Yang, J. Nichols, J. S. Hall, I. Eyres, W. Mansfield, and A. Smith. 2009. "Klf4 Reverts Developmentally Programmed Restriction of Ground State Pluripotency." *Development* 136 (7): 1063–69. https://doi.org/10.1242/dev.030957.

Guo, Ge, Ferdinand Von Meyenn, Fatima Santos, Yaoyao Chen, Wolf Reik, Paul Bertone, Austin Smith, and Jennifer Nichols. 2016. "Naive Pluripotent Stem Cells Derived Directly from Isolated Cells of the Human Inner Cell Mass." *Stem Cell Reports* 6 (4): 437–46. https://doi.org/10.1016/j.stemcr.2016.02.005.

Guppy, Michael, Erich Greiner, and Karl Brand. 1993. "The Role of the Crabtree Effect and an Endogenous Fuel in the Energy Metabolism of Resting and Proliferating Thymocytes." *European Journal of Biochemistry* 212 (1): 95–99.

https://doi.org/10.1111/j.1432-1033.1993.tb17637.x.
Hadjimichael, Christiana, Konstantina Chanoumidou, Christoforos Nikolaou, Antonios Klonizakis, Gesthimani Ioanna Theodosi, Takis Makatounakis, Joseph Papamatheakis, and Androniki Kretsovali. 2017. "Promyelocytic Leukemia Protein Is an Essential Regulator of Stem Cell Pluripotency and Somatic Cell Reprogramming." *Stem Cell Reports* 8 (5): 1366–78. https://doi.org/10.1016/j.stemcr.2017.03.006.
Hawkins, Kate E., Shona Joy, Juliette M.K.M. Delhove, Vassilios N. Kotiadis, Emilio Fernandez, Lorna M. Fitzpatrick, James R. Whiteford, et al. 2016. "NRF2 Orchestrates the Metabolic Shift during Induced Pluripotent Stem Cell Reprogramming." *Cell Reports* 14 (8): 1883–91. https://doi.org/10.1016/j.celrep.2016.02.003.
Hayashi, Katsuhiko, Hiroshi Ohta, Kazuki Kurimoto, Shinya Aramaki, and Mitinori Saitou. 2011. "Reconstitution of the Mouse Germ Cell Specification Pathway in Culture by Pluripotent Stem Cells." *Cell* 146 (4): 519–32. https://doi.org/10.1016/j.cell.2011.06.052.
Heard, Edith. 2004. "Recent Advances in X-Chromosome Inactivation." *Current Opinion in Cell Biology* 16 (3): 247–55. https://doi.org/10.1016/j.ceb.2004.03.005.
Hensley, Christopher T., Brandon Faubert, Qing Yuan, Naama Lev-Cohain, Eunsook Jin, Jiyeon Kim, Lei Jiang, et al. 2016. "Metabolic Heterogeneity in Human Lung Tumors." *Cell* 164 (4): 681–94. https://doi.org/10.1016/j.cell.2015.12.034.
Hitosugi, Taro, Sumin Kang, Matthew G Vander Heiden, Tae-Wook Chung, Shannon Elf, Katherine Lythgoe, Shaozhong Dong, et al. 2009. "Tyrosine Phosphorylation Inhibits PKM2 to Promote the Warburg Effect and Tumor Growth." *Science Signaling* 2 (97): ra73 LP-ra73. https://doi.org/10.1126/scisignal.2000431.
Horiuchi, Yuta, Daiki Nakatsu, Fumi Kano, and Masayuki Murata. 2017. "Pyruvate Kinase M1 Interacts with A-Raf and Inhibits Endoplasmic Reticulum Stress-Induced Apoptosis by Activating MEK1/ERK Pathway in Mouse Insulinoma Cells." *Cellular Signalling* 38: 212–22. https://doi.org/https://doi.org/10.1016/j.cellsig.2017.07.017.
Imamura, Kuchi, and Takehiko Tanaka. 1982. "[25] Pyruvate Kinase Isozymes from Rat." *Methods in Enzymology* 90 (C): 150–65. https://doi.org/10.1016/S0076-6879(82)90121-5.
Israelsen, William J., Talya L. Dayton, Shawn M. Davidson, Brian P. Fiske, Aaron M. Hosios, Gary Bellinger, Jie Li, et al. 2013. "PKM2 Isoform-Specific Deletion Reveals a Differential Requirement for Pyruvate Kinase in Tumor Cells." *Cell* 155 (2): 397–409. https://doi.org/10.1016/j.cell.2013.09.025.
Jacks, Tyler E., Alba Luengo, Arjun Bhutkar, Talya L. Dayton, Kathryn M. Miller, Matthew G. Vander Heiden, William J. Israelsen, Shawn M. Davidson, Vasilena Gocheva, and Clary B. Clish. 2016. "Germline Loss of PKM2 Promotes Metabolic Distress and Hepatocellular Carcinoma." *Molecular Cancer Research* 14 (4 Supplement): PR04–PR04. https://doi.org/10.1158/1557-3125.devbiolca15-pr04.
Jiang, Yuhui, Xinjian Li, Weiwei Yang, David H. Hawke, Yanhua Zheng, Yan Xia, Kenneth Aldape, et al. 2014. "PKM2 Regulates Chromosome Segregation and Mitosis Progression of Tumor Cells." *Molecular Cell* 53 (1): 75–87. https://doi.org/10.1016/j.molcel.2013.11.001.
Jiang, Yuhui, Yugang Wang, Ting Wang, David H Hawke, Yanhua Zheng, Xinjian Li, Qin Zhou, et al. 2014. "PKM2 Phosphorylates MLC2 and Regulates Cytokinesis of

Tumour Cells." *Nature Communications* 5 (1): 5566. https://doi.org/10.1038/ncomms6566.

Joo, Jin Young, Hyun Woo Choi, Min Jung Kim, Holm Zaehres, Natalia Tapia, Martin Stehling, Koo Sung Jung, Jeong Tae Do, and Hans R. Schöler. 2014. "Establishment of a Primed Pluripotent Epiblast Stem Cell in FGF4-Based Conditions." *Scientific Reports* 4: 7477. https://doi.org/10.1038/srep07477.

Jurica, Melissa S, Andrew Mesecar, Patrick J Heath, Wuxian Shi, Thomas Nowak, and Barry L Stoddard. 1998. "The Allosteric Regulation of Pyruvate Kinase by Fructose-1,6-Bisphosphate." *Structure* 6 (2): 195–210. https://doi.org/10.1016/S0969-2126(98)00021-5.

Kalkan, Tüzer, Susanne Bornelöv, Carla Mulas, Evangelia Diamanti, Tim Lohoff, Meryem Ralser, Sjors Middelkamp, Patrick Lombard, Jennifer Nichols, and Austin Smith. 2019. "Complementary Activity of ETV5, RBPJ, and TCF3 Drives Formative Transition from Naive Pluripotency." *Cell Stem Cell* 24 (5): 785-801.e7. https://doi.org/10.1016/j.stem.2019.03.017.

Kalkan, Tüzer, and Austin Smith. 2014. "Mapping the Route from Naive Pluripotency to Lineage Specification." *Philosophical Transactions of the Royal Society B: Biological Sciences* 369 (1657): 20130540-. https://doi.org/10.1098/rstb.2013.0540.

Kinoshita, Masaki, and Austin Smith. 2018. "Pluripotency Deconstructed." *Development, Growth & Differentiation* 60 (1): 44–52. https://doi.org/10.1111/dgd.12419.

Kojima, Yoji, Keren Kaufman-Francis, Joshua B. Studdert, Kirsten A. Steiner, Melinda D. Power, David A.F. Loebel, Vanessa Jones, et al. 2014. "The Transcriptional and Functional Properties of Mouse Epiblast Stem Cells Resemble the Anterior Primitive Streak." *Cell Stem Cell* 14 (1): 107–20. https://doi.org/10.1016/j.stem.2013.09.014.

Kondoh, Hiroshi, Matilde E Lleonart, Yasuhiro Nakashima, Masayuki Yokode, Makoto Tanaka, David Bernard, Jesus Gil, and David Beach. 2007. "A High Glycolytic Flux Supports the Proliferative Potential of Murine Embryonic Stem Cells." *Antioxidants & Redox Signaling* 9 (3): 293–99. https://doi.org/10.1089/ars.2006.1467.

Konno, Masamitsu, Hideshi Ishii, Jun Koseki, Nobuhiro Tanuma, Naohiro Nishida, Koichi Kawamoto, Tatsunori Nishimura, et al. 2015. "Pyruvate Kinase M2, but Not M1, Allele Maintains Immature Metabolic States of Murine Embryonic Stem Cells." *Regenerative Therapy* 1: 63–71. https://doi.org/10.1016/j.reth.2015.01.001.

Lee, Jungwoon, Hye Kyoung Kim, Yong-Mahn Han, and Jungho Kim. 2008. "Pyruvate Kinase Isozyme Type M2 (PKM2) Interacts and Cooperates with Oct-4 in Regulating Transcription." *The International Journal of Biochemistry & Cell Biology* 40 (5): 1043–54. https://doi.org/https://doi.org/10.1016/j.biocel.2007.11.009.

Levine, Arnold J, and Anna M Puzio-Kuter. 2010. "The Control of the Metabolic Switch in Cancers by Oncogenes and Tumor Suppressor Genes." *Science* 330 (6009): 1340 LP – 1344. https://doi.org/10.1126/science.1193494.

Liang, Ji, Ruixiu Cao, Xiongjun Wang, Yajuan Zhang, Pan Wang, Hong Gao, Chen Li, et al. 2017. "Mitochondrial PKM2 Regulates Oxidative Stress-Induced Apoptosis by Stabilizing Bcl2." *Cell Research* 27 (3): 329–51. https://doi.org/10.1038/cr.2016.159.

Liang, Jiancong, Ma Wan, Yi Zhang, Peili Gu, Huawei Xin, Sung Yun Jung, Jun Qin, et al. 2008. "Nanog and Oct4 Associate with Unique Transcriptional Repression Complexes in Embryonic Stem Cells." *Nature Cell Biology* 10 (6): 731–39.

https://doi.org/10.1038/ncb1736.
Ma, Rong, Qing Liu, Shutao Zheng, Tao Liu, Doudou Tan, and Xiaomei Lu. 2019. "PKM2-Regulated STAT3 Promotes Esophageal Squamous Cell Carcinoma Progression via TGF-B1-Induced EMT." *Journal of Cellular Biochemistry* 120 (7): 11539–50. https://doi.org/10.1002/jcb.28434.
Manders, EMM, FJ Verbeek, and JA Aten. 1993. "Measurement of Co-Localization of Objects in Dual-Colour Confocal Images." *Journal of Microscopy* 169 (3): 375–82. https://doi.org/10.1111/j.1365-2818.1993.tb03313.x.
Martin, G R. 1981. "Isolation of a Pluripotent Cell Line from Early Mouse Embryos Cultured in Medium Conditioned by Teratocarcinoma Stem Cells." *Proceedings of the National Academy of Sciences* 78 (12): 7634 LP – 7638. https://doi.org/10.1073/pnas.78.12.7634.
Morfouace, M., L. Lalier, L. Oliver, M. Cheray, C. Pecqueur, P. F. Cartron, and F. M. Vallette. 2014. "Control of Glioma Cell Death and Differentiation by PKM2-Oct4 Interaction." *Cell Death and Disease* 5 (1): e1036-8. https://doi.org/10.1038/cddis.2013.561.
Morgani, Sophie, Jennifer Nichols, and Anna Katerina Hadjantonakis. 2017. "The Many Faces of Pluripotency: In Vitro Adaptations of a Continuum of in Vivo States." *BMC Developmental Biology* 17 (1): 10–12. https://doi.org/10.1186/s12861-017-0150-4.
Morita, Mami, Taku Sato, Miyuki Nomura, Yoshimi Sakamoto, Yui Inoue, Ryota Tanaka, Shigemi Ito, et al. 2018. "PKM1 Confers Metabolic Advantages and Promotes Cell-Autonomous Tumor Cell Growth." *Cancer Cell* 33 (3): 355-367.e7. https://doi.org/10.1016/j.ccell.2018.02.004.
Nabbi, Arash, and Karl Riabowol. 2015. "Rapid Isolation of Nuclei from Cells in Vitro." *Cold Spring Harbor Protocols* 2015 (8): 769–72. https://doi.org/10.1101/pdb.prot083733.
Nakatsu, Daiki, Yuta Horiuchi, Fumi Kano, Yoshiyuki Noguchi, Taichi Sugawara, Iseki Takamoto, Naoto Kubota, Takashi Kadowaki, and Masayuki Murata. 2015. "L-Cysteine Reversibly Inhibits Glucose-Induced Biphasic Insulin Secretion and ATP Production by Inactivating PKM2." *Proceedings of the National Academy of Sciences of the United States of America* 112 (10): E1067–76. https://doi.org/10.1073/pnas.1417197112.
Nichols, Jennifer, and Austin Smith. 2009. "Naive and Primed Pluripotent States." *Cell Stem Cell* 4 (6): 487–92. https://doi.org/10.1016/j.stem.2009.05.015.
Niwa, Hitoshi, Jun Ichi Miyazaki, and Austin G. Smith. 2000. "Quantitative Expression of Oct-3/4 Defines Differentiation, Dedifferentiation or Self-Renewal of ES Cells." *Nature Genetics* 24 (4): 372–76. https://doi.org/10.1038/74199.
Noguchi, T, K Yamada, H Inoue, T Matsuda, and T Tanaka. 1987. "The L- and R-Type Isozymes of Rat Pyruvate Kinase Are Produced from a Single Gene by Use of Different Promoters." *Journal of Biological Chemistry* 262 (29): 14366–71. http://www.jbc.org/content/262/29/14366.abstract.
Ohinata, Yasuhide, Hiroshi Ohta, Mayo Shigeta, Kaori Yamanaka, Teruhiko Wakayama, and Mitinori Saitou. 2009. "A Signaling Principle for the Specification of the Germ Cell Lineage in Mice." *Cell* 137 (3): 571–84. https://doi.org/10.1016/j.cell.2009.03.014.
Ohtsuka, Satoshi, Yoko Nakai-Futatsugi, and Hitoshi Niwa. 2015. "LIF Signal in Mouse Embryonic Stem Cells." *JAK-STAT* 4 (2): 1–9.

https://doi.org/10.1080/21623996.2015.1086520.
Ohtsuka, Satoshi, Satomi Nishikawa-Torikai, and Hitoshi Niwa. 2012. "E-Cadherin Promotes Incorporation of Mouse Epiblast Stem Cells into Normal Development." *PLoS ONE* 7 (9). https://doi.org/10.1371/journal.pone.0045220.
Otsu, Nobuyuki. 1979. "A Threshold Selection Method from Gray-Level Histograms." *IEEE Transactions on Systems, Man and Cybernetics* 20 (1): 62–66. https://doi.org/0018-9472/79/0100-0062$00.75.
Pearson, Karl, and Olaus Magnus Friedrich Erdmann Henrici. 1896. "VII. Mathematical Contributions to the Theory of Evolution.—III. Regression, Heredity, and Panmixia." *Philosophical Transactions of the Royal Society of London. Series A, Containing Papers of a Mathematical or Physical Character* 187 (January): 253–318. https://doi.org/10.1098/rsta.1896.0007.
Prakasam, Gopinath, Rajnish Kumar Singh, Mohammad Askandar Iqbal, Sunil Kumar Saini, Ashu Bhan Tiku, and Rameshwar N K Bamezai. 2017. "Pyruvate Kinase M Knockdown–Induced Signaling via AMP-Activated Protein Kinase Promotes Mitochondrial Biogenesis, Autophagy, and Cancer Cell Survival." *Journal of Biological Chemistry* 292 (37): 15561–76. https://doi.org/10.1074/jbc.M117.791343.
Prigione, Alessandro, Beatrix Fauler, Rudi Lurz, Hans Lehrach, and James Adjaye. 2010. "The Senescence-Related Mitochondrial/Oxidative Stress Pathway Is Repressed in Human Induced Pluripotent Stem Cells." *STEM CELLS* 28 (4): 721–33. https://doi.org/10.1002/stem.404.
Qi, Hailong, Xianling Ning, Chang Yu, Xin Ji, Yan Jin, Michael A McNutt, and Yuxin Yin. 2019. "Succinylation-Dependent Mitochondrial Translocation of PKM2 Promotes Cell Survival in Response to Nutritional Stress." *Cell Death & Disease* 10 (3): 170. https://doi.org/10.1038/s41419-018-1271-9.
Qin, Shengtang, Danli Yang, Kang Chen, Haolan Li, Liqiang Zhang, Yuan Li, Rongrong Le, Xiaojie Li, Shaorong Gao, and Lan Kang. 2017. "Pkm2 Can Enhance Pluripotency in ESCs and Promote Somatic Cell Reprogramming to IPSCs." *Oncotarget* 8 (48): 84276. https://doi.org/10.18632/ONCOTARGET.20685.
Rodrigues, Ana Sofia, Marcelo Correia, Andreia Gomes, Sandro L. Pereira, Tânia Perestrelo, Maria Inês Sousa, and João Ramalho-Santos. 2015. "Dichloroacetate, the Pyruvate Dehydrogenase Complex and the Modulation of MESC Pluripotency." *PLoS ONE* 10 (7): e0131663. https://doi.org/10.1371/journal.pone.0131663.
Shi, Xiangguang, Lingchong You, and Ruo-yu Luo. 2019. "Glycolytic Reprogramming in Cancer Cells: PKM2 Dimer Predominance Induced by Pulsatile PFK-1 Activity." *Physical Biology* 16 (6): 66007. https://doi.org/10.1088/1478-3975/ab3f5a.
Shimada, Nobukazu, Toshie Shinagawa, and Shunsuke Ishii. 2008. "Modulation of M2-Type Pyruvate Kinase Activity by the Cytoplasmic PML Tumor Suppressor Protein." *Genes to Cells* 13 (3): 245–54. https://doi.org/10.1111/j.1365-2443.2008.01165.x.
Silva, Jose, and Austin Smith. 2008. "Capturing Pluripotency." *Cell* 132 (4): 532–36. https://doi.org/10.1016/j.cell.2008.02.006.
Smith, Austin. 2017. "Formative Pluripotency: The Executive Phase in a Developmental Continuum." *Development* 144 (3): 365–73. https://doi.org/10.1242/dev.142679.
Takahashi, Saori, Shin Kobayashi, and Ichiro Hiratani. 2018. "Epigenetic Differences between Naïve and Primed Pluripotent Stem Cells." *Cellular and Molecular Life*

Sciences 75 (7): 1191–1203. https://doi.org/10.1007/s00018-017-2703-x.
Taniguchi, Kohei, Nobuhiko Sugito, Minami Kumazaki, Haruka Shinohara, Nami Yamada, Yoshihito Nakagawa, Yuko Ito, et al. 2015. "MicroRNA-124 Inhibits Cancer Cell Growth through PTB1/PKM1/PKM2 Feedback Cascade in Colorectal Cancer." *Cancer Letters* 363 (1): 17–27. https://doi.org/10.1016/J.CANLET.2015.03.026.
Tesar, Paul J., Josh G. Chenoweth, Frances A. Brook, Timothy J. Davies, Edward P. Evans, David L. Mack, Richard L. Gardner, and Ronald D.G. McKay. 2007. "New Cell Lines from Mouse Epiblast Share Defining Features with Human Embryonic Stem Cells." *Nature* 448 (7150): 196–99. https://doi.org/10.1038/nature05972.
Wang, H.-J., Y.-J. Hsieh, W.-C. Cheng, C.-P. Lin, Y.-S. Lin, S.-F. Yang, C.-C. Chen, et al. 2014. "JMJD5 Regulates PKM2 Nuclear Translocation and Reprograms HIF-1 -Mediated Glucose Metabolism." *Proceedings of the National Academy of Sciences* 111 (1): 279–84. https://doi.org/10.1073/pnas.1311249111.
Wei, Libin, Yuanyuan Dai, Yuxin Zhou, Zihao He, Jingyue Yao, Li Zhao, Qinglong Qiqiang Guo, et al. 2018. "Pyruvate Kinase M2 Is a PHD3-Stimulated Coactivator for Hypoxia-Inducible Factor 1." *Development* 8 (1): 1–16. https://doi.org/10.1016/j.cell.2011.03.054.
Wei, Libin, Yuanyuan Dai, Yuxin Zhou, Zihao He, Jingyue Yao, Li Zhao, Qinglong Guo, and Lin Yang. 2017. "Oroxylin A Activates PKM1/HNF4 Alpha to Induce Hepatoma Differentiation and Block Cancer Progression." *Cell Death & Disease* 8 (7): e2944. https://doi.org/10.1038/cddis.2017.335.
Weinhouse, SIDNEY, OTTO Warburg, DEAN Burk, and ARTHUR L Schade. 1956. "On Respiratory Impairment in Cancer Cells." *Science* 124 (3215): 267 LP – 272. https://doi.org/10.1126/science.124.3215.267.
Wolff, Barbara, Jean-Jacques Sanglier, and Ying Wang. 1997. "Leptomycin B Is an Inhibitor of Nuclear Export: Inhibition of Nucleo-Cytoplasmic Translocation of the Human Immunodeficiency Virus Type 1 (HIV-1) Rev Protein and Rev-Dependent MRNA." *Chemistry & Biology* 4 (2): 139–47. https://doi.org/https://doi.org/10.1016/S1074-5521(97)90257-X.
Wong, Carmen Chak Lui, Sandy Leung Kuen Au, Aki Pui Wah Tse, Iris Ming Jing Xu, Robin Kit Ho Lai, David Kung Chun Chiu, Larry Lai Wei, et al. 2014. "Switching of Pyruvate Kinase Isoform l to M2 Promotes Metabolic Reprogramming in Hepatocarcinogenesis." *PLoS ONE* 9 (12). https://doi.org/10.1371/journal.pone.0115036.
Wong, Nicholas, Jason De Melo, and Damu Tang. 2013. "PKM2, a Central Point of Regulation in Cancer Metabolism." *International Journal of Cell Biology* 2013. https://doi.org/10.1155/2013/242513.
Wu, Yong, Vadim Zinchuk, Olga Grossenbacher-Zinchuk, and Enrico Stefani. 2012. "Critical Evaluation of Quantitative Colocalization Analysis in Confocal Fluorescence Microscopy." *Interdisciplinary Sciences: Computational Life Sciences* 4 (1): 27–37. https://doi.org/10.1007/s12539-012-0117-x.
Yamada, K, and T Noguchi. 1999. "Regulation of Pyruvate Kinase Gene Expression." *Biochem. J* 337: 1–11. https://doi.org/PMC1219928.
Yang, W., and Z. Lu. 2015. "Pyruvate Kinase M2 at a Glance." *Journal of Cell Science* 128 (9): 1655–60. https://doi.org/10.1242/jcs.166629.
Yang, Weiwei, and Zhimin Lu. 2013. "Nuclear PKM2 Regulates the Warburg Effect."

Cell Cycle 12 (19): 3154–58. https://doi.org/10.4161/cc.26182.

Yang, Weiwei, Yan Xia, Haitao Ji, Yanhua Zheng, Ji Liang, Wenhua Huang, Xiang Gao, Kenneth Aldape, and Zhimin Lu. 2011. "Nuclear PKM2 Regulates β-Catenin Transactivation upon EGFR Activation." *Nature* 480 (7375): 118–22. https://doi.org/10.1038/nature10598.

Yang, Weiwei, Yanhua Zheng, Yan Xia, Haitao Ji, Xiaomin Chen, Fang Guo, Costas A. Lyssiotis, Kenneth Aldape, Lewis C. Cantley, and Zhimin Lu. 2012. "ERK1/2-Dependent Phosphorylation and Nuclear Translocation of PKM2 Promotes the Warburg Effect." *Nature Cell Biology* 14 (12): 1295–1304. https://doi.org/10.1038/ncb2629.

Ying, Qi-Long, Jason Wray, Jennifer Nichols, Laura Batlle-Morera, Bradley Doble, James Woodgett, Philip Cohen, and Austin Smith. 2008. "The Ground State of Embryonic Stem Cell Self-Renewal." *Nature* 453 (7194): 519–23. https://doi.org/10.1038/nature06968.

Zhang, Jin, Jing Zhao, Perrine Dahan, Vivian Lu, Cheng Zhang, Hu Li, and Michael A. Teitell. 2018. "Metabolism in Pluripotent Stem Cells and Early Mammalian Development." *Cell Metabolism* 27 (2): 332–38. https://doi.org/10.1016/j.cmet.2018.01.008.

Zhou, Wenyu, Michael Choi, Daciana Margineantu, Lilyana Margaretha, Jennifer Hesson, Christopher Cavanaugh, C. Anthony Blau, et al. 2012. "HIF1α Induced Switch from Bivalent to Exclusively Glycolytic Metabolism during ESC-to-EpiSC/HESC Transition." *EMBO Journal* 31 (9): 2103–16. https://doi.org/10.1038/emboj.2012.71.

Zhou, Ying, Srinjan Basu, Ernest Laue, and Ashwin A Seshia. 2016. "Single Cell Studies of Mouse Embryonic Stem Cell (MESC) Differentiation by Electrical Impedance Measurements in a Microfluidic Device." *Biosensors & Bioelectronics* 81 (July): 249–58. https://doi.org/10.1016/j.bios.2016.02.069.

Zhu, Hui, Shijun Hu, and Julie Baker. 2014. "JMJD5 Regulates Cell Cycle and Pluripotency in Human Embryonic Stem Cells." *Stem Cells (Dayton, Ohio)*, 1–17. https://doi.org/10.1002/stem.1724.

Zinchuk, Vadim, Yong Wu, and Olga Grossenbacher-Zinchuk. 2013. "Bridging the Gap between Qualitative and Quantitative Colocalization Results in Fluorescence Microscopy Studies." *Scientific Reports* 3 (1): 1365. https://doi.org/10.1038/srep01365.

Chapter 4

4.0.0. Chapter Title: Flow cytometric characterization of pluripotent cell protein markers in naïve, formative, and primed pluripotent stem cells

A version of this Chapter has been submitted for publication in *Methods in Molecular Biology.*

4.0.1. CRediT Author Statement:

Joshua Dierolf: Conceptualization, Methodology, Validation, Formal Analysis, Investigation, Writing – Original Draft, Writing – Review & Editing, Visualization

Kristin Chadwick: Conceptualization, Validation

Courtney Brooks: Conceptualization, Methodology, Investigation

Dean Betts: Resources, Writing – Review & Editing, Funding Acquisition

Andrew Watson: Writing – Review & Editing

4.0.2. Summary:

Here we describe methodologies to characterize, delineate, and quantify pluripotent cells between naïve, formative, and primed pluripotent state mouse embryonic stem cell (mESCs) populations using flow cytometric analysis. This methodology can validate pluripotent states, sort individual cells of interest and determine the efficiency of transitioning naïve mESCs to a primed-like state as mouse epiblast-like cells (mEpiLCs) and on to fully primed mouse epiblast stem cells (mEpiSCs). Quantification of the cell surface markers: SSEA1(CD15) and CD24, introduces an effective method of distinguishing individual cells from a population by their respective positioning in the pluripotent spectrum. Additionally, this protocol can be used to demarcate and sort cells via fluorescently activated cell sorting for downstream applications. Flow cytometric analysis within mESCs, mEpiLCs, and mEpiSCs can be efficiently completed using these optimized protocols.

4.1.0. Introduction:

Flow cytometry is a method of single cell analysis utilizing a microfluidic system where individual cells are directed, single file, through a laser, or series of lasers. Cell size and granularity can be assessed using flow cytometry through the analysis of laser light scatter. The measurement of side-scatter shows the level of granularity, or, the amount of light that reflects off the individual cell and intracellular interface, whereas the forward-scatter parameter is a measure of the light that passes around the cell in question. Taken together, an understanding of the size and intracellular complexity of the cells in a population can be quantified and organized into subpopulations (Leif 1986). Cells can be sorted through the process of fluorescently activated cell sorting (FACS) following the process of gating out specific traits of a population for downstream applications.

Several methods of mouse epiblast cell-like cell (mEpiLCs) generation have been devised (Morgani, Nichols, and Hadjantonakis 2017). This protocol have utilizes ground state mouse embryonic stem cell (mESCs) transitioned into mEpiLCs over 48, 72, and 92 hours in transitioning media containing Activin A and Fibroblast growth factor 5 (Fgf5), replacing mESC media containing leukemia inhibitory factor (LIF) and a small molecule cocktail of inhibitors for Glycogen synthase kinase 3 beta (GSK3b) and Mitogen-activated protein kinase, kinase (MEK) (Hayashi et al. 2011). This flow cytometric analysis methodology includes quantification of the cell surface markers: Stage-Specific Embryonic Antigen-1 (SSEA1/CD15) and Cluster of differentiation 24 (CD24). SSEA1 is a naïve pluripotency associated cell surface protein marker that is expressed in mESCs (Solter and Knowles 1978). Alternatively, CD24 is an expressed primarily in primed mEpiSCs and has decreased expression in naïve mESCs (Shakiba et al. 2015). Together,

I propose that SSEA1 and CD24 can be used to discriminate between either end of the pluripotent spectrum in human and mouse pluripotent stem cells (PSCs), and can also be used to distinguish formative pluripotent state mouse epiblast-like cells (mEpiLCs) as well (Shakiba et al. 2015). Additional methods of flow cytometric normalization, practises, and troubleshooting are beyond the scope of this chapter, however, for these additional details, we refer the reader to following excellent resources (Hahne et al. 2010; Herzenberg et al. 2006).

4.2.0. Materials:

1. Washing Solution: Sterile Dulbecco's Phosphate Buffered Saline (no magnesium, no calcium) (DPBS(-/-))(DPBS(-/-))(Gibco^{TM} 14190144).
2. Flow Cytometry Staining Buffer – 10 % Fetal bovine serum (Embryonic stem-cell FBS, qualified, US origin (Gibco 16141061)) in DPBS(-/-) filter sterilized.
3. Trypan Blue Solution (ThermoFisher Scientific 15250061).
4. Fixing Agent: 4 % paraformaldehyde (Sigma Aldrich, St Louis MO) diluted in DPBS(-/-).
5. Cell passaging agent (StemPro Accutaseâ).
6. Antibody dilutions:
    - Live/Dead: Live/Dead viability dye such as Zombie Aqua™ Fixable Viability Kit (BioLegend 423101), diluted 1:1000/1 million cells.
    - SSEA1: Brilliant Violet 421™ anti-mouse/human CD15 (SSEA-1) Antibody (BioLegend 125613) diluted at 5 mL/1 million cells.

- CD24: APC/Cyanine7 anti-mouse CD24 Antibody (BioLegend 101821) diluted at 0.25 mg/1 million cells.

7. 20-40 µM sterile cell strainers (Falcon™ Cell Strainers 08-771-1).
8. Flow tubes and corresponding caps, specific to your flow cytometer of choice.

4.3.0. Methods:

In the following protocol, I describe how to characterize and distinguish between pluripotent stem cell populations representing naïve, formative, and primed pluripotent states using flow cytometry. Methods for using both live and fixed cell preparations are detailed. Live cell staining may be used for downstream sorting of purified populations, and additional experimentation such as omics data analysis or differentiation assays, whereas fixed cell staining can be sorted for downstream applications limited to non-viable cells, such as protein and transcript abundance studies. This methodology is useful in determining the transition efficiency of generating primed-like mEpiLCs from mESCs in comparison to primed mEpiSCs by a comparison of SSEA1 and CD24 cell surface expression levels. These markers can be compared for both human and mouse PSCs (Shakiba et al. 2015).

During the experimental planning step, aim to grow your pluripotent stem cells into their third, fourth, and fifth (P_X+3/4/5 minimum) passage following cryopreservation thaw. This will allow for 3 biological replicates. To analyze geometric mean, mode, or median data, each biological replicate should be analyzed in the same flow cytometric experimental session. If you are only looking at pluripotent marker gating, each

biological replicate can be run on their own session only if the full set of controls are used for each run. Additionally, grow cells to a quantity that allows for 3 technical replicates of each biological replicate of each cell type to be analyzed. Regardless of gating scheme, ensure colonies are morphologically healthy with little to no signs of differentiation and with similarly spaced-out cell densities.

Individual treatment groups require having an unstained control cell population, a single stain control of each protein marker, a full minus one (FMO) tube containing all protein markers except for one, and lastly a full stain sample containing each protein marker, each of these needs to be completed for each cell type examined. Additionally, a live/dead control is necessary to avoid autofluorescence readings produced by examining dead and ruptured cells. This can be accomplished by using a 50/50 % mixture of live and dead cells stained using a viability dye (e.g., Zombie Aqua) that penetrates dead cells only. Laser intensity compensation should be completed on the unstained and single stained specimens instead of traditionally compensation beads (*see* **Note 1)**. Always consult a spectral overlap calculator prior to ordering and running a multi-stained flow cytometry experiment to ensure individual readings can be differentiated from each other. The Spectral Viewer by BD Biosciences (San Jose, CA) is especially useful if you are using a BD Biosciences flow cytometer. Prior to a running a complete experiment, it is advised that an antibody titration series be completed for each new cell type and stain, this can be accomplished by testing the recommended controls. See Table 4.1 for recommended starting set-up for mouse epiblast stem cells.

Table 4.1. Recommended Set-up for a single cell type.

Tube	Treatment/Specimen (mEpiSC)	Stain		
		Live/Dead	SSEA1	CD24
1.	Unstained			
2.	50% Live/50%Dead	Zombie Aqua		
3.	Single stain	Zombie Aqua		
4.	Single stain		BV421	
5.	Single stain			APC
6.	Full minus one		BV421	APC
7.	Full minus one	Zombie Aqua		APC
8.	Full minus one	Zombie Aqua	BV421	
9.	Full – n1	Zombie Aqua	BV421	APC
10.	Full – n2	Zombie Aqua	BV421	APC
11.	Full – n3	Zombie Aqua	BV421	APC

4.3.1. Live pluripotent stem cell preparation.

Twenty-four hours prior to the day of harvest, remove cells for live/dead cell compensation. This can be accomplished by leaving a conical tube of cells out of the incubator in DPBS(-/-) overnight. Combine 200,000 dead cells with 200,000 live cells. Aim for approximately 400,000 cells overall for the live/dead treatment. Live cells benefit from the addition of 10 mM rho kinase inhibitor (Y-27632; STEMCELL Technologies). This should be added gently to fresh, pre-warmed (37 °C) media on cells for 1 hour in an incubator (*see* **Note 2**). Lift cells from their dish into a single cell

suspension for 5 minutes incubated at 37 °C using StemPro Accutase, cover the entire growth surface area to be effective, agitation is not necessary (*see* **Note 3**). Transfer the lifted cells to pre-warmed (37 °C) media and centrifuged (244 rcf) for 3 minutes or until pelleted (*see* **Note 4**). Aspirate supernatant and perform a viability cell count using trypan blue with a hemocytometer or similar cell counting method (Strober 1997). Each treatment should have a minimum of 400,000 cells. Divide cells into sterile, labelled, and capped flow tubes, reconstituted in 100 µL/treatment with flow cytometry staining buffer (FCSB). Stain live/dead viability treatments by incubating for 30 minutes in a light-tight box at room temperature (*see* **Note 5**). For treatments without live/dead staining skip this step and proceed to adding the appropriate fluorophore. Wash treatments with 2 mL of FCSB, centrifuge (244 rcf) for 3 minutes. Aspirate the supernatant and reconstitute with 100 µL of FCSB. Add appropriate fluorophore conjugated antibodies taking note of product concentration/cell count, gently vortex and incubate for 30 minutes in a light-tight box at room temperature. All samples, except for the unstained controls, are now light sensitive and should always be handled in dim lighting conditions. Wash treatments with 2 mL of FCSB, centrifuge (244 rcf) for 3 minutes. Reconstitute with 200 µL of FCSB and gently vortex. Pipette the cell suspension over an upside-down 20 µm cell strainer. Wash with 100 uL of FCSB. Flip cell strainer and pipette from the inside to get residual cells held by surface tension. Proceed immediately to running cells through a flow cytometer or FACS sorting for optimal results.

4.3.2. Fixed pluripotent stem cell preparation.

Twenty-Four hours prior to the day of harvest, remove cells for live/dead cell compensation. This can be accomplished by leaving a conical tube of cells out of the incubator in DPBS(-/-) overnight (*see* **Note 1**.). Aim for approximately 400,000 cells. Lift cells from their plate; enzymatic lifting works well. Colonies need to be separated into single cells, cover the growth surface with lifting agent for 5 minutes in an incubator (*see* N**ote 5**). Centrifuge (244 rcf) the single cell suspension for 3 minutes. Aspirate supernatant and perform a viability cell count using trypan blue with a hemocytometer or similar cell counting method(Strober 1997). Each treatment should have a minimum of 400,000 cells. Divide cells into sterile, labelled, and capped flow tubes, reconstituted in 100 µL/treatment with flow cytometry staining buffer (FCSB). Reconstitute in DPBS(-/-) (100 mL x tubes required), divide into flow tubes. Stain live/dead viability treatments by incubating for 30 minutes in a light-tight box at room temperature (*see* **Note 5**). For treatments without live/dead staining skip this step and proceed to fixation. Wash treatments with 2 mL of FCSB and centrifuge (244 rcf) for 3 minutes. Aspirate the supernatant and reconstitute with 100 mL of FCSB. Wash treatments with 2 mL of FCSB and centrifuge (244 rcf) for 3 minutes. Aspirate the supernatant and add appropriate 500 mL of fixative agent (freshly made and chilled 4 % paraformaldehyde in DPBS(-/-) is recommended for cell surface marker analysis), incubate for 10 minutes in a fume hood on ice (*see* **Notes 1 and 6**). Wash with 2 mL of DPBS(-/-) and centrifuge (244 rcf) for 3 minutes. Aspirate supernatant and reconstitute with 100 µL of PBS(-/-) per treatment. Add appropriate fluorophore conjugated antibodies taking note of product concentration/cell count, gently vortex and incubate for 1 hour in a light-tight box at on ice. All samples (except for unstained controls) are now light sensitive and should be

handled in dim lighting conditions. Wash once with 2 mL of DPBS(-/-) and centrifuge (244 rcf) for 3 minutes. Aspirate supernatant and reconstitute with 200 µL of DPBS(-/-) and gently vortex. Pipette the cell suspension over an upside-down 20 µm cell strainer and wash with 100 µL of DPBS(-/-). Flip the cell strainer and pipette from the inside to get residual cells held by surface tension. Leave tubes in the fridge in a light-tight box until you are ready to run on a flow cytometer. Run on a flow cytometer within 24 hours of staining for optimal results.

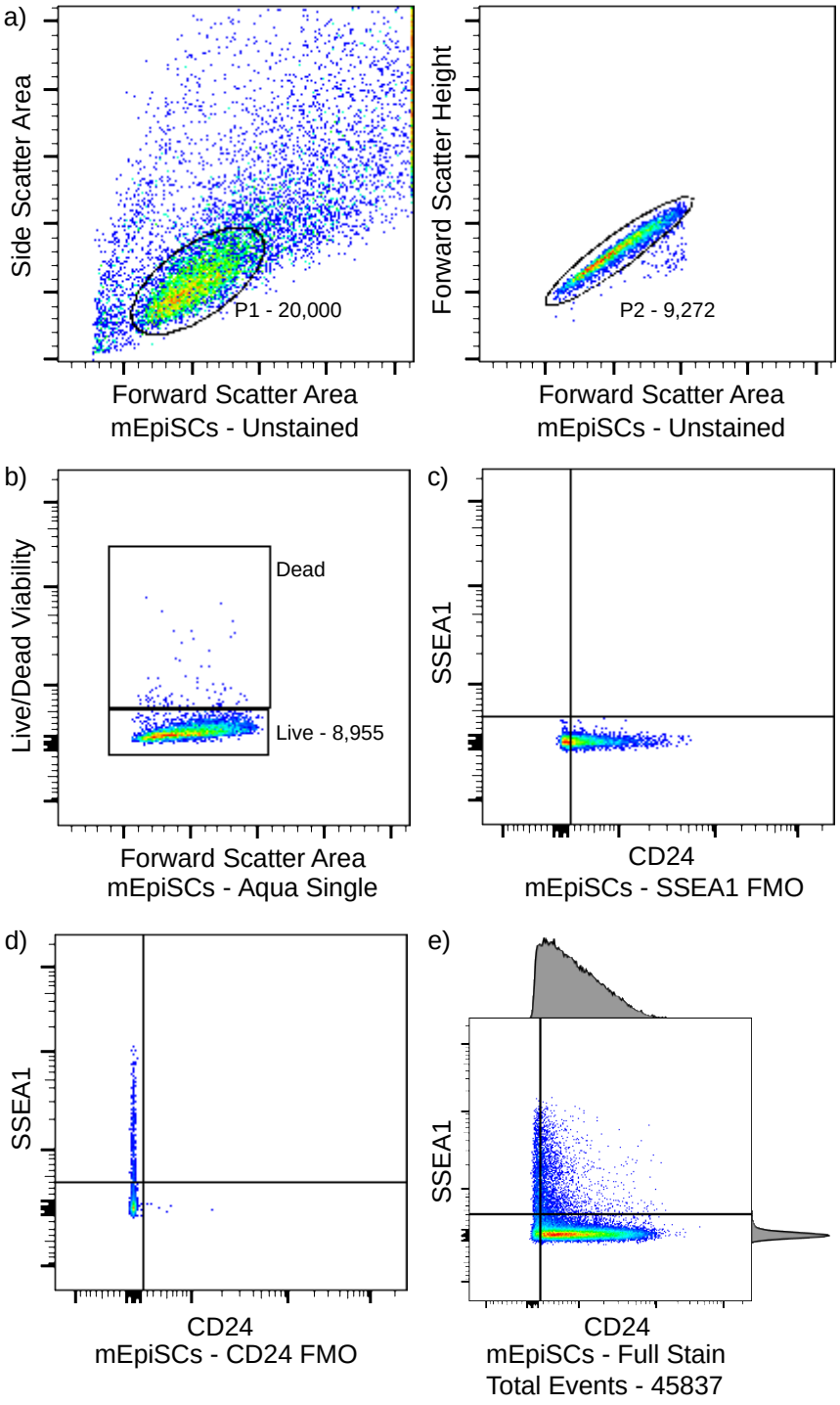
a)
Side Scatter Area
P1 - 20,000
Forward Scatter Area
mEpiSCs - Unstained
Forward Scatter Height
P2 - 9,272
Forward Scatter Area
mEpiSCs - Unstained
b)
Live/Dead Viability
Dead
Live - 8,955
Forward Scatter Area
mEpiSCs - Aqua Single
c)
SSEA1
CD24
mEpiSCs - SSEA1 FMO
d)
SSEA1
CD24
mEpiSCs - CD24 FMO
e)
SSEA1
CD24
mEpiSCs - Full Stain
Total Events - 45837

Figure 4.1. Flow cytometric characterization of SSEA1 and CD24 and gating strategy of mEpiSCs.

a) Side-scatter-area versus forward-scatter-area flow plot detailing granularity of light refracting off subcellular structures and cell size by light passing over the same individual cell events. This population display can show subpopulations within the data. In mEpiSCs, examine P1, the lower population if grown on MEFs. Forward-scatter area versus forward-scatter-height further delineates the shape of cells passing through the cytometer as population P2. b) Gating of viability-stained samples. Cells expressing the viability stain are not living, the live population on interest is compared to either the Live/Dead single stain or Live/Dead FMO specimens. c) SSEA1 versus CD24 channel expression with crosshair gating of the SSEA1 FMO specimen with the x-axis threshold set just above the main population of cells. d) SSEA1 versus CD24 channel expression with crosshair gating of the CD24 FMO specimen with the y-axis threshold set just to the right of the main population of cells. The x-axis threshold of c) is maintained.
e) SSEA1 versus CD24 channel expression with crosshair gating of the fully stained specimen with both the x-axis and y-axis thresholds maintained. Adjunct histograms can further distinguish the event density of the plot.

4.3.3. Flow Cytometric Analysis.

Flow cytometric analysis will depend largely on the cytometer the user has selected. For the development of this methodology, a BD FACSCanto™ Cell Analyzer flow cytometer was used, however, all the steps outlined will be consistent for any current flow cytometer. Regardless of the cytometer used, these steps should be followed to ensure consistent and qualified results. Consult with the manufacturer for setting individual laser parameters and ensure proper cleaning and maintenance has been completed prior to any use. Daily quality control checks need to be completed using qualified beads to optimize results.

Compensation was completed using BD FACSDiva™ Software. Gating was completed using BD FlowJo™ Software. While other post-flow cytometric analysis software is available, FlowJo™ currently provides the most comprehensive and advanced methods of flow cytometric analysis. The following gating strategy can be applied in most situations, however, if FlowJo is not your software of choice, start at Step 3. Each cell population refinement can be brought into the subsequent step for a final gated flow plot (*see* **Note 7**).

Import or drag individual .fsc files into FlowJo. Drag unstained, single stained treatments of each cell type into the compensation tab. Post-flow cytometric compensation can now be improved using FlowJo's Compensation Wizard. Compensated samples will be indicated with a colored 3x3 grid marker. Begin examining the unstained sample, setting the x- and y- axes to forward-scatter-area and side-scatter-area respectively, gate out the main population of cells. A tightly, set polygonal gate works well (Figure 4.1.a) (*see*

Note 8). Now, compare the Live/Dead stain only specimen to either the Live/Dead FMO or the unstained specimen. Examine these using forward-scatter-area versus the appropriate Live/Dead corresponding channel. A simple box gate scheme should suffice for both a live and dead gate (Figure 4.1. b). This step and the following steps can be portrayed using biexponential axes. Open both the SSEA1 FMO and CD24 FMO specimens. Set the x- and y- axes to the corresponding CD24 and SSEA1 laser channel respectively. Choose the crosshair gating option and set the crosshair above and to the right of each population (Figure 4.1.c, d). These options can be performed in either order. Finally, apply the complete gating scheme to the fully stained specimen. If possible, add adjunct histogram to show the event density (Figure 4.1.e) (*see* **Note 9**).

4.3.4. Statistical Representations

If each biological replicate was run during the same session, FlowJo can accurately calculate the geometric mean, mode, and median for an analysis relatively synonymous to that of densitometry in immunoblotting studies. These options can be found under statistical options following gating.

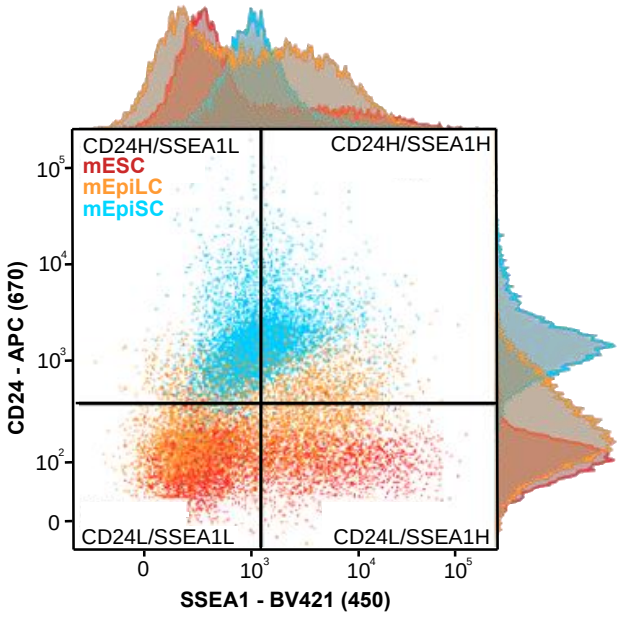

Figure 4.2. Flow cytometric expression of SSEA1 and CD24 during naïve to primed transitioning in mESCs, mEpiLCs, and mEpiSCs.

mESCs, mEpiLCs (72 hours of transitioning), and mEpiSCs examined for SSEA1 and CD24 run on a flow cytometry within a single session can be compared within a single flow plot to demonstrate the shifting of transitioning formative state mEpiLCs towards a primed-like pluripotent fate. Overlay of flow cytometric plots is best represented with adjunct histograms as pseudo-coloring of the individual events in an overlay is not distinguishable between groups.

Typical percentages of each population you may encounter can be found in Table 4.2.

Table 4.2. Quadrant event frequencies of SSEA1/CD24 cell surface marker expression in mESCs, mEpiLCs, and mEpiSCs.

Cell Type	SSEA1H/CD24 L (%Event±SD)	SSEA1H/CD24 H (%Event±SD)	SSEA1L/CD24 H (%Event±SD)	SSEA1L/CD24 L (%Event±SD)
Naïve mESCs	29.8±1.9	3.2±1.4	6.1±2.9	61.0±3.2
Formative, 48- hour mEpiLCs	31.1±18.5	1.8±1.2	1.9±0.3	65.2±19.4
Primed-like 96-hour mEpiLCs	38.6±5.2	14.9±10.9	5.9±2.5	40.3±14.1
Primed mEpiSCs	0.7±0.2	21.1±7.6	74.4±9.4	3.6±4.6

4.4.0. Notes:

1. *Growing mEpiSCs is optimal on a layer of MEF feeders. mEpiSCs are much smaller than MEFs and examining side-scatter and forward-scatter attributes can be used as a form of size exclusion. This method of gating is limited, and it is preferential to run samples both fixed and feeder-free when possible. Otherwise include a pluripotent marker not expressed on MEFs, especially in the case of a FACS study.*

2. *In the case of metabolism related scientific studies, consider avoiding feeding cells prior to or during the flow cytometry or immunofluorescent imaging process to maintain consistency and avoid spiking of metabolites and corresponding enzymatic processes/pathways.*

3. *Live/Dead cell compensation requires that you have a mix of live and dead cells. Some protocols use heated water (typically 65 °C) however mESCs can withstand 65 °C for 30 minutes, maintaining >98 % viability. Traditional compensation beads will not work with Live/Dead stains.*

4. *Spectral overlap of fluorophores can confound flow cytometry results depending on the stain and the flow cytometer used. Several spectral overlap calculators are available, and it is highly recommended that all stains be reviewed and applied appropriately to the correct flow cytometry laser configurations.*

5. *It is often recommended that compensation beads are used with single stains for flow cytometry. However, pluripotent stem cell marker expression will fluorescence brighter in PSCs than current commercially available compensation beads.*

6. *Fluorochromes such as phycoerythrin (PE) or allophycocyanin (APC) are large protein molecules and will be affected the same way as other proteins by the fixation so try to avoid alcohols. However, small fluorochromes such as AlexaFluor488 or FITC are generally unaffected by whichever fixative is used.*

7. *Doing this instead of importing the .wsp file containing the experiment will result in the x- and y- axes being flipped. This is a longstanding issue with FlowJo but may be corrected in the future.*

8. *This population can be refined by setting the x- and y- axes to forward-scatter-area and forward-scatter-height respectively, further gate out the main population of cells. A tightly, set polygonal gate works well (Fig. 4.2.a)).*

9. *This can be especially useful if combining and comparing several cell types or treatments and the pseudo-color display option can't be selected. See Figure 4.2. for a comparison of mESCs, mEpiLCs, and mEpiSCs overlayed.*

4.5.0. Discussion:

This protocol is specifically designed to sort naïve, formative, and primed pluripotent stem cell states. Studies examining newly derived or altered mPSCs could find such methods useful in validating pluripotent state, calculating transitioning efficiency of generating various pluripotent states, or following genetic manipulation (Kinoshita et al. 2020; Hayashi et al. 2011; Shakiba et al. 2015; Vidal, Stadtfeld, and Apostolou 2015). As pluripotency is described as a continuum, this method is invaluable for studying differences between cell types found in the developing epiblast. Originally, these methods have focused on sorting differences between naïve mESCs and primed mEpiSCs (Shakiba et al. 2015).

Here we uniquely describe how this procedure can be extended to also sort cells designated as the formative stage of pluripotency (Shakiba et al. 2015). As formative state cells are the only known pluripotent cell type capable of primordial germ cell differentiation, this method is applicable and necessary for the investigation of mechanisms controlling the differentiation of naïve, mESCs transitioning to a formative pluripotent state and onward to specialized germ cell-like cells following bone morphogenetic protein (BMP) treatment (Hayashi et al. 2011). During the development of this methodology, a non-transient formative state was described in mouse and human embryonic stem cells (Kinoshita et al. 2020). With the addition of Fgf/nodal signalling, Dr. Austin Smith's group, which originally hypothesized the formative pluripotent state, utilized tankyrase inhibitor to inhibit Wnt signalling in cells explanted from the inner cell mass of embryonic day 5.5 mouse embryos (Kinoshita et al. 2020). Previously, the formative state could only be captured for 24-48 hours as a transient population, with this

new methodology, cells can be passaged for >20 passages maintaining characteristics of the formative state. The protocols outlined in this methodology paper could be applied to this landmark study in generating stable formative pluripotent lines (Hayashi et al. 2011). Given proper bone morphogenetic protein stimuli, formative state cells can efficiently differentiate into primordial germ-like cells unlike any other pluripotent stem cell stage. Using this flow cytometric method, one can quantify the transitioning efficiency of formative state cells from mESCs compared to explanted formative state cells to determine differences in chemically transitioned and native states *in vitro*.

Traditionally, reprogramming somatic human cells and explanting embryonic stem cells from human embryos results in pluripotent stem cells representing the primed pluripotent state. Recently, naïve and formative state human pluripotent stem cells have been derived from both embryonic and adult origins (Ware et al. 2014; Giulitti et al. 2019; Kinoshita et al. 2020). The described methodology is applicable in the study of naïve pluripotent reversion from the primed pluripotent state and from somatic fates via reprogramming. From the human naïve pluripotent state, it is possible to transition to formative state and capture the transitioning efficiency as well as compare transitioned cells (i.e., naïve-like cells) to the traditional primed state as previous studies have compared naïve and primed mouse pluripotent states (Shakiba et al. 2015). The addition of CD40, a cell surface pluripotency marker associated with the primed pluripotent state, could additionally be utilized (Shakiba et al. 2015). Through previous attempts in the mouse system, we observed that CD24 differences were more apparent than CD40.

Currently, naïve, formative, and primed pluripotency discrimination can be completed through transcript abundance studies, epigenetic landscape differences, differentiation assays, and chimeric contributions (Kinoshita et al. 2020; Morgani, Nichols, and Hadjantonakis 2017). This novel method has the added benefit of potential downstream applications through the option of fluorescently activated cell sorting (FACS) of distinct, purified cell populations. Following FACS, sorted fixed cells can be examined for protein or transcript abundance studies and perhaps single cell analysis or proteomics and live cells can be re-plated into more homogenous populations for expansion and differentiation assays. With the advent of stable formative pluripotent states, the described methodology with the addition of FACS could allow for the study of subpopulations for improved studies into the development of germ cell differentiation. Future improvements to this protocol are likely to be optimized using stable and pure formative state PSC lines. A comparative study examining the transition of mESCs to formative mEpiLCs compared to actual explanted formative state cells and primed mEpiSCs examining the transition throughout the pluripotent spectrum within a smaller time interval would be telling of the developmental changes that take place.

4.6.0. Acknowledgements:

Flow cytometry was completed in at the London Regional Flow Cytometry Facility at Robarts Research Institute of Western University. mESC and mEpiSC pluripotent stem cell lines were graciously gifted from Dr. Janet Rossant. This research was funded by a Canadian Institutes of Health Research operating grant to A.J.W. and D.H.B. and Natural Sciences and Engineering Research Council of Canada grant to D.H.B. The funding sources played no role in design, data collection, analysis, decision to publish, or preparation of this study and manuscript.

4.7.0. References:

Giulitti, Stefano, Marco Pellegrini, Irene Zorzan, Paolo Martini, Onelia Gagliano, Margherita Mutarelli, Michael Johannes Ziller, et al. 2019. "Direct Generation of Human Naive Induced Pluripotent Stem Cells from Somatic Cells in Microfluidics." *Nature Cell Biology* 21 (2): 275–86. https://doi.org/10.1038/s41556-018-0254-5.

Hahne, Florian, Alireza Hadj Khodabakhshi, Ali Bashashati, Chao-Jen Wong, Randy D Gascoyne, Andrew P Weng, Vicky Seyfert-Margolis, et al. 2010. "Per-Channel Basis Normalization Methods for Flow Cytometry Data." *Cytometry Part A* 77A (2): 121–31. https://doi.org/https://doi.org/10.1002/cyto.a.20823.

Hayashi, Katsuhiko, Hiroshi Ohta, Kazuki Kurimoto, Shinya Aramaki, and Mitinori Saitou. 2011. "Reconstitution of the Mouse Germ Cell Specification Pathway in Culture by Pluripotent Stem Cells." *Cell* 146 (4): 519–32. https://doi.org/10.1016/j.cell.2011.06.052.

Herzenberg, Leonore A, James Tung, Wayne A Moore, Leonard A Herzenberg, and David R Parks. 2006. "Interpreting Flow Cytometry Data: A Guide for the Perplexed." *Nature Immunology* 7 (7): 681–85. https://doi.org/10.1038/ni0706-681.

Kinoshita, Masaki, Michael Barber, William Mansfield, Yingzhi Cui, Daniel Spindlow, Giuliano Giuseppe Stirparo, Sabine Dietmann, Jennifer Nichols, and Austin Smith. 2020. "Capture of Mouse and Human Stem Cells with Features of Formative Pluripotency." *Cell Stem Cell*. https://doi.org/https://doi.org/10.1016/j.stem.2020.11.005.

Leif, Robert C. 1986. "Practical Flow Cytometry." *Cytometry* 7 (1): 111–12. https://doi.org/https://doi.org/10.1002/cyto.990070119.

Morgani, Sophie, Jennifer Nichols, and Anna Katerina Hadjantonakis. 2017. "The Many Faces of Pluripotency: In Vitro Adaptations of a Continuum of in Vivo States." *BMC Developmental Biology* 17 (1): 10–12. https://doi.org/10.1186/s12861-017-0150-4.

Shakiba, Nika, Carl A. White, Yonatan Y. Lipsitz, Ayako Yachie-Kinoshita, Peter D. Tonge, Samer M.I. Hussein, Mira C. Puri, et al. 2015. "CD24 Tracks Divergent Pluripotent States in Mouse and Human Cells." *Nature Communications* 6: 7329. https://doi.org/10.1038/ncomms8329.

Solter, D, and B B Knowles. 1978. "Monoclonal Antibody Defining a Stage-Specific Mouse Embryonic Antigen (SSEA-1)." *Proceedings of the National Academy of Sciences* 75 (11): 5565 LP – 5569. https://doi.org/10.1073/pnas.75.11.5565.

Strober, Warren. 1997. "Trypan Blue Exclusion Test of Cell Viability." *Current Protocols in Immunology* 21 (1): A.3B.1-A.3B.2. https://doi.org/https://doi.org/10.1002/0471142735.ima03bs21.

Vidal, Simon E., Matthias Stadtfeld, and Eftychia Apostolou. 2015. "F-Class Cells: New Routes and Destinations for Induced Pluripotency." *Cell Stem Cell* 16 (1): 9–10. https://doi.org/10.1016/j.stem.2014.12.007.

Ware, C. B., A. M. Nelson, B. Mecham, J. Hesson, W. Zhou, E. C. Jonlin, A. J. Jimenez-Caliani, et al. 2014. "Derivation of Naive Human Embryonic Stem Cells." *Proceedings of the National Academy of Sciences* 111 (12): 4484–89. https://doi.org/10.1073/pnas.1319738111.

Chapter 5

A version of this Chapter is being submitted for publication.

5.0.0. Title: Modulation of PKM1/2 levels by steric-blocking morpholinos alters the metabolic and pluripotent state of murine pluripotent stem cells.

5.0.1. Author contributions:

CRediT Author Statement:

Joshua G. Dierolf: Conceptualization, Methodology, Validation, Formal Analysis, Investigation, Writing – Original Draft, Writing – Review & Editing, Visualization

Hailey Hunter: Methodology, Writing – Review & Editing

Dean H. Betts: Resources, Writing – Review & Editing, Funding Acquisition, Supervision

Andrew J. Watson: Writing – Review & Editing, Funding Acquisition, Supervision

5.1.0. Abstract:

Metabolism is implicated in playing both an active and passive role in embryonic development, cell pluripotency, and cell-fate, however, little is known regarding the role of metabolic state in the recently described formative pluripotent state. This developmental pluripotent continuum is accompanied by a metabolic switch from a bivalent metabolism (both glycolysis and oxidative phosphorylation) in naïve cells, to predominantly glycolysis in primed cells. Metabolic preferences promote the maintenance and generation of various pluripotent states. I have investigated the role of pyruvate kinase muscle isoforms (PKM1/2) in naïve, formative, and primed mouse embryonic stem cells through modulation of PKM1/2 mRNA transcripts using steric-blocking morpholinos that downregulate PKM2 and upregulate PKM1. I have examined these effects in naïve, formative, and primed cell states by quantifying the effects of PKM1/2 modulation on pluripotent and metabolic transcripts and by measuring shifts in the populations of cells expressing naïve and primed markers by flow cytometry. I found that modulating PKM1 and PKM2 levels alters the transition from the naïve state into a formative and primed-like pluripotent states. Therefore, I conclude that PKM1/2 actively contributes to mechanisms that oversee early stem pluripotency and their progression towards a primed pluripotent state.

5.2.0. Introduction:

Pluripotent stem cells (PSCs) are characterized by their unlimited self-renewal and potential to specialize into cell types of the adult organism. Approximately 3.5 days following fertilization (E3.5), the mouse embryo contains a niche of cells within the

blastocyst and encircled by the trophectoderm called the inner cell mass (ICM) of the pre-implantation embryo (Evans and Kaufman 1981; Martin 1981). This niche of 10-20 cells represents the earliest pluripotent stem cell (PSC) population of the developing embryo and these cells are the origin of the primary germ layers that result in the formation of the fetus. These cells also represent the origins of mouse embryonic stem cells (ESCs) that are important research models for unraveling early developmental cell fate control mechanisms and are also key resources for the development of cell-based therapeutics. PSCs of the developing mouse can be explanted from the embryo until E8.0, however, several key differences underlying changes in their pluripotency arise between the E3.5 and E8.0 (Morgani, Nichols, and Hadjantonakis 2017). Some of these differences include developmentally programmed changes in gene expression, epigenetic landscape, metabolic preferences, and ability to contribute to all germ cell layers and chimeric development (Nichols and Smith 2009; Zhou et al. 2012). Explanted mouse ESCs (mESCs) between E3.5 and E4.5 and mouse epiblast stem cells (mEpiSCs) from between E7.25 and E8.0 both express core pluripotency genes including sex determining region Y – box 2 (Sox2), octamer-binding transcription factor 4 (Oct4), and Nanog (lower in mouse epiblast stem cells; mEpiSCs), however, mESCs express pluripotency associated genes such as reduced expression 1 (Rex1), platelet endothelial cell adhesion molecule 1 (Pecam-1), and orphan nuclear receptor Esrrb at greater levels than mEpiSCs (Wray et al. 2011). Conversely, mEpiSCs express pluripotency genes such as Zinc finger protein 2 (Zic2), T(Brachyury), and Cerberus (Cer1) more so than mESCs (Morgani, Nichols, and Hadjantonakis 2017). Metabolically, mESCs are bivalent in their preference for metabolic pathways utilizing both glycolysis and oxidative phosphorylation (OXPHOS). However, mEpiSCs are preferentially univalent, using aerobic glycolysis, similar to the

preferences of most cancer cells, where regardless of oxygen availability glycolysis takes on precedence despite OXPHOS being capable of generating more adenosine triphosphate (ATP) (Zhou et al. 2012). Primed cells, adult stem cells, and typical cancer cells with high rates of proliferation opt for glycolysis in this manner to generate metabolic precursors for other anabolic processes (Vander Heiden, Cantley, and Thompson 2009; Mathieu and Ruohola-Baker 2017). Recent studies have indicated there is an intermediate state of pluripotency existing between the naïve and primed ends of the pluripotent spectrum referred to as 'formative pluripotency', representative of the E5.5-E6.0 post-implantation epiblast (Smith 2017). Therefore, E3.5-E4.5, E5.5-6.0, and E7.25-E8.0 represent distinct states of the pluripotent continuum, and are referred to as naïve, formative, and primed pluripotent states respectively, and represent the ICM cells of the pre- and post-implantation epiblast (Nichols and Smith 2009; Morgani, Nichols, and Hadjantonakis 2017; Osorno et al. 2012; Kinoshita et al. 2020).

This newly defined formative pluripotent state is consistent within the phased progression model suggesting that all differentiating naïve cells must phase through the formative, then primed state before exiting pluripotency. The exception to this rule is germ cell lineages, however, it is this exception that supports the phased progression model as formative state cells have the potential to become primordial germ cells. The formative pluripotent state and the phased progression model rely on the concept of germ line competence. When mESCs and are incorporated into chimeras and allowed to develop, germ cells arise, however, when mESCs are cultured *in vitro* they do not produce primordial germ cell-like cells (mPGCLCs) (Hayashi et al. 2011). In contrast, ICM cells of the E5.5-E6.0 mouse embryo (formative interval) can readily differentiate into

mPGCLCs through addition of bone morphogenic protein 4 (Bmp4) (Ohinata et al. 2009). Developmentally, germ line competency occurs during the interval between naïve and primed pluripotent states and the phased progression model hypothesis adds that somatic cell differentiation competency is also gained at this time. The switch from metabolic bivalency to aerobic glycolysis also begins during this transition (Kalkan et al. 2017). Ground state mESCs that are chemically transitioned towards a primed pluripotent state through the replacement of LIF/2i with activin and fibroblast growth factor (Fgf) supplementation (FA), hereafter referred to as mouse epiblast-like cells (mEpiLCs), do not fully commit to primed pluripotency and exhibit an intermediate potency with the potential to differentiate into mPGCLCs (Guo et al. 2009; Hayashi et al. 2011). Formative state mEpiLCs show increased expression of genes including *de novo* DNA methyltransferase 3a/b (Dnmt3a/b), fibroblast growth factor 5 (Fgf5), Sal-like protein 2 (Sall2), Sox3, and POU domain class 3 transcription factor 1 (Oct6; Pou3f1), following a decrease in Nanog expression (Smith 2017; Buecker et al. 2014).

There is a growing body of evidence showing that not only are the metabolic preferences of naïve and primed pluripotent states are distinct, but metabolic preferences also act to promote developmental processes, maintain pluripotency state, and enable cell fate decisions (Dahan et al. 2019; Tsogtbaatar et al. 2020; P. Wei et al. 2018). The concept of metabolic remodelling and reprogramming has been demonstrated in a variety of stem cells including T cell fate control, direct reprogramming of glial cells to neurons, neuronal metabolic preferences during differentiation, and improving stemness through mitochondrial function by nicotinamide adenine dinucleotide (NAD) repletion (Buck et al. 2016; Gascón et al. 2016; H. Zhang et al. 2016; Zheng et al. 2016). Regarding

metabolic preferences, glycolysis and OXPHOS play a primary role in pluripotent state differences (Zhou et al. 2012). On either end of the pluripotent continuum, naïve and primed states observe unique preferential metabolic phenotypes. Naïve cells are metabolically bivalent, *in vitro* colonies use both glycolytic and oxidative phosphorylation processes, whereas primed cell colonies are preferentially glycolytic representing a trend referred to as the 'Warburg Effect' (WE). These *in vitro* metabolic preferences may exist as a by-product of their *in vivo* correlate's metabolism due to restricted physiological oxygen access of the pre- and post- implantation cell niches. The recently described and stabilized intermediate pluripotent state, the formative state, has yet to be metabolically profiled, however, as this interval is representative of the recently post-implantation blastocyst, it may indicate a bias for aerobic glycolysis (Kinoshita et al. 2020; Smith 2017).

A key metabolic enzyme that not only links glycolysis and OXPHOS but is also a hallmark factor in the WE is pyruvate kinase muscle isoforms 1/2 (Pkm1/2 (transcript), PKM1/2 (protein)). Pkm1/2 is an allosterically regulated and alternatively spliced gene that produces the pyruvate kinase enzyme responsible for the catalysis of a phosphoryl group from phosphoenolpyruvate in glycolysis to form pyruvate, and the phosphoryl group is transferred to adenosine diphosphate to form ATP (Jurica et al. 1998; Valentini et al. 2000). PKM2 is implicated in cancer and the WE and recently PKM1 has been shown to have a contributing role to small cell lung cancer (W. Yang and Lu 2015; Growth 2018; L. Wei et al. 2017). PKM2 impinges on OXPHOS when nuclear translocated, and upregulates glycolytic activity that favors lactate production of acetyl

Co-A over a mitochondrial OXPHOS fate – a hallmark of the WE (Wang et al. 2014; Weiwei Yang and Lu 2013).

As PKM1/2 are implicated in aerobic glycolysis and proliferation, it is critical to investigate their contributions to naïve and primed cell pluripotency. Previous attempts to study the role of PKM1/2 in naïve and primed pluripotent states did not consider the intermediate, formative phases of the pluripotent continuum (Qin et al. 2017; Konno, Ishii, et al. 2015; Prigione et al. 2014). This study utilized steric-blocking morpholinos to modulate PKM1 and PKM2 isoforms in naïve and primed mouse pluripotent stem cells and during the chemical transitioning to formative, primed-like stem cells from the naïve state. The outcomes include effects to Pkm1 and Pkm2 transcript abundance in naïve, formative, primed-like, and primed pluripotent stem cells, and the impact of modulating Pkm1/2 on metabolic and pluripotent state. I also determined the impact of altering Pkm1/2 during transitioning mESCs-to-formative and formative-to-primed-like pluripotency. This study demonstrates that downregulation of PKM2 alone through splice modifications results in altered metabolic transcript abundance and promotes naïve-to-primed transitioning in formative mEpiLCs and downregulation of PKM2 and upregulation of PKM1 results in a new population of naïve and primed marker expressing cells in primed-like mEpiLCs. This study promotes metabolism as a driver of pluripotency and development, demonstrates how to delineate intermediate states from ground and primed pluripotency and provides evidence of PKM1 having a role in the pluripotent developmental process.

5.3.0. Methods:

5.3.1. Stem cell culture conditions:

Mouse embryonic stem cells (mESCs, R1 strain – 129X1 x 129S1 (gifted from Dr. Janet Rossant, The Hospital for Sick Children, Toronto, Ontario, Canada), formative and primed-like mouse epiblast-like cells (mEpiLCs, chemically converted R1 mESCs over 48 and 96 hours) and primed mouse epiblast stem cells (mEpiSCs, strain – 129S2 ((gifted from Dr. Janet Rossant, The Hospital for Sick Children, Toronto, Ontario, Canada); were cultured in the following base media; a 1:1 mixture of KnockOut DMEM/F12 (Thermo Fisher Scientific 12660012) and Neurobasal Media (Thermo Fisher Scientific 21103049) with 0.1% 2-Mercaptoethanol (Gibco 21985-029), 0.25% GlutaMAX (Thermo Fisher Scientific 35050061), 1.0% N2 Supplement (100x) (Thermo Fisher Scientific 17502048), and 2.0% B27 Supplement (50x) (Thermo Fisher Scientific 17504044) (Supp. Figure 1a). mESCs and mEpiLCs were cultured on 0.1% porcine gelatin (Sigma-Aldrich G2500) and mEpiSCs and MEFs were cultured on 10 μg/mL/cm^2 fibronectin (Roche 11051407001). Base media for the culture of mESCs were supplemented with 1000 units/mL ESGRO Recombinant mouse LIF protein (EMD Millipore ESG1107), and 2i small molecule inhibitors: 1 μM PD0325901 (Reagents Direct 39-C68) and 3μM CHIR99021 (Reagents Direct 27-H76). Base media for the culture of mEpiLCs and mEpiSCs were supplemented with 20ng/mL Activin A from mouse (Sigma-Aldrich SRP6057) and 12 ng/mL Fgf-2 from mouse (Sigma-Aldrich SRP3038). mESCs were passaged using StemPro™ Accutase™ (Thermo Fisher Scientific A1110501) and centrifuged at 300 x g for 5 minutes. Primed mouse epiblast stem cells were cultured in the base medium and supplements as mEpiLCs were along with a substratum of irradiated mouse embryonic

fibroblasts (MEFs). One hour prior to passaging, growth medium was replaced. Passaging was completed using Gentle Cell Dissociation Buffer (GCDB) (Gibco 13151-014) for 5 minutes at room temperature. Lifted cells were then centrifuged at 244 x g for 3 minutes and plated at a seeding density of 1:12 onto MEFs. RNA and protein abundance studies were completed by excluding MEFs for feeder-free conditions and passaging mEpiSCs once with StemPro™ Accutase™ (Thermo Fisher Scientific A1110501) followed by a GCDB passage, this resulted in a clean and healthy population of feeder-free mEpiSCs ready for transcript and protein abundance studies. Cells were utilized within three to five passages following cryopreservation when possible and studies were carried out in biological triplicate.

5.3.2. siRNA Transfection:

mESCs were grown to approximately 70-80% confluency and washed with fresh, pre-warmed (37 °C) LIF/2i supplemented media. Transfection was completed using the lipid-based carrier Lipofectamine3000 (ThermoFisher L3000001) and optimal siRNA and carrier concentrations were assessed using a FITC fluorescein conjugated siRNA control quantitatively via flow cytometry qualitatively by fluorescent imaging. Lipofectamine3000 was diluted in 50 µL of Opti-MEM (FisherScientific 31985070) prior to mixing with siRNA and incubated together at room temperature for 15 minutes. Cells were washed with Opti-MEM once and the Lipofectamine3000 and siRNA solution in Opti-MEM were incubated on the cells for 5 hours. Cells were then aspirated and given fresh media. Pkm1/2 siRNA design constructs were made with the aid of ThermoFisher's Life Sciences Solutions division. Specificity assessment was then completed using qPCR and immunoblotting.

5.3.3. Morpholino Delivery:

Morpholinos were transfected into mESCs, formative mEpiLCs and mEpiSCs through the scrape delivery method (Partridge et al. 1996). In brief, once cells achieved approximately 70-80% confluency, fresh pluripotent specific media supplemented with 5, 10, or 20 μM morpholino (as a series for optimization and 20 μM for experimental studies) (fluorescein-tagged control, PKM MO 1 or PKM MO 2 morpholino) that had been 2 μm filter sterilized was ejected onto a PBS(+/+) washed growth surface (either gelatin or fibronectin). The MO supplemented media was swirled for 10 seconds both clockwise and counterclockwise before being allowed to incubate at room temperature for 1 minute. Rubber policeman cell scrapers (Sarstedt 83.3951) were used vertically across the plate, then perpendicularly. Cells co-endocytosed the morpholinos through now open transient pores for 10 minutes without permitting the cells to reattach to their substratum. Transfected cells were replated onto larger growth spaces and allowed to incubate for 24 hours before downstream applications including fluorescent imaging, immunoblotting, transcript abundance and flow cytometry studies. Transfected cells were compared by phase contrast to determine if morphology was influenced. Imaging of fluorescently transfected cells and phase contrast microscopy was completed using a Leica DMI 6000B. Morpholino design, targeting sites and post-transfection changes to PKM1/2 protein can be found in Table 5.1. Experimental timelines for morpholino transfection and cell fate transitioning are detailed in Figure 5.01.a-b.

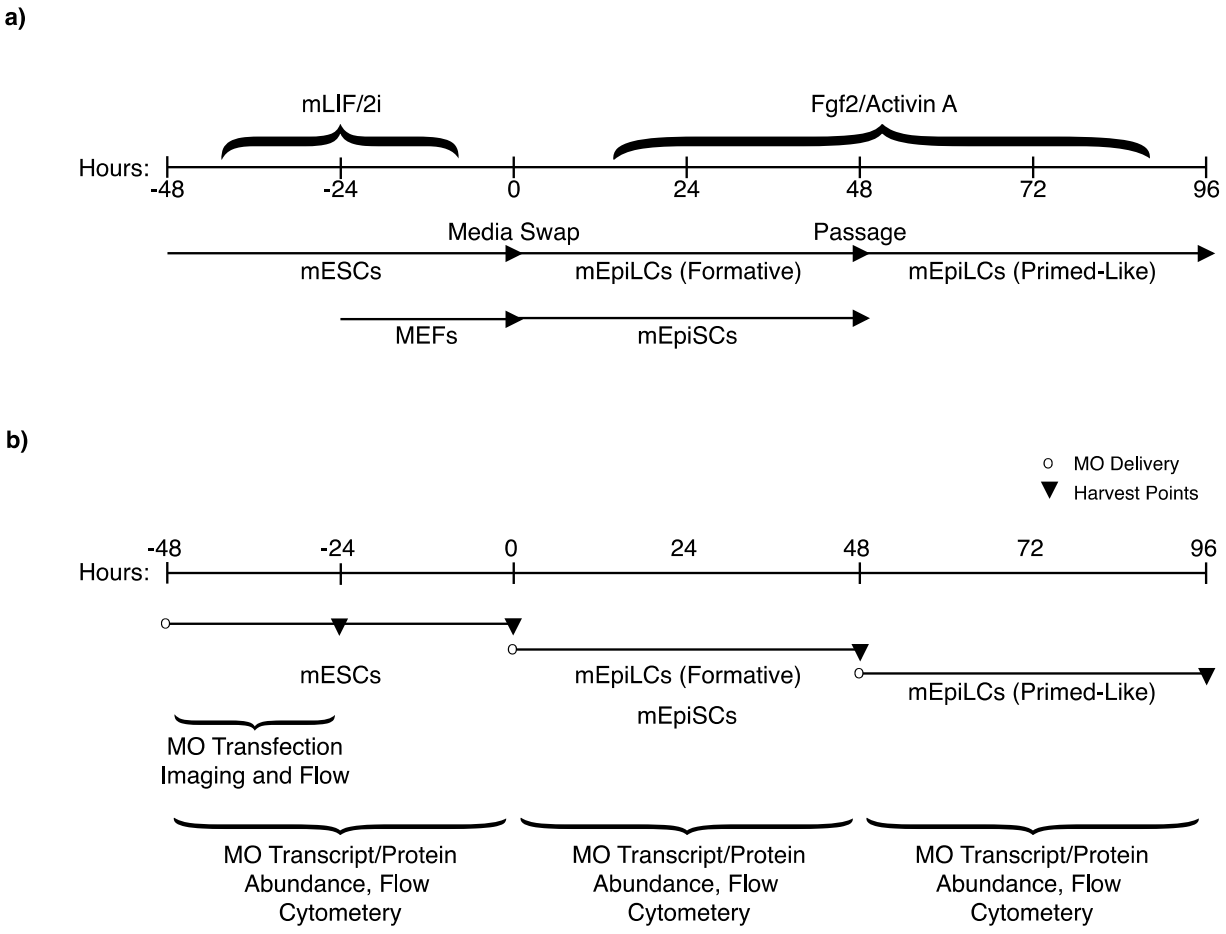

Figure 5.01. mESC, mEpiLC, and mEpiSC culture and timing schematic.

Ground state, naïve mESCs, formative/primed-like transitioning to mEpiLCs, and primed mEpiSCs experimental planning schematic. a) Experimental plating set-up and media transitioning from mESCs into formative and primed-like mEpiLCs through media supplementation and timing. b) Morpholino scrape delivery and incubation timelines described per cell type in each experimental study component.

Table 5.1. Morpholino Design.

Name	Target	Design
PKM MO 1	Pkm-202-i8e9	CCGAGCTATCTGTAAGGTTTAGGGT
PKM MO 2	(Pkm-201-e8i9)	ACTGCCGCCTCCTACCTGCCAGA

5.3.4. Transcript Abundance:

RNA isolation was completed using a RNeasy RNA isolation kit (Qiagen 74104) and Trizol (Ambion 15596018) hybrid protocol followed by DNAse treatment (Invitrogen AM1906). cDNA synthesis was completed using iScript (BioRad 170-8891) on 500 ng of RNA. Quantitative PCR was completed using SensiFAST™ SYBR® No-ROX Kit (FroggaBio BIO-98020). Optimal annealing temperatures for each primer were tested in temperature gradients followed by a dilution series to determine primer efficiencies. Relative transcript abundance was calculated using the Pfaffl method of quantification, normalized to mESCs not treated with a morpholino and relative to α-Tubulin transcript abundance(Pfaffl 2001). Forward and reverse primer designs and annealing temperatures are available in Table 5.2. TaqMan PCR was completed using TaqMan™ Advanced Master Mix (Thermo Fisher Scientific 4444557). Relative transcript abundance was calculated using the ΔΔCt method of quantification, normalized to mESCs not treated with a morpholino and relative to Hprt transcript abundance (Livak and Schmittgen 2001). The fold change in transcript abundance levels for both qPCR and TaqMan studies was calculated and expressed as $\log_2$.

Table 5.2. PCR Primers

Gene Name	Potency/ Role	Efficiency (%)	Annealing Temperature (℃)	Sequence (F = Forward, R = Reverse; 5' – 3')
α-Tubulin	House keeping	101.0	57.0-63.0	F- AACCAGATGGTGAAATGTGACCCT R- CACAGTGGGAGGCTGGTAGTTAAT
Pecam	Naïve	90.0	63.0	F- CAAGGCCAAACAGAAACCCG R- GCCTTCCGTTCTCTTGGTGA
Rex1	Naïve	96.6	63.0	F- AGAAGAAAGCAGGATCGCCT R- TATGACTCACTTCCAGGGGG
Esrrb	Naïve	103.7	63.0	F- CAGGCAAGGATGACAGACG R- GAGACAGCACGAAGGACTGC
Lef1	Formative	108.1	57.0	F- AGAAGAAGAAGAGGAAGAGAGAGAAGC R- AGATGTAGGCAGCTGTCATTCTGG
Dnmt3	Formative	99.0	63.0	F- GGCAAGGACGACGTTTTGTG R- GTTGGACACGTCCGTGTAGTGAG
Pou1fc	Formative	99.0	60.0	F- TTTCTCAAGTGTCCCAAGCC R- ACCACCTCCTTCTCCAGTTG
Zic2	Primed	90.0	63.0	F- GGTGACCCACGTCTCTGTG R- CGGATGTGGTTGACCAGTTT
Cer1	Primed	99.8	60.0	F- ACCTATGTGTGGATGGCTGC R- AGATCCGGCTTGTCTTCTGC
T(Bra)	Primed	104.1	60.0	F- CGGTGGCGAGAGAAGTGAAG R- CTTCCCTGCGCTCTCTGTG
Hk2	Glycolysis	91.8	63.0	F- CCTGCTACAGGTCCGAGCCATCTT R- GAGGATGAAGCTTGTACAGTGTCC
Gpi	Glycolysis	102.3	63.0	F- AACCGGCCGACCAACTCAAT TGTG R- TGCCGTCCAGCTCTGGCTCAATTT
Pgam1	Glycolysis	94.0	63.0	F- TACGCAGACCTTACTGAAGACCAG R- AGCTCCATGATGGCCTCTTCTGAG
Ldha	Glycolysis	98.7	63.0	F- GCAGACAAGGAGCAGTGGAAGGAG R- ACACTGAGGAAGACATCCTCATTG
Pfkl	Glycolysis	103.1	63.0	F- AATGTGCTGGGCCACTTGCAGCAG R- TGACCGGACTGAAGGCCACTACCT
Aldoa	Glycolysis	101.2	63.0	F- ATGAGGAGATTGCCATGGCAACGG R- TTTAGAGCAGAGGCCTGCAGGGCT
Eno1	Glycolysis	98.5	63.0	F- ACCAACCCTAAGCGGATTGCCAAG R- AGTCTTGATCTGCCCAGTGCAGAG
Mdh2	OXPHOS	104.7	63.0	F- AGAAGTCGTGAAGGCCAAGG R- AGTGATCTTGCCAATGCCCA

Fh1	OXPHOS	98.4	63.0	F- CGGTTTCGCAGAAAAGGTGG R- ACAGCAACGTGATTCCCCAT
Sdha	OXPHOS	90.5	63.0	F- AGAGATACGCACCTGTTGCC R- ACTGGGATGGGCTCCTTAGT
Suclg1	OXPHOS	108.7	63.0	F- GGTGAAATTGGTGGTCACGC R- AAGGACACTACAGGCTTGGC
Cs	OXPHOS	104.0	63.0	F- TGCCGGTTTGTCTACCCTTC R- GGCAGGATGAGTTCTTGGCT
Idh2	OXPHOS	97.8	63.0	F- TCTTCACCCCAAAGGATGGC R- TCTGGTGTTCTCGGTAATGGC

5.3.5. Protein Abundance:

Cells were washed with chilled (PBS(+/+)) (Gibco 14040-133) and lysed with Pierce™ RIPA Buffer (Thermo Fisher Scientific 89900) supplemented with 1X Phosphatase Inhibitor Cocktail Set 2 (Calbiochem 5246251) and 1X Protease Inhibitor Cocktail Set 1 (Calbiochem 539131). Protein quantification was completed using a Pierce™ BCA Protein Assay kit (Thermo Fisher Scientific 23225). Loading mixes were prepared at 20 µg in MilliQ H_2O, LDS (NuPAGE™ LDS Sample Buffer (4X) Invitrogen NP0007) and Reducing Agent (NuPAGE™ Sample Reducing Agent (10X) Invitrogen NP0004) at 70°C for 10 minutes before loading in NuPAGE™ 4-12% Bis-Tris Gels (Invitrogen NuPAGE NP0336). 1x MOPS (BOLT Invitrogen B000102) and 500 µL of antioxidant containing dithiothreitol (Thermo Fisher Scientific NP0009) was added and electrophoresis was completed at 200V for 50 minutes. Proteins were transferred to a PVDF membrane at 100V over 2 hours. The protein transferred PVDF membrane (EMD Immobilon IPVH00010) was blocked in 5% bovine serum albumin (BSA) (ALB001) for pPKM2 and 5% skimmed milk (Carnation) for PKM1 and PKM2 in 1x Tris-Buffered Saline with 0.1% Tween 20 for 1 hour at room temperature with end-to-end agitation. Primary antibodies were incubated overnight at 4 °C with end-to-end rotation. HRP-conjugated secondary antibodies were incubated for 1 hour at room temperature with end-to-end rotation. Membranes were imaged with Luminata Classico Western HRP Substrate (EMD WBLUC0500) and stripped using Restore Western Blot Stripping Buffer (Thermo Fisher Scientific 21059). Bands of interest were compared to β-ACTIN. Primary and secondary antibodies and their concentrations are listed in Table 5.3.

Table 5.3. Western blot antibody/marker list

Primary Antibody/Marker	**Concentration**	**Secondary Antibody**	**Concentration**
β-ACTIN A3854	1:50000	N/A: HRP-linked	N/A: HRP-linked
PKM1 15821-1-AP	1:5000, 5% TBST	Anti-rabbit IgG, HRP-linked Antibody #7074 Cell Signaling Technology	1:2000-10,000, 5% Milk in TBST
pPKM2 (Tyr105) 3827S	1:5000, 5% BSA in TBST	Anti-rabbit IgG, HRP-linked Antibody #7074 Cell Signaling Technology	1:2000-10,000, 5% BSA in TBST
PKM2 15822-1-AP	1:5000, 5% Skim milk in TBST	Anti-rabbit IgG, HRP-linked Antibody #7074 Cell Signaling Technology	1:2000 5% Milk in TBST

5.3.6. Flow Cytometry:

mPSCs were lifted with StemPro™ Accutase™ (Thermo Fisher Scientific A1110501) incubated at 37 °C for 5 minutes. Centrifugation steps were completed at 244 x g for 3 minutes. Dead cell compensation and gating was completed using a 50% mixture of live and dead mESCs stained with Zombie Aqua™ Fixable Viability Kit (BioLegend 423101) and incubated in the light-tight container at room temperature for 30 minutes. Cells were washed with 2 mL of flow cytometry staining buffer (FCSB) containing: 90% PBS (-/-), 10% FBS (qualified, ESC grade), and fixed with 4% paraformaldyde (PFA) in PBS (-/-). Fixed cells were washed with PBS(-/-), centrifuged and divided into unstained, single, full-minus-one and full stained combinations of each cell type. Fixed cells were stained with conjugated antibodies for 1 hour in a light-tight box at room temperature prior to washing, centrifugation and resuspension in PBS(-/-) and ejected through a 40 µm cell strainer (Fisherbrand™ Sterile Cell Strainers 22-363-547) with a final wash of 100 µL of PBS (-/-). Flow cytometry was completed on a FACSCanto flow cytometer. Antibodies and their concentrations are listed in Table 5.4.

Table 5.4. Flow cytometry antibody/marker list

Primary Antibody/Marker	**Concentration**	**Secondary Antibody**	**Concentration**
CD24 138505	0.25 µg/1 million cells	N/A: Conjugated	N/A: Conjugated
SSEA1 125614	5 µL/1 million cells	N/A: Conjugated	N/A: Conjugated

5.3.7. Statistical Analyses:

Statistics were completed using a one- and two-way ANOVAs where applicable. Characterization by flow cytometry of SSEA1/CD24 in mPSCs was completed using a one-way ANOVA with Tukey's multiple comparisons test. Flow cytometric analysis of transfection efficiency compared random control morpholino groups using a one-way ANOVA with Tukey's multiple comparisons test. Immunoblotting for protein abundance in the influence of PKM1/2 morpholinos utilized a one-way ANOVA with a Dunnett's multiple comparisons test. Determining the influence of PKM1/2 morpholinos on transitioning formative and primed-like mEpiLCs as quantified by flow cytometry of SSEA1/CD24 in mPSCs was completed using a one-way ANOVA with Dunnett's multiple comparisons test. Transcript abundance studies examining the influence of PKM1/2 morpholinos on mPSCs was accomplished using a two-way ANOVA with Dunnett's multiple comparisons test.

5.4.0. Results:

5.4.1. Formative and primed-like mEpiLCs can be distinguished from primed mEpiSCs through SSEA1 and CD24 cell surface expression.

mEpiLCs can be distinguished from naïve mESCs and primed mEpiSCs based on Stage - Specific Embryonic Antigen-1 (SSEA1) and Cluster of differentiation 24 (CD24) expression (Figure 5.02.a-e). Representative flow cytometry plots demonstrate cell population quantification (%) of pluripotent cells with high and low expression of SSEA1 and CD24 (Figure 5.02.b-e). There was a significant difference between group mean

values of pluripotent cell types expressing high levels of SSEA1 and low levels of CD24 ($F(3,8)=8.993$, $p=0.0061$) (Figure 5.02.a). Tukey's multiple comparisons post hoc test determined that the percentage of mEpiSCs expressing high levels of SSEA1 and low levels of CD24 was significantly greater than mESCs, mEpiLCs (formative), or mEpiLCs (primed-like) ($p=0.0253$, $p=0200$, $p=0.0058$ respectively) (Figure 5.02.a). Moreover, there was a significant difference between group mean values of pluripotent cell types expressing high levels of SSEA1 and CD24 ($F(3,8)=5.777$, $p=0.0212$) (Figure 5.01.a). Tukey's multiple comparisons post hoc test determined that the percentage of mEpiSCs expressing high levels of SSEA1 and CD24 was significantly greater than mESCs or mEpiLCs (formative) ($p=0.0458$, $p=0.0319$ respectively) (Figure 5.02.a). There was also a significant difference between group mean values of pluripotent cell types expressing low levels of SSEA1 and high levels of CD24 ($F(3,8)=142.9$, $p<0.0001$) (Figure 5.02.a). Tukey's multiple comparisons test determined that the percentage of mEpiSCs expressing low levels of SSEA1 and high levels of CD24 was significantly greater than mESCs, mEpiLCs (formative), or mEpiLCs (primed-like) ($p=<0.0001$ in all instances) (Figure 5.02.a). Lastly, there was a significant difference between group mean values of pluripotent cell types expressing low levels of SSEA1 and CD24 ($F(3,8)=15.54$, $p<0.0011$) (Figure 5.02.a). Tukey's multiple comparisons test determined that the percentage of mEpiSCs expressing low levels of SSEA1 and CD24 was significantly greater than mESCs, mEpiLCs (formative), or mEpiLCs (primed-like) ($p=0.0021$, $p=0013$, $p=0.0276$ respectively) (Figure 5.02.a).

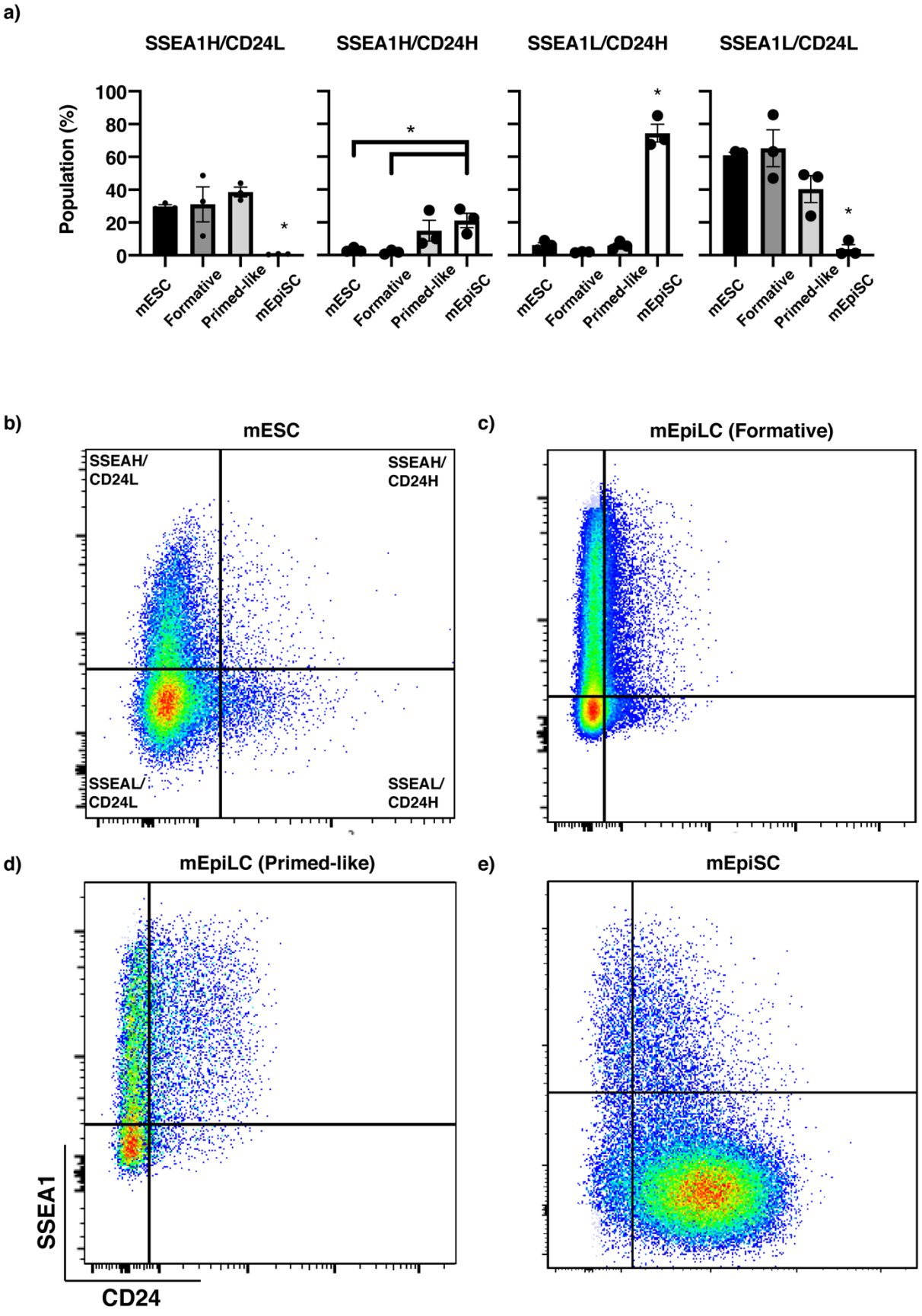
a)
SSEA1H/CD24L
SSEA1H/CD24H
SSEA1L/CD24H
SSEA1L/CD24L
Population (%)
100
80
60
40
20
0
mESC
Formative
Primed-like
mEpiSC
b)
mESC
SSEAH/ CD24L
SSEAH/ CD24H
SSEAL/ CD24L
SSEAL/ CD24H
c)
mEpiLC (Formative)
d)
mEpiLC (Primed-like)
SSEA1
CD24
e)
mEpiSC

Figure 5.02. mESC, mEpiLC (Formative), mEpiLC (Primed-like), and mEpiSC SSEA1 and CD24 cell surface marker characterization.

Delineation of naïve mESCs, formative and primed-like mEpiLCs, and mEpiSCs by a) flow cytometric analysis of SSEA1 and CD24 cell surface marker expression. Biexponential scale flow plots represent portrayals of SSEA1-compensated Brilliant Violet 421 on a 450 nm laser versus CD24-compensated APC on a 670 nm laser of b) mESCs, c) formative mEpiLC, d) primed-like mEpiLC, and e) mEpiSC. Data shown as mean±SEM of treatments compared in biological triplicate as a one-way ANOVA with a Tukey's multiple comparisons relative to the control of each corresponding cell type; * $p<0.05$, n=3 biological replicates.

5.4.2. Efficient transfection of siRNAs and morpholino oligonucleotide delivery into mESCs.

Transfection efficiency was determined using a FITC Fluorescein tagged control siRNA at 10, 30, 50 pmol concentrations delivered into mESCs using the lipid-based carrier Lipofectamine3000 at 1.5 and 3.0 µL volumes, further diluted in 50 µL of Opti-MEM. Optimal siRNA concentration and carrier volume were determined to be 30 pmol in 3µL respectively using flow cytometry relative to no siRNA and carrier controls (Figure 5.03.). mESCs transfected with the optimized parameters of Pkm1/2 siRNA constructs (Table 5.5.) were assessed at 24-, 48-, and 72-hours post-transfection by a transcript abundance study (Figure 5.04.a-c). Initial results show an upregulation of Pkm1/2 transcript abundance following siRNA transcript, with a slow leveling off towards 72 hours post-transfection. Importantly, a scrambled siRNA control influenced Pkm1/2 transcript (Figure 5.04.a,b) and protein abundance (Figure 5.05.) drawing skepticism as to the true specificity of the siRNA constructs. Originally, this project sought to determine the role of PKM1/2 in mESCs exiting the naïve state during a chemically driven conversion to mEpiLCs. Our first knockdown strategy was centered around using small interfering ribonucleic acids (siRNAs) specific to either PKM isoform, and PKM total (both isoforms 1 and 2). Our initial troubles came from difficulties efficiently transfecting and validating siRNAs in mESCs, and after several approaches I was able to transfect a control siRNA tagged with a fluoresceine conjugate A as determined by flow cytometry (Figure 5.03.). I used flow cytometry to assess an optimal concentration of siRNA and lipid-based carrier, determining optimal transfection parameters of 30.0 pmol siRNA with 3.0 µL of Lipofectamine3000.

These results led us to re-examining our knockdown strategy using an targeted morpholino approach.

a)

No siRNA, 0.0 uL Lipofectamine

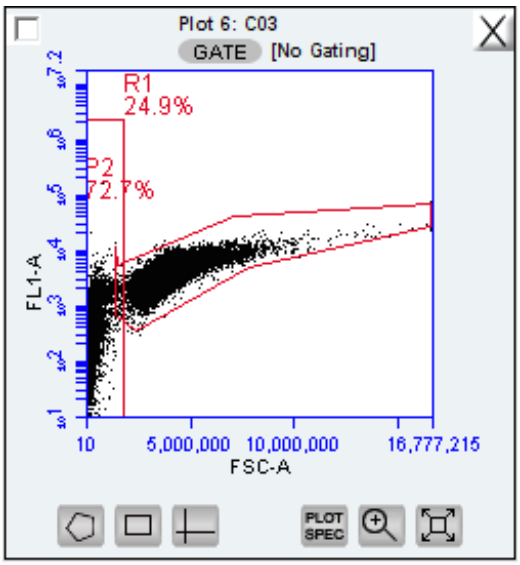

b)

30 pmol siRNA, 3.0 uL Lipofectamine

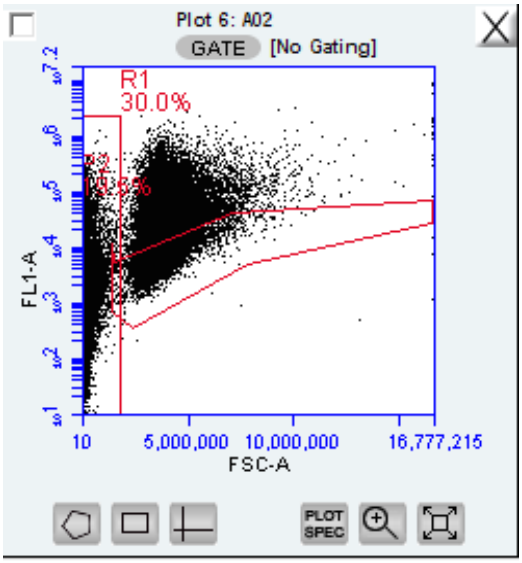

c)

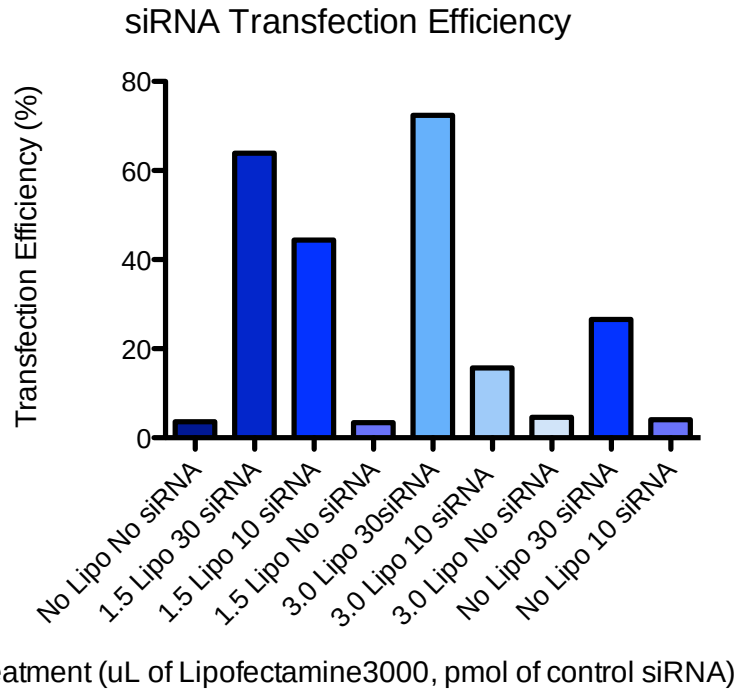

Treatment (uL of Lipofectamine3000, pmol of control siRNA)

Figure 5.03. mESCs can be efficiently transfected using Lipofectamine3000. Cells were transfected using Lipofectamine3000 and FITC Fluorescein Conjugate-A. gating comparison between the greatest transfection efficiency of **a)** no siRNA and no transfection agent, and b) 30 pmol of siRNA and 3µL of Lipofectaine3000. **c)** Transfection efficiencies comparing combinations of transfection agent and siRNA quantities using a C6 Accuri flow cytometer, n=1.

Following validation of the transfection process, I assessed our PKM1/2 siRNA designs. These siRNAs were designed with the help of ThermoFisher bioinformatics team and 3 different sets of siRNAs targeting each isoform were made (Table 5.5.). These siRNA constructs were transfected into mESCs, and RNA was extracted after 24, 48, and 72 hours of incubation at 10.0, 30.0, and 50.0 pmol concentrations (Figure 5.04.). Examining the transcript abundance of these constructs following transfection demonstrated that increases and decreases in Pkm1/2 that were not compatible with our current question regarding downregulating Pkm1/2. Optimal siRNA constructs were tested in mESCs for PKM1/2 protein abundance (Figure 5.05.). Unfortunately, there was a significant influence of the scramble control siRNA on protein abundance and a lack of either PKM1 or PKM2 isoform specificity.

Table 5.5. siRNA construct designs

Construct	Sense	Anti-Sense
Pkm1-A	CAGCAGCUUUGAUAGUUCUTT	AGAACUAUCAAAGCUGCUGCT
Pkm1-B	GGAGGCCUCUUAUAAGUGUTT	ACACUUAUAAGAGGCCUCCAC
Pkm1-C	UGAUAGCUCGGGAGGCUGATT	UCAGCCUCCCGAGCUAUCAGG
Pkm2-A	CCAUUAUCGUGCUCACCAATT	UUGGUGAGCACGAUAAUGGCC
Pkm2-B	AUCUACCACUUGCAGCUAUTT	AUAGCUGCAAGUGGUAGAUGG
Pkm2-C	GCUAUUCGAGGAACUCCGCTT	GCGGAGUUCCUCGAAUAGCTG
Pkm-Total	-Targets exon 4	

Custom Silencer Select siRNA constructs designed to target Pkm1, Pkm2, and Pkm total specifically.

a)

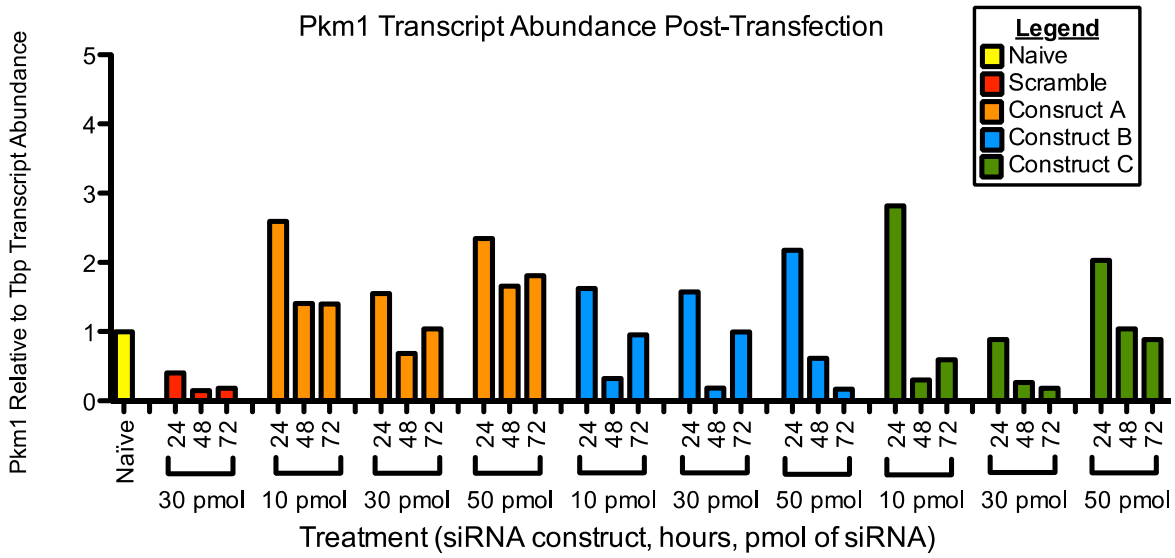
Pkm1 Transcript Abundance Post-Transfection
Legend
Naive
Scramble
Consruct A
Construct B
Construct C
Pkm1 Relative to Tbp Transcript Abundance
0
1
2
3
4
5
Naïve
24
48
72
30 pmol
10 pmol
30 pmol
50 pmol
10 pmol
30 pmol
50 pmol
10 pmol
30 pmol
50 pmol
Treatment (siRNA construct, hours, pmol of siRNA)

b)

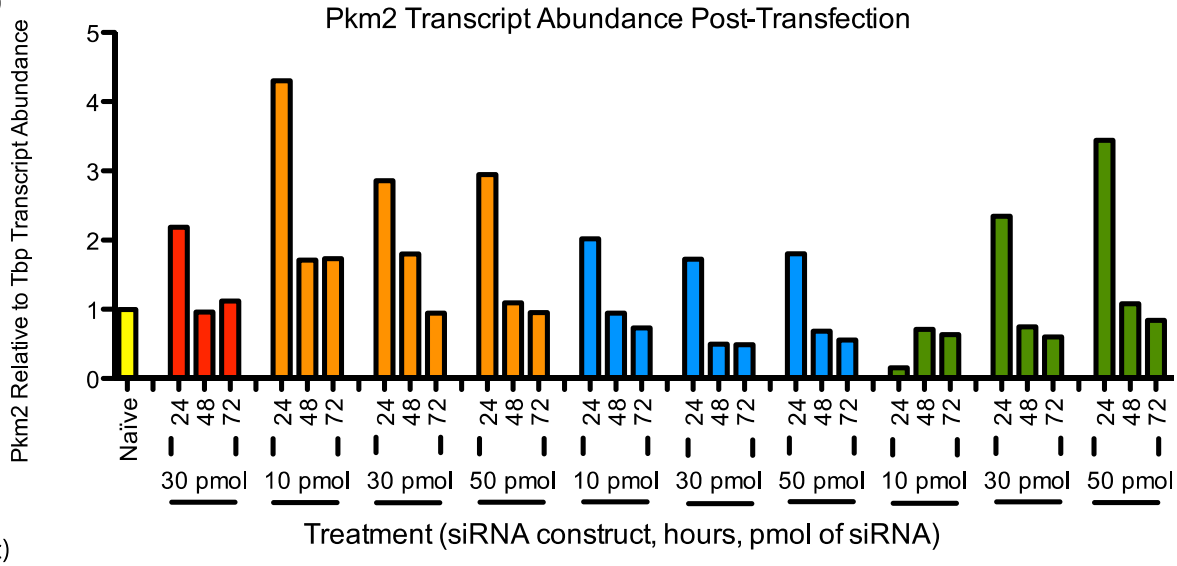
Pkm2 Transcript Abundance Post-Transfection
Pkm2 Relative to Tbp Transcript Abundance
0
1
2
3
4
5
Naïve
24
48
72
30 pmol
10 pmol
30 pmol
50 pmol
10 pmol
30 pmol
50 pmol
10 pmol
30 pmol
50 pmol
Treatment (siRNA construct, hours, pmol of siRNA)

c)

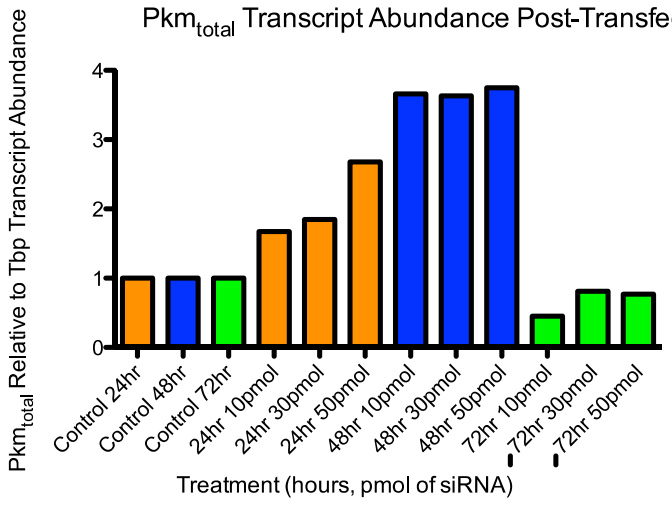
Pkm$_{total}$ Transcript Abundance Post-Transfection
Pkm$_{total}$ Relative to Tbp Transcript Abundance
0
1
2
3
4
Control 24hr
Control 48hr
Control 72hr
24hr 10pmol
24hr 30pmol
24hr 50pmol
48hr 10pmol
48hr 30pmol
48hr 50pmol
72hr 10pmol
72hr 30pmol
72hr 50pmol
Treatment (hours, pmol of siRNA)

Figure 5.04. PKM1/2 siRNA transfected mESCs altered Pkm1/2 transcript abundance.

Cell culture conditions included N2B27 media supplemented with LIF and 2i in 20% oxygen conditions over 3 days**.** Cells were transfected using custom designed Silencer Select siRNAs, Lipofectamine3000 and Opti-MEM. mRNA abundance relative to *Tbp* and calculated using △△Ct algorithm., **A)** *Pkm1*, **B)** *Pkm2* **C)** *Pkm Total* transcript abundance studies for 24-, 48-, and 72-hour time points. Treatments were measured using technical triplicates, n = 1.

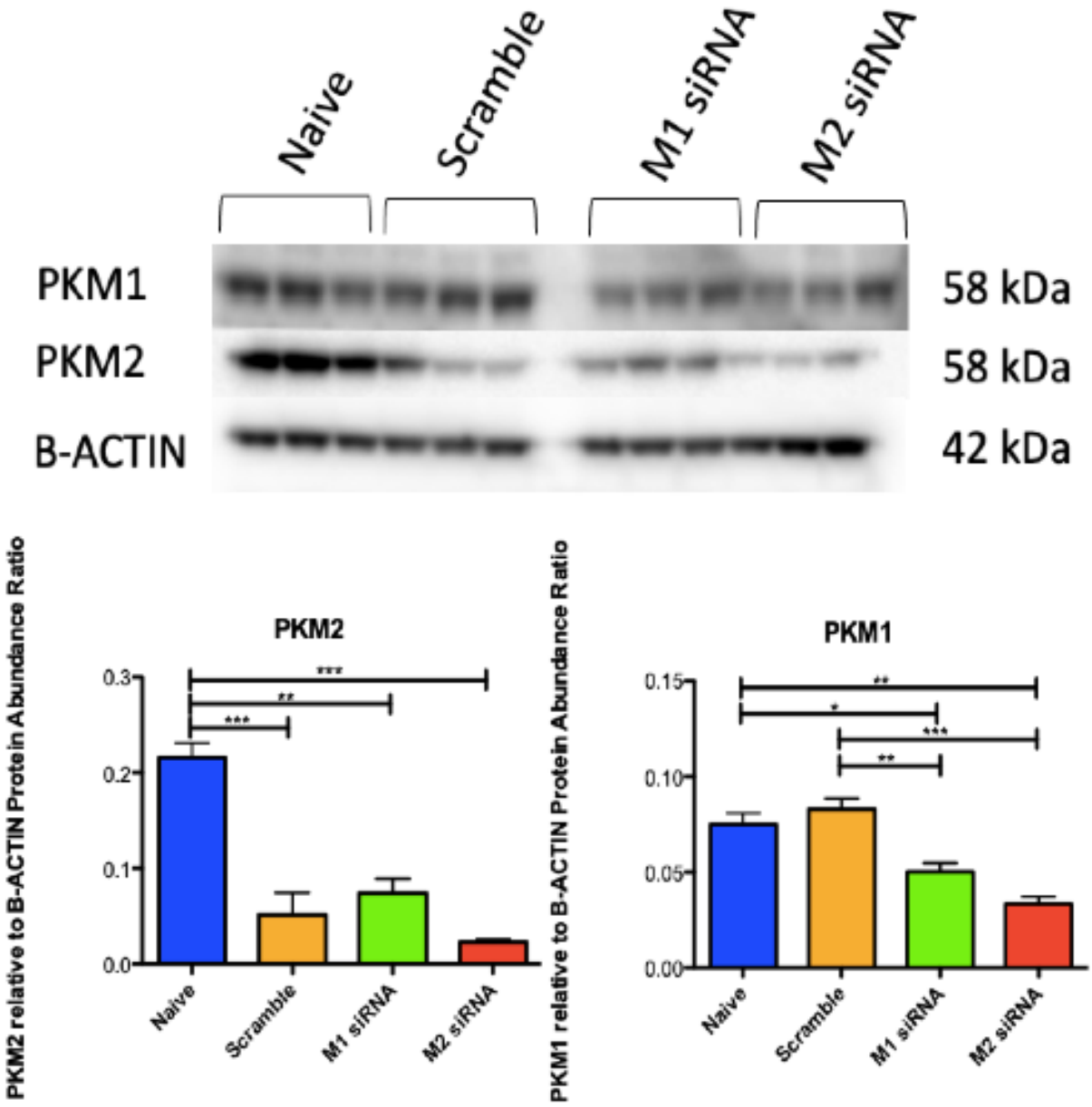

Figure 5.05. Most optimal siRNA constructs for PKM1 and PKM2 influence protein abundance in mESCs.

Naïve mESCs treated with a scramble control siRNA, PKM1, and PKM2 designed custom silencer siRNAs transfected with Lipofectamine 3000 show a downregulation of PKM2 protein abundance. PKM1 and PKM2 siRNAs alone downregulated PKM1 protein abundance. Protein densitometry was compared relative to β-ACTIN and samples were run in biological triplicate, error bars represent mean±SEM, *$p<0.05$.

Random control Morpholinos tagged with a fluorescein label were scrape delivered into mESCs as a concentration series of 5, 10, or 20 μM (Figure 5.03.a-c). At 10 μM, tagged control morpholinos were detectable by fluorescent microscopy (Figure 5.06.a). Scrape delivered cells were measured via flow cytometry for transfection efficiency as assessed by FITC+ events relative to the total live cell population and mean fluorescence intensity as measured by geometric mean of fluorescent events (Figure 5.06.b, c). There was a significant concentration-dependent difference between FITC+ cell events using random control morpholino treatments as determined by a one-way ANOVA ($F(2,6)=45.77$, $p=0.0002$) (Figure 5.06.b). The concentration series for FITC+ events demonstrated: 5 μM (mean=73.9%, SEM=2.1), 10 μM (mean=94.7%, SEM=2.3), and 20 μM (mean=98.0, SEM=1.3) (Figure 5.06.b).

a)

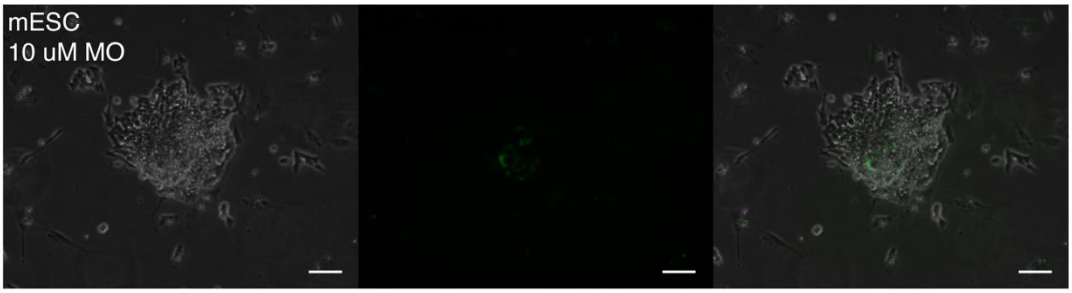

b)

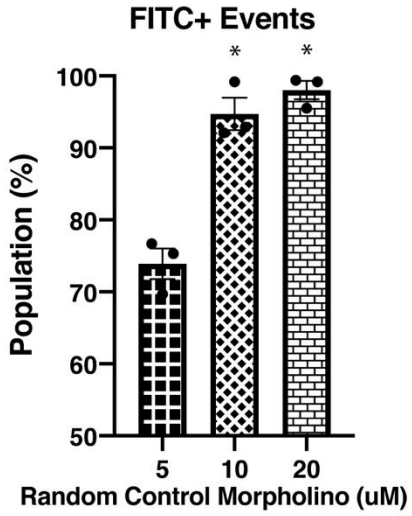

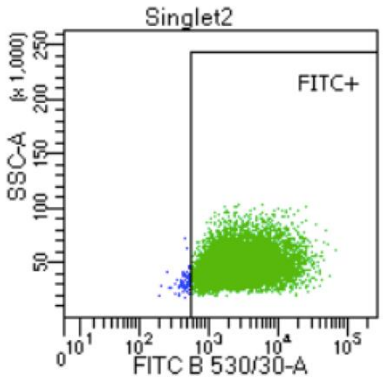

mESC
20uM Control MO
#FITC+ 98.03±2.20

c)

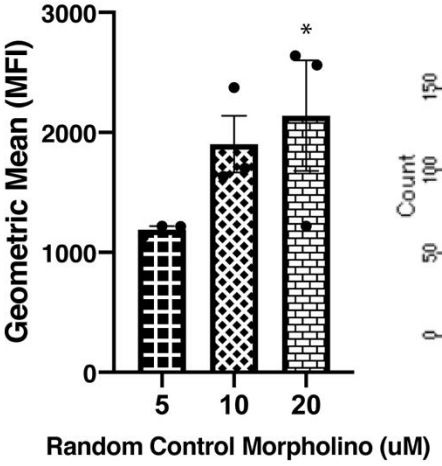

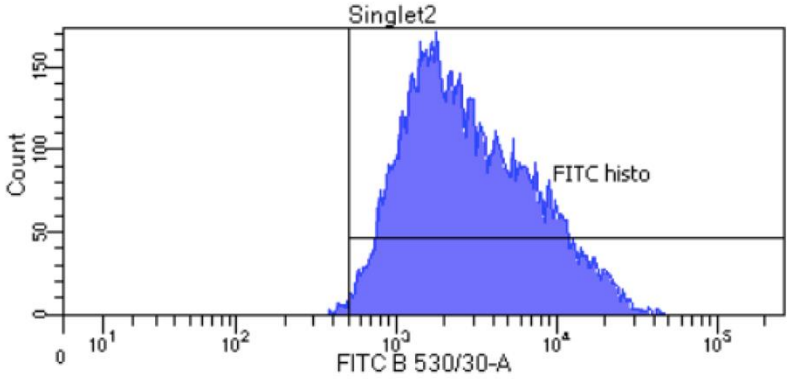

Figure 5.06. mESCs can be efficiently and effectively transfected with morpholinos by scrape delivery at 20 μM.

Scrape delivered morpholinos tagged with a fluorescein label were visible in a) mESCs as demonstrated by fluorescent phase contrast microscopy at concentration of 10 μM. Scale bars represent 75 μm. Transfection of morpholinos was optimized by comparing 5, 10, and b) 20μM fluorescein-tagged control morpholinos as determined through c) FITC+ frequency relative to total population and d) geometric mean by flow cytometric analysis of FITC wavelength laser channel. Data shown as mean±SEM of treatments compared in biological triplicate; * $p<0.05$, n=3 biological replicates.

5.4.4. Steric-blocking Morpholinos affects PKM1 and PKM2 protein levels.

Forty-eight hours-post 20 μM morpholino scrape delivery produced significant changes to PKM1 and PKM2 protein levels in mESCs (Figure 5.07.a, Figure 5.01.b). The transfection of a random control morpholino did not affect PKM1 or PKM2 protein abundance compared to mESCs scraped without a morpholino (Figure 5.04.a-f). There was a significant difference between group mean values of PKM1 protein abundance following Morpholino treatments as determined by a one-way ANOVA ($F(3,8)=52.21$, $p<0001$) (Figure 5.07.b). There was a significant difference between group mean values of PKM2 protein abundance following morpholino treatments as determined by a one-way ANOVA ($F(3,8)=4.619$, $p=0.0371$) (Figure 5.07.c). A Dunnett's multiple comparison test determined that the addition of the PKM1 designed Morpholino, now referred to as 'PKM MO 1' significantly decreased PKM2 protein abundance ($p=0.0212$) (Figure 5.07.b, c). The PKM2 designed morpholino, now referred to as 'PKM MO 2' significantly decreased PKM2 protein abundance ($p=0.0480$) and significantly increased PKM1 protein abundance ($P<0.0001$) (Figure 5.07.b, c). There was a significant increase in the ratio of PKM1:PKM2 protein abundance with the addition of the PKM MO 2 ($p<0.0001$) (Figure 5.07.e). There was a significant increase in the ratio of PKM1:PKM2 protein abundance with the addition of the PKM MO 1 and the PKM MO 2 ($p=0.0082$ and $p<0.0001$) (Figure 5.07.e). There was a significant increase in the ratio of pPKM2:PKM2 protein abundance with the addition of the PKM MO 1 and the PKM MO 2 ($p=0.0082$ and $p<0.0001$) (Figure 5.07.f).

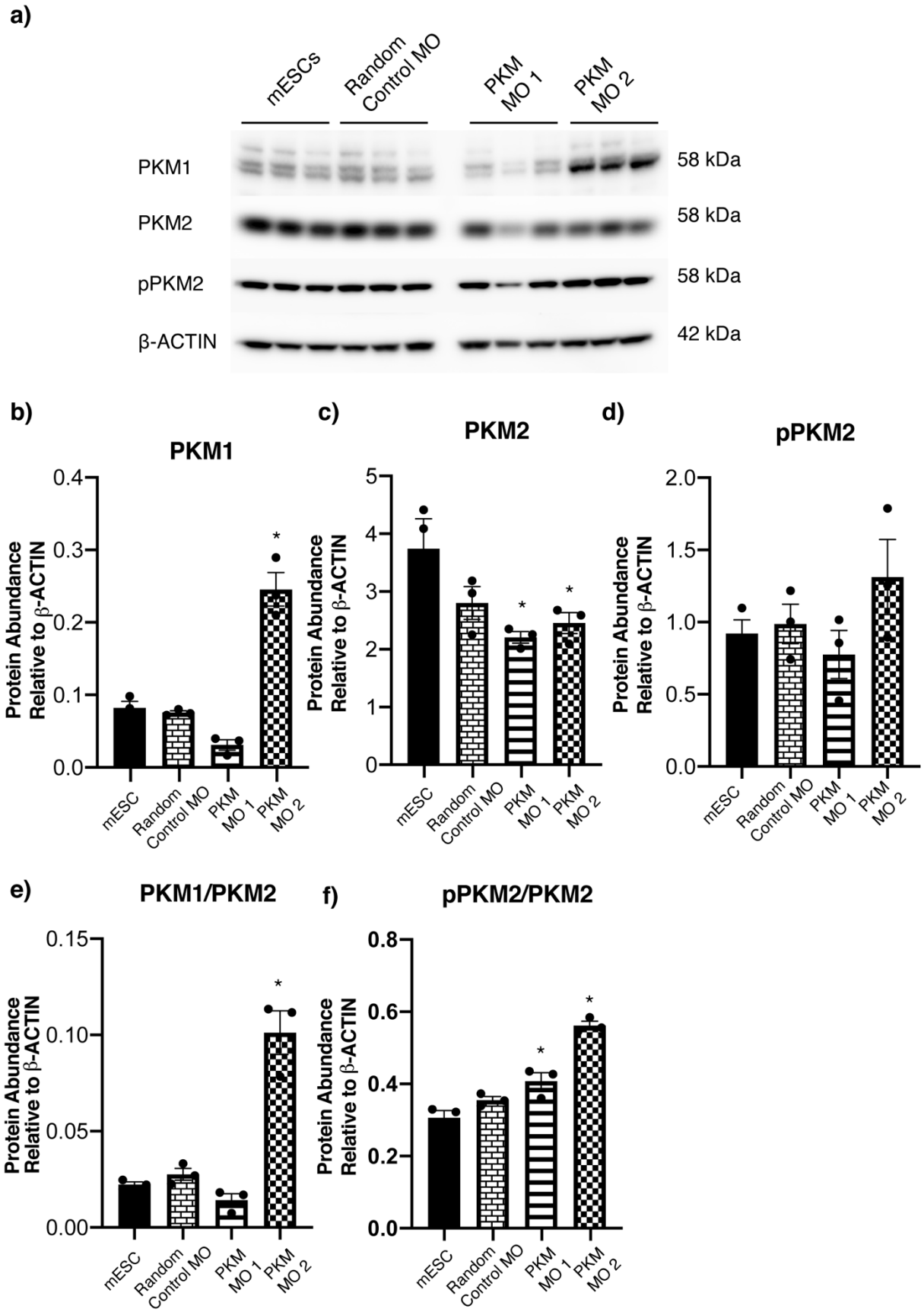
a)
mESCs
Random Control MO
PKM MO 1
PKM MO 2
PKM1
PKM2
pPKM2
β-ACTIN
58 kDa
58 kDa
58 kDa
42 kDa
b)
PKM1
c)
PKM2
d)
pPKM2
Protein Abundance Relative to β-ACTIN
mESC
Random Control MO
PKM MO 1
PKM MO 2
e)
PKM1/PKM2
f)
pPKM2/PKM2

Figure 5.07. Splice-modifying morpholinos modulate PKM1 and PKM2 protein abundance in mESCs.

a) Representative PKM1/2 immunoblotting of morpholino transfected mESCs demonstrates b) upregulation of PKM1 and c) downregulation of PKM2 by transfecting the PKM MO2, whereas PKM MO1 significantly downregulates PKM2. The PKM MO 2 additionally e) upregulates protein abundance of PKM1/PKM2 ratio. There was d) no significant change in pPKM2 with the inclusion of a PKM morpholino. Data shown as mean±SEM of treatments compared in biological triplicate as a one-way ANOVA with a Tukey's multiple comparisons test; * $p<0.05$, n=3 biological replicates.

5.4.5. Pkm1/2 transcript abundance is altered in mESCs, formative mEpiLCs, primed-like mEpiLCs, and mEpiSCs following PKM1/2 spliceosome modification.

A two-way ANOVA was conducted to examine the influence of treating each pluripotent state with the PKM MO 1 or PKM MO 2 morpholinos at 20 μM on Pkm1/2 transcript abundance levels (Figure 5.08.a-c). There was a statistically significant interaction, meaning the effects of different pluripotent cell types depends on each morpholino treatment, for Pkm1 (Figure 5.08.a) and Pkm2 (Figure 5.08.b) transcript abundance, but not the Pkm1/Pkm2 (Figure 5.08.c) transcript abundance ratio, ($F(6,24)=11.92$, $p<0.001$), ($F(6,24)=2.695$, $p=0.0382$), and ($F(6,24)=1.904$, $p=0.1214$) respectively between pluripotent cell type and morpholino treatment. Simple main effect analysis demonstrated that within pluripotent cell types, the addition of PKM MO 1 or PKM MO 2 morpholinos significantly influenced Pkm1 transcript abundance ($F(3,24)=6.253$, $p=0.0027$, and $F(2,24)=25.86$, $p<0.001$ respectively). Simple main effect analysis also demonstrated that pluripotent cell type and the addition of PKM MO 1 or PKM MO 2 morpholinos significantly influenced Pkm1/Pkm2 transcript abundance ratio ($F(3,24)=14.26$, $p<0.0001$, and $F(2,24)=21.79$, $p<0.0001$ respectively). Based on Dunnett's multiple comparisons tests relative to the control treatment of each pluripotent cell type, adding a PKM MO 2 morpholino significantly enhanced Pkm1 transcript abundance in mESCs ($p<0.0001$), mEpiLC (formative) ($p=0.0006$), and mEpiSCs ($p=0.0080$), and Pkm1/Pkm2 transcript abundance ratio in mESCs ($p=0.0023$) and mEpiLCs (formative) ($p=0.0025$). Based on Dunnett's multiple comparisons tests relative to the control treatment of each pluripotent cell type, treatment with the PKM

MO 2 morpholino significantly reduced Pkm1 and Pkm2 transcript abundance in mEpiLC (primed-like) ($p=0.0025$ and $p=0.0497$, respectively).

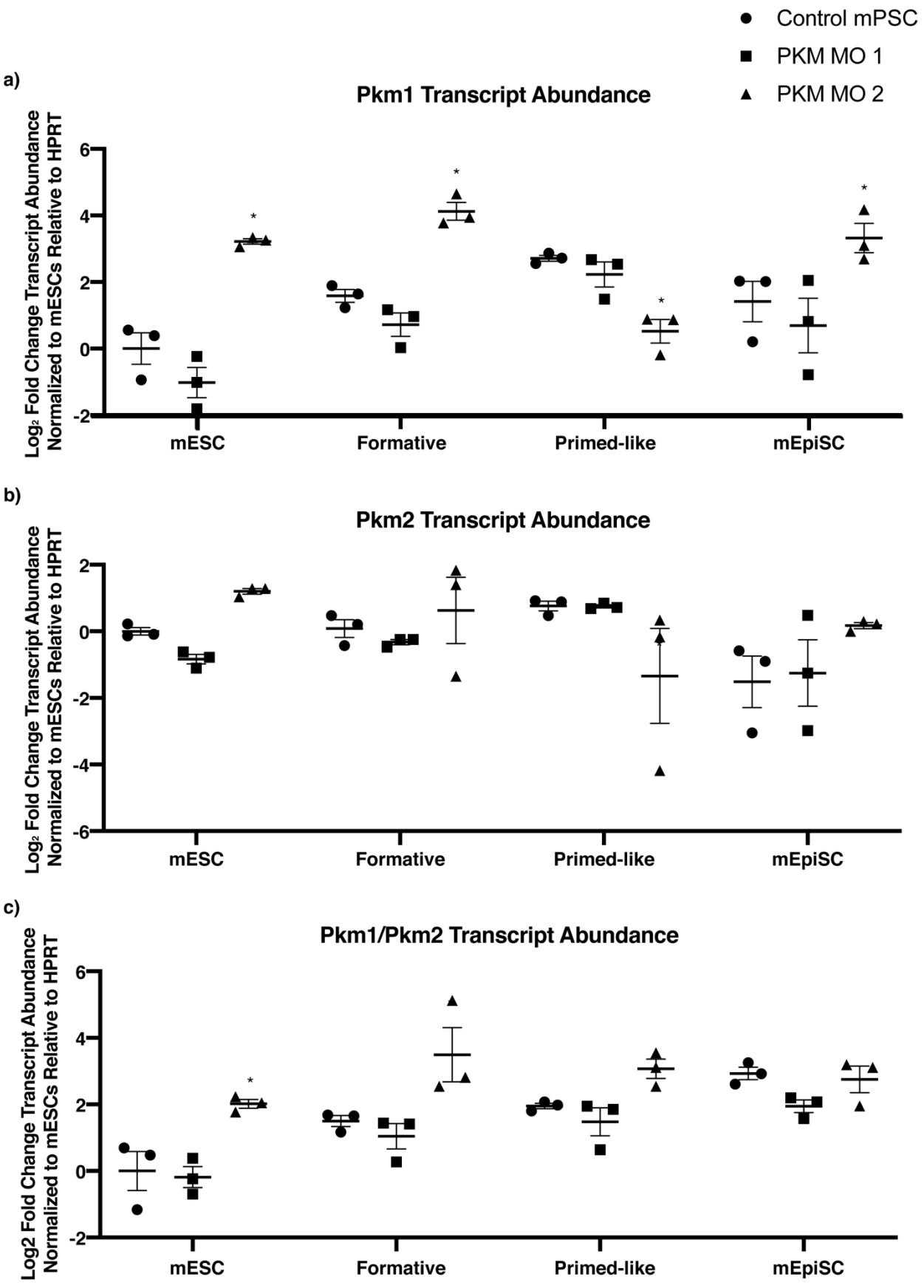
Control mPSC
PKM MO 1
PKM MO 2
a)
Pkm1 Transcript Abundance
Log2 Fold Change Transcript Abundance Normalized to mESCs Relative to HPRT
6
4
2
0
-2
mESC
Formative
Primed-like
mEpiSC
b)
Pkm2 Transcript Abundance
Log2 Fold Change Transcript Abundance Normalized to mESCs Relative to HPRT
2
0
-2
-4
-6
mESC
Formative
Primed-like
mEpiSC
c)
Pkm1/Pkm2 Transcript Abundance
Log2 Fold Change Transcript Abundance Normalized to mESCs Relative to HPRT
6
4
2
0
-2
mESC
Formative
Primed-like
mEpiSC

Figure 5.08. PKM morpholinos influence Pkm1/2 transcript abundance in naïve mESCs, formative mEpiLCs, primed-like mEpiLC, and primed mEpiSCs. Delivery of the PKM MO 2 significantly influences a) Pkm1 transcript abundance in mESCs, formative mEpiLCs, primed-like mEpiLCs, and mEpiSCs relative to control cells of each pluripotent state. b) Pkm2 transcript abundance was significantly downregulated in mEpiLCs with PKM2 morpholino delivery. mESCs and formative mEpiLCs c) Pkm1 to Pkm2 transcript abundance ratio was upregulated following PKM2 morpholino transfection. Data shown as mean±SEM of treatments compared in biological triplicate as a two-way ANOVA with a Dunnett's multiple comparisons relative to the control of each corresponding cell type; * $p<0.05$, n=3 biological replicates run in technical triplicate. Data represents Log_2 of fold change relative to Hprt and normalized to control mESCs.

5.4.6. Decreased PKM2 and increased PKM2 protein abundance by morpholino modulation decreases glycolytic genes Eno1 and Hk2 transcript abundance in primed mEpiSCs.

A two-way ANOVA was conducted that examined the influence of treatment with PKM MO 1 or PKM MO 2 morpholinos (20 μM) on glycolytic and oxidative phosphorylation (OXPHOS) metabolic transcript abundance following transfection in mESCs, transitioning mEpiLCs to the formative and primed-like pluripotent states and mEpiSCs over 48 hours. There was no significant interaction for the glycolysis genes Hexokinase 2 (Hk2), Lactate dehydrogenase A (Ldha), Phosphofructokinase 1 (Pfk1), and Alpha-enolase (Eno1) transcript abundance (Figure 5.09.a), however, there was a statistically significant difference in transcript abundance between pluripotent cell types ($F3,24)=38.12, p<0.0001$), ($F(3,24)=13.80$, $p<0.0001$), ($F(3,24)=5.361$, $p=0.0057$), and ($F(3,24)=4.815$, $p<0.0092$) respectively. Based on Dunnett's multiple comparisons tests relative to the control treatment of each pluripotent cell type, treatment with the PKM MO 2 morpholino significantly reduced Eno1 and Hk2 transcript abundance in mEpiSCs ($p=0.0268$ and $p=0.0128$ respectively). There was no significant interaction for the OXPHOS genes Isocitrate dehydrogenase 2 (Idh2), malate dehydrogenase 2 (Mdh2), and Succinate-CoA ligase (Suclg1) transcript abundance (Figure 5.06.b), however, there was a statistically significant difference in transcript abundance was observed between pluripotent cell types ($F(3,24)=10.35$, $p=0.0001$),($F(3,24)=6.679$, $p=0.0019$), and ($F(3,24)=3.299$, $p=0.0375$).

a)

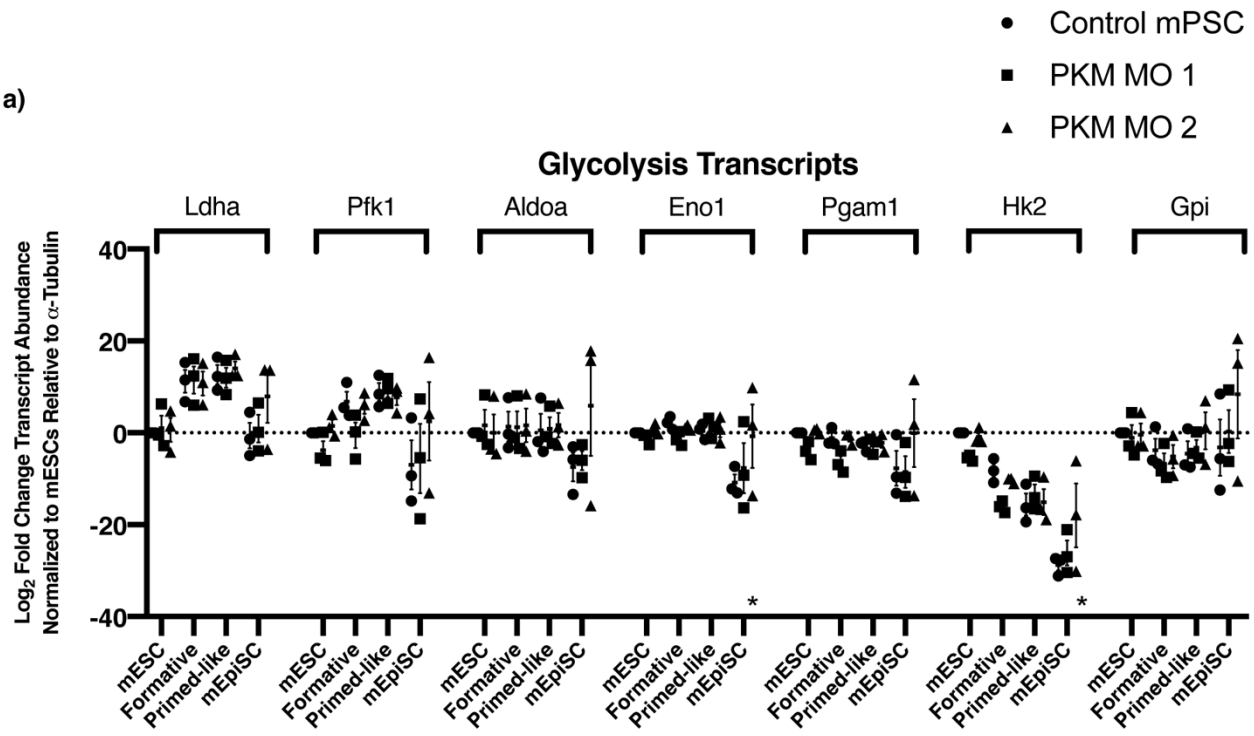
Control mPSC
PKM MO 1
PKM MO 2
Glycolysis Transcripts
Ldha
Pfk1
Aldoa
Eno1
Pgam1
Hk2
Gpi
Log2 Fold Change Transcript Abundance Normalized to mESCs Relative to α-Tubulin
40
20
0
-20
-40
*
*
mESC
Formative
Primed-like
mEpiSC

b)

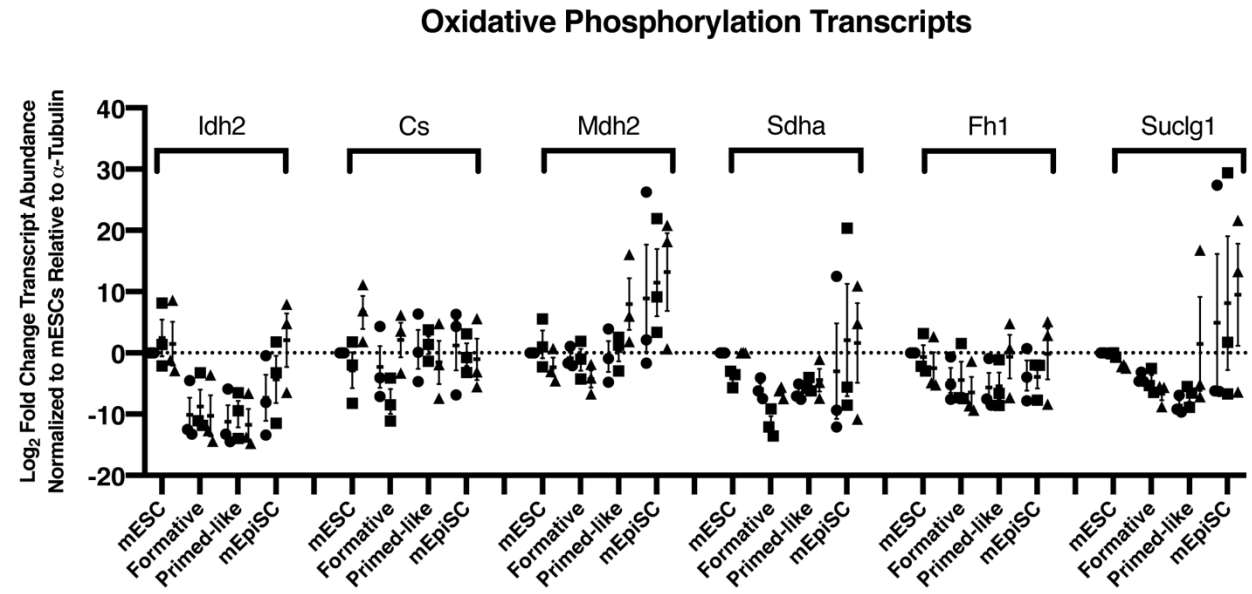
Oxidative Phosphorylation Transcripts
Idh2
Cs
Mdh2
Sdha
Fh1
Suclg1
Log2 Fold Change Transcript Abundance Normalized to mESCs Relative to α-Tubulin
40
30
20
10
0
-10
-20
mESC
Formative
Primed-like
mEpiSC

Figure 5.09. PKM morpholinos influence key glycolytic transcript abundance markers in naïve mESCs, formative mEpiLCs, primed-like mEpiLC, and primed mEpiSCs.

Quantification of transcript abundance following scrape delivery of 20 μM PKM MO 1 and PKM MO 2 morpholinos into mPSCs over 48 hours. Transcript markers include a) glycolysis genes Hk2, Gpi, Pfkl, Aldoa, Pgam1, Eno1, and Ldha, and b) oxidative phosphorylation genes Cs, Idh2, Suclg2, Sdh-a, Fh, and Mdh2. Transcript abundance was compared using the Pfaffl method and data is shown as mean±SEM of treatments compared in biological triplicate as a two-way ANOVA with a Dunnett's multiple comparisons relative to the control of each corresponding cell type; * $p<0.05$, n=3 biological replicates run in technical triplicate. Data represents Log_2 of fold change relative to α-Tubulin and normalized to control mESCs.

5.4.7. PKM1/2 modulation does not alter naïve, formative, or primed pluripotency associated transcripts in mESCs, formative mEpiLCs, primed-like mEpiLCs, and mEpiSCs.

A two-way ANOVA was conducted that examined the influence of treating with the PKM MO 1 or PKM MO 2 morpholinos on transcript abundance of naïve, formative, and primed pluripotent associated transcripts. There was no significant interaction for the naïve pluripotency genes Rex1, Pecam, or Esrrb transcript abundance (Figure 5.09.a), however, there was observed a statistically significant difference in transcript abundance between pluripotent cell types ($F(3,24)=54.98$, $p<0.0001$), ($F(3,24)=15.93$, $p<0.0001$), and ($F(3,24)=25.06$, $p<0.0001$) respectively. There was no significant interaction for the formative pluripotency genes Lef1 (Lymphoid Enhancer Binding Factor 1), Dnmt3b, or Pou1fc transcript abundance (Figure 5.09.b), however, there was a statistically significant differences in transcript abundance between pluripotent cell types ($F(3,24)=7.380$, $p=0.0011$), ($F(3,24)=60.28$, $p<0.0001$), and ($F(3,24)=85.18$, $p<0.0001$) respectively. There was no significant interaction for the primed pluripotency genes Zic2, Cer1, or T(Brachyury) transcript abundance (Figure 5.09.c), however, there was an observed statistically significant difference in transcript abundance between pluripotent cell types ($F(3,24)=4.071$, $p=0.0180$), ($F(3,24)=27.79$, $p<0.0001$), and ($F(3,24)=70.40$, $p<0.0001$) respectively.

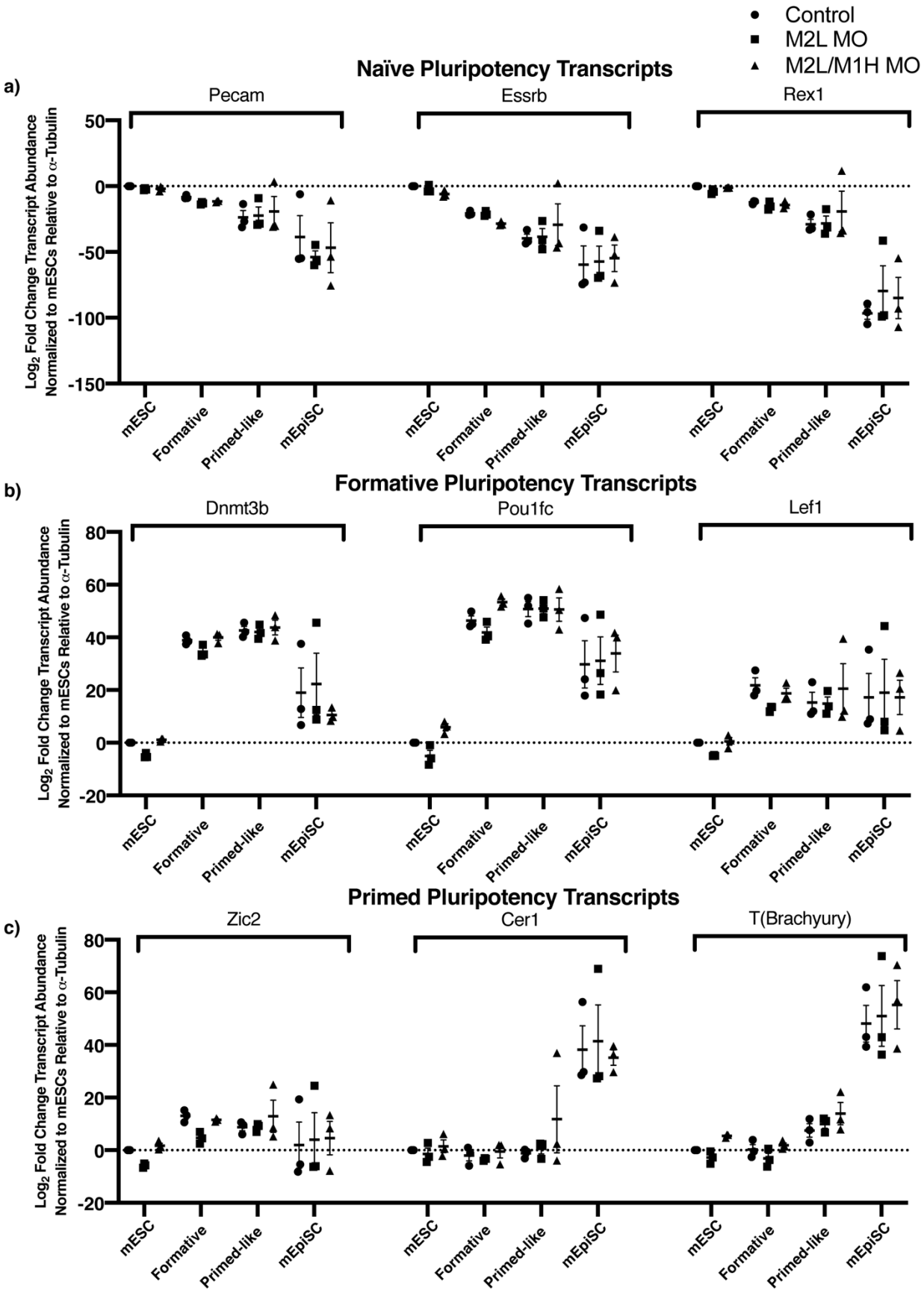
Control
M2L MO
M2L/M1H MO
a)
Naïve Pluripotency Transcripts
Pecam
Essrb
Rex1
Log2 Fold Change Transcript Abundance Normalized to mESCs Relative to α-Tubulin
50
0
-50
-100
-150
mESC
Formative
Primed-like
mEpiSC
b)
Formative Pluripotency Transcripts
Dnmt3b
Pou1fc
Lef1
80
60
40
20
0
-20
c)
Primed Pluripotency Transcripts
Zic2
Cer1
T(Brachyury)

Figure 5.010. PKM morpholinos do not influence key naïve, formative, and primed pluripotency transcript abundance markers in naïve mESCs, formative mEpiLCs, primed-like mEpiLC, and primed mEpiSCs.

Quantification of transcript abundance following scrape delivery of 20 μM PKM MO 1 and PKM MO 2 morpholinos into mPSCs over 48 hours. Transcript markers include a) naïve pluripotency associated genes Pecam, Esrrb, and Rex1, b) formative pluripotency associated genes Dnmt3b, Pou1fc, and Lef1, and c) primed pluripotency associated genes Zic2, Cer1, and T(Brachury). Transcript abundance was compared using the Pfaffl method and data is shown as mean±SEM of treatments compared in biological triplicate as a two-way ANOVA with a Dunnett's multiple comparisons relative to the control of each corresponding cell type; * $p<0.05$, n=3 biological replicates run in technical triplicate. Data represents Log_2 of fold change relative to α-Tubulin and normalized to control mESCs.

5.4.8. PKM1/2 modification alters SSEA1 and CD24 ratios in transitioning mESCs into formative state and formative mEpiLCs into primed-like state mEpiLCs.

There was an observed a significant difference between group mean values of morpholino treatments expressing low levels of SSEA and high levels of CD24 in formative mEpiLCs as determined by a one-way ANOVA ($F(2,6)=8.167$, $p=0.0194$) (Figure 5.11.a). A Dunnett's multiple comparison test detected that the percentage of mEpiLCs (formative) transfected with the PKM MO 1 morpholino (Figure 5.11.c) was significantly enhanced compared to control mEpiLCs ($p=0.0128$). There was an observed significant difference between group mean values of morpholino treatments expressing high levels of SSEA and CD24 in primed-like mEpiLCs as determined by a one-way ANOVA ($F(2,6)=8.486$, $p=0.0178$) (Figure 5.11.a). A Dunnett's multiple comparison test determined that the percentage of mEpiLCs (primed-like) transfected with the PKM MO 1 (Figure 5.12c.) and PKM MO 2 morpholinos (Figure 5.12.d) was significantly greater than control mEpiLCs for SSEA1 high and CD24 high events ($p=0.0264$ and $p=0.0172$ respectively).

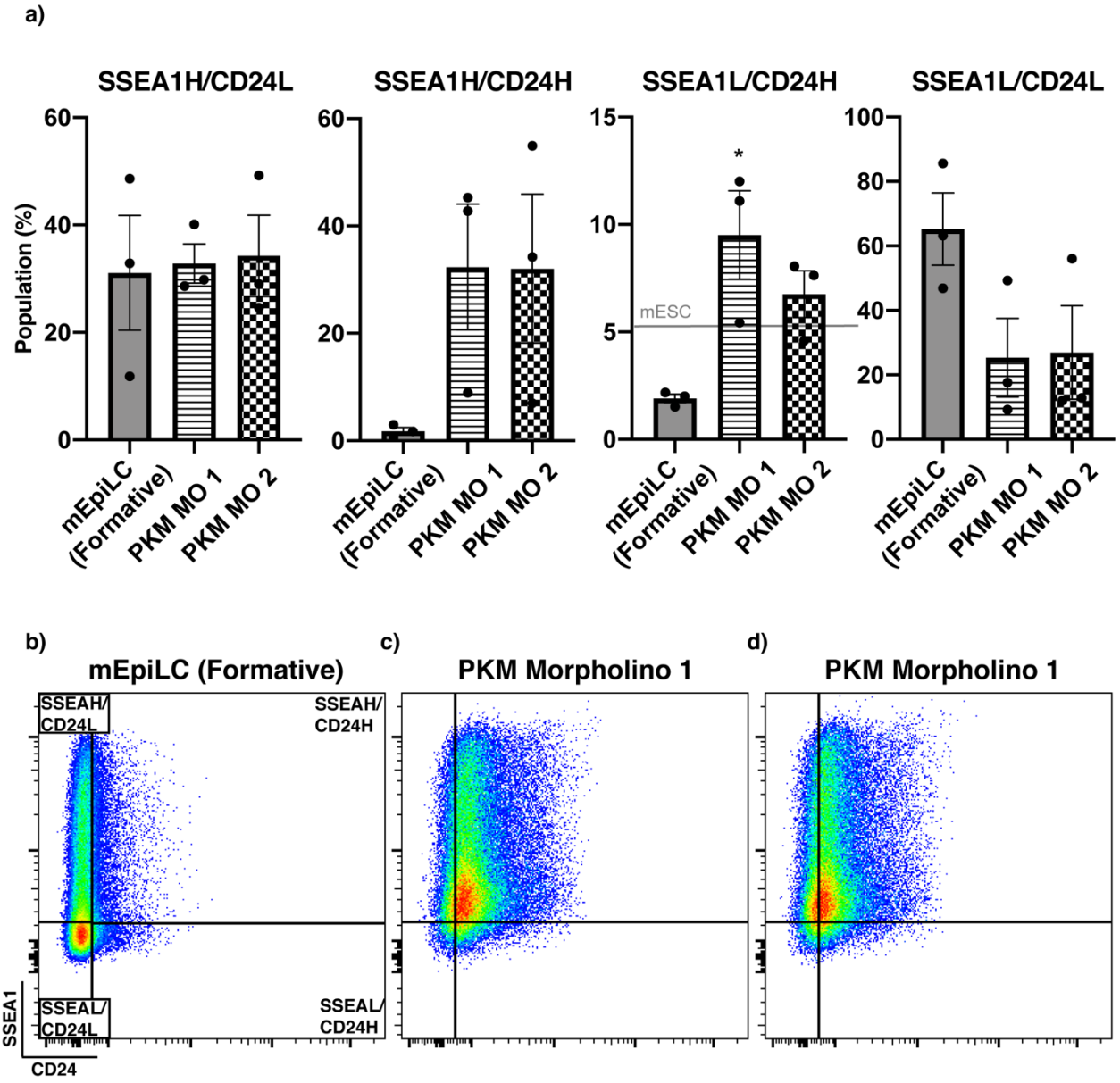
a)
SSEA1H/CD24L
SSEA1H/CD24H
SSEA1L/CD24H
SSEA1L/CD24L
Population (%)
mESC
*
mEpiLC (Formative)
PKM MO 1
PKM MO 2
b)
mEpiLC (Formative)
c)
PKM Morpholino 1
d)
PKM Morpholino 1
SSEAH/ CD24L
SSEAH/ CD24H
SSEAL/ CD24L
SSEAL/ CD24H
SSEA1
CD24

Figure 5.11. Influence of downregulating PKM on SSEA1 and CD24 expression in transitioning formative mEpiLCs.

Scrape delivery of 20 μM PKM MO 1 and PKM MO 2 morpholinos into mESCs transitioned over 48 hours into formative mEpiLCs compared by a) SSEA1 and CD24 cell surface markers by flow cytometry. Transitioning into formative b) mEpiLCs with the addition of c) PKM MO 1 morpholinos and significantly increased the population of SSEA1H and CD24H cells and both PKM MO 1 and d) PKM MO 2 delivery resulted in decreased SSEA1L and CD24L cell populations. Biexponential scale flow plots represent portrayals of SSEA1-compensated Brilliant Violet 421 on a 450 nm laser versus CD24-compensated APC on a 670 nm laser. Data shown as mean±SEM of treatments compared in biological triplicate as a one-way ANOVA with a Dunnett's multiple comparisons relative to the control of each corresponding cell type; * $p<0.05$, n=3 biological replicates.

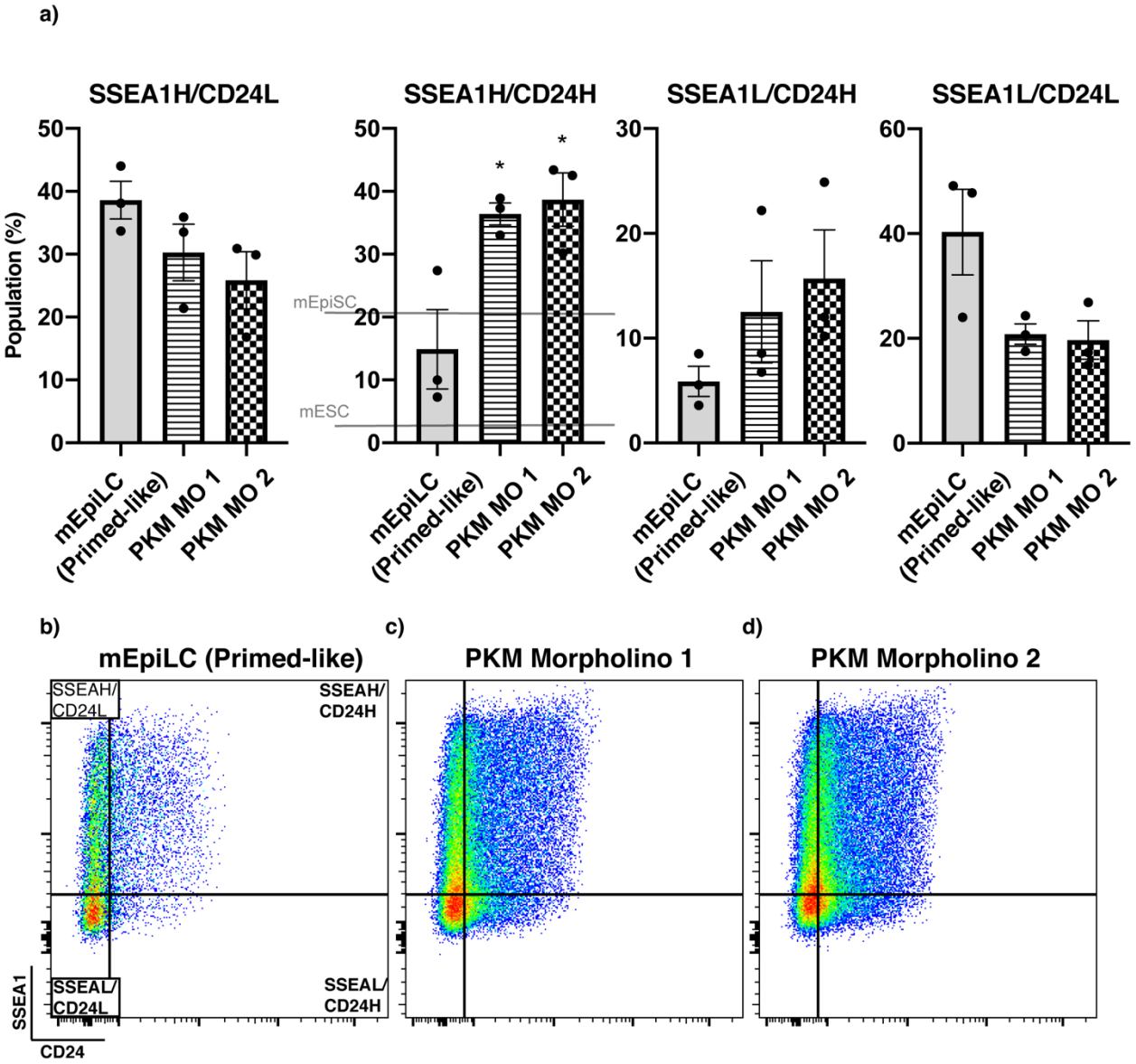
a)
SSEA1H/CD24L
SSEA1H/CD24H
SSEA1L/CD24H
SSEA1L/CD24L
Population (%)
mEpiSC
mESC
mEpiLC (Primed-like)
PKM MO 1
PKM MO 2
b)
c)
d)
mEpiLC (Primed-like)
PKM Morpholino 1
PKM Morpholino 2
SSEAH/ CD24L
SSEAH/ CD24H
SSEAL/ CD24L
SSEAL/ CD24H
SSEA1
CD24

Figure 5.12. Influence of downregulating PKM on SSEA1 and CD24 expression in transitioning primed-like mEpiLCs.

Scrape delivery of 20 μM PKM MO 1 and PKM MO 2 morpholinos into formative mEpiLCs transitioned over 48 hours into primed-like, mEpiLCs compared by a) SSEA1 and CD24 cell surface markers by flow cytometry. Transitioning into primed-like b) mEpiLCs with the addition of c) PKM MO 1 morpholinos and d) PKM MO 2 morpholino delivery significantly increased the population of SSEA1H and CD24H cells and decreased SSEA1L and CD24L cell populations. Biexponential scale flow plots represent portrayals of SSEA1-compensated Brilliant Violet 421 on a 450 nm laser versus CD24-compensated APC on a 670 nm laser. Data shown as mean±SEM of treatments compared in biological triplicate as a one-way ANOVA with a Dunnett's multiple comparisons relative to the control of each corresponding cell type; * $p<0.05$, n=3 biological replicates.

5.5.0. Discussion:

There is a growing body of evidence promoting metabolism as having an active role in cell pluripotency, differentiation, and development (Tsogtbaatar et al. 2020; Dahan et al. 2018; J. Zhang et al. 2018). Within the cells of the early embryo and the pluripotent spectrum, pyruvate kinase muscle isoforms 1 and 2 are suggested to play a variety of roles (Konno, Koseki, et al. 2015; Konno, Ishii, et al. 2015; Jacks et al. 2016). Isoform specific lentiviral overexpression of either Pkm1 or Pkm2 in mESCs significantly increased the pluripotency associated genes Nanog, Eras, and Rex1 transcript abundance, but did not influence specialization when subjected with differentiation media (Qin et al. 2017). This same study found that when Pkm1/2 were downregulated via shRNA, the same pluripotency transcripts were significantly downregulated. Additionally, Pkm1/2 are implicated in the reprogramming of somatic cells to naïve mESCs as downregulating total Pkm1/2 via shRNA significantly hindered induced pluripotent stem cell (iPSC) generation as quantified by measuring alkaline phosphatase staining (Qin et al. 2017). Alternatively, overexpression of Pkm2, but not Pkm1 significantly increased alkaline phosphatase staining during reprogramming, suggesting that Pkm2 is the PKM isoform that facilitates iPSC generation. The metabolic switch from OXPHOS to glycolysis is linked to activation of hypoxia inducible factor 1α (HIF-1α), where PKM2 interacts with the HIF1α subunit promoting transactivation domain function as well as p300 recruitment to the HIF1α's response element during somatic cell reprogramming (Luo et al. 2011). This interaction promotes the WE and thus the switch from OXPHOS to aerobic glycolysis (Palsson-McDermott et al. 2015). The reprogramming of human OXPHOS reliant somatic cells to iPSCs results in primed pluripotent stem cells (hESCs) which

exhibit an aerobic glycolytic metabolic preference, a metabolic transition not far from the naïve-to-primed bivalency to glycolytic transition of mESCs-to-mEpiSCs (Zhou et al. 2012). In the presence of differentiation media, naïve mESCs with a Pkm2 allele knock-in resist differentiation compared to the Pkm1 knock-in as measured by a microarray analysis (Konno, Ishii, et al. 2015). Additionally, the Pkm2 allele knock-in enhances methionine metabolism during differentiation suggesting a pro-oxidative role (Konno, Ishii, et al. 2015). In Chapter 3, I demonstrate that PKM1 and PKM2 protein abundance significantly increases in formative mEpiLCs, therefore, knocking down Pkm2 during this transition could destabilize the pro-oxidative controls necessary for the developmental transition through the formative state during differentiation.

Despite employing an isoform targeted approach of the exclusive splice sites between PKM1 and PKM2, the results of the protein abundance study demonstrate that one of constructs downregulated PKM2 with an upregulation to PKM1. This is not a typical expectation when using morpholinos but is potentially related to the morpholino in question binding across splice regulatory proteins. In this case, the alternative splicing mechanism of PKM1/2 could be impacted by altering splice suppressor and enhancer proteins binding to pre-mRNAs. This would cause a feedback mechanism leading to unintended splicing edits. This alteration has been demonstrated previously in a study examining PKM2 and myotonic dystrophy (Gao and Cooper 2013).

Between either end of the pluripotent spectrum exists a recently described and poorly understood executive, formative stage, of which, metabolic trends and PKM expression have yet to be fully delineated (Smith 2017). Our results demonstrate that altering PKM

through spliceosome modification, influences metabolic and pluripotent cell surface marker expression. Contrary to the hypothesized direction that transitioning formative and primed-like mEpiLCs would take, knocking down PKM1/2 promoted primed pluripotency associated cell surface marker expression and promoted an enhanced population of cells expressing high levels of the naïve cell surface marker SSEA1 and the primed cell surface marker CD24. Notably, there was no significant differences in pluripotency associated transcripts following the addition of morpholinos from their non-transfected control states. While previous research has found Pkm2 to play an important role in naïve pluripotency maintenance and reprogramming from somatic cells to either naïve or primed states, these results demonstrate that Pkm1/2 splice modifications do alter the pluripotent phenotype in transitioning formative and primed-like pluripotent states towards a primed state. It has been demonstrated that naïve mESCs express high levels SSEA1 and primed mEpiSCs express high levels of CD24, potentially the downregulation of PKM2 and upregulation of PKM1 promotes formative state cell expression, however, at this time little is known regarding formative state metabolic preferences (Shakiba et al. 2015). Profiling true, stable formative state cells would confirm this potential cell surface marker trend and the role of PKM1/2 during transitioning. This investigation sheds light on the metabolic preference of formative state cells through our transcript abundance study. I demonstrate a downregulation of OXPHOS transcripts such as Idh2 and an increase in glycolytic transcripts such as Ldha, these trends suggest the initiation of the WE and reflect the *in vivo* correlate following post-implantation of the blastocyst. Of note, the transcript abundance study found key differences between the formative mEpiLCs and primed mEpiSCs, including an increase in OXPHOS transcripts in Mdh2 and Suclg1 for primed cells, these markers are known to regulate tumor growth and are

players in the WE, suggesting that the formative state has not fully adhered to aerobic glycolysis (Kitazawa et al. 2020). As metabolically bivalent cells, naïve mESCs transitioning to the formative state rewire their transcriptional and epigenetic landscape, gaining the competency to differentiate into other cell types (Smith 2017; Kinoshita and Smith 2018). Previous studies demonstrate that reactive oxygen species (ROS)-mediated interactions with mitochondria and nuclear functions are clearly implicated in stem cell fate and potency (Bigarella, Liang, and Ghaffari 2014). As PKM1 plays a critical role in the metabolic shunting of pyruvate towards an OXPHOS fate as acetyl-CoA in the mitochondria, the ROS generated by increased PKM1 may further impinge upon the developmental progression of the pluripotent continuum and lineage competency. This upregulation could promote metabolic reprogramming by inducing a shift to OXPHOS or an OXPHOS-burst to increase ROS and stabilize hypoxia inducible factor 1α (HIF-1α), such an event could be verified by examining extracellular acidification rate and oxygen consumption rate. The master metabolic regulator HIF-1α is activated during instances of hypoxia, decreased ROS and the glycolytic shift towards primed pluripotency. PKM2 can interact with HIF1α to further promote the WE (Prigione et al. 2014). Through PKM2 reduction and PKM1 upregulation, these findings suggest that PKM2 reduction promoted the primed CD24 high cell surface marker population when generating formative state mEpiLCs and may conversely indicate a role for PKM1 in promoting naïve pluripotency. Upregulation of PKM1 appears to have stunted the influence of PKM2 reduction, potentially as a compensatory mechanism. This study demonstrates that formative and primed-like pluripotent states can be effectively distinguished from the naïve, ground, and primed pluripotent states using flow cytometry for the cell surface

markers SSEA1 and CD24. This finding can be utilized to determine transitioning and differentiation efficiencies within the pluripotent continuum and exit during cell lineage specification. Previously, only naïve and primed states have been examined using these markers and here I demonstrate that unique expression dynamics could additionally be utilized for fluorescently activated cell sorting for downstream studies and population purifications (Shakiba et al. 2015). This method should be used in the study of primordial germ cell-like cell generation along with somatic lineage competency during pluripotent development.

The results of the transcript abundance demonstrate that the glycolysis genes Pgam1 and Gpi significantly decreased in primed mEpiSCs following PKM2 downregulation. This is not surprising as Pkm2, Pgam1, and Gpi are heavily implicated in WE and biosynthesis; downregulating a key protein such as PKM2 appears to have downstream effects on other WE associated genes and may disrupt aerobic glycolysis in cells that have achieved true primed pluripotency (Hitosugi et al. 2012; de Padua et al. 2017). Importantly, the genes Hk2 and Eno1 significantly increased in primed mEpiSCs, and Hk2 also significantly increased in primed-like mEpiLCs following PKM2 downregulation and PKM1 upregulation. This follows the currently described preferences for primed pluripotency, and exit of the naïve state, by promoting a glycolytic preference over OXPHOS, and elevated WE transcription of these two critical genes (Capello et al. 2016). The transcript abundance results also demonstrate that the OXPHOS genes Mdh2, Fh1, and Suclg1 all significantly increased when PKM2 was downregulated and PKM1 was upregulated in primed-like mEpiLCs. This further promotes the primed pluripotent state as Mdh2 is implicated in feeding the WE through nicotinamide adenine dinucleotide regeneration

(NAD), thus supporting the glycolytic shift (Hanse et al. 2017). Fumarate hydratase (Fh1) works to process the accumulated fumarate, which in turn works to activate hypoxia response (Isaacs et al. 2005; Frezza et al. 2011). The increased PKM1 may contribute towards compensating towards fumarate accumulation, however, increased Fh1 relative to the control primed-like cells and even the naïve mESCs is unexpected and may play a new role in generating the unique naïve SSEA1 high coupled with primed CD24 high population. Suclg1 works to generate ADP and succinyl-CoA in the tricarboxylic acid cycle and can work to promote substrate level phosphorylation even in the absence of oxygen, and thus can work within the shift towards aerobic glycolysis model in primed-like mEpiLCs (Chinopoulos and Seyfried 2018). Metabolic profiling on the protein level through immunoblots and non-denaturing gels paired with live cell acute measure of extracellular acidification rate and oxygen consumption rate will help to elucidate metabolic trends in the formative state and PSCs treated with PKM morpholinos. As both the downregulated PKM2 and the combination of downregulation of PKM2 and upregulation of PKM1 yielded similar levels (mean of 36.4% and 38.7% respectively) of unique population of SSEA1 high and CD24 high primed-like mEpiLCs, the effects of PKM1 upregulation are either not strong enough to compensate or do not have a role in the transition out of the formative state to primed state pluripotency. This trend could additionally be in response to, or in addition to the significant increase in the ratio of PKM1/PKM2 with the PKM MO 2 treatment. In summary, the metabolic transcript abundance results demonstrate modulating PKM1 and PKM2 expression appears to impact the primed-like mEpiSCs and primed mEpiSCs (Figure 5.13). This may promote the unique population of naïve and primed cell surface marker expressing cells in the primed-like mEpiSCs, and likely disrupts primed pluripotency in mEpiSCs by

displacing the WE (Figure 5.12.). My strategy of targeting PKM1/2 splice events resulted in an elevated ratio of phosphorylated-PKM2 (pPKM2), the conformation associated with the WE, to total-PKM2, lysates showing the cumulative expression of both homo-tetrameric and dimeric (pPKM2) conformations. This result implicates pPKM2 as playing a role in generating this novel expression pattern of SSEA1 high and CD24 high expressing cells following the transition from the formative state to a primed-like pluripotency. Previously, in Chapter 3, I demonstrated maintenance of the ratio of PKM1/PKM2 protein abundance throughout the pluripotent continuum in murine cells, by modulating the ratio of pPKM2/PKM2 with morpholinos, a further promotion of the WE and enhanced metabolic shifting from bivalency to aerobic glycolysis is possible.

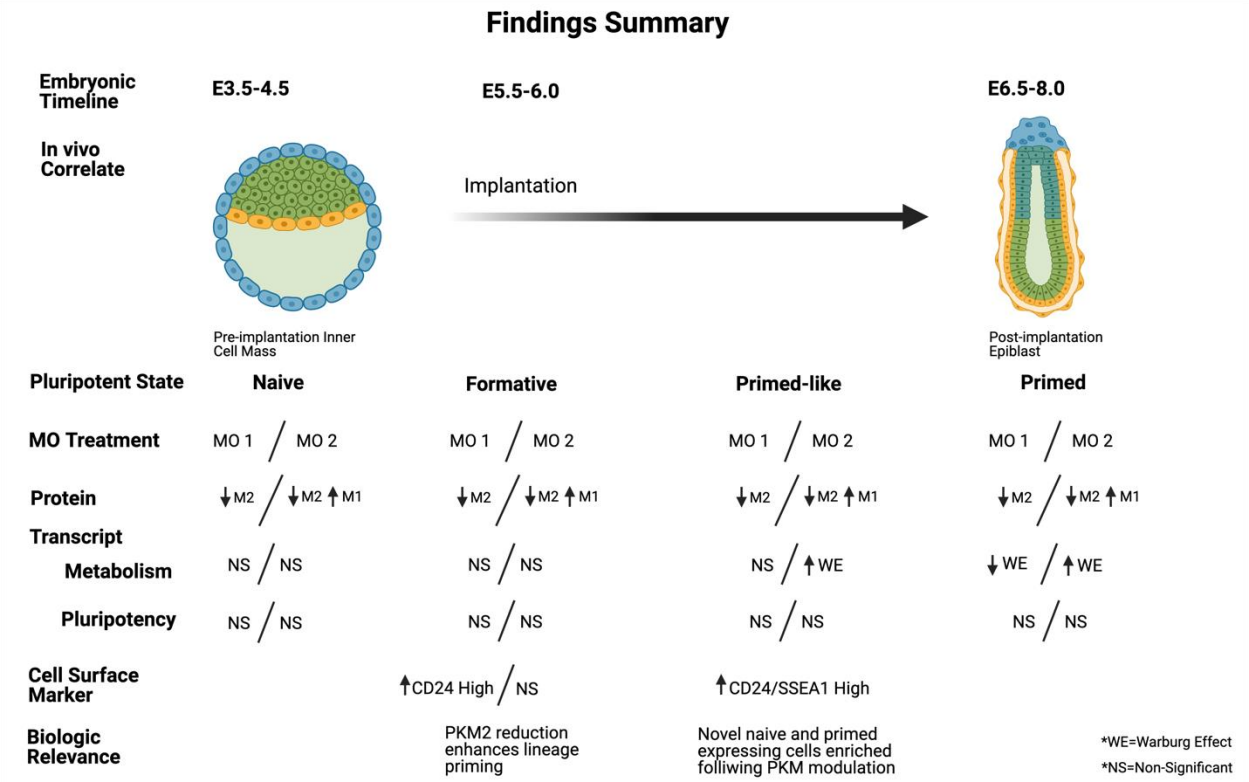

Figure 5.13. Summary of Chapter 5 research findings.

The influence of PKM1/2 morpholinos on protein and transcript abundance, and cell surface marker expression in mESCs, mEpiLCs (formative and primed-like), and mEpiSCs. mPSCs representing the states of the pluripotent continuum treated with PKM morpholinos result in altered metabolic transcripts related to the WE in primed-like mEpiLCs and primed mEpiSCs. There was no difference found in pluripotency associated transcripts across the spectrum with the addition of PKM morpholinos, however, the cell surface markers for the pluripotency proteins SSEA1 and CD24 were altered in mESCs transitioning to the formative state and from formative mEpiLCs transitioning to primed-like mEpiLCs.

Here, I demonstrate that downregulating PKM2 alone promotes primed pluripotent stem cell populations (CD24 High) when generating formative state mEpiLCs. Importantly, downregulating PKM2 with PKM1 upregulation does result in a significant increase in CD24 High expressing cells. In this instance, the pro-OXPHOS nature of Pkm1 may promote the bivalent nature of mESCs to counter the pro-transitioning influence of downregulating PKM2. Through germline deletion of PKM2 in mice, it was found that PKM1 becomes the predominant isoform in all cells of the developing PKM2-null mouse compensating for the loss of PKM2, the traditional predominant form during development (Jacks et al. 2016). These results suggest that downregulating PKM2 appears to yield a population expressing both naïve and primed cell surface markers. Interestingly, another intermediate pluripotent cell state referred to as 'f-class' cells have been shown to contain a similar population of SSEA1+/CD24+ cells (Vidal, Stadtfeld, and Apostolou 2015; Urbanska et al. 2017). These f-class cells are generated in rare populations following extended transgene expression of reprogramming factors Oct4, Klf4. Sox2 and c-Myc (Vidal, Stadtfeld, and Apostolou 2015). When the formative pluripotent state was hypothesized, the notion that formative cells could occupy the transcriptional profile of both naïve and primed states was suggested, potentially disrupting the fine-tuning pro-oxidative controls associated with the Pkm2 isoform during a transition that promotes the formative state *in vitro* (Smith 2017). The lack of PKM1 specificity introduced us to an unexpected beneficial strategy that being that our Pkm1/2 morpholinos can induce both downregulation of PKM2 alone and downregulation of PKM2 while simultaneously upregulating PKM1. This occurrence has been demonstrated previously using morpholinos on the alternative spliced gene Proteolipid protein 1 (Plp1/DM20), where Plp1 shift to DM20 alternative splicing (Tantzer et al. 2018). The cause for the lack of

specificity in the targeted morpholino approach could be due to a duplication mutation as the exclusive exons share a very similar sequence, downstream mutations could further change the exonic structure. A PKM1 specific morpholino is necessary to delineate the role of the M1 isoform in maintaining individual pluripotent states and pluripotent transitioning. A CRISPR or TALEN strategy is possible for an alternatively spliced isoform such as PKM1/2, however, PKM1/2 specificity has been shown using shRNAs, germline loss of function and lentiviral allele-knock in (Qin et al. 2017; Konno, Ishii, et al. 2015; Jacks et al. 2016). When taken together, this study promotes PKM1 and PKM2 having a role in the WE as upregulation in formative and primed-like mEpiLCs and mEpiSCs promotes WE genes and primed pluripotency associated CD24 expression. This is surprising as PKM2 is associated with the WE, and PKM1 has only recently been implicated in specific cancers, this finding promotes both isoforms as having a potential role in development and the pluripotent continuum (L. Wei et al. 2017; Morita et al. 2018). These findings promote Pkm1 and Pkm2 having distinct roles in metabolism and pluripotency along with contributing to the growing body of evidence that metabolism is a driver of pluripotency state.

5.6.0. Acknowledgements:

Flow cytometry was completed at the London Regional Flow Cytometry Facility at Robarts Research Institute of The University of Western Ontario, London, Ontario, Canada. Pluripotent cell lines were generously gifted from Dr. Janet Rossant from The Hospital for Sick Children, Toronto, Ontario, Canada. Morpholinos were designed by Dr. Jon Moulton of Gene Tools LLC, Philomath, Oregon, USA. This research was funded by a Canadian Institutes of Health Research operating grant to A.J.W. and D.H.B. and Natural Sciences and Engineering Research Council of Canada grant to D.H.B. The funders had no role in study design, data collection and analysis, decision to publish, or preparation of the manuscript.

Additional information:

The authors have no competing interests to disclose.

5.7.0. References:

Bigarella, Carolina L, Raymond Liang, and Saghi Ghaffari. 2014. "Stem Cells and the Impact of ROS Signaling." *Development* 141 (22): 4206 LP – 4218. https://doi.org/10.1242/dev.107086.

Buck, Michael D, David O'Sullivan, Ramon I Klein Geltink, Jonathan D Curtis, Chih-Hao Chang, David E Sanin, Jing Qiu, et al. 2016. "Mitochondrial Dynamics Controls T Cell Fate through Metabolic Programming." *Cell* 166 (1): 63–76. https://doi.org/10.1016/j.cell.2016.05.035.

Buecker, Christa, Rajini Srinivasan, Zhixiang Wu, Eliezer Calo, Dario Acampora, Tiago Faial, Antonio Simeone, Minjia Tan, Tomasz Swigut, and Joanna Wysocka. 2014. "Reorganization of Enhancer Patterns in Transition from Naive to Primed Pluripotency." *Cell Stem Cell* 14 (6): 838–53. https://doi.org/10.1016/j.stem.2014.04.003.

Capello, Michela, Sammy Ferri-Borgogno, Chiara Riganti, Michelle Samuel Chattaragada, Moitza Principe, Cecilia Roux, Weidong Zhou, Emanuel F Petricoin, Paola Cappello, and Francesco Novelli. 2016. "Targeting the Warburg Effect in Cancer Cells through ENO1 Knockdown Rescues Oxidative Phosphorylation and Induces Growth Arrest." *Oncotarget* 7 (5): 5598–5612. https://doi.org/10.18632/oncotarget.6798.

Chinopoulos, Christos, and Thomas N Seyfried. 2018. "Mitochondrial Substrate-Level Phosphorylation as Energy Source for Glioblastoma: Review and Hypothesis." *ASN Neuro* 10: 1759091418818261. https://doi.org/10.1177/1759091418818261.

Dahan, Perrine, Vivian Lu, Robert M.T. Nguyen, Stephanie A.L. Kennedy, and Michael A. Teitell. 2018. "Metabolism in Pluripotency: Both Driver and Passenger?" *Journal of Biological Chemistry*, February, jbc.TM117.000832. https://doi.org/10.1074/JBC.TM117.000832.

Dahan, Perrine, Vivian Lu, Robert M T Nguyen, Stephanie A L Kennedy, and Michael A Teitell. 2019. "Metabolism in Pluripotency: Both Driver and Passenger?" *The Journal of Biological Chemistry* 294 (14): 5420–29. https://doi.org/10.1074/jbc.TM117.000832.

Dierolf, Joshua G, Andrew J Watson, and Dean H Betts. 2020. "Differential Localization Patterns of Pyruvate Kinase Isoforms in Murine Naïve, Formative and Primed Pluripotent States." *BioRxiv*, January, 2020.04.12.036251. https://doi.org/10.1101/2020.04.12.036251.

Evans, M. J., and M. H. Kaufman. 1981. "Establishment in Culture of Pluripotential Cells from Mouse Embryos." *Nature*. https://doi.org/10.1038/292154a0.

Frezza, Christian, Liang Zheng, Ori Folger, Kartik N Rajagopalan, Elaine D MacKenzie, Livnat Jerby, Massimo Micaroni, et al. 2011. "Haem Oxygenase Is Synthetically Lethal with the Tumour Suppressor Fumarate Hydratase." *Nature* 477 (7363): 225–28. https://doi.org/10.1038/nature10363.

Gao, Zhihua, and Thomas A Cooper. 2013. "Reexpression of Pyruvate Kinase M2 in Type 1 Myofibers Correlates with Altered Glucose Metabolism in Myotonic Dystrophy." *Proceedings of the National Academy of Sciences* 110 (33): 13570 LP – 13575. https://doi.org/10.1073/pnas.1308806110.

Gascón, Sergio, Elisa Murenu, Giacomo Masserdotti, Felipe Ortega, Gianluca L Russo, David Petrik, Aditi Deshpande, et al. 2016. "Identification and Successful

Negotiation of a Metabolic Checkpoint in Direct Neuronal Reprogramming." *Cell Stem Cell* 18 (3): 396–409. https://doi.org/10.1016/j.stem.2015.12.003.

Growth, Cell-autonomous Tumor Cell. 2018. "PKM1 Confers Metabolic Advantages and Promotes Article PKM1 Confers Metabolic Advantages and Promotes Cell-Autonomous." *Cancer Cell* 33 (3): 355-367.e7. https://doi.org/10.1016/j.ccell.2018.02.004.

Guo, G., J. Yang, J. Nichols, J. S. Hall, I. Eyres, W. Mansfield, and A. Smith. 2009. "Klf4 Reverts Developmentally Programmed Restriction of Ground State Pluripotency." *Development* 136 (7): 1063–69. https://doi.org/10.1242/dev.030957.

Hanse, E A, C Ruan, M Kachman, D Wang, X H Lowman, and A Kelekar. 2017. "Cytosolic Malate Dehydrogenase Activity Helps Support Glycolysis in Actively Proliferating Cells and Cancer." *Oncogene* 36 (27): 3915–24. https://doi.org/10.1038/onc.2017.36.

Hayashi, Katsuhiko, Hiroshi Ohta, Kazuki Kurimoto, Shinya Aramaki, and Mitinori Saitou. 2011. "Reconstitution of the Mouse Germ Cell Specification Pathway in Culture by Pluripotent Stem Cells." *Cell* 146 (4): 519–32. https://doi.org/10.1016/j.cell.2011.06.052.

Heiden, Matthew Vander, Lewis Cantley, and Craig Thompson. 2009. "Understanding the Warburg Effect: The Metabolic Requiremetns of Cell Proliferation." *Science* 324 (5930): 1029–33. https://doi.org/10.1126/science.1160809.Understanding.

Hitosugi, Taro, Lu Zhou, Shannon Elf, Jun Fan, Hee-Bum Kang, Jae Ho Seo, Changliang Shan, et al. 2012. "Phosphoglycerate Mutase 1 Coordinates Glycolysis and Biosynthesis to Promote Tumor Growth." *Cancer Cell* 22 (5): 585–600. https://doi.org/10.1016/j.ccr.2012.09.020.

Isaacs, Jennifer S, Yun Jin Jung, David R Mole, Sunmin Lee, Carlos Torres-Cabala, Yuen-Li Chung, Maria Merino, et al. 2005. "HIF Overexpression Correlates with Biallelic Loss of Fumarate Hydratase in Renal Cancer: Novel Role of Fumarate in Regulation of HIF Stability." *Cancer Cell* 8 (2): 143–53. https://doi.org/10.1016/j.ccr.2005.06.017.

Jacks, Tyler E., Alba Luengo, Arjun Bhutkar, Talya L. Dayton, Kathryn M. Miller, Matthew G. Vander Heiden, William J. Israelsen, Shawn M. Davidson, Vasilena Gocheva, and Clary B. Clish. 2016. "Germline Loss of PKM2 Promotes Metabolic Distress and Hepatocellular Carcinoma." *Molecular Cancer Research* 14 (4 Supplement): PR04–PR04. https://doi.org/10.1158/1557-3125.devbiolca15-pr04.

Jurica, Melissa S, Andrew Mesecar, Patrick J Heath, Wuxian Shi, Thomas Nowak, and Barry L Stoddard. 1998. "The Allosteric Regulation of Pyruvate Kinase by Fructose-1,6-Bisphosphate." *Structure* 6 (2): 195–210. https://doi.org/10.1016/S0969-2126(98)00021-5.

Kalkan, Tüzer, Nelly Olova, Mila Roode, Carla Mulas, Heather J Lee, Isabelle Nett, Hendrik Marks, et al. 2017. "Tracking the Embryonic Stem Cell Transition from Ground State Pluripotency." *Development* 144 (7): 1221 LP – 1234. https://doi.org/10.1242/dev.142711.

Kinoshita, Masaki, Michael Barber, William Mansfield, Yingzhi Cui, Daniel Spindlow, Giuliano Giuseppe Stirparo, Sabine Dietmann, Jennifer Nichols, and Austin Smith. 2020. "Capture of Mouse and Human Stem Cells with Features of Formative Pluripotency." *Cell Stem Cell*. https://doi.org/https://doi.org/10.1016/j.stem.2020.11.005.

Kinoshita, Masaki, and Austin Smith. 2018. “Pluripotency Deconstructed.” *Development, Growth & Differentiation* 60 (1): 44–52. https://doi.org/10.1111/dgd.12419.

Kitazawa, Masashi, Tomohisa Hatta, Yusuke Sasaki, Kazuhiko Fukui, Koji Ogawa, Eriko Fukuda, Naoki Goshima, et al. 2020. “Promotion of the Warburg Effect Is Associated with Poor Benefit from Adjuvant Chemotherapy in Colorectal Cancer.” *Cancer Science* 111 (2): 658–66. https://doi.org/10.1111/cas.14275.

Konno, Masamitsu, Hideshi Ishii, Jun Koseki, Nobuhiro Tanuma, Naohiro Nishida, Koichi Kawamoto, Tatsunori Nishimura, et al. 2015. “Pyruvate Kinase M2, but Not M1, Allele Maintains Immature Metabolic States of Murine Embryonic Stem Cells.” *Regenerative Therapy* 1: 63–71. https://doi.org/10.1016/j.reth.2015.01.001.

Konno, Masamitsu, Jun Koseki, Koichi Kawamoto, Naohiro Nishida, Hidetoshi Matsui, Dyah Laksmi Dewi, Miyuki Ozaki, et al. 2015. “Embryonic MicroRNA-369 Controls Metabolic Splicing Factors and Urges Cellular Reprograming.” *PLoS ONE* 10 (7): e0132789. https://doi.org/10.1371/journal.pone.0132789.

Livak, Kenneth J, and Thomas D Schmittgen. 2001. “Analysis of Relative Gene Expression Data Using Real-Time Quantitative PCR and the 2−ΔΔCT Method.” *Methods* 25 (4): 402–8. https://doi.org/https://doi.org/10.1006/meth.2001.1262.

Luo, Weibo, Hongxia Hu, Ryan Chang, Jun Zhong, Matthew Knabel, Robert O’Meally, Robert N. Cole, Akhilesh Pandey, and Gregg L. Semenza. 2011. “Pyruvate Kinase M2 Is a PHD3-Stimulated Coactivator for Hypoxia-Inducible Factor 1.” *Cell* 145 (5): 732–44. https://doi.org/10.1016/j.cell.2011.03.054.

Martin, G R. 1981. “Isolation of a Pluripotent Cell Line from Early Mouse Embryos Cultured in Medium Conditioned by Teratocarcinoma Stem Cells.” *Proceedings of the National Academy of Sciences* 78 (12): 7634 LP – 7638. https://doi.org/10.1073/pnas.78.12.7634.

Mathieu, Julie, and Hannele Ruohola-Baker. 2017. “Metabolic Remodeling during the Loss and Acquisition of Pluripotency.” *Development (Cambridge, England)* 144 (4): 541–51. https://doi.org/10.1242/dev.128389.

Morgani, Sophie, Jennifer Nichols, and Anna-Katerina Hadjantonakis. 2017. “The Many Faces of Pluripotency: In Vitro Adaptations of a Continuum of in Vivo States.” *BMC Developmental Biology* 17 (1): 7. https://doi.org/10.1186/s12861-017-0150-4.

Morita, Mami, Taku Sato, Miyuki Nomura, Yoshimi Sakamoto, Yui Inoue, Ryota Tanaka, Shigemi Ito, et al. 2018. “PKM1 Confers Metabolic Advantages and Promotes Cell-Autonomous Tumor Cell Growth.” *Cancer Cell* 33 (3): 355-367.e7. https://doi.org/10.1016/j.ccell.2018.02.004.

Nichols, Jennifer, and Austin Smith. 2009. “Naive and Primed Pluripotent States.” *Cell Stem Cell* 4 (6): 487–92. https://doi.org/10.1016/j.stem.2009.05.015.

Ohinata, Yasuhide, Hiroshi Ohta, Mayo Shigeta, Kaori Yamanaka, Teruhiko Wakayama, and Mitinori Saitou. 2009. “A Signaling Principle for the Specification of the Germ Cell Lineage in Mice.” *Cell* 137 (3): 571–84. https://doi.org/10.1016/j.cell.2009.03.014.

Osorno, Rodrigo, Anestis Tsakiridis, Frederick Wong, Noemí Cambray, Constantinos Economou, Ronald Wilkie, Guillaume Blin, Paul J Scotting, Ian Chambers, and Valerie Wilson. 2012. “The Developmental Dismantling of Pluripotency Is Reversed by Ectopic Oct4 Expression.” *Development* 139 (13): 2288 LP – 2298. https://doi.org/10.1242/dev.078071.

Padua, Monique Cunha de, Giulia Delodi, Milica Vučetić, Jérôme Durivault, Valérie

Vial, Pascale Bayer, Guilhermina Rodrigues Noleto, Nathalie M Mazure, Maša Ždralević, and Jacques Pouysségur. 2017. “Disrupting Glucose-6-Phosphate Isomerase Fully Suppresses the ‘Warburg Effect’ and Activates OXPHOS with Minimal Impact on Tumor Growth except in Hypoxia.” *Oncotarget* 8 (50): 87623–37. https://doi.org/10.18632/oncotarget.21007.

Palsson-McDermott, Eva M, Anne M Curtis, Gautam Goel, Mario A R Lauterbach, Frederick J Sheedy, Laura E Gleeson, Mirjam W M van den Bosch, et al. 2015. “Pyruvate Kinase M2 Regulates Hif-1α Activity and IL-1β Induction and Is a Critical Determinant of the Warburg Effect in LPS-Activated Macrophages.” *Cell Metabolism* 21 (1): 65–80. https://doi.org/10.1016/j.cmet.2014.12.005.

PARTRIDGE, MICHAEL, ALEXANDRA VINCENT, PAULA MATTHEWS, JOHN PUMA, DAVID STEIN, and JAMES SUMMERTON. 1996. “A Simple Method for Delivering Morpholino Antisense Oligos into the Cytoplasm of Cells.” *Antisense and Nucleic Acid Drug Development* 6 (3): 169–75. https://doi.org/10.1089/oli.1.1996.6.169.

Pfaffl, M W. 2001. “A New Mathematical Model for Relative Quantification in Real-Time RT-PCR.” *Nucleic Acids Research* 29 (9): e45–e45. https://doi.org/10.1093/nar/29.9.e45.

Prigione, Alessandro, Nadine Rohwer, Sheila Hoffmann, Barbara Mlody, Katharina Drews, Raul Bukowiecki, Katharina Blümlein, et al. 2014. “HIF1α Modulates Cell Fate Reprogramming through Early Glycolytic Shift and Upregulation of PDK1-3 and PKM2.” *Stem Cells* 32 (2): 364–76. https://doi.org/10.1002/stem.1552.

Qin, Shengtang, Danli Yang, Kang Chen, Haolan Li, Liqiang Zhang, Yuan Li, Rongrong Le, Xiaojie Li, Shaorong Gao, and Lan Kang. 2017. “Pkm2 Can Enhance Pluripotency in ESCs and Promote Somatic Cell Reprogramming to IPSCs.” *Oncotarget* 8 (48): 84276. https://doi.org/10.18632/ONCOTARGET.20685.

Shakiba, Nika, Carl A. White, Yonatan Y. Lipsitz, Ayako Yachie-Kinoshita, Peter D. Tonge, Samer M.I. Hussein, Mira C. Puri, et al. 2015. “CD24 Tracks Divergent Pluripotent States in Mouse and Human Cells.” *Nature Communications* 6: 7329. https://doi.org/10.1038/ncomms8329.

Smith, Austin. 2017. “Formative Pluripotency: The Executive Phase in a Developmental Continuum.” *Development* 144 (3): 365–73. https://doi.org/10.1242/dev.142679.

Tantzer, Stephanie, Karen Sperle, Kaitlin Kenaley, Jennifer Taube, and Grace M Hobson. 2018. “Morpholino Antisense Oligomers as a Potential Therapeutic Option for the Correction of Alternative Splicing in PMD, SPG2, and HEMS.” *Molecular Therapy - Nucleic Acids* 12 (September): 420–32. https://doi.org/10.1016/j.omtn.2018.05.019.

Tsogtbaatar, Enkhtuul, Chelsea Landin, Katherine Minter-Dykhouse, and Clifford D L Folmes. 2020. “Energy Metabolism Regulates Stem Cell Pluripotency .” *Frontiers in Cell and Developmental Biology* . https://www.frontiersin.org/article/10.3389/fcell.2020.00087.

Urbanska, Marta, Maria Winzi, Katrin Neumann, Shada Abuhattum, Philipp Rosendahl, Paul Müller, Anna Taubenberger, Konstantinos Anastassiadis, and Jochen Guck. 2017. “Single-Cell Mechanical Phenotype Is an Intrinsic Marker of Reprogramming and Differentiation along the Mouse Neural Lineage.” *Development* 144 (23): 4313 LP – 4321. https://doi.org/10.1242/dev.155218.

Valentini, Giovanna, Laurent Chiarelli, Riccardo Fortini, Maria L. Speranza, Alessandro Galizzi, and Andrea Mattevi. 2000. “The Allosteric Regulation of Pyruvate Kinase:

A Site-Directed Mutagenesis Study." *Journal of Biological Chemistry* 275 (24): 18145–52. https://doi.org/10.1074/jbc.M001870200.

Vidal, Simon E., Matthias Stadtfeld, and Eftychia Apostolou. 2015. "F-Class Cells: New Routes and Destinations for Induced Pluripotency." *Cell Stem Cell* 16 (1): 9–10. https://doi.org/10.1016/j.stem.2014.12.007.

Wang, H.-J., Y.-J. Hsieh, W.-C. Cheng, C.-P. Lin, Y.-S. Lin, S.-F. Yang, C.-C. Chen, et al. 2014. "JMJD5 Regulates PKM2 Nuclear Translocation and Reprograms HIF-1 -Mediated Glucose Metabolism." *Proceedings of the National Academy of Sciences* 111 (1): 279–84. https://doi.org/10.1073/pnas.1311249111.

Wei, Libin, Yuanyuan Dai, Yuxin Zhou, Zihao He, Jingyue Yao, Li Zhao, Qinglong Guo, and Lin Yang. 2017. "Oroxylin A Activates PKM1/HNF4 Alpha to Induce Hepatoma Differentiation and Block Cancer Progression." *Cell Death & Disease* 8 (7): e2944. https://doi.org/10.1038/cddis.2017.335.

Wei, Peng, Katja K Dove, Claire Bensard, John C Schell, and Jared Rutter. 2018. "The Force Is Strong with This One: Metabolism (Over)Powers Stem Cell Fate." *Trends in Cell Biology* 28 (7): 551–59. https://doi.org/https://doi.org/10.1016/j.tcb.2018.02.007.

Wray, Jason, Tüzer Kalkan, Sandra Gomez-Lopez, Dominik Eckardt, Andrew Cook, Rolf Kemler, and Austin Smith. 2011. "Inhibition of Glycogen Synthase Kinase-3 Alleviates Tcf3 Repression of the Pluripotency Network and Increases Embryonic Stem Cell Resistance to Differentiation." *Nature Cell Biology* 13 (7): 838–45. https://doi.org/10.1038/ncb2267.

Yang, W., and Z. Lu. 2015. "Pyruvate Kinase M2 at a Glance." *Journal of Cell Science* 128 (9): 1655–60. https://doi.org/10.1242/jcs.166629.

Yang, Weiwei, and Zhimin Lu. 2013. "Nuclear PKM2 Regulates the Warburg Effect." *Cell Cycle* 12 (19): 3154–58. https://doi.org/10.4161/cc.26182.

Zhang, Hongbo, Dongryeol Ryu, Yibo Wu, Karim Gariani, Xu Wang, Peiling Luan, Davide D'Amico, et al. 2016. "NAD^+ Repletion Improves Mitochondrial and Stem Cell Function and Enhances Life Span in Mice." *Science (New York, N.Y.)* 352 (6292): 1436–43. https://doi.org/10.1126/science.aaf2693.

Zhang, Jin, Jing Zhao, Perrine Dahan, Vivian Lu, Cheng Zhang, Hu Li, and Michael A. Teitell. 2018. "Metabolism in Pluripotent Stem Cells and Early Mammalian Development." *Cell Metabolism* 27 (2): 332–38. https://doi.org/10.1016/j.cmet.2018.01.008.

Zheng, Xinde, Leah Boyer, Mingji Jin, Jerome Mertens, Yongsung Kim, Li Ma, Li Ma, Michael Hamm, Fred H Gage, and Tony Hunter. 2016. "Metabolic Reprogramming during Neuronal Differentiation from Aerobic Glycolysis to Neuronal Oxidative Phosphorylation." *ELife* 5 (June). https://doi.org/10.7554/eLife.13374.

Zhou, Wenyu, Michael Choi, Daciana Margineantu, Lilyana Margaretha, Jennifer Hesson, Christopher Cavanaugh, C. Anthony Blau, et al. 2012. "HIF1α Induced Switch from Bivalent to Exclusively Glycolytic Metabolism during ESC-to-EpiSC/HESC Transition." *EMBO Journal* 31 (9): 2103–16. https://doi.org/10.1038/emboj.2012.71.

Chapter 6

6.0.0. General Discussion.

Pluripotent stem cells (PSCs) are hallmarked by two key traits: i) they can divide in the undifferentiated state indefinitely and ii) they have the potential to specialize into any cell type of the adult organism including the germ cells. These traits are referred to as self-renewal, trilineage differentiation, and germ cell specialization. Pluripotency is described as a developmental continuum reflecting *in vivo* embryological origins as individual states (Nichols and Smith 2009; Morgani, Nichols, and Hadjantonakis 2017). The cells of the developing inner cell mass (ICM) of the pre-implantation embryo can be explanted and grown *in vitro*, with cells of this developmental stage are referred to as having naïve pluripotency (Evans and Kaufman 1981; Martin 1981). Recently an executive, intermediate pluripotent state has been described, also known as formative pluripotency (Smith 2017). Immediately following implantation cells enter the formative interval and towards the end of pluripotency, cells exhibit primed pluripotency. These three phases represent sequential developmental intervals of the phased progression model of pluripotency, whereby a developing cell of the embryo needs to progress throughout each phase before specializing through the progress of differentiation (Smith 2017). Naïve, formative, and primed pluripotency represent distinct intervals of pluripotent development and have only recently been stably produced into cell lines instead of transiently existing states (Kinoshita et al. 2020). Aside from their developmental timeline, one distinguishing feature of these pluripotent states is their metabolic preference (Zhou et al. 2012). Naïve PSCs utilize both glycolysis and oxidative phosphorylation (OXPHOS), whereas primed PSCs use aerobic glycolysis, a trait also

preferential in most cancer cells commonly referred to as the ‘Warburg Effect’ (Zhou et al. 2012). The formative pluripotent state has yet to have its metabolic preferences delineated and requires further investigation. Based on our transcript abundance study in Chapter 5, the formative pluripotent state appears to show the onboarding of an increase in aerobic glycolytic transcripts and a decrease in oxidative phosphorylation transcripts.

My project investigated the rate limiting and last step of glycolysis, metabolic enzymes pyruvate kinase muscle isoforms 1 and 2 (PKM1/2). PKM2 has been found to regulate endothelial-to-mesenchymal transition in cancer cells and is known to enhance the reprogramming of adult cells into pluripotent cells (Hamabe et al. 2014; Qin et al. 2017). When a PKM1 allele is knocked into naïve mouse ESCs (mESCs) grown in differentiation media, the result is increased endoderm transcripts, whereas with a PKM2 allele knock-in there is a resistance to differentiation (Konno et al. 2015). Currently, we have a limited understanding of PKM1/2’s role in embryonic development, formative pluripotency, and transitioning between pluripotent states.

While there has been extensive research into characterizing naïve and primed pluripotent states, current understanding of how ESCs transition between states and formative state pluripotency is not well known (Zhou et al. 2012). In particular, what is known regarding how ESCs exit from naïve state through differentiation stimulus is poorly understood (Kalkan and Smith 2014). Several models have been published regarding the transition of naïve cells to a primed-like pluripotent state *in vitro,* and artificially transitioned cells retain the transcriptional circuitry and traits of their *in vivo* correlates to serve as an effective method of study (Guo et al. 2009). This work aims to delineate the

investigation's main question by verifying if modulating PKM1 or PKM2 will influence the maintenance of the naïve or primed states, and to alter the generation of the formative or primed-like pluripotency when transitioning from a naïve pluripotent state.

One aspect of my investigation regarding metabolic preferences and cell culture conditions that appeared to show an influence in pluripotency was altering oxygen tension. Oxygen tension was promising as primed pluripotency is associated with aerobic glycolysis, potentially, this trend is intrinsically programmed due to the developmental origins of *in vivo* post-implantation epiblast (Shyh-Chang and Ng 2017). This trend holds true during the reprogramming process of somatic cells to primed PSCs (Mathieu and Ruohola-Baker 2017). Oxygen tension works to influence metabolic enzymes important in pluripotent conversion such as HIF-1α (Zhou et al. 2012). It is well documented that human PSCs prefer low oxygen cell culture conditions, this works to promote primed pluripotency (Lees et al. 2019). Naïve mESCs, transitioning formative mEpiLCs, and primed mEpiSCs can be cultured at normoxic (~21% oxygen tension) and low oxygen (hypoxic ~2-5% and 5% oxygen tension in this study). Morphologically, mEpiSCs grew more proficiently showing their characteristic flattened morphology (Figure 6.1.).

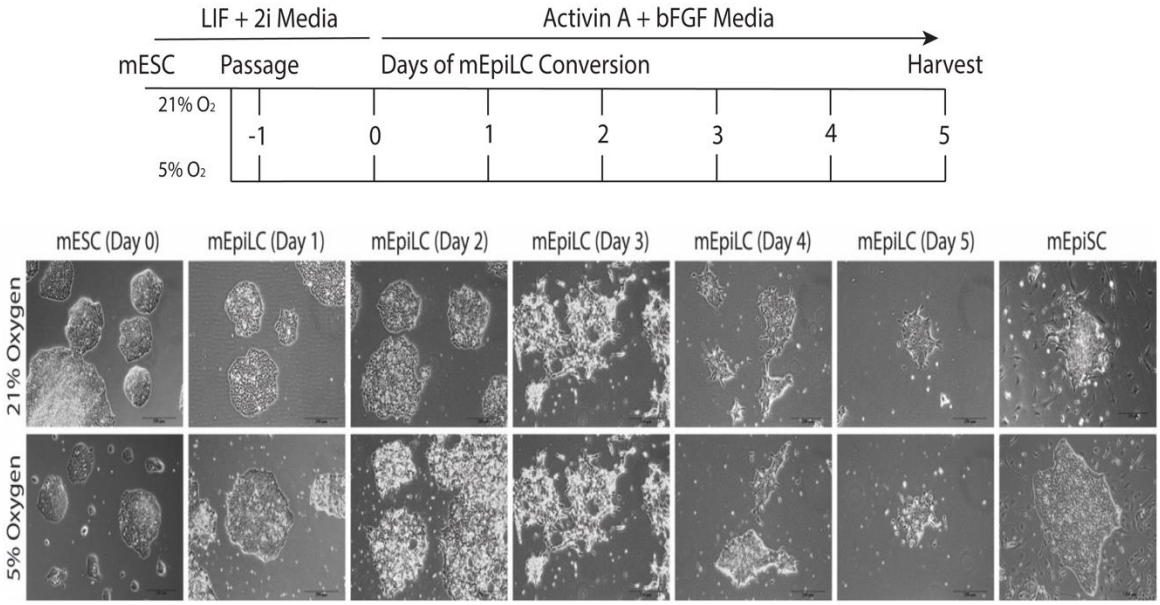

Figure 6.1. Phase contrast imaging of naïve mESCs, chemically transitioned of formative, and primed-like mEpiLCs.

Naïve mESCs can be chemically transitioned from glistening, domed colonies characteristic of the naïve pluripotent state, into flattened colonies like the primed pluripotent cells of the post-implantation epiblast. This conversion can be accomplished through the swapping of required growth factors from LIF/2i conditions to FA media. Cells were cultured in both 21% oxygen representative of normoxic conditions and 5% oxygen conditions, referred to as hypoxic. Phased contract microscopy was completed on 10x objective. Scale bars represent 200 μm.

To study the influence of oxygen tension on each pluripotent state we additionally examined protein lysates for metabolic and pluripotency and early lineage markers (Figure 6.2.). Naïve mESCs, mEpiLCs transitioning over 5 days (each day harvested), primed mEpiSCs, and as a somatic cell control, mouse embryonic fibroblasts (MEFs) were grown in both 21% oxygen to simulate normoxic conditions and 5% oxygen to simulate hypoxic conditions.

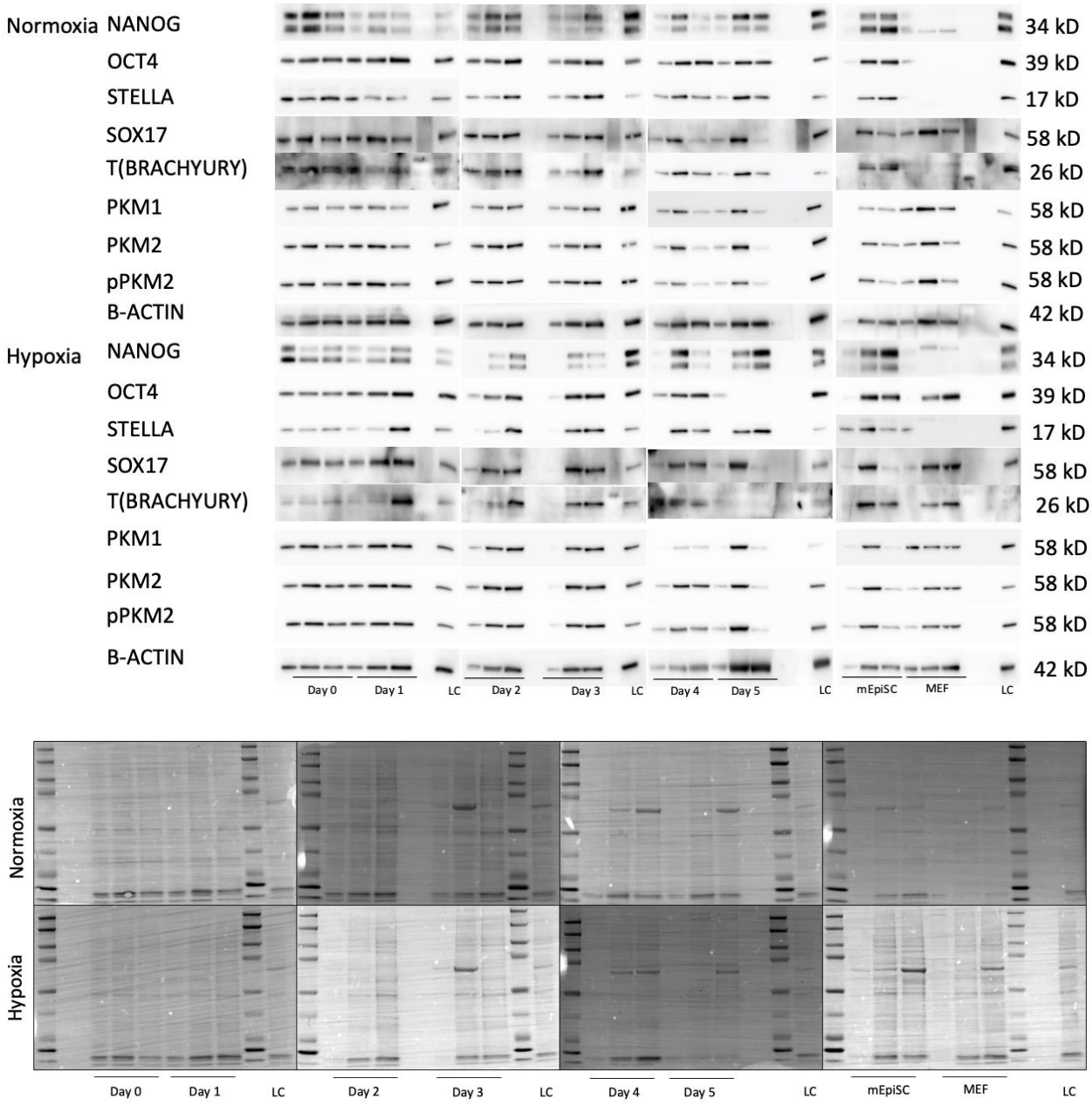

Figure 6.2. Immunoblotting and Ponceau staining of mESCs, transitioning mEpiLCs, mEpiSCs, and MEFs in normoxic and hypoxic cell culture conditions.

Naïve mESCs, transitioning mEpiLCs, mEpiSCs, and MEFs immunoblotted for pluripotency and metabolic protein markers. Cells were grown in 21% oxygen (atmospheric/normoxic) and 5% oxygen (hypoxic) conditions. Each lane represents an individual biological replicate, and each cell type was run in biological triplicate.

Examining the protein abundance of 21% and 5% oxygen tensions revealed differential metabolic and pluripotent expression patterns throughout the pluripotent continuum (Figure 6.3.A-G). My findings suggest that primed mEpiSCs show a beneficial influence of culture in 5% oxygen over 21% as demonstrated with a statistically significant increase in T(BRACHYURY) protein abundance for low oxygen conditions (Figure 6.3.C). A significant decrease in NANOG confers an exit of the naïve state in transitioning mEpiLCs (Figure 6.3.D) (Kinoshita and Smith 2018). While a decrease in NANOG is expected, a drop in OCT4 is not, potentially the finding of a significant decrease in OCT4 protein abundance between 21% and 5% conditions in 4 to 5 days of transitioning mEpiLCs may suggest that the formative pluripotent state has an elevate degree of preference for OXPHOS (Figure 6.3.E). Early in the transitioning process (days 1 and 2) indicate that hypoxic conditions promote the primed pluripotency associated protein SOX17 (Figure 6.3.F) (Kinoshita and Smith 2018). It is hypothesized that the early post-implantation epiblast cell of the murine embryo should reflect the decreased oxygen availability (Mathieu and Ruohola-Baker 2017). This may explain why the greatest metabolic protein abundance changes in PKM1, pPKM2, and PKM2 reflect the early formative transitioning mEpiLCs and the metabolically bivalent mESCs. There was a significant increase in PKM1 for hypoxic conditions relative to normoxic conditions in naïve mESCs and 1 day of transitioning mEpiLCs (Figure 6.3.A) and a significant increase in pPKM2/PKM2 in mESCs and mEpiLCs transitioning on days 1-3 (Figure 6.3.B).

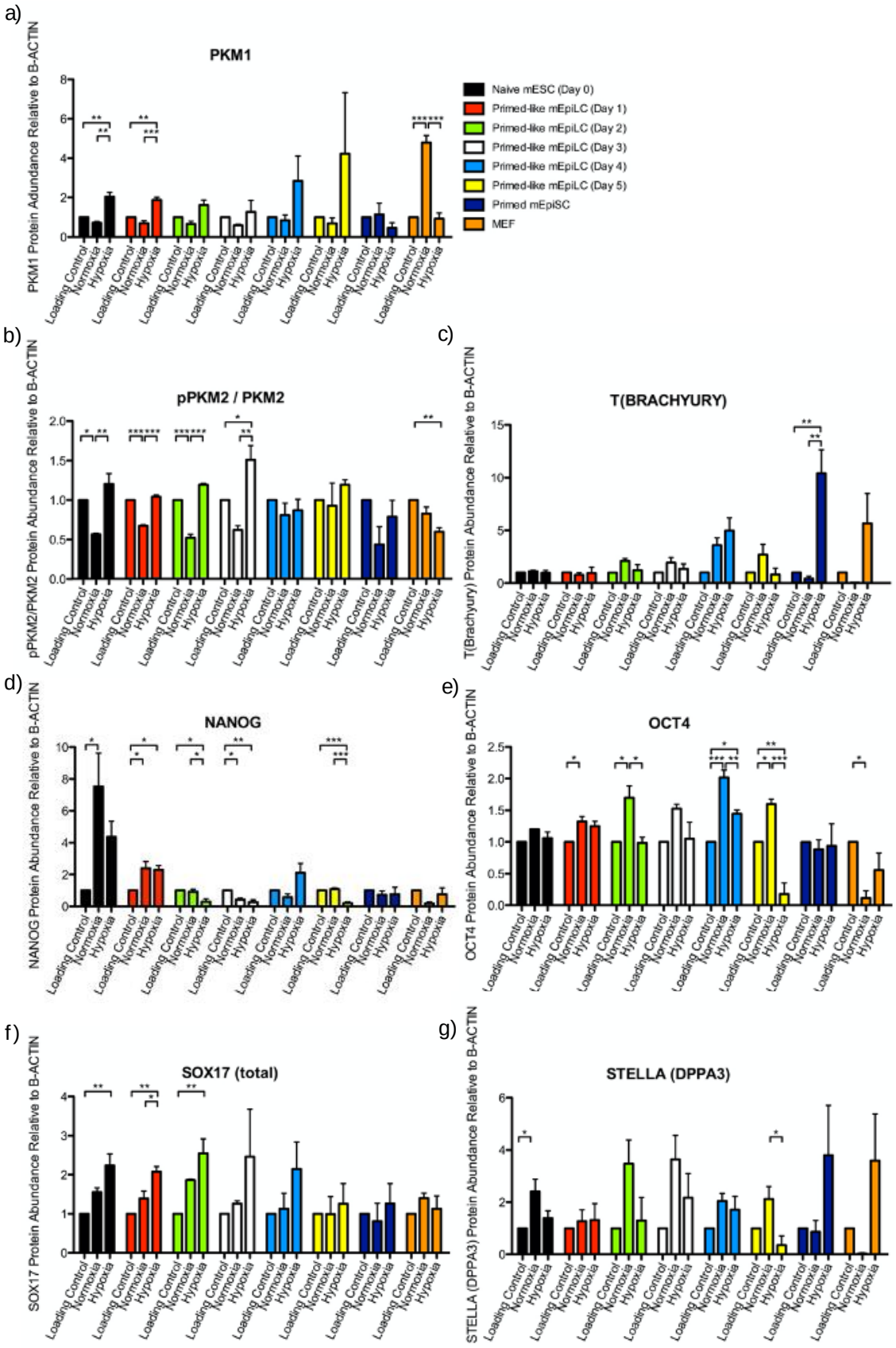
a)
PKM1
PKM1 Protein Adundance Relative to B-ACTIN
Naive mESC (Day 0)
Primed-like mEpiLC (Day 1)
Primed-like mEpiLC (Day 2)
Primed-like mEpiLC (Day 3)
Primed-like mEpiLC (Day 4)
Primed-like mEpiLC (Day 5)
Primed mEpiSC
MEF
b)
pPKM2 / PKM2
pPKM2/PKM2 Protein Abundance Relative to B-ACTIN
c)
T(BRACHYURY)
T(Brachyury) Protein Abundance Relative to B-ACTIN
d)
NANOG
NANOG Protein Abundance Relative to B-ACTIN
e)
OCT4
OCT4 Protein Abundance Relative to B-ACTIN
f)
SOX17 (total)
SOX17 Protein Abundance Relative to B-ACTIN
g)
STELLA (DPPA3)
STELLA (DPPA3) Protein Abundance Relative to B-ACTIN
Loading Control
Normoxia
Hypoxia

Figure 6.3. Metabolic and pluripotent state associated protein abundance in naïve mESCs, transitioning mEpiLCs, primed mEpiSCs, and somatic MEFs.

Naïve mESCs, transitioning mEpiLCs (over 5 days of chemical transitioning), primed mEpiSCs, and somatic MEFs were compared relative to a loading control consisting of a combination of each lysate. Metabolic and pluripotency associated markers were compared by densitometry and normalized to the loading control. Data consists of mean densitometry$\pm$SEM, run in biological triplicate, *$p>0.05$.

6.1.0. Summary of Findings:

My research contributes to evidence that metabolism has an active and passive role in development and pluripotency. I have found differences in PKM1/2 expression and subcellular localization between naïve, formative, and primed mouse embryonic stem cells. Metabolism has been thought of as a by-product of cell fate, but this idea has been challenged as metabolism has now been found to be as a necessary driver of development (Zhang et al. 2018; Dahan et al. 2019; Tsogtbaatar et al. 2020). By better understanding the role of metabolism during the transition between naïve and primed PSCs, *in vitro* research can more closely recapitulate the *in vivo* mammalian development of pre-gastrulation embryos.

In Chapter 2, I detail a novel, comprehensive methodology in colocalization. This methodology is beneficial in the study of nuclear and cytoplasmic protein localization of pluripotent stem cells (PSCs). Due to the increased nuclear to cytoplasmic size ratio of PSCs, my method utilizes the addition of 3D imaging, background negation, and an additional nuclear reference relative to the nuclear pluripotency marker of comparison to the protein of interest for validation. This methodology was used to demonstrate nuclear and cytoplasmic colocalization of PKM1/2 in naïve mESCs, formative mEpiLCs, and primed mEpiSCs relative to OCT4 and GAPDH localization, validated with Hoechst nuclear staining. These findings show that it is critical to run positive and negative references relative to dual fluorophore colocalization and that in the case of mouse embryonic stem cells (mESCs), the spatial overlap data may not be sufficient to reach quality colocalization assessment compared to correlation data when considering the qualifying standards (Zinchuk, Wu, and Grossenbacher-Zinchuk 2013). I observed that

the MOC metrics in PSCs were insufficient to delineate nuclear and cytoplasmic distinctions by colocalization and that the PCC metric was a highly effective and viable tool for such distinction and analysis. To increase the power of traditional colocalization studies, I did not simply analyze single images, but I also employed orthogonal projections of stacks examining the data of individual slices to characterize the localization patterns of a true three-dimensional structure. Additionally, I accounted for the inherent flaws of the MOC calculation by examining only the individual colonies and individual cells in the orthogonal and airyscanned images respectively to prevent autofluorescence or background pixel offset. Using this methodology, my research demonstrates that PKM1 and PKM2 have a moderate correlation and a strong spatial overlap to the nuclear localized OCT4 and the cytoplasmic localized GAPDH in naïve mESCs. In formative state mEpiLCs, there is a significant decrease in spatial overlap of PKM1 and PKM2 localization relative to GAPDH. Additionally, there was a strong correlation of PKM1 to OCT4 and a moderate correlation of PKM1 to GAPDH, whereas PKM2 had a weak correlation to both OCT4 and GAPDH in mEpiLCs. Finally, primed mEpiSCs had a strong overlap of PKM1 and PKM2 to the localization of OCT4 and GAPDH, but only a weak correlation of PKM1 and PKM2 relative to OCT4 and a moderate correlation to GAPDH. These results provide evidence of differential subcellular localization patterns of PKM1/2, which are traditionally localized to the cytoplasm. Nuclear translocation of each isoform may indicate non-canonical roles for this metabolic gene similar to documented roles within cells exhibiting the Warburg Effect (Wei et al. 2017; Weiwei Yang and Lu 2013).

In Chapter 5, I utilized a novel method of naïve, formative, primed-like, and primed pluripotent state delineation by flow cytometry, quantifying the pluripotent state associated cell surface markers SSEA1 and CD24. This methodology allowed for the distinguishing of unique SSEA1/CD24 expression for each state and allowed for the transitioning efficiency to be determined following the addition of pre-mRNA splice morpholinos designed to target PKM1 and PKM2. This study demonstrated that altering PKM1/2 expression by morpholinos modulated SSEA1/CD24 expression in transitioning pluripotent states within the pluripotent continuum and works to promote the notion that metabolism is a driver of development. As such, blocking pre-mRNA splicing of PKM1 and PKM2 during a naïve-to-primed transition of mESCs to mEpiLCs modulates the exit from naivety and initiation of primed pluripotency. Specifically, downregulation of PKM2 promotes the frequency of cell events expressing the primed pluripotency cell surface marker CD24 in naïve mESCs transitioning to the formative pluripotent state. Additionally, downregulation of PKM2 alone or coupled with upregulation of PKM1 increases the frequency of cells expressing high levels of both the naïve cell surface marker SSEA1 and the primed marker CD24 when transitioning from the formative state to a primed-like pluripotency. Modulation of PKM1/2 with either targeted approach increased the ratio of pPKM2 (homodimeric conformation attributed to the Warburg Effect) to total PKM2 (homo-tetrameric and dimeric conformations), giving rise to the likely possibility that pPKM2 plays a role in generating this novel expression pattern. This enhanced ratio has been postulated to indicate a shift towards biosynthesis over energetic processes (W. Yang and Lu 2015; Zahra et al. 2020). In Chapter 3, I demonstrate the stable ratio of PKM1/PKM2 is demonstrated throughout the pluripotent continuum, thus a perturbation of this ratio likely would further promote the Warburg

Effect and enhance the metabolic shift from bivalency to aerobic glycolysis. Colocalization data by confocal microscopy, and flow cytometric results and analysis using the comprehensive techniques are detailed in Chapters 2 and 4, and are respectively summarized in Figure 6.4.

Collectively, I demonstrate differential nuclear localization of PKM1 and PKM2 in mPSCs across the pluripotent continuum. My initial observations of the presence of nuclear PKM1 appeared to be the first of its kind, and only recently has been shown in hepatoma cells (Wei et al. 2017). Coupled with nuclear fractionation data, my comprehensive methodology to colocalization, detailed in Chapter 2, works to clearly demonstrate nuclear PKM1/2 in mPSCs across the spectrum, detailed in Chapter 3. These findings indicate a potential non-canonical role outside of metabolic processing for PKM1/2 within the developmental process. My study proceeded to delineate the influence of modulating PKM1/2 through spliceosome modifying morpholinos to alter PKM1/2 expression in each pluripotent and during a transition throughout the continuum. In chapter 5, I found that altering PKM1/2 expression had little impact on metabolic transcripts associated with glycolysis and OXPHOS or pluripotency transcripts, however, there was an impact on key pluripotency cell surface marker expression during transitioning. Modulation of PKM1 and PKM2 in cells chemically transitioning from naïve mESCs into formative mEpiLCs and subsequently into primed-like mEpiLCs indicate that PKM1/2 are drivers of the development of the pluripotent continuum. Decreasing PKM2 protein abundance during the in the transition to the formative state increases expression of the primed pluripotency cell surface marker CD24. By either

downregulating PKM2 or downregulating PKM2 while upregulating PKM1 formative state mEpiLCs developing into primed-like mEpiLCs exhibit a novel subset of cells expressing both the naïve pluripotency cell surface marker SSEA1 and CD24. Using the methodology of I describe in Chapter 4, I delineated between these mPSCs with a model of PKM1/2 modulation, and demonstrate a means of discrimination for the formative state. Together, these results demonstrate a novel differential nuclear expression pattern of PKM1/2 across the pluripotent continuum and by modulating expression of PKM1/2 key pluripotency cell surface markers are influenced indicating a role in pluripotent state transitioning.

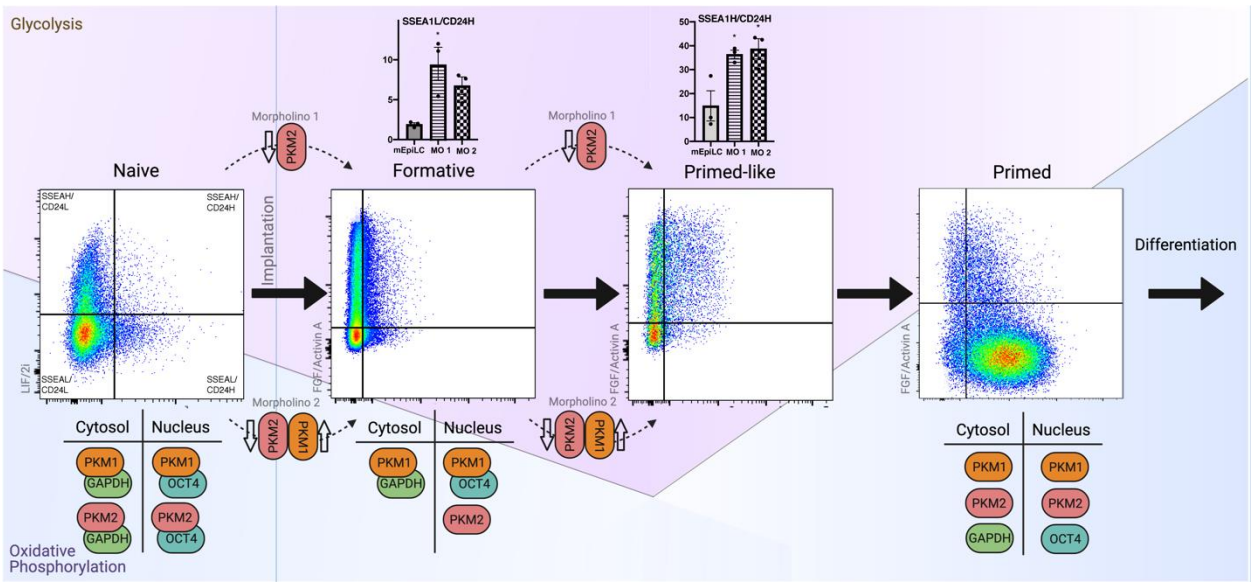

Figure 6.4. Thesis summary of colocalization and flow cytometric results.
During the developmental transition of naïve-to-primed pluripotent states in mouse embryonic stem cells, there is a switch in metabolic preference from bivalent oxidative phosphorylation and glycolysis in the naïve state, to aerobic glycolysis in primed stem cells. Using my improved colocalization technique, I examined orthogonal projections with references to known nuclear and cytoplasmic markers, I determined that PKM1 and PKM2 proteins are differentially expressed in nuclear and cytoplasmic regions of PSCs throughout the pluripotent continuum, importantly, overlap of proteins indicates potential biomolecular interaction of the protein of interest PKM1/2 and either OCT4 or GAPDH, the nuclear and cytoplasmic reference respectively. To elucidate the potential role that PKM1/2 has within the development of the pluripotent continuum, I utilized a morpholino strategy targeting PKM1/2 splice modifications during chemical transitioning between naïve-to-formative and formative-to-primed-like pluripotent states. Alteration of PKM1/2 (downregulation of PKM2 or downregulation of PKM2 coupled with upregulation of PKM1) through the addition of splice modifying morpholinos resulted in an increased frequency of cells expressing high levels of the cell surface marker SSEA1 and CD24 during a formative-to-primed-like pluripotent state transition. Taken together, these results promote non-canonical roles for PKM1 and PKM2 in mPSCs across the pluripotent continuum.

6.2.0. Research Limitations:

This thesis was limited by PKM MO targeting specificity, limited metabolic profiling of live cells and protein abundance analyses of metabolic and pluripotent sates. After several designs, attempts, and redesigns, my PKM1 and PKM2 knockdown strategy failed to be specific exclusively for one or the other isoform. However, I made the most of this lack of specificity to further promote the individual role of decreasing PKM2 alone and upregulating PKM1 concomitantly with a reduction in PKM2. To truly show the role of PKM1/2 during this period of development, an inducible overexpression model of each isoform should be employed. Originally, I attempted to employ a strategy of small interfering RNAs (siRNA), however, this method did was not truly convincing. The details of my siRNA study attempts are described in Chapter 5 (Figures 5.11.-13.). The main issue with the siRNA investigation was a lack of PKM1 or PKM2 specificity by protein abundance (Chapter 5., Figure 5.13.) and an apparent upregulation of Pkm1 and Pkm2 transcript abundance (Chapter 5., Figure 5.12.). Additionally, the scrambled control siRNA resulted in an influence of the siRNA transcript and protein abundance. These conflicting results may be a result of the heterogenous transcriptional landscape in naïve cells and epigenetic rewiring during development and transitioning. Naïve and primed cells can be distinguished in terms of their DNA methylation including changes to promotor-interactions and chromatin state maps (Chovanec et al. 2021; Messmer et al. 2019). Future studies could include an inducible overexpression model that would allow for the study of increasing either isoform during developmental transitioning from transient states such as the formative and primed-like states. With the recent advent of a stably cultured formative pluripotent stem cell line, an inducible overexpression model is not necessary to study the transition towards a primed-like state. The addition of studying

acute live cell extracellular acidification rate and oxygen consumption rate, measure of glycolysis and oxidative phosphorylation in each pluripotent state treated with PKM1/2 modulation would demonstrate the metabolic reprogramming effect of PKM1/2. Running this acute study in live cells and the newly derived stable formative state cells would remove the limitation of knowing metabolic preferences within these cells and their modulated states following morpholino incorporation. Finally, using my comprehensive colocalization methodology described in Chapter 2, I demonstrate nuclear PKM1 in Chapter 3, however, this strategy was limited in proving nuclear translocation without the addition of ChIP-sequencing coupled with single cell RNA-sequencing. The addition of these powerful molecular techniques would greatly benefit this study to transcriptional regulation of PKM1 during pluripotency transitioning.

6.3.0. Future Experiments:

A final and definitive method of characterizing the metabolic profiles of naïve, formative, and primed cells will include examining extracellular acidification (ECAR) and oxygen consumption rates (OCR) which correspond to glycolysis and OXPHOS respectively. The Betts laboratory owns and operates a Seahorse XF^e Extracellular Flux Analyzer, which is used to measure ECAR and OCR in live cells. This technology has been shown to be effective in comparing naïve and primed cells based on metabolic demands and can show the influence of altering PKM splicing in live cells (Zhou et al. 2012). Agilent, the company who created the Seahorse has expressed interest in us to profile the formative pluripotent state. This could be a valuable part in better understanding the role of metabolism in cell fate decisions and developmental processes. Metabolic readouts

following adjustments PKM1/2 expression in naïve, formative and primed PSCs will provide valuable insight into PKM1/2's role in glycolytic shifting during developmental progression. Future experiments should consider culturing mPSCs in low oxygen conditions (5% oxygen) as we demonstrate an upregulation of metabolic and pluripotency associated proteins (Figure 6.1.-3.).

Future studies should also include a stable line of formative state murine pluripotent stem cells. These cells can be generated with the inclusion of tankyrase inhibitor with FA media (Kinoshita et al. 2020). True formative state stem cells extracted from murine ICM from E5.5-E6.0 would be ideal in a comparison of explanted naïve mESCs and primed mEpiSCs. It would be especially interesting to see if the unique SSEA1 high/CD24 high population corresponds with an increased expression of CD61 as expected of primordial germ cell differentiation (Kinoshita et al. 2020). This may allude to PKM1/2 being implicated in direct conversion of germ cell specialization.

Precise targeted disruption of PKM1/2 demonstrated by isoform specificity should be further explored. This study utilized a PKM2 downregulation and PKM2 downregulation with PKM1 upregulation strategy using the tools we had at our disposal. Future studies should utilize either a knockdown or knockout approach and overexpression specific to each isoform. Additionally, the combination of such tactics to produce a knockdown or knockout of one isoform and an overexpression of the other would further promote the roles of each isoform and perhaps further validate our morpholino results in primed-like mEpiSCs and cell expressing both CD24 and SSEA1. The incorporation of inducible overexpression of PKM1 or PKM2 would also work to further promote if PKM1/2 is

necessary or sufficient to maintain or hinder pluripotency and developmental transitioning.

Finally, the colocalization study would greatly benefit from a mass spectroscopy study of nuclear PKM1/2 and co-immunoprecipitation study with OCT4. Previous studies have used mass spectroscopy to study nuclear PKM2 interactions with JMJD5 (Wang et al. 2014). This study should begin with a non-denaturing gel of each pluripotent state examining dimeric and tetrameric PKM2 levels, this has been completed in other cell types and is possible to complete (Verma and Patel 2019). The work of this thesis demonstrates differences in each conformation; however, this experiment would further solidify differences and allow for downstream analysis by mass spectroscopy. These aspects work to promote nuclear translocation during development. Future studies into the role of nuclear PKM1 during this time interval is necessary to promote non-canonical roles of this metabolic enzyme that traditionally is not known to translocate into nuclear compartments (Wei et al. 2017). To delineate novel targets of PKM1 and PKM2 within the nucleus, ChIP-sequencing and single cell RNA sequencing could be employed to identify potential regulatory targets of metabolism and pluripotency.

Additionally, evidence of the role of PKM1/2 during a naïve-to-primed transition could be provided by a pharmacological approach. There are a variety of commercially available chemical PKM1/2 inhibitors and activators. Inhibitors such as shikonin, a Chinese herb derivative, have been reported to knockdown greater than 50% of PKM2 activity with no apparent influence on PKM1 (Chen et al. 2011). While chemical inhibitors are readily available, there is a tendency to focus on PKM2 or PKM total,

leaving PKM1 partially or fully functioning. Chemical inhibitors such as DASA-58 and TEPP-46 work as a PKM2 activator, specifically enabling the homotetramer conformation and destabilizing the homodimer by preventing phosphorylation (Anastasiou et al. 2012). Alternatively, promyelocytic leukemia protein works in the opposite fashion by maintaining the nuclear localizing PKM2 homodimer and destabilizing the homotetramer thus promoting aerobic glycolysis and the Warburg Effect (Shimada, Shinagawa, and Ishii 2008).

6.4.0. Significance of Findings:

This area of research promotes metabolism as having an active role in pluripotent development, rather than a passive role as a by-product of differentiation. Knowing whether PKM1/2 has a role in early development has yet to be determined and this project has further clarified that role. Efficient transitioning of naïve and primed pluripotent states has regenerative medicine implications as well in terms of disease modelling or the scaling up of cells. Human ESCs (hESCs) isolated from blastocysts are traditionally representative of the primed state and while hESCs are pluripotent, induction towards a naïve state is for desirable for improved scalability and the enhanced ability to be feeder-free (Vallier 2005). Reprogramming somatic cells or inducing primed cells to a more naïve-like state is becoming an increasing important area of research that will yield benefits regenerative medicine.

From a therapeutic standpoint, this aim works to transition mESCs to formative mEpiLCs (48 hours of transitioning in FA media), and primed-like mEpiLCs (72≤ hours of

transitioning in FA media) in a more homogenous and stable population. Currently, induced pluripotent stem cells (iPSCs) are favored over ESCs for disease modelling, despite both being equally capable (Halevy and Urbach 2014). Despite reduced reprogramming efficiency and epigenetic memory, the preference for iPSCs is largely due to challenges associated with ESCs legalities and genome editing. However, several diseases are better portrayed using ESCs largely due to epigenetic memory and landscape. In a comparison of X-linked autosomal diseases, it was found that disorders such as Turner's Syndrome, epigenetic silencing in Fragile X Syndrome and Huntington's Disease are better modelled using ESCs than iPSCs (Halevy and Urbach 2014).

In summary, my investigation of differential pyruvate kinase muscle isoform expression in naïve-to-primed mESC development promotes PKM1 and PKM2 having an important role in *in vitro* pluripotency throughout the pluripotent continuum and may suggest a developmental link as these cells have appear to demonstrate a metabolic preference bias like their *in vivo* counterparts of the pre- and post- implantation blastocyst. Differential localization patterns of PKM1/2 through the pluripotent continuum demonstrate subcellular changes to nuclear and cytoplasmic localization and potential interaction of both isoforms to the pluripotency protein OCT4 may indicate a role in governing pluripotency. The presence of nuclear PKM1 was a first of its kind observation and indicates a potential non-metabolic role. Modulation of PKM1/2 does not drastic alter metabolic or pluripotency transcript abundance, however, when transitioning between the naïve and formative state, downregulation of PKM2 enhances CD24 expression, a key protein associated with primed pluripotency. Additionally, when transitioning from a formative state to a primed-like pluripotency, the downregulation of PKM2 and

downregulation of PKM2 with upregulation of PKM1 increases the frequency of cells expression both SSEA1 and CD24, characteristics of both naïve and primed cells. Using the methodology findings of Chapter 4, I demonstrate that the formative pluripotency state can be distinguished from both the naïve and primed states. My refined colocalization and flow cytometric methodology further the field of molecular techniques and fill benefit downstream analysis and applications such as improved cell sorting. The results of this thesis support my governing hypothesis that PKM1/2 is differentially localized during the development of PSCs in the pluripotent continuum and altering PKM1/2 expression appears to modulate developmental progression during transition from the naïve pluripotent state and formative state. My thesis sheds light on the role of metabolism and pyruvate shuttling during early development and has the potential to enhance our knowledge of mechanisms controlling pluripotent cell conversion, ultimately benefiting disease modelling and cell replacement therapies. The findings of my works promote PKM1/2 as having a non-canonical role outside of metabolic processing during developing stem cells of the pluripotency continuum and further promotes metabolism as a driver of pluripotency and development.

6.5.0. References:

Anastasiou, Dimitrios, Yimin Yu, William J. Israelsen, Jian Kang Jiang, Matthew B. Boxer, Bum Soo Hong, Wolfram Tempel, et al. 2012. "Pyruvate Kinase M2 Activators Promote Tetramer Formation and Suppress Tumorigenesis." *Nature Chemical Biology* 8 (10): 839–47. https://doi.org/10.1038/nchembio.1060.

Chen, J., J. Xie, Z. Jiang, B. Wang, Y. Wang, and X. Hu. 2011. "Shikonin and Its Analogs Inhibit Cancer Cell Glycolysis by Targeting Tumor Pyruvate Kinase-M2." *Oncogene* 30 (42): 4297–4306. https://doi.org/10.1038/onc.2011.137.

Chovanec, Peter, Amanda J Collier, Christel Krueger, Csilla Várnai, Claudia I Semprich, Stefan Schoenfelder, Anne E Corcoran, and Peter J Rugg-Gunn. 2021. "Widespread Reorganisation of Pluripotent Factor Binding and Gene Regulatory Interactions between Human Pluripotent States." *Nature Communications* 12 (1): 2098. https://doi.org/10.1038/s41467-021-22201-4.

Dahan, Perrine, Vivian Lu, Robert M T Nguyen, Stephanie A L Kennedy, and Michael A Teitell. 2019. "Metabolism in Pluripotency: Both Driver and Passenger?" *The Journal of Biological Chemistry* 294 (14): 5420–29. https://doi.org/10.1074/jbc.TM117.000832.

Evans, M. J., and M. H. Kaufman. 1981. "Establishment in Culture of Pluripotential Cells from Mouse Embryos." *Nature*. https://doi.org/10.1038/292154a0.

Guo, G., J. Yang, J. Nichols, J. S. Hall, I. Eyres, W. Mansfield, and A. Smith. 2009. "Klf4 Reverts Developmentally Programmed Restriction of Ground State Pluripotency." *Development* 136 (7): 1063–69. https://doi.org/10.1242/dev.030957.

Halevy, Tomer, and Achia Urbach. 2014. "Comparing ESC and IPSC—Based Models for Human Genetic Disorders." *Journal of Clinical Medicine* 3 (4): 1146–62. https://doi.org/10.3390/jcm3041146.

Hamabe, Atsushi, Masamitsu Konno, Nobuhiro Tanuma, Hiroshi Shima, Kenta Tsunekuni, Koichi Kawamoto, Naohiro Nishida, et al. 2014. "Role of Pyruvate Kinase M2 in Transcriptional Regulation Leading to Epithelial–Mesenchymal Transition." *Proceedings of the National Academy of Sciences* 111 (43): 15526 LP – 15531. https://doi.org/10.1073/pnas.1407717111.

Kalkan, Tüzer, and Austin Smith. 2014. "Mapping the Route from Naive Pluripotency to Lineage Specification." *Philosophical Transactions of the Royal Society B: Biological Sciences* 369 (1657): 20130540-. https://doi.org/10.1098/rstb.2013.0540.

Kinoshita, Masaki, Michael Barber, William Mansfield, Yingzhi Cui, Daniel Spindlow, Giuliano Giuseppe Stirparo, Sabine Dietmann, Jennifer Nichols, and Austin Smith. 2020. "Capture of Mouse and Human Stem Cells with Features of Formative Pluripotency." *Cell Stem Cell*. https://doi.org/https://doi.org/10.1016/j.stem.2020.11.005.

Kinoshita, Masaki, and Austin Smith. 2018. "Pluripotency Deconstructed." *Development, Growth & Differentiation* 60 (1): 44–52. https://doi.org/10.1111/dgd.12419.

Konno, Masamitsu, Hideshi Ishii, Jun Koseki, Nobuhiro Tanuma, Naohiro Nishida, Koichi Kawamoto, Tatsunori Nishimura, et al. 2015. "Pyruvate Kinase M2, but Not M1, Allele Maintains Immature Metabolic States of Murine Embryonic Stem Cells." *Regenerative Therapy* 1: 63–71. https://doi.org/10.1016/j.reth.2015.01.001.

Lees, Jarmon G, Timothy S Cliff, Amanda Gammilonghi, James G Ryall, Stephen Dalton, David K Gardner, and Alexandra J Harvey. 2019. "Oxygen Regulates

Human Pluripotent Stem Cell Metabolic Flux." Edited by Antonio C Campos de Carvalho. *Stem Cells International* 2019: 8195614. https://doi.org/10.1155/2019/8195614.

Martin, G R. 1981. "Isolation of a Pluripotent Cell Line from Early Mouse Embryos Cultured in Medium Conditioned by Teratocarcinoma Stem Cells." *Proceedings of the National Academy of Sciences* 78 (12): 7634 LP – 7638. https://doi.org/10.1073/pnas.78.12.7634.

Mathieu, Julie, and Hannele Ruohola-Baker. 2017. "Metabolic Remodeling during the Loss and Acquisition of Pluripotency." *Development (Cambridge, England)* 144 (4): 541–51. https://doi.org/10.1242/dev.128389.

Messmer, Tobias, Ferdinand von Meyenn, Aurora Savino, Fátima Santos, Hisham Mohammed, Aaron Tin Long Lun, John C Marioni, and Wolf Reik. 2019. "Transcriptional Heterogeneity in Naive and Primed Human Pluripotent Stem Cells at Single-Cell Resolution." *Cell Reports* 26 (4): 815-824.e4. https://doi.org/10.1016/j.celrep.2018.12.099.

Morgani, Sophie, Jennifer Nichols, and Anna Katerina Hadjantonakis. 2017. "The Many Faces of Pluripotency: In Vitro Adaptations of a Continuum of in Vivo States." *BMC Developmental Biology* 17 (1): 10–12. https://doi.org/10.1186/s12861-017-0150-4.

Nichols, Jennifer, and Austin Smith. 2009. "Naive and Primed Pluripotent States." *Cell Stem Cell* 4 (6): 487–92. https://doi.org/10.1016/j.stem.2009.05.015.

Qin, Shengtang, Danli Yang, Kang Chen, Haolan Li, Liqiang Zhang, Yuan Li, Rongrong Le, Xiaojie Li, Shaorong Gao, and Lan Kang. 2017. "Pkm2 Can Enhance Pluripotency in ESCs and Promote Somatic Cell Reprogramming to IPSCs." *Oncotarget* 8 (48): 84276. https://doi.org/10.18632/ONCOTARGET.20685.

Shimada, Nobukazu, Toshie Shinagawa, and Shunsuke Ishii. 2008. "Modulation of M2-Type Pyruvate Kinase Activity by the Cytoplasmic PML Tumor Suppressor Protein." *Genes to Cells* 13 (3): 245–54. https://doi.org/10.1111/j.1365-2443.2008.01165.x.

Shyh-Chang, Ng, and Huck-Hui Ng. 2017. "The Metabolic Programming of Stem Cells." *Genes & Development* 31 (4): 336–46. https://doi.org/10.1101/gad.293167.116.

Smith, Austin. 2017. "Formative Pluripotency: The Executive Phase in a Developmental Continuum." *Development* 144 (3): 365–73. https://doi.org/10.1242/dev.142679.

Tsogtbaatar, Enkhtuul, Chelsea Landin, Katherine Minter-Dykhouse, and Clifford D L Folmes. 2020. "Energy Metabolism Regulates Stem Cell Pluripotency ." *Frontiers in Cell and Developmental Biology* . https://www.frontiersin.org/article/10.3389/fcell.2020.00087.

Vallier, L. 2005. "Activin/Nodal and FGF Pathways Cooperate to Maintain Pluripotency of Human Embryonic Stem Cells." *Journal of Cell Science* 118 (19): 4495–4509. https://doi.org/10.1242/jcs.02553.

Verma, Kirtika, and Ashok Patel. 2019. "Pyruvate Kinase M2 Serves as Blockade for Nucleosome Repositioning and Abrogates Chd7 Remodeling Activity." *PLOS ONE* 14 (2): e0211515. https://doi.org/10.1371/journal.pone.0211515.

Wang, H.-J., Y.-J. Hsieh, W.-C. Cheng, C.-P. Lin, Y.-S. Lin, S.-F. Yang, C.-C. Chen, et al. 2014. "JMJD5 Regulates PKM2 Nuclear Translocation and Reprograms HIF-1 -Mediated Glucose Metabolism." *Proceedings of the National Academy of Sciences* 111 (1): 279–84. https://doi.org/10.1073/pnas.1311249111.

Wei, Libin, Yuanyuan Dai, Yuxin Zhou, Zihao He, Jingyue Yao, Li Zhao, Qinglong Guo,

and Lin Yang. 2017. “Oroxylin A Activates PKM1/HNF4 Alpha to Induce Hepatoma Differentiation and Block Cancer Progression.” *Cell Death & Disease* 8 (7): e2944. https://doi.org/10.1038/cddis.2017.335.

Yang, W., and Z. Lu. 2015. “Pyruvate Kinase M2 at a Glance.” *Journal of Cell Science* 128 (9): 1655–60. https://doi.org/10.1242/jcs.166629.

Yang, Weiwei, and Zhimin Lu. 2013. “Nuclear PKM2 Regulates the Warburg Effect.” *Cell Cycle* 12 (19): 3154–58. https://doi.org/10.4161/cc.26182.

Zahra, Kulsoom, Tulika Dey, Ashish, Surendra Pratap Mishra, and Uma Pandey. 2020. “Pyruvate Kinase M2 and Cancer: The Role of PKM2 in Promoting Tumorigenesis .” *Frontiers in Oncology* . https://www.frontiersin.org/article/10.3389/fonc.2020.00159.

Zhang, Jin, Jing Zhao, Perrine Dahan, Vivian Lu, Cheng Zhang, Hu Li, and Michael A. Teitell. 2018. “Metabolism in Pluripotent Stem Cells and Early Mammalian Development.” *Cell Metabolism* 27 (2): 332–38. https://doi.org/10.1016/j.cmet.2018.01.008.

Zhou, Wenyu, Michael Choi, Daciana Margineantu, Lilyana Margaretha, Jennifer Hesson, Christopher Cavanaugh, C. Anthony Blau, et al. 2012. “HIF1α Induced Switch from Bivalent to Exclusively Glycolytic Metabolism during ESC-to-EpiSC/HESC Transition.” *EMBO Journal* 31 (9): 2103–16. https://doi.org/10.1038/emboj.2012.71.

Zinchuk, Vadim, Yong Wu, and Olga Grossenbacher-Zinchuk. 2013. “Bridging the Gap between Qualitative and Quantitative Colocalization Results in Fluorescence Microscopy Studies.” *Scientific Reports* 3: 1–5. https://doi.org/10.1038/srep01365.

Ethics Approval:

Ethics approval was not necessary for this study. Cell were obtained in a laboratory with permission to use stem cells in a level 2+ capable research environment.

Copyright releases from publications:

Currently not available.

Curriculum Vitae:

JOSHUA DIEROLF

EDUCATION

Western University, Ontario, Canada *2015 – 2021*
PhD. Candidate, Physiology and Pharmacology Specialization in Developmental Biology

Western University, Ontario, Canada *2010 – 2015*
Bachelors of Science, Honours Specialization in Biology.

SUMMARY OF QUALIFICATIONS

Pluripotent Stem Cell Expert

- Productive researcher studying the role of metabolism on pluripotent stem cell maintenance and development.
- Comprehensive knowledge of naive, formative and primed pluripotent stem cells.

Research Scientist

- Consistently worked in a range of academic and industrial research environments.
- Taken roles ranging from being a cleaner, mentor, research assistant and graduate student.
- Expertise shown in cell culture, molecular experiments and 3D printing.
- Professional research topics include organic chemistry, dental biochemistry, diabetic exercise physiology and pluripotent stem cell biology.
- Extensive training in planning experiments, executing studies and writing grants and research articles.

Innovator

- My greatest ability is to think outside of the box and make working solutions.
- I have developed new laboratory techniques using flow cytometry and confocal colocalization.
- Designed and 3D printed solutions to common lab and home problems and I am working on patenting a biomedical innovation for research scientists studying cell migration.
- I have proven my ability to troubleshoot and market biomedical innovations as I have been awarded first place in Ontario's Proteus Biomedical Innovation competition working to commercialize the Artificial Placenta, and ECMO alternative for premature babies.

PERSONAL ATTRIBUTES

Entrepreneurial
My strongest attribute is to think outside of the box and work towards commercializing new solutions and innovations. I am passionate about considering the commercialization potential of new innovations and work out the best ways to pitch these concepts. As such, I have won a provincial biomedical pitching competition and worked to commercialize a neonatal lung assistance device and have completed competitive graduate level biomedical innovation courses at my university.

Results Oriented
In an attempt to work more efficiently and mitigate lost resources and wasted time, I continue to hone my ability to answer research problems while limiting trial and error. During my studies, I have attained expert level proficiency in my techniques to ensure that I am operating and publishing top tier results. In doing so I have outlined new methods to improve colocalization experiments in biological samples and outlined a novel method of formative state pluripotent stem cell delineation.

Critical Thinking
Throughout my PhD. project, I have had to cultivate my problem solving and brainstorming abilities to tackle hurdles ranging from repairing sensitive laboratory equipment to designing novel approaches. I am confident in my ability to examine problems, make an action plan and coordinate with experts if necessary. To solve several issues in my lab and at my university, I have taken a think outside of the box approach and made my own solution by 3D printing. In doing so, I have been approached by faculty to help them with research problem and I am currently working on commercializing my own biomedical innovation.

Dedication
I have been interested in developmental biology from an early age. My training in martial arts has made me disciplined enough to not give up after failure. As a researcher, failure is inevitable, but learning from mistakes and improving upon them is a skill I continue to master. The harder decisions I have had to make include admitting the limits of my system and making the move onto new aspects when appropriate.

PHD. PROJECT

Thesis title: Characterization and modulatory influence of pyruvate kinase muscle isoforms 1 and 2 within the murine pluripotent continuum.

- Pioneered a project to understand the influence of PKM1/2 metabolism on early development. Discovered a new method of distinguishing formative pluripotent stem cells from naïve and primed pluripotent stem cells by flow cytometry using the cell surface markers SSEA1 and CD24 in cells of the early mouse embryo.
- Characterized and delineated differences in the rate limiting enzyme of glycolysis; pyruvate kinase muscle isoforms 1 and 2 (PKM1/2).
- Quantified differential localization and expression of these isoforms as well as indicate a novel nuclear presence of PKM1 suggesting a potential non-canonical role during development.
- Currently adjusting PKM1/2 expression and metabolite available during chemical transitioning of naïve cells towards a primed-like fate to elucidate roles of metabolism in pluripotency and early development.

TECHNICAL SKILLS

Cell Culture	Aseptic technique, Transfection, hPSCs, mPSCs, MEFs, HEK
Animal Models	Mouse & Rat handling & injections for teaching & diabetes research
Immunofluorescence	Expert Flow cytometry & Colocalization
Gene Editing	Design and use of: siRNA, CRISPR, Morpholino
Molecular/Wet Lab	RNA & Protein isolation, Immunocytochemistry, cDNA synthesis, qPCR, BCA, Immunoblotting, Protein fractionation
Specialized Equipment	FACSCanto Flow cytometer, Zeiss LSM800 Confocal microscope, FDM/Resin 3D printers

COMPUTER SKILLS

3D Printing	TinkerCad, Blender, Cura
Programming	Swift 3, R/Python, Java, Latex, HTML, Visual Basic
Software	MS Office, FlowJo, Prism, Image Lab, Photoshop/Illustrator, Zeiss/Leica suites

INDUSTRIAL/WORK EXPERIENCE

Tradewave Inc. 2016 - 2018(Consultant)
New Technology Services Lead

· Maintaining databases, designed websites and programmed applications for a variety of local, national & international e-commerce clients.
· Troubleshot programming issues across platforms and research companies to make custom website demonstrations.
· Successfully promoted the company to key clients and laid the group work for product and service presentations for future clients.

ALS Environmental 2013 - 2014(Internship)
Laboratory Analyst

· Extracted petroleum hydrocarbons, polycyclic aromatic hydrocarbons, oil/grease pesticides and herbicides from water, waste and soil samples.
· Adapted to an organic chemistry-based environment and thrived by honing my laboratory and analytical skills.
· Calibrated and maintained a variety of analytical equipment.

Family Karate Centres 2004 - 2017(Sensei)
Head Instructor

· Planned and executed Karate and Aikido classes for students of all ages.
· Was responsible for directing a team of instructors and leading classes.
· Pioneered a self-defence curriculum and achieve high levels of success in Southwestern Ontario. Additionally, I provided first aid, cleaning, sales, and administrative roles.

PUBLICATIONS

Ngan SY, Quach H, **Dierolf JG,** Lee J, Wong AP. (2021). Modelling human lung epithelial cell fate specification using pluripotent stem cells *Nature Methods*, (2021), Publication in works.

Quach H, Huang E, **Dierolf JG,** Wong AP. (2021). A Developmental Link to Cystic Fibrosis Lung Disease Pathogenesis *Stem Cell Reports - Review*, (2021), Publication in works.

Lee J, Yiming X, Huang E, **Dierolf JG,** Wong AP. (2021). Current strategies in Cystic Fibrosis gene therapy *Stem Cell Reports - Review*, (2021), Publication in works.

Dierolf JG, Watson AJ, Betts DH. (2021). 3D immunofluorescent image colocalization quantification in mouse epiblast stem cells *Methods in Molecular Biology*, (2021), Submitted and awaiting publication.

Dierolf JG, Brooks C, Chadwick K, Watson AJ, Betts DH. (2021). Flow cytometric characterization of pluripotent cell protein markers in nave, formative, and primed pluripotent stem cells *Methods in Molecular Biology*, (2021), Submitted and awaiting publication.

Dierolf JG, Hunter H, Watson AJ, Betts DH. (2021). Modulation of PKM1/2 levels by steric-blocking morpholinos alters the metabolic and pluripotent state of murine pluripotent stem cells. *Scientific Reports*, (2021), In Submission Process - Scientific Reports.

Dierolf JG, Watson AJ, Betts DH. (2021). Differential localization patterns of pyruvate kinase isoforms in murine nave, formative and primed pluripotent states *Experimental Cell Research*, (2021), Submitted and awaiting publication. Preprint available: "BioRxiv"

Dierolf JG, (2020). Till & McCulloch Meetings 2020: A tale of self-renewal. Signals Blog, *November*(2020), CCRM

Dierolf JG, (2020). Info for all, minus the paywall. Signals Blog, *January*(2020), CCRM

Tobias IC, Isaac RR, **Dierolf JG,** Khazaee R, Cumming RC, Betts DH. (2018). Metabolic plasticity during transition to naïve-like pluripotency in canine embryo-derived stem cells. *Stem Cell Research*, *30*(2018), 23-33.

Goiko M, **Dierolf J,** Gleberzon JS, Liao Y, Grohe B, Goldberg HA, de Bruyn JR, Hunter GK. (2014). Peptides of Matrix Gla Protein Inhibit Nucleation Growth of Hydroxyapatite Calcium Oxalate Monohydrate Crystals. *PLoS One*, *8*(2015): e80344.

AWARDS AND BURSARIES

"Cells I See" TMM Competition - National Meeting Grand Prize (2019)
Monetary Value: $750
Awarding Organization: CCRM/SCN

RNA Sequencing Workshop(2019)
Monetary Value: approx.$1200
Awarding Organization: OIRM/SCN

Graduate Student Innovation Scholars(2019)
Monetary Value: $1500
Awarding Organization: IVEY/WorlDiscoveries

Proteus Innovation Competition(2019)
Monetary Value: $5000
Awarding Organization: Propel

Intellectual Property and Entrepreneurship(2018)
Monetary Value: $350
Awarding Organization: SCN

B3 Bench to Bedside Therapeutic Workshop(2017)
Monetary Value: $350
Awarding Organization: SCN

TMM Conference; Toronto, Ontario(2016-2019)
Monetary Value: approx. $1000+ per year
Awarding Organization: OIRM

Developmental Biology Poster Winner(2016)
Monetary Value: $200
Awarding Organization: Western University

COMMITTEES

Stem Cell Network Trainee Communications Committee – National Chair

- I have spearheaded subcommittees planning events at the national conference TMM.
- I invite key players in the regenerative medicine stem cell biology field and planned workshops geared towards preparing trainees and postdocs in scientific storytelling, grant and abstract writing and innovation.
- As the National Chair, I am in charge of planning and guiding a team of 10+ stem cell experts to plan our yearly meetings trainee events using the resources provided by the Stem Cell Network.
- Finally, I was invited to host a fireside talk with a stem cell recipient at out national meeting.

Stem Cell Network Trainee Education Committee – Member

- In this committee, I attend planning meetings for trainee events and webinars.
- I provide input from the standpoint of the chair of the trainee communications committee.

Stem Cell Network - TMM2020 Code of Conduct Committee – Member

- Support and promote a welcoming, inclusive, safe, productive, harassment-free TMM conference environment for all participants, where all are treated with dignity and respect.

Western Stem Cell Group – Coordinator

- Plan monthly meetings stem cell research labs at Western University.
- Guide meetings, introduce speakers, seek sponsorship from industry, share community news, plan events and monitor finances.
- Invite science companies including Stem Cell Technologies and Synthego to give talks and work on collaborations with the Western University community.
- Instruct technique and research presentations to the Western community with this platform.

Graduate Student Council – Secretary

- Administer internal voting, taking minutes and leading departmental events.
- Provide feedback on important community efforts and frequently volunteer my time.

Stem Cell Talks London – Planning Committee (founding member)

- Present basic stem cell biology to local high school classes.
- Help to coordinate a yearly stem cell outreach symposium.

Former Position - Graduate Student Council – Health & Safety Officer

- Provide feedback on important community efforts and frequently volunteer my time.

TEACHING EXPERIENCE

Stem Cell Biology and Regenerative Medicine (2020)
This course entailed 4th year students to learn about adult stem cell biology and their uses in regenerative medicine. I was head teaching assistant in this course and I was responsible for planning and implementing a blog assignment system that students would have to take a stance and defend their position on. During this course I also taught review sessions and both proctored and graded exams.

Understanding Pluripotency: The physiology of stem cell fate and function (2018 – 2019)
As the sole teaching assistant for this course, I was responsible for responding to student inquiries on a daily basis. My role was to mark and provide feedback on writing assignments and examinations throughout the course. This fourth year stem cell course gave me the opportunity to share my passion and knowledge of pluripotency as a mentor to several students interested in stem cell research in graduate studies

Human Physiology (2016 – 2017)
As a teaching assistant for the Physiology Department, I taught weekly tutorials to second year undergraduates based on lecture materials. Tutorial sizes were between 30 and 40 students and I would design my own lesson plan and activities based on the materials of the week to reinforce concepts.

Physiology Laboratory (2015)
My experience as a teaching assistant in this laboratory course included guiding students through experiments ranging from frog and rat dissections to measuring human saccades and renal output.

PRESENTATIONS

Oral

Stem Cell Recipient Fireside Interview - Online Platform talk
TMM2021 – November, 2020

Child Health Research Day - Platform talk
Online Conference (Pandemic) – May 27, 2020
"Differential localization patterns of pyruvate kinase isoforms in murine naive, formative and primed pluripotent states"

Public Seminar - Physiology and Pharmacology Department - Platform talk
Online Seminar (Pandemic) – May 11, 2020
"Pyruvate kinase muscle isoforms 1 and 2 evolve through mouse nave, formative and primed pluripotency development"

London Health Research Day - Platform talk
London Convention Centre – 2019
"Characterization of PKM1/2 in mouse embryonic stem cells"

CIHR Trainee Showcase
Western University – 2018
"Steric blocking of PKM1 enhances nave to primed pluripotency conversion in murine embryonic stem cells"

Western Stem Cell Group
Western University – 2015, 2016, 2017, 2018, 2019
2018 "Delineating the metabolic role of PKM1/2 isoforms in mouseembryonic stem cell pluripotency "
2016 "Dismantling the metabolic roles of pyruvate kinase muscle isoforms in maintaining nave pluripotency"

Stem Cells Inked: Metabolism and Cell Fate
OIRM – 2017

Developmental Biology Trainee Showcase 2016
Western University – 2016

Ontario Biology Day 2015
Carleton University – 2015
"The bioenergetic regulation of canine embryonic stem cells"

Scientific Posters
Till & McCulloch Conference
Canada – 2016, 2017, 2018, 2019
2019 "Nuclear translocation of pyruvate kinase muscle isoforms 1 and 2 in naive and primed mouse embryonic stem cells."
2018 "Knockdown of PKM1 enhances nave to primed pluripotency conversion in murine embryonic stem cells."
2017 "Delineating the metabolic role of pyruvate kinase muscle isoforms in regulating pluripotent stem cell state conversion."
2016 "Delineating the metabolic role of pyruvate kinase muscle isoforms in mouse embryonic stem cell pluripotency."

Developmental Biology Research Day
Western University – 2016, 2017, 2018
2018 "Delineating the metabolic role of pyruvate kinase muscle isoforms in mouse embryonic stem cell pluripotency"
2017 "Delineating the metabolic role of pyruvate kinase muscle isoforms in regulating pluripotency"
2016 "Delineating the metabolic role of pyruvate kinase muscle isoforms in mouse embryonic stem cell pluripotency"

London Health Research Day
London, ON – 2016, 2017, 2018
2018 "Delineating the metabolic role of pyruvate kinase muscle isoforms in mouse embryonic stem cell pluripotency "
2017 "Characterizing the metabolic role of pyruvate kinase muscle isoforms in mouse embryonic stem cell pluripotency"
2016 "Dismantling the metabolic roles of pyruvate kinase isoforms in maintaining nave pluripotency"

Physiology Pharmacology Research Day
Western University – 2015, 2016
2016 "Delineating the metabolic role of pyruvate kinase muscle isoforms in mouse embryonic stem cell pluripotency"
2015 "Dismantling the metabolic roles of pyruvate kinase isoforms in maintaining nave pluripotency"